University of Nottingham
UK | CHINA | MALAYSIA

Faculty of Engineering

Chemical and Environmental Engineering Department

# Vertical annular flow characteristics for air/silicone oil system

**Yousuf Abdullah Al-Aufi**

**B.Sc., M.Sc.**

Thesis submitted to the University of Nottingham for the degree of Doctor of Philosophy

September 2017

*Dedicated to..*

*My entire loving and supporting family*

*and my dearest homeland , Oman*

*Yousuf Al-aufi*

*September 2017*

# ABSTRACT

Annular flow is one of the most common two-phase flow regimes observed in industrial applications. In annular flow, the liquid flows partly as a thin film along the pipe wall and partly as droplets entrained in the turbulent gas core. Most of the previous studies about the characteristics of annular flow and the developed correlations were conducted using an air/water system. This thesis reports an investigation about the characteristics of the annular flow regime and a development of liquid film thickness measurement using an ultrasonic technique in air/water and air/silicone oil systems.

Experiments were carried on an upward vertical annular flow test facility with 34.5 mm inner diameter (ID) using air/water and air/silicone oil two-phase systems. Time-varying of total pressure drop, liquid film thickness and wall shear stress were measured. The total pressure drop was measured using a remote seal differential pressure transducer and the wall shear stress was measured using a glue-on hot film sensor.

An ultrasonic technique was developed to measure the liquid film thickness. It was evaluated using static and dynamic measurements. For static measurements, it was compared with the liquid film thickness calculated based on knowledge of liquid volume and area of the test rig. For dynamic measurements, it was compared with two well-known conductance measurement techniques (Multi Pin Film Sensor and concentric probe) in falling film and upward vertical annular flow test facilities respectively. The relative error between the ultrasonic

technique and the other two techniques was within ±5%. A new processing method for ultrasonic measurement called Baseline removal method was developed for measuring liquid film thickness less than 0.5 mm.

The influence of gas and liquid superficial velocities, viscosity and surface tension on the measured parameters was studied using both systems. Both systems showed similar trend behavior with increasing gas and liquid superficial velocities even there was a difference in fluid properties. The results were also compared with the existing correlations developed using an air/water system to predict each one of the measured parameters. Most of the tested correlations predicted the total pressure drop, liquid film thickness and wall shear stress with relative deviation of ±50% or even higher in some cases.

# LIST OF PUBLICATIONS

**Yousuf AlAufi**, Nicholas J Watson, Barry J. Azzopardi, Buddhika N. Hewakandamby, Georgios Dimitrakis, Abbas Hasan and Alexander N. Kalashnikov (2016). Thin Film Thickness Measurements using Ultrasonic pulse echo technique. Proceedings of 9th International Conference on Multiphase Flow (ICMF), Firenze-Italy, 2016.

Abbas Hasan, B. Azzopardi1, B. Hewakandamby, **Yousuf AlAufi**, N.J. Watson, and Shara K. Mohammed (2016). Experimental characterization of interfacial wave structure of a falling liquid film in a vertical large pipe diameter. Proceedings of 9th International Conference on Multiphase Flow (ICMF), Firenze-Italy, 2016.

Abbas Hasan, B. Azzopardi, B. Hewakandamby, Shara K. Mohammed and **Yousuf AlAufi** (2017). An experimental study of a falling liquid film in a vertical pipe. Proceedings of 10th World Congress of Chemical Engineering conference (WCCE), Spain, October 2017 (Accepted extended abstract).

**Yousuf AlAufi**, Nicholas J Watson, Buddhika N. Hewakandamby, Georgios Dimitrakis, Abbas Hasan and Holmes M. Two phase annular flow thin film thickness measurement using ultrasonic pulse echo. (In preparation).

Abbas Hasan, B. Hewakandamby, **Yousuf AlAufi**, N.J. Watson, and Shara K. Mohammed. An experimental study of interfacial wave structure of freely falling liquid films in a vertical large pipe diameter. (In preparation).

# TABLE OF CONTENTS

# LIST OF FIGURES

# LIST OF TABLES

# NOMENCLATURE LIST

| Symbol | Meaning | unit |
|---|---|---|
| A | Area | ($m^2$) |
| A | Constant in Equation 3.6 | (-) |
| a | Overheating ratio | (-) |
| B | Constant in Equation 3.6 | (-) |
| C | Constant in Table 2.1 | (-) |
| $C_{B1}$ | Constant in Table 2.2 | (-) |
| $C_{B2}$ | Constant in Table 2.2 | (-) |
| $C_{B3}$ | Constant in Table 2.2 | (-) |
| $C_{B4}$ | Constant in Table 2.2 | (-) |
| $c, c_w, c_L$ | Speed of sound | (m/s) |
| $d_o$, D, ID | Pipe internal diameter | (m) |
| $D_1$ | Height between $P_1$ tapping and transmitter | (m) |
| $D_2$ | Height between $P_2$ tapping and transmitter | (m) |
| d | Pipe outside diameter | (m) |
| $E_{acq}$ | Measured voltage from Anemometer Bridge | (V) |
| $E_{corr}$ | Corrected voltage from Anemometer Bridge | (V) |
| $E, E_f$ | Entrainment Fraction | (-) |
| $E_{max}$ | Maximum Entrainment Fraction | (-) |
| $f, f_{lo}, f_l$ | Liquid friction factor | (-) |
| $f_{go}, f_g$ | Gas friction factor | (-) |
| $f_{TP}$ | Two-phase friction factor | (-) |
| $f_D$ | Darcy friction factor | (-) |
| $f, f_o$ | Frequency | (Hz) |
| $Fr_F$ | Froude number in equation (2.20) | (-) |
| $Fr_{BB}$ | Froude number in equation (2.28) | (-) |
| $Fr_g$ | Gas Froude number | (-) |
| $Fr_l$ | Liquid Froude number | (-) |
| $G_L$ | Liquid mass flux | ($kg/m^2s$) |
| $G_G$ | Gas mass flux | ($kg/m^2s$) |
| g | Acceleration due to gravity | ($m/s^2$) |
| H | Level height | (m) |

| | | |
|---|---|---|
| h | Heat transfer coefficient from heated wall to the fluid | ($w/m^2k$) |
| k | Thermal conductivity of the liquid | (w/m k) |
| k | Adiabatic compressibility | ($Pa^{-1}$) |
| $Ku_g$ | Kutateladze number | (-) |
| $l$ | Distance between the two tapping holes | (m) |
| $\dot{m}_l$ | Liquid mass flux | ($kg/m^2s$) |
| $\dot{m}_g$ | Gas mass flux | ($kg/m^2s$) |
| $\dot{m}_{le}$ | Liquid entrainment mass flux | ($kg/m^2s$) |
| $\dot{m}_{TP}$ | Total two-phase mass flux | ($kg/m^2s$) |
| $N_{\mu_l}$ | Non-dimensional viscosity number | (-) |
| $P$ | Channel perimeter | (m) |
| $P_1$ | Pressure at low side | (Pa) |
| $P_2$ | Pressure at high side | (Pa) |
| $\Delta P$ | Pressure drop | (Pa) |
| $Q_l$ | Liquid volumetric flowrate | ($m^3/s$) |
| R | Reflection coefficient | (-) |
| $Re, Re_{sl}$ | Liquid Reynolds number | (-) |
| $Re_{lf}$ | Liquid film Reynolds number | (-) |
| $Re_{LFC}$ | Critical liquid film Reynolds number | (-) |
| $R_{var}$ | Variable resistance in the anemometer bridge | (ohm) |
| $R_1$ , $R_{int}$ | Internal resistances in the bridge | (ohm) |
| $R_{var}$ | Variable resistance in the anemometer bridge | (ohm) |
| $R$ , $R_w$ | Resistance of the probe at its operating temperature | (ohm) |
| $R_c$ | Resistance of the cable to the hot film probes | (ohm) |
| $R_{ps}$ | Resistance of the probe support | (ohm) |
| $R_{ref}$ | Sensor resistance at reference temperature | (ohm) |
| $T_w$ | Operating temperature | ($^oC$) |
| $T_{ref}$ | Reference temperature | ($^oC$) |
| $T_{acq}$ | Acquisition of actual flow temperature | ($^oC$) |
| $T$ | Period of complete wave cycle | (s) |
| T | Transmission coefficient | (-) |
| $u^*, u_\tau$ | Friction velocity | (m/s) |

| | | |
|---|---|---|
| $U_g^*$ | Wallis parameter | (-) |
| $U_R$ | Slip ratio | (-) |
| $U_{sg}$ | Gas superficial velocity | (m/s) |
| $U_{sl}$ | Liquid superficial velocity | (m/s) |
| $We_F$ | Weber number in equation (2.21) | (-) |
| We | Weber number in equation (2.39 and 2.44) | (-) |
| $We_g''$ | Modified gas Weber number | (-) |
| x | Quality | (-) |
| X | Lockhart Martinelli parameter | (-) |
| V | Volume | ($m^3$) |
| V | Voltage | (V) |
| $Z$ | Acoustic impedance of a medium | ($kg/m^2s$) |

**Greek symbols**

| | | |
|---|---|---|
| $\beta$ | Inclination angle | (deg) |
| $\delta$ | Liquid film thickness | (m) |
| $\delta_l^+$ | Dimensionless liquid film thickness | (-) |
| $\delta_{th}$ | Theoretical liquid film thickness | (m) |
| $\delta_T$ | Thermal boundary layer | (m) |
| $\delta_w$ | Wall thickness | (m) |
| $\epsilon$ | Relative pipe roughness | (m) |
| $\varepsilon_l(0)$ | Parameter defined by equation (2.26) | (-) |
| $\varepsilon_g$ | Gas void fraction | (-) |
| $\varepsilon_{gH}$ | Homogenous void fraction | (-) |
| $\emptyset_l^2$ | Liquid multiplier | (-) |
| $\emptyset_g^2$ | Gas multiplier | (-) |
| $\mu_l$ | Liquid Dynamic viscosity | (kg/ms) |
| $\mu_g$ | Gas Dynamic viscosity | (kg/ms) |
| $\mu_W$ | Water Dynamic viscosity | (kg/ms) |
| $\mu_{TPH}$ | Two-phase homogeneous viscosity | (kg/ms) |
| $v$ | Kinematic viscosity | ($m^2/s$) |
| $\rho_l$ | Liquid density | ($kg/m^3$) |

| | | |
|---|---|---|
| $\rho_g$ | Gas density | (kg/m$^3$) |
| $\rho_W$ | Water density | (kg/m$^3$) |
| $\rho_A$ | Air density | (kg/m$^3$) |
| $\rho_{TPH}$ | Homogeneous density | (kg/m$^3$) |
| σ | Surface tension | (N/m) |
| $\sigma_W$ | Water Surface tension | (N/m) |
| $\tau_o,\ \tau_w$ | Wall shear stress | (Pa, N/m$^2$) |
| $\tau_c$ | Characteristic shear stress | (Pa, N/m$^2$) |
| $\tau_i$ | Interfacial shear stress | (Pa, N/m$^2$) |
| $\lambda$ | Wavelength of ultrasonic signal | (m) |
| $f$ | Wave frequency of ultrasonic signal | (Hz) |
| $\alpha_{ref}$ | Temperature coefficient of resistance at $T_{ref}$ | (1/$^o$C) |
| $\alpha$ | Parameter defined in equation (2.43) | (-) |
| $\alpha$ | Thermal diffusivity of the liquid | (m$^2$/s) |

# ACKNOWLEDGMENTS

First, praise to the God Almighty for his blessings on me which enabled me to complete this thesis on time. I would like to thank Ministry of Higher Education in Oman for their financial support of my study.

My thanks and gratitude is to my supervisors Dr Buddhika Hewakandamby, Dr Nicholas Watson, Dr Georgios Dimitrakis and Professor Barry Azzopardi. Without their constructive comments, excellent support, continuous encouragement and motivation this work would not be completed. I would like to extend my thanks to Dr Abbas Hassan for his guidance and help in the experiments on falling film rig. Also I would like to thank Dr Melvin Holmes and Professor Malcom Povey from Leeds University for their help and support in measurements of silicone oil speed of sound.

I would also like to express my thanks to all technicians in L3 Laboratory (Phil, Mel, Fred, Reg, Alex, Karl, Paul, Mick and Marion) for their help and support during my experimental work.

Many thanks to my friends and colleagues for their support and encouragement during my study, Mustapha, Ibrahim, Rajab, Komonibo, Shara, Joao, Josep, Matthew, Shamal, Zoe and Katerina.

A special thanks and unlimited gratitude to my lovely family; Maryam, Basma, Baraah, Ibrahim, Noor and Basil for their support, encouragement and patience throughout the duration of my study. Many thanks to my family in Oman; my parents, brothers and sisters for their support, prayers and wishing me the best in my study.

# CHAPTER 1

# INTRODUCTION

## 1.1. Introduction

Simultaneous flow of two or more phases in pipes has been observed in a wide range of industries including petroleum production, power generation, chemical manufacturing and processing. This kind of simultaneous flow of two or more phases interacting together is known as multiphase flow. These flows can take many forms among which a liquid flowing in tandem with its vapour in applications such as condensers and reboilers and in pneumatic conveyors where suspended solids flow in an air stream. Moreover in the oil and gas industry, one can observe oil, gas, water and sand flowing together. In addition, industries such as sewage treatment, air conditioning and refrigeration also deal with the multiphase flow. However multiphase flow is not limited only to channel flow systems, it can also be observed in more complex geometries such as stirred vessels, heat exchangers and phase separators (Hewitt, 1978, Azzopardi, 2006).

Measurements of multiphase flow parameters such as flowrate, void fraction, pressure drop and liquid film thickness are crucial in design and control process equipment (Hamad and He, 2010). As an example, accurate measurement of multiphase flowrates helps in well optimisation in the oil and gas industries and defines the life cycle of producing fields. Knowledge of multiphase flow measurement parameters contributes to define the optimum design of equipment

at minimum capital cost, predict operational limits and for diagnosing future operational faults to ensure efficient and safe operation. Therefore, it is essential to know the effects of phase change and its interaction. Also, understanding of multiphase flow will help in selecting the right measurement techniques.

Multiphase flow is a complex phenomenon and many experimental and theoretical studies have been carried out especially on two-phase flow. These studies lead to the formulation of a vast number of equations and correlations to address its behaviour and effect. However, many of these equations and correlations are empirical (Azzopardi, 2006) and there is still a lack of good prediction due to the limitation of the available measurement techniques and hence the lack of accurate experimental data for two-phase flow (Hamad and He, 2010).

In some cases, many of these equations and correlations were purely a fit to experimental data which are valid for the conditions studied. However, there are constants which have been fitted in these correlations based on the experimental data. Their number should be minimised if they cannot be excluded (Azzopardi, 2006).

## 1.2. Motivation

Two-phase flows are the most common in nature as well as in industrial applications (Hewitt and Hall-Taylor, 1970). It is the least understood section of the fluid mechanics due to the complexities of the deforming interfaces and the dynamic dispersity of the phases in each other. Of the flow regimes occur in two-phase flows in industrial applications, annular flow is the most frequently observed two-phase flow pattern (Azzopardi, 2006). Risers in oil platforms, boiler tubes in power generation, and industrial condensers are to name few applications where the annular flow exists. In annular flow, the liquid flows partly as a thin film along the pipe wall and partly as droplets entrained in the turbulent gas core. Information about its characteristics such as liquid film behaviour and frictional pressure drop is important. Knowledge of the liquid film thickness is necessary to avoid dry-out situations where the liquid film is completely removed from contact with the channel's wall (Hewitt and Hall-Taylor, 1970). Frictional pressure drop information is useful because it is related to the energy required to drive the two-phase flow system where knowledge about shear stress plays a dominant role (Hewitt and Hall-Taylor, 1970, Alekseenko et al., 1994, Azzopardi, 2006).

Film interface is associated with large disturbance waves which play a big role in the amount of droplet entrainment, shear stress at the interface and heat transfer in annular flow. Therefore, measuring the film thickness and shear stress simultaneously will help to understand the effects of the disturbance wave and

develop a model to predict the structure of the interfacial area (Hewitt, 1978, Hagiwara. Y, 1988, Govan et al., 1989, Azzopardi, 2006, Ayaz et al., 2013).

As discussed above, the disturbance waves are considered as the main source of droplet entrainment in the gas core. This droplet entrainment contributes to the pressure drop and affects the film thickness (Hewitt and Hall-Taylor, 1970 and Azzopardi, 2006). In addition, the disturbance waves affect the interfacial shear stress and hence the wall shear stress. There are many investigations that have been performed in annular flow using an air/water system to understand the relationship between liquid film thickness, pressure drop and wall shear stress. These studies include Martin (1983), Owen (1986), Wolf (1995) in a small pipe diameter (32mm) and Zangana (2011) in a large pipe diameter (127mm). However, this relationship has not yet been examined with liquids other than water. Therefore, it is important to examine this relationship with other liquids.

Most of the correlations in use to predict pressure drop, film thickness and wall shear stress were developed using water as the liquid phase and steam or air as the gas phase in gas-liquid two-phase flow systems. For this particular reason, these correlations need to be tested through measurements of various flows where the physical properties are different from water.

Several measurement techniques were developed over the past decades for measuring film thickness and wall shear stress. Most of these measurements were developed using an air/water system as will be discussed in Chapter 2. The advantages and limitations of those techniques have been reviewed by different researchers and can be found in the literature including Winter (1977),

Alekseenko et al. (1994), Hanratty and Campbell (1996), Clark (2002) and Naughton and Sheplak (2002). Finding one measurement technique which can completely satisfy all the specified requirements is a difficult task. In addition, the application and requirement of one technique might not be the same for the other technique which makes it difficult to combine two techniques in the same geometry (Clark, 2002). In the current study, the silicone oil was used as a liquid phase. Accurate measurement of these parameters is important and finding techniques that can be used with silicone oil are one of the main challenges in the current study.

## 1.3. Aims

From the discussion in Section 1.2, the aim of the current study can be summarised as following:

- Investigate and understand the relationship between the pressure drop, film thickness and wall shear stress on upward annular flow using an air/silicone oil system.
- Test existing correlations to predict the pressure drop, film thickness and wall shear stress using an air/silicone oil system.

The experiments were conducted on a vertical test facility with 34.5mm inner diameter (ID) where more detail and description is available in Chapter 3. Different gas and liquid flow rates were studied using air/water and air/silicone oil systems.

## 1.4. Objectives

The objectives of this research are to concentrate on:

- Develop or test available measurement techniques of film thickness and wall shear stress that can be used simultaneously using an air/silicone oil system.
- Obtain experimental data using an air/water annular flow in order to investigate the effect of liquid and gas superficial velocity and the relationship between wall shear stress, film thickness and pressure drop.
- Obtain experimental data using an air/silicone oil annular flow and compare them with the air/water results in order to investigate the effect of liquid and gas superficial velocity and the relationship between wall shear stress, film thickness and pressure drop.
- Assess the existing correlations of pressure drop, film thickness and wall shear stress against collected experimental data.

## 1.5. Thesis Outline

This thesis is divided into seven main Chapters:

**Chapter one** provides a general introduction about multiphase flow and information about the motivation, aim and objective of this study.

**Chapter two** contains information about two-phase flow pattern and their maps. In separate sections, film thickness and wall shear stress measuring techniques

are evaluated and their applicability to be used with an air/silicone oil system is assessed.

**Chapter three** describes the experiment test facilities and the instrumentation with their calibration.

**Chapters four, five and six** presents the results about the pressure drop, film thickness and wall shear stress using air/water and air/silicone oil systems. In each chapter, the effect of gas and liquid superficial velocity, viscosity and surface tension are discussed. In addition, the results of each parameter were used to test the available correlations to predict each of them. In chapter five, development of an ultrasonic pulse echo technique to measure the liquid film thickness is also discussed. The validation process of the ultrasonic using static and dynamic film is presented.

**Chapter seven** outlines the conclusions and recommendation for future work.

# CHAPTER 2

# LITERATURE REVIEW

## 2.1. Gas-Liquid Two-phase Flow

### 2.1.1. Flow Patterns of Gas-Liquid Flow

Simultaneous flow of gas and liquid in a pipe is the most common multiphase flow combination that can be found in industry. As a result, there is a large volume of research that has been carried out to study the complex behaviour of such flows. The complexity arises not only from the presence of two distinct phases but also from the discontinuous nature and the instance of the continuously deforming interface. This deforming interface and the distribution of the phases lead to distinct flow patterns, generally known as 'flow regimes'. The flow of the two phases simultaneously would lead to the establishment of a periodically measuring flow structure (regimes) and would transform into another depending on the geometry of the pipe arrangement and flow rates variations (Levy, 1999). An example of different pipe geometries which can be found in an offshore oil and gas facility is shown in Figure 2.1.

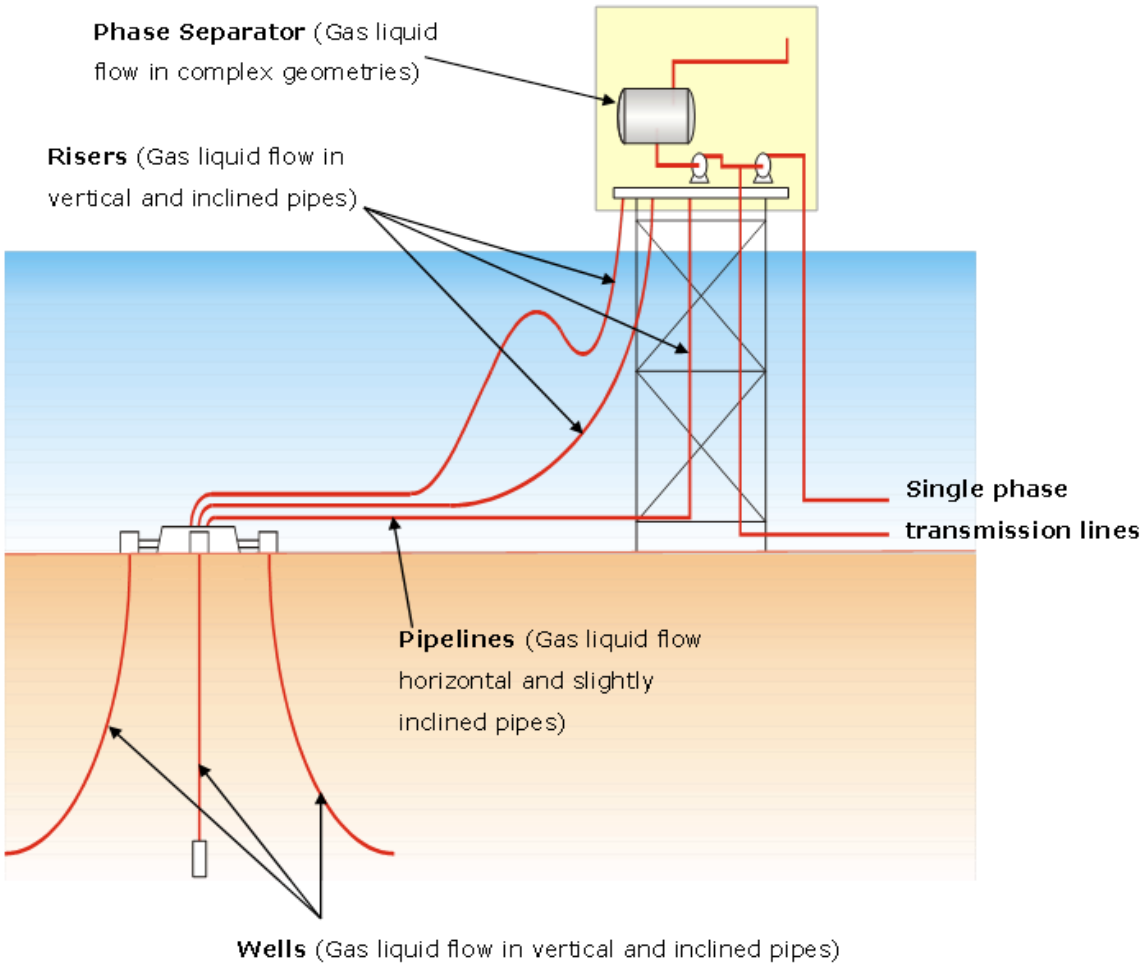


Figure 2.1: Schematic of an offshore oil and gas facility with different pipe geometries (Azzopardi, 2006)

Figure 2.2 and Figure 2.3 illustrated the typical flow regimes for vertical and horizontal gas-liquid flow.

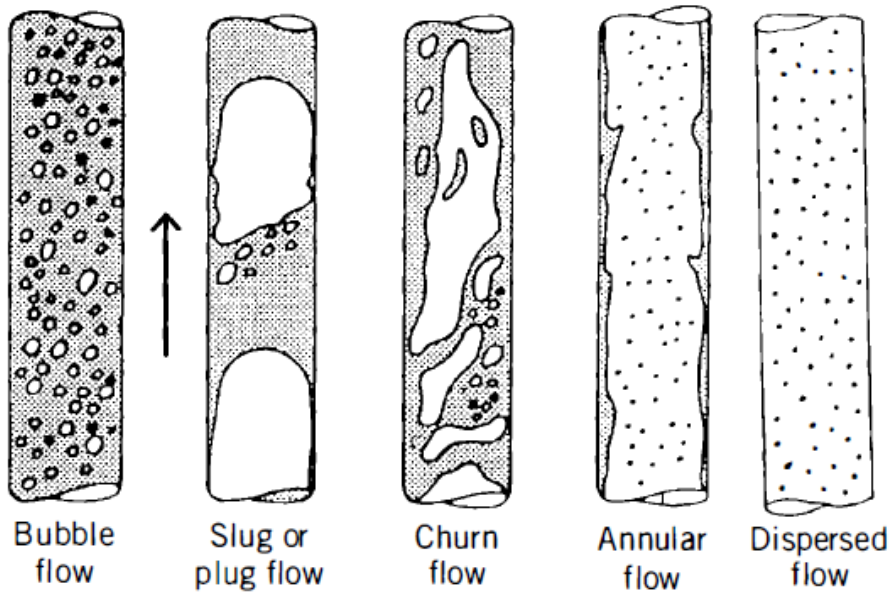


Figure 2.2: Flow Pattern in Vertical Flow Direction (Levy, 1999)

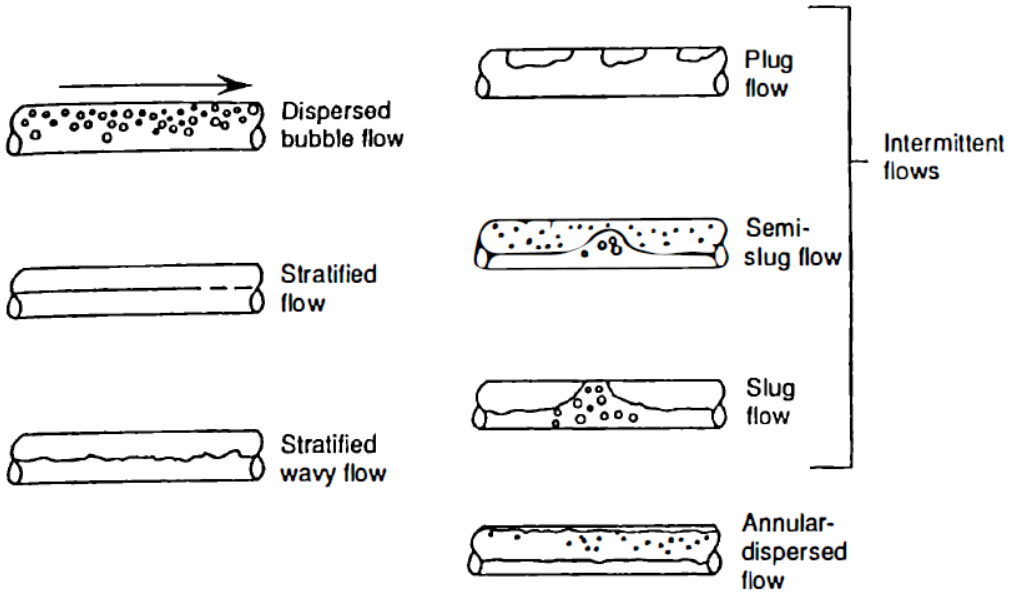


Figure 2.3: Flow Pattern in Horizontal Flow Direction (Levy, 1999)

A brief description of these flow regimes is given below where for more detail description refer to Hewitt and Hall-Taylor (1970), Alekseenko et al. (1994) and Azzopardi (2006). In vertical gas-liquid flow, when the gas flow rates change with a constant liquid flow rate, different flow regimes can be observed as shown in Figure 2.2. At low gas flow rates, bubble flow regime exists where gas bubbles of different shape and size are dispersed and uniformly distributed in the liquid phase. When the gas flow rate increases, bubbles starts to coalesce and form large bullet-shaped bubble equivalent to pipe diameter with a thin liquid film surrounding it known as Taylor bubbles. This flow regime called slug flow in which Taylor bubble is separated by slugs of liquid contains a dispersion of small bubbles. The transition from bubble to slug takes place at void fraction around 0.25 to 0.3 as suggested by Taitel et al. (1980). The Taylor bubbles in the slug flow break into an unstable pattern with a further increase in the gas flow rate. This makes the liquid oscillate up and down in the tube forming the churn/froth flow regime. Cheng et al. (1998) and Ohnuki and Akimoto (2000) indicated that slug flow pattern doesn't occur in larger diameter pipes (0.15 - 0.2 m) where there is a direct transition from bubble to churn. Then, annular flow regime occurs when the gas flow rate is high enough to make the liquid flows partly upwards as a thin film along the pipe wall and partly as droplets entrained in the turbulent gas core. Increasing the gas flow rate further makes the liquid to be dispersed as drops in the gas and the gas occupied most of the cross-sectional area. This flow regime is known as dispersed flow.

The regimes in the horizontal gas-liquid flow have a similar pattern to that in vertical flow except stratified flow is present in which separation of the two phases occurs. However, for horizontal flow, the gas phase occupies the upper part and the liquid phase will be displaced towards the bottom of the channel due to gravitational forces acting on it.

Visual inspection is usually used to identify the flow patterns. However, when visual access is difficult, the flow patterns are recognised by analysis of pressure gradient, void fraction or combination of the void fraction and probability density function (PDF) (Omebere-Iyari and Azzopardi, 2007). Figure 2.4 illustrates the study by Costigan and Whalley (1997) using the void fraction and probability density function (PDF) technique for flow pattern analysis.

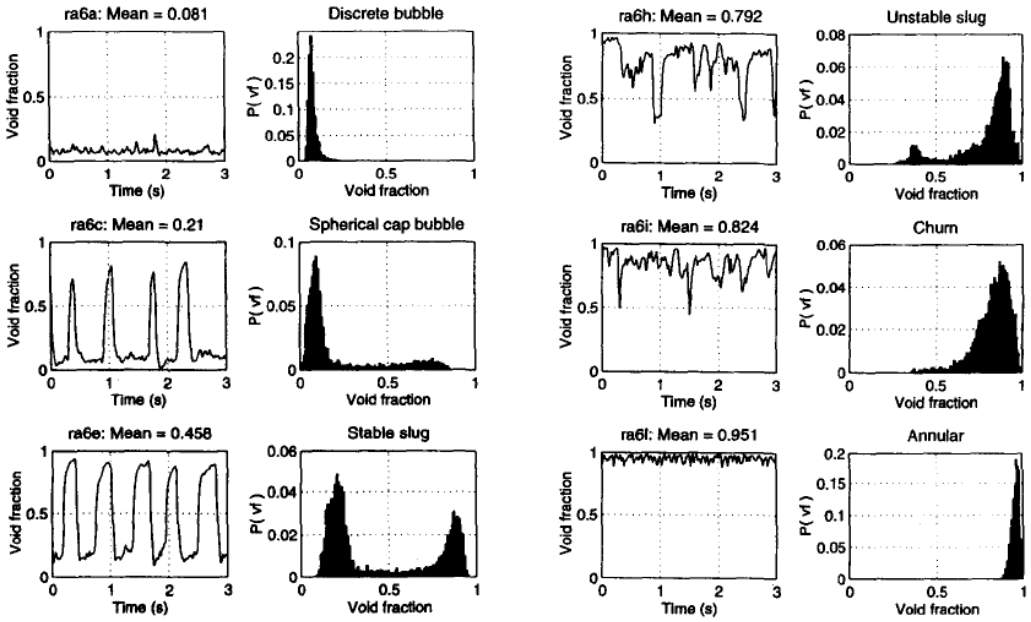


Figure 2.4: Void fraction traces with their probability density function (PDF) Costigan and Whalley (1997).

### 2.1.2. Flow Patterns Map

In order to obtain accurate data, it is crucial to select the right correlation and measurement technique. Therefore, understanding and determining which flow regime is present in a given section of pipeline is important. Additionally, knowledge about the flowing conditions at which each flow regime will happen is necessary which can be achieved by having flow pattern map that can be used as a common predicting method suitable for different process flowing conditions, properties and geometries.

The flow pattern map represents the observation of flow patterns where the transitional boundary between each of them is plotted on a two-dimensional log-log axes graph. However, there is no common flow pattern map because flow pattern maps tend to be created from experimental observation and not from fluid mechanics theory (Levy, 1999). It is clearly noticed the difference in the available flow pattern maps in the literature. Several flow pattern maps are structured using superficial velocity or momentum flux of the respective phases or dimensionless groups, such as the Froude number and the Reynolds number. There is no set rule to what parameters the axis of such map should be used. On the other hand, there is no clear distinction when the transition will happen between two flow regimes. As an example, if a flow condition is close to any border on a flow pattern map, then this indicates that the flow pattern at that point is likely to be transitional between the two flow patterns exist either side of the boundary line. The most popular flow map for vertical flow is the one produced by Hewitt and Roberts (1969) as shown in Figure 2.5. In this map, the various flow patterns are plotted in terms of the momentum fluxes which are the

product of the square of the superficial velocity and the phase density of the respective phases.

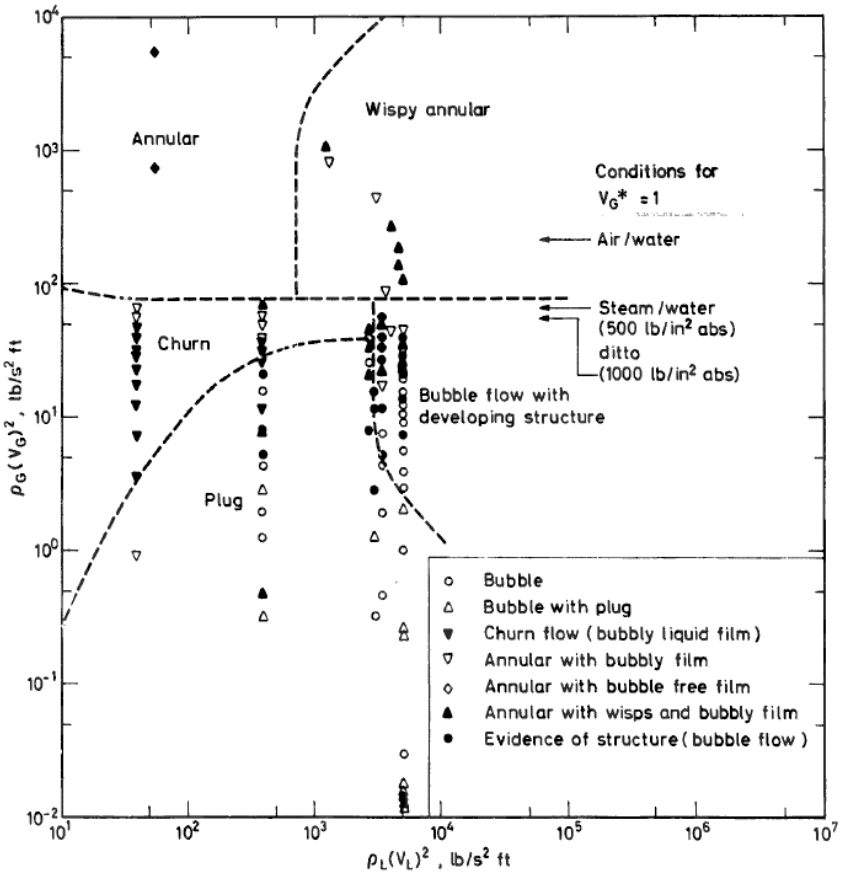


Figure 2.5: Vertical upward flow pattern map (Hewitt and Roberts, 1969)

In contrast, the most widely known flow map for horizontal flow is the one plotted by Baker (1954) which is based on industrial data. The Baker map was modified by (Scott, 1963) where transition zones were added as shown in Figure 2.6. In this map, the $G_L$ and $G_G$ are the mass fluxes of the liquid and gas phases respectively and the parameters $\lambda_B = \left[\left(\frac{\rho_G}{\rho_A}\right)\left(\frac{\rho_L}{\rho_W}\right)\right]^{0.5}$ and $\psi_B = \left(\frac{\sigma_W}{\sigma}\right)\left[\frac{\mu_L}{\mu_W}\left(\frac{\rho_W}{\rho_L}\right)^2\right]^{\frac{1}{3}}$ represent correction factors for fluid physical

properties in which $\rho$ is the density, σ is the surface tension, $\mu$ is viscosity and subscripts G, L, A and W refer to the corresponding values for gas, liquid, air and water at atmospheric pressure.

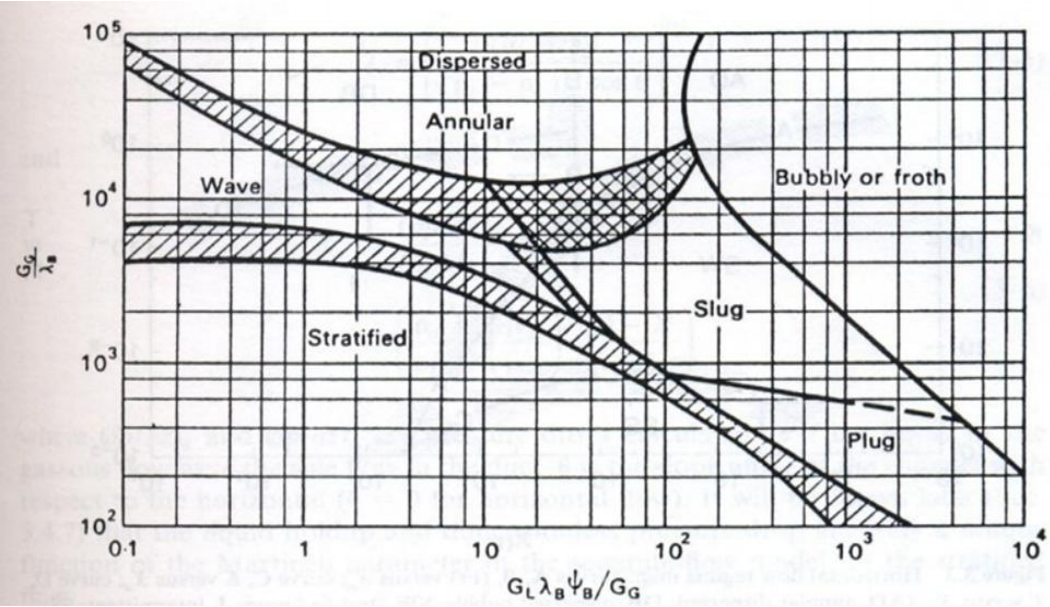


Figure 2.6: Horizontal flow pattern map for (Scott (1963))

There is a poor agreement between existing flow pattern maps as shown in Figure 2.7 which illustrates the poor agreement in churn to annular flow boundary proposed by Sekoguchi and Mori (1997) plotted in a dimensional version of the flow pattern map from Hewitt and Roberts (1969) as reported by Van der Meulen (2012).

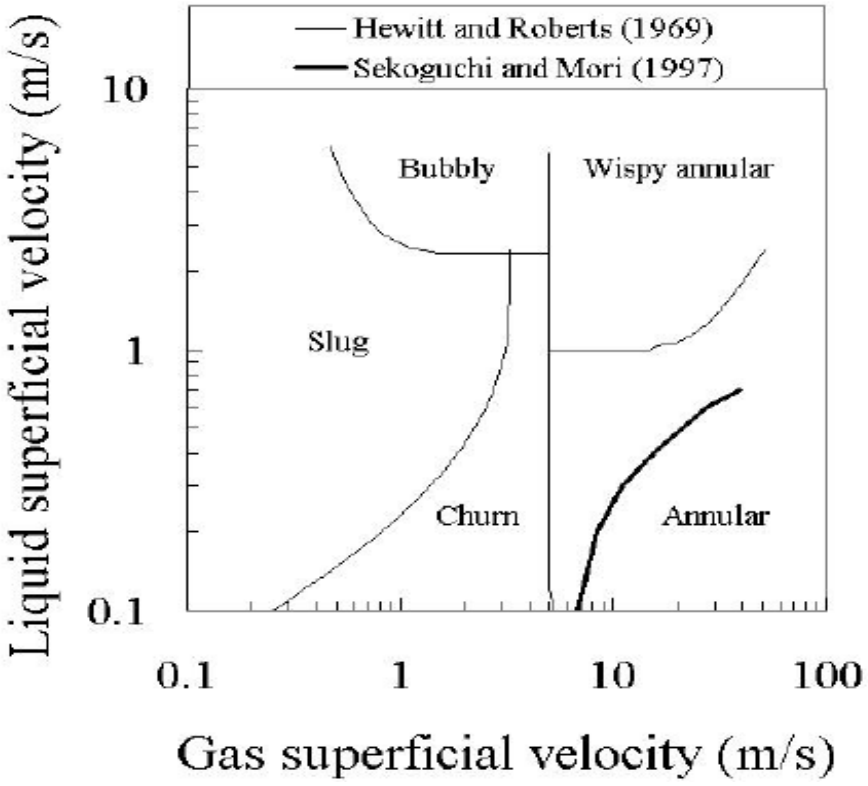


Figure 2.7: Different flow pattern transitions to annular flow. (Van der Meulen, 2012)

### 2.1.3. Flow Model

There is no one common mathematical expression or empirical correlation that could adequately address the many existing variations of each flow regime. Each flow regime has its model and correlation which is only suitable for that regime and valid in the range of the condition studied. Therefore, there are several models that have been developed within a single flow pattern and it can be hard to choose between them as they might not be valid for the condition intend to study. Each model depends on flow rate, pressure drop, gas volume fraction and fluid properties (Density, viscosity) (Hewitt and Hall-Taylor, 1970, Levy, 1999, Azzopardi, 2006).

## 2.2. Pressure drop

Pressure drop is one of the important parameter in equipment and pipeline design. It governs the pumping requirement to move the fluids through pipelines. In addition, the relationship between the flow rate and pressure drop is important to determine heat or mass transfer coefficients. The great importance of pressure drop prediction is reflected in the large number of models and correlations in the literature (Hewitt, 1982, Azzopardi, 2006). Two-phase pressure drop can be calculated using homogenous flow model and separated flow model. In the separated flow model, the frictional pressure drop can be calculated using Chisholm (1967), Friedel (1979) and Beggs and Brill (1973) correlations. Both models are derived from the momentum balance of flow through the element of channel with constant cross-sectional area. The total two-phase pressure drop $\left(\frac{\mathrm{dp}}{\mathrm{dz}}\right)_{\mathrm{TP}}$ is calculated from the sum of frictional pressure drop,$\left(\frac{\mathrm{dp}}{\mathrm{dz}}\right)_{\mathrm{f}}$, gravitational pressure drop $\left(\frac{\mathrm{dp}}{\mathrm{dz}}\right)_{\mathrm{g}}$ and accelelaration pressure drop $\left(\frac{\mathrm{dp}}{\mathrm{dz}}\right)_{\mathrm{acc}}$ as per below equation:

$$-\left(\frac{\mathrm{dp}}{\mathrm{dz}}\right)_{\mathrm{TP}} = -\left(\frac{\mathrm{dp}}{\mathrm{dz}}\right)_{\mathrm{f}} - \left(\frac{\mathrm{dp}}{\mathrm{dz}}\right)_{\mathrm{g}} - \left(\frac{\mathrm{dp}}{\mathrm{dz}}\right)_{\mathrm{acc}} \tag{2.1}$$

In the current study, the acceleration pressure drop is negligible because it is assumed that the system is fully developed and at equilibrium. Therefore, it will not be considered in the following discussion. More details about pressure drop can be found in different text book including Hewitt and Hall-Taylor (1970), Hewitt (1982), Azzopardi (2006) and Hanratty (2013).

### 2.2.1. Homogenous flow model

The homogenous flow model treats the two-phase flow as a single phase flow where both gas and liquid are assumed travelling at the same velocity. All the properties of the two-phase flow are considered as homogeneously mixed where the average is calculated. The total pressure drop can be calculated using the following expression:

$$-\left(\frac{dp}{dz}\right)_{TP} = -\left(\frac{dp}{dz}\right)_{f} - \left(\frac{dp}{dz}\right)_{g} \tag{2.2}$$

$$-\left(\frac{dp}{dz}\right)_{f} = \tau_o \frac{P}{A} = \frac{4f_{TP}}{D}\frac{\dot{m}_{TP}^2}{2\rho_{TPH}} \tag{2.3}$$

$$-\left(\frac{dp}{dz}\right)_{g} = g\rho_{TPH} \tag{2.4}$$

where $\tau_o$ is wall shear stress, P is the channel perimeter, A is the cross-sectional area, $f_{TP}$ is the two-phase friction factor, $\dot{m}_{TP}$ is the total mass flux of both phases, D is the pipe internal diameter, $\rho_{TPH}$ is the homogeneous two-phase density and g is the gravitational acceleration.

The homogeneous two-phase density ($\rho_{TPH}$) is given by the following equation:

$$\frac{1}{\rho_{TPH}} = \frac{x}{\rho_g} + \frac{(1-x)}{\rho_l} \tag{2.5}$$

where x is the quality which is defined as the mass flux of the gas phase ($\dot{m}_g$) divided by the total mass flux of both phases as shown in equation (2.6):

$$x = \frac{\dot{m}_g}{\dot{m}_g + \dot{m}_l} \tag{2.6}$$

The two phase friction factor ($f_{TP}$) is calculated using a single phase correlation allowing for pipe roughness (e/D) where the single phase Reynolds number is replaced with the two phase Reynolds number ($Re_{TPH}$) which is:

$$Re_{TPH} = \frac{\dot{m}_{TP} D}{\mu_{TPH}} \tag{2.7}$$

where $\mu_{TPH}$ is the two-phase homogenous viscosity and is calculated by the following equation as suggested by Cicchitti et al. (1960):

$$\mu_{TPH} = \mu_g x + \mu_l (1 - x) \tag{2.8}$$

## 2.2.2. Separated flow model

The separated flow model treats the two-phase flow as a two separated single phase flow where there is no interaction between them. The total pressure drop can be calculated using the following expression:

$$-\left(\frac{dp}{dz}\right)_{TP} = -\left(\frac{dp}{dz}\right)_f - \left(\frac{dp}{dz}\right)_g \tag{2.2}$$

$$-\left(\frac{dp}{dz}\right)_f = \tau_o \frac{P}{A} = \frac{4f_l}{D} \frac{\dot{m}_{TP}^2}{2\rho_l} \emptyset_l^2 \tag{2.9}$$

$$-\left(\frac{dp}{dz}\right)_g = g\left[\varepsilon_g \rho_g + (1 - \varepsilon_g)\rho_l\right] \tag{2.10}$$

where $f_l$ is the liquid friction factor, $\emptyset_l^2$ is the liquid multiplier factor and $\varepsilon_g$ is the gas void fraction.

The gas void fraction ($\varepsilon_g$) is given by the following equation:

$$\varepsilon_g = \frac{1}{1+U_R\frac{(1-x)\rho_g}{x\rho_l}} \tag{2.11}$$

where $U_R$ is known as the slip velocity ratio which can be calculated using the correlation suggested by Chisholm (1972):

$$U_R = \left[1 - x\left(1 - \frac{\rho_l}{\rho_g}\right)\right]^{0.5} \tag{2.12}$$

The frictional pressure drop can be calculated using Chisholm (1967), Friedel (1979) and Beggs and Brill (1973) correlations. These correlations treated the two-phase flow as all flow as liquid where liquid multiplier factor ($\emptyset_l^2$) is used in equation (2.9) (Azzopardi, 2006).

**<u>Chisholm (1967) correlation:</u>**

Lockhart and Martinelli (1949) defined the liquid and gas multiplier factors using the following expression:

$$\left(\frac{dp}{dz}\right)_f = \emptyset_l^2\left(\frac{dp}{dz}\right)_l = \emptyset_g^2\left(\frac{dp}{dz}\right)_g \tag{2.13}$$

where $\left(\frac{dp}{dz}\right)_l$ and $\left(\frac{dp}{dz}\right)_g$ are the pressure drops for the liquid phase and gas phase flowing alone.

They related these parameters with a parameter $X^2$ which is defined as:

$$X^2 = \frac{\left(\frac{dp}{dz}\right)_l}{\left(\frac{dp}{dz}\right)_g} \tag{2.14}$$

This relationship is presented in graphical form as shown in Figure 2.8. Lockhart and Martinelli (1949) suggested four groups depending on whether the phase alone flows were laminar (viscous) or turbulent. These groups are shown in Figure 2.8 for each phase as vv, vt, tv and tt where v=viscous and t= turbulent.

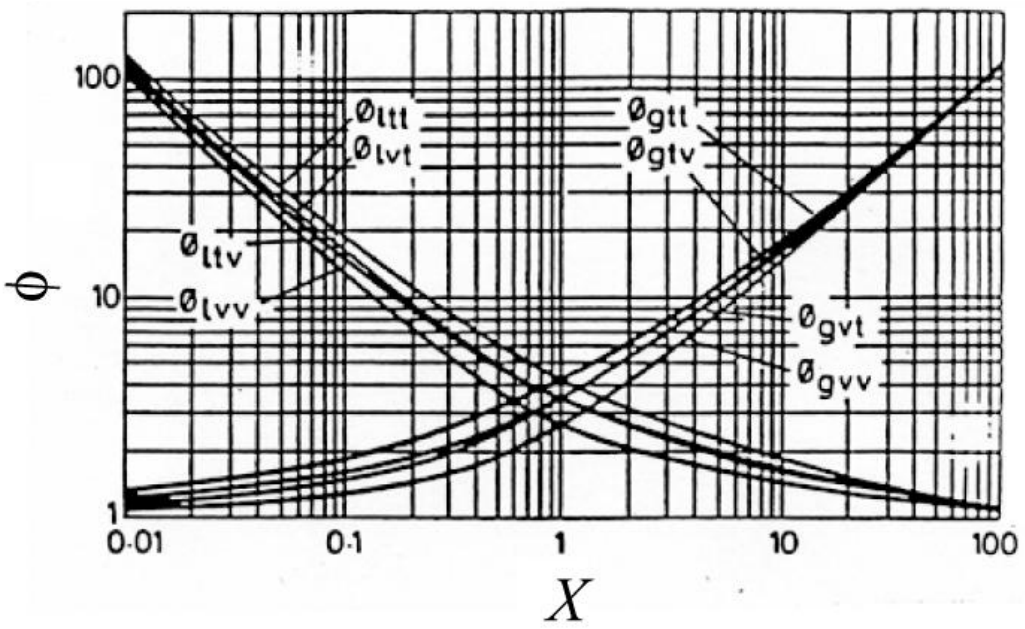


Figure 2.8: Lockhart and Martinelli (1949) parameters relationship for pressure drop multiplier.

Chisholm (1967) represented this graphical form by an analytical form as following:

$$\emptyset_l^2 = 1 + \frac{C}{X} + \frac{1}{X^2} \tag{2.15}$$

$$\emptyset_g^2 = 1 + CX + X^2 \tag{2.16}$$

where C is a constant which depends on the nature of the phase alone flows.

The value of C as suggested by Chisholm (1967) are shown in Table 2.1:

| Liquid | Gas | Subscript | C |
|---|---|---|---|
| Turbulent | Turbulent | tt | 20 |
| Viscous | Turbulent | vt | 12 |
| Turbulent | Viscous | tv | 10 |
| Viscous | Viscous | vv | 5 |

Table 2.1: The value of C as suggested by Chisholm (1967).

**Friedel (1979) Correlation:**

Friedel (1979) proposed a correlation to calculate the liquid multiplier only for the frictional pressure as follow:

$$\emptyset_{lo}^2 = A_1 + A_2 \tag{2.17}$$

$$A_1 = (1-x)^2 + x^2\left(\frac{\rho_l}{\rho_g}\right)\left(\frac{f_{go}}{f_{lo}}\right) \tag{2.18}$$

$$A_2 = \frac{3.24x^{0.78}(1-x)^{0.224}\left(\frac{\rho_l}{\rho_g}\right)^{0.91}\left(\frac{\mu_g}{\mu_l}\right)^{0.19}\left(1-\frac{\mu_g}{\mu_l}\right)^{0.7}}{Fr_F^{0.045}We_F^{0.035}} \tag{2.19}$$

$$Fr_F = \frac{\dot{m}_{TP}^2}{\rho_{TPH}^2 gD} \tag{2.20}$$

$$We_F = \frac{\dot{m}_{TP}^2 D}{\rho_{TPH}\sigma} \tag{2.21}$$

This correlation is for horizontal and vertical upward flow. $f_{go}$ and $f_{lo}$ are the single phase friction if all the flow were liquid or gas respectively.

**Beggs and Brill (1973) correlation:**

Beggs and Brill (1973) proposed a correlation to calculate the frictional pressure drop that can be used for different pipe orientation. The frictional pressure drop can be calculated using the following expression:

$$\left(\frac{dp}{dz}\right)_f = \frac{0.5 f_{TP} \dot{m}_{TP} (u_{gs} + u_{ls})}{D} \quad (2.22)$$

$$f_{TP} = f_l \exp(S) \quad (2.23)$$

$$S = \frac{\ln(y)}{(-0.0523 + 3.182 \ln(y) - 0.8725 [\ln(y)]^2 + 0.01853 [\ln(y)]^4)} \quad (2.24)$$

outside the interval $1.0 < y < 1.2$

$$S = \ln(2.2y - 1.2) \quad (2.25)$$

within $1.0 < y < 1.2$

$$y = \frac{(1 - \varepsilon_{gH})}{(1 - \varepsilon_g)^2} \quad (2.26)$$

$$\varepsilon_g = 1 - \varepsilon_l(0)[1 - C_{B4} \sin(1.8\beta) - 0.333 \sin^3(1.8\beta)] \quad (2.27)$$

$$\varepsilon_l(0) = \frac{C_{B1} (1 - \varepsilon_{gH})^{C_{B2}}}{Fr_{BB}^{C_{B3}}} \quad (2.28)$$

$$Fr_{BB} = \frac{(u_{gs} - u_{ls})^2}{gD} \quad (2.29)$$

The constants $C_{B1}$ to $C_{B4}$ are given in Table 2.2:

| Constant | $Fr_{BB} < L_1$ | $Fr_{BB} > L_1$ and $L_2$ | $L_1 < Fr_{BB} < L_2$ |
|---|---|---|---|
| $C_{B1}$ | 0.98 | 1.065 | 0.845 |
| $C_{B2}$ | 0.4846 | 0.5824 | 0.5351 |
| $C_{B3}$ | 0.0868 | 0.0609 | 0.0172 |
| $C_{B4}$ (up flow) | Eq (2.31) | 0 | Eq (2.30) |
| $C_{B4}$ (down flow) | Eq (2.32) | Eq (2.32) | Eq (2.32) |

Table 2.2: Constants for Beggs and Brill (1973) correlation.

$$C_{B4} = \varepsilon_{gH} \ln\left[\frac{2.96\left(1-\varepsilon_{gH}\right)^{0.305} N_{lv}^{0.0978}}{Fr_{BB}^{0.4473}}\right] \quad (2.30)$$

$$C_{B4} = \varepsilon_{gH} \ln\left[\frac{0.011 N_{lv}^{3.539}}{\left(1-\varepsilon_{gH}\right)^{3.768} Fr_{BB}^{1.614}}\right] \quad (2.31)$$

$$C_{B4} = \varepsilon_{gH} \ln\left[\frac{4.7 N_{lv}^{0.1244}}{\left(1-\varepsilon_{gH}\right)^{0.3692} Fr_{BB}^{0.5056}}\right] \quad (2.32)$$

$$N_{lv} = u_{ls}\left(\frac{\rho_l}{g\sigma}\right)^{0.25} \quad (2.33)$$

$$L_1 = \exp\left(-4.62 - 3.757X_b - 0.481X_b^2 - 0.0207X_b^3\right) \quad (2.34)$$

$$L_2 = \exp\left(1.061 - 4.602X_b - 1.609X_b^2 - 0.179X_b^3 + 0.000635X_b^5\right) \quad (2.35)$$

$$X_b = \ln\left(1 - \varepsilon_{gH}\right) \quad (2.36)$$

The $\varepsilon_{gH}$ is the homogenous void fraction that can be calculated using equation (2.11) at $U_R$=1.

## 2.3. Entrainment

In annular two-phase flow, part of the liquid film is entrained as small droplets in the gas core. This mechanism is known as droplet entrainment or entrainment fraction. The entrainment fraction ($E_f$) is defined as the ratio between the liquid entrainment mass flux ($\dot{m}_{le}$) and the total liquid mass flux ($\dot{m}_l$) as per the following expression (Azzopardi, 2006):

$$E_f = \frac{\dot{m}_{le}}{\dot{m}_l} \tag{2.37}$$

The liquid film is associated with disturbance waves which are the main source of droplet entrainment (Azzopardi, 1997, Barbosa et al., 2002). There are two mechanisms by which the droplets are torn from the waves reported in the literature. These two mechanisms were identified by Azzopardi (1983) which are bag break-up and ligament break-up as shown in Figure 2.9. The bag break-up occurred at low gas and liquid flow rates where ligament break-up occurred at high gas and liquid flow rates. More detail about these mechanisms and how they happened can be found in Azzopardi (1997) and Azzopardi (2006). Pan and Hanratty (2002) reported that the entrainment fraction increased by increasing the gas and liquid flow rates, pipe diameter and gas density and by decreasing the surface tension. On the other hand, the liquid is deposited back into the liquid film which is known as droplet deposition. At the equilibrium condition at which the rate of entrainment is equal to the rate of deposition, the droplet entrainment in the gas core becomes steady. The interchange between the entrainment and deposition is account for 20% of the pressure gradient according to Fore and Dukler (1995) and this was supported by Pan et al. (2015b) who indicated that it is account for 14.5% of the pressure gradient.

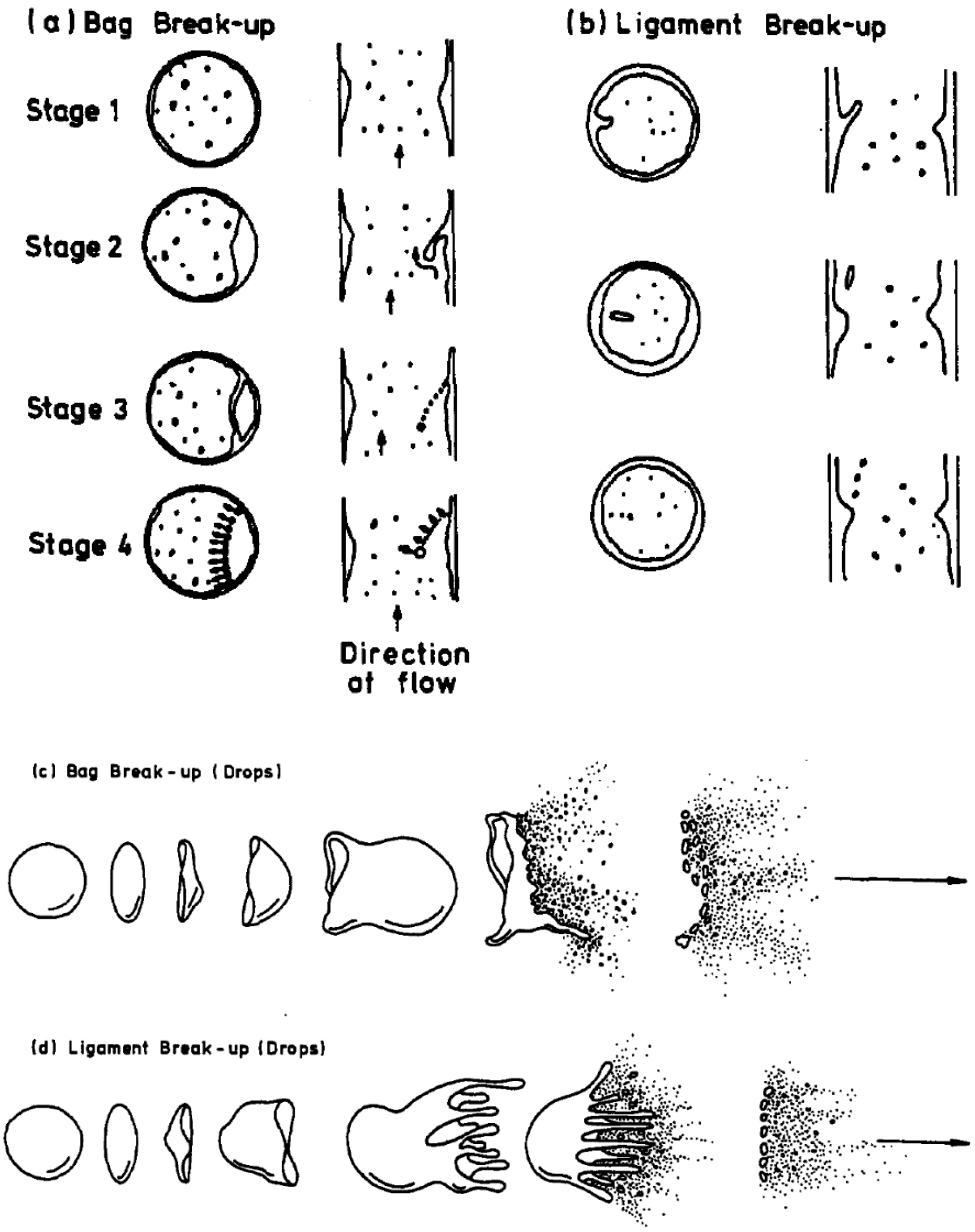


Figure 2.9: Entrainment Mechanisms - Bag break-up and Ligament break-up

(Azzopardi, 1997)

### 2.3.1. Entrainment Prediction Correlations

Predicting the entrainment fraction is important for estimating the pressure drop, flow rate, liquid holdup and dry-out in annular flow (Sawant et al., 2008, Al-Sarkhi et al., 2012). Due to the difficulty of measuring the entrainment rate, many correlations were developed from the available measured entrainment data in the literature to predict the entrainment fraction (Magrini et al., 2012). The most popular correlations for vertical annular two-phase flow include Oliemans et al. (1986), Ishii and Mishima (1989), Sawant et al. (2008) and recently Al-Sarkhi et al. (2012). In the current study, all these correlations were compared to find the correlation which can be used for predicting entrainment fraction of air/water and air/silicone oil systems as discussed in Chapter 4. The Al-Sarkhi et al. (2012) correlation was selected as it showed an improvement in the predicting entrainment compared to Sawant et al. (2008) correlation when compared with available entrainment measured data as shown by Al-Sarkhi et al. (2012) . A brief description about each of these correlations is given below:

**Oliemans et al. (1986) correlation**

Harwell databank was used by Oliemans et al. (1986) to correlate the entrainment fraction. This data includes air/water, air/ethanol and water/steam systems. The entrainment fraction ($E_f$) is correlated by the following expression:

$$\frac{E_f}{(1-E_f)} = 10^{-2.52}\rho_l^{1.08}\rho_g^{0.8}\mu_l^{0.27}\mu_g^{0.28}\sigma^{-1.8}D^{1.72}U_{sl}^{0.7}U_{sg}^{1.44}g^{0.46} \quad (2.38)$$

where $\rho_l$ and $\rho_g$ are the liquid and gas densities, $\mu_l$ and $\mu_g$ are the liquid and gas viscosities, $\sigma$ is the surface tension, D is the pipe internal diameter, $U_{sg}$ and $U_{sl}$ are the gas and liquid superficial velocities and g is gravitational acceleration.

**Ishii and Mishima (1989) correlation**

The correlation of Ishii and Mishima (1989) was developed based on force balance between the interfacial shear force and surface tension force. The droplet entrainment would occur when the retaining force of surface tension is exceeded by the interfacial shear force exerted by the gas flow. The correlation consists of two dimensionless numbers which are a modified gas Weber number (We) and a liquid Reynolds number ($Re_{sl}$). The correlation was developed from the database of air/water system. The entrainment fraction ($E_f$) can be calculated from the following form:

$$E_f = \tanh\left[7.25 \times 10^{-7} We^{1.25} Re_{sl}^{0.25}\right] \quad (2.39)$$

$$We = \frac{\rho_g U_{sg}^2 D}{\sigma}\left(\frac{\rho_l - \rho_g}{\rho_g}\right)^{1/3} \quad (2.40)$$

$$Re_{sl} = \frac{\rho_l U_{sl} D}{\mu_l} \quad (2.41)$$

**Sawant et al. (2008) correlation**

Sawant et al. (2008) correlation was developed on a similar basis as Ishii and Mishima (1989) correlation where both modified gas Weber number (We) and a liquid Reynolds number (Re) are used. However, the power of the density ratio in the modified gas Weber number (We) was (1/4) instead of (1/3) to incorporate

the pressure effect. It was verified using experimental data of air/water system. The entrainment fraction ($E_f$) is given by the following expression:

$$E_f = E_{max}\tanh[\alpha We^{1.25}] \quad (2.42)$$

$$E_{max} = 1 - \frac{Re_{sl,lim}}{Re_{sl}} \quad (2.43)$$

$$\alpha = 2.31 \times 10^{-4} Re_{sl}^{-0.35} \quad (2.44)$$

$$We = \frac{\rho_g U_{sg}^2 D}{\sigma}\left(\frac{\rho_l - \rho_g}{\rho_g}\right)^{1/4} \quad (2.45)$$

$$Re_{sl,lim} = 250\ln(Re_{sl}) - 1265 \quad (2.46)$$

$$Re_{sl} = \frac{\rho_l U_{sl} D}{\mu_l} \quad (2.47)$$

**Al-Sarkhi et al. (2012) correlation**

The Al-Sarkhi et al. (2012) correlation used the same correlation of Sawant et al. (2008). However, they have used different equation for calculating the maximum entrainment fraction derived from experimental data of air/water system.

$$E_{max} = E_{max\,lim}\left[1 - \exp\left(-\left(\frac{Re_{sl}}{1400}\right)^{0.6}\right)\right] \quad (2.48)$$

where

$E_{max\,lim}$ is the maximum entrainment fraction which is equal to one.

## 2.4. Liquid Film Thickness Measurement

The film in the annular flow is driven by the interfacial shear imparted by the gas flow and this coupling of momentum between the two phases lead to various interfacial behaviours. While there are capillary waves propagating on the film, large coherent waves (in pipes with small diameters) travel on the film at a much larger speed intermittently. Though intermittent, these waves seem to have somewhat regular periodicity for a given liquid and gas flow rates (Thwaites et al., 1976, Azzopardi, 1997, Azzopardi, 2006). These highly dynamic, complex interfacial phenomena which are dependent on the gas and liquid flow rates and the physical properties of the two phases present one of the greatest challenges in developing theoretical models describing the hydrodynamics of the film fully (Thwaites et al., 1976). However, capturing the characteristics of the liquid film is essential for the development of predictive models (Hewitt and Hall-Taylor, 1970, Azzopardi, 2006) that would be used in equipment design as well as to develop safe operational practices. To this end, developing phenomenological models underpinned by the measurements of the local film thickness and flow rates should be considered. The local liquid film thickness measurements provide information to estimate the gas void fraction, hence the liquid and gas velocities (Tibiriçá et al., 2010). Furthermore, such measurements provide means to test the existing correlations for their fidelity.

Various measurement techniques of liquid film thickness have been developed since 1960's because of the difficulty to get an accurate measurement as the film thickness is generally less than 10 millimetres (Clark, 2002). Alekseenko et al. (1994) stated that due to the complexity of the film surface wave structure, there are no measuring techniques available to completely satisfy all the specified requirements. There have been many studies about the available liquid film thickness measurement techniques that can be found in literature in Hewitt and Hall-Taylor (1970), Hewitt (1978), Alekseenko et al. (1994), Shedd and Newell (1997), Boyer et al. (2002). Nevertheless, the latest intensive review has been done by Clark (2002) who summarised the main techniques used in liquid film thickness measurements by defining the difference between them and their classification. The liquid film thickness measurement techniques have been classified in three different methods by Collier and Hewitt (1964) as per Hewitt (1978) and Clark (2002). These methods are film average methods, localised methods and point methods. In 2002, Clark proposed an additional fourth method which is spatial methods. Each of these methods and techniques falls under it will be discussed in details. The review in the current study focuses to look for a technique that can work on non-conducting medium, not intrusive and provide information about the film characteristics (i.e. waves).

### 2.4.1. Film average methods

These methods involve measurement of the average film thickness over a substantial length of the liquid film. They are unable to provide information about the characteristics of the liquid film thickness (i.e. waves) and the instantaneous measurements where much of the research interest is directed today. As the information on the structure of the interface is desired in the current work, these techniques were not considered for application. However, a brief review of the available techniques is included which are holdup measurements and weighing method.

**Hold-up measurements**

The Hold-up measurement technique works by isolating a section of the liquid film and measuring its volume as shown in Figure 2.10. Then, the average liquid film thickness is calculated with a knowledge of the length of the isolated section and pipe internal diameter. As per Hewitt and Hall-Taylor (1970), the early literature on the use of the method for falling films was presented by Hewitt et al. (1961). The total isolation of the film is the main difficulty in implementation. The use of this method to calculate the average film thickness from the measured total liquid hold-up is questionable especially at high mass flow rates where the entrained droplets in the gas have been assumed negligible.

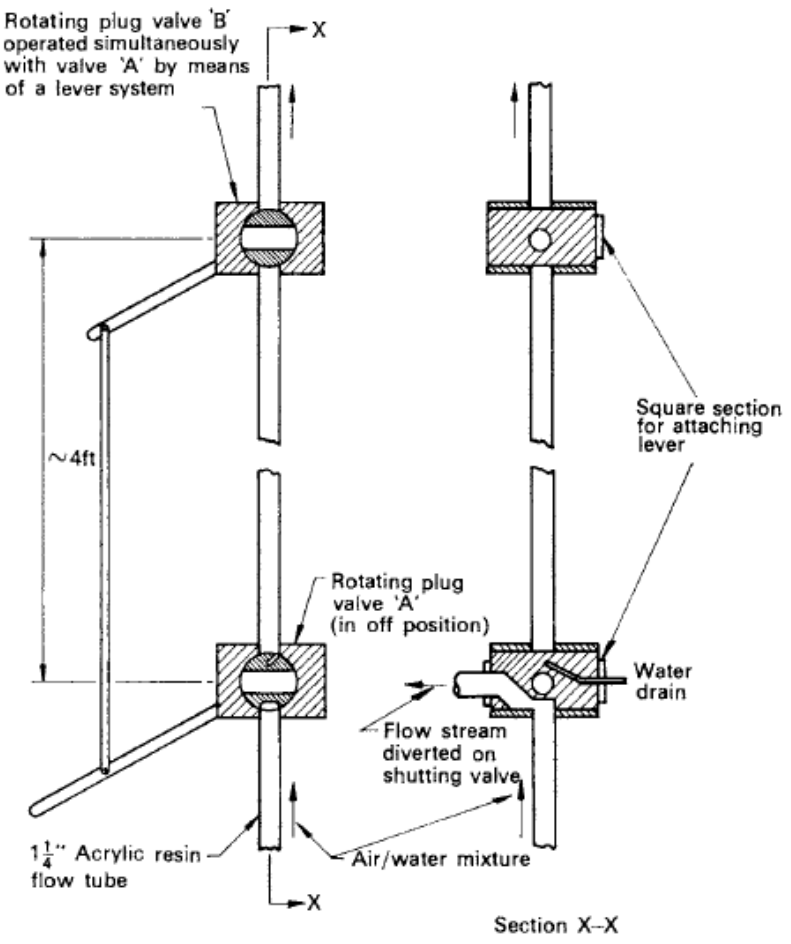


Figure 2.10: Hold-up Measurements, (Hewitt and Hall-Taylor (1970))

## Weighing Methods

The weighing method is similar to Hold-up measurements except it measures the weight hold-up test section during operation. In order to reduce systematic errors due to the friction and forces caused by the experimental support, it is critical to carefully design the entry and exit to the test section (Collier and Hewitt (1964)). This method is not recommended for conditions with the gas flow because of the frictional forces induced (Hewitt and Hall-Taylor (1970)).

## 2.4.2. Localized methods

These methods include techniques in which localised measurements of the thickness of the film is obtained. Most common techniques used to measure film thickness belong to this group because they can be implemented very easy and can be used in the most flow systems. These methods include capacitance measurements, conductance probe, radioactive absorption and emission and ultrasonic pulse echo.

**Capacitance Probes**

Capacitance probe is a technique which can be used where the test fluid is non-conductive, non-transparent or immiscible with dyestuffs. It works by taken the advantage of the difference in dielectric constant between liquid and gas where the local capacitance is measured using a pair of electrodes that will be a function of the thickness of the film between them. Different capacitive thickness sensors were presented by Alekseenko et al. (1994) which are shown schematically in Figure 2.11.

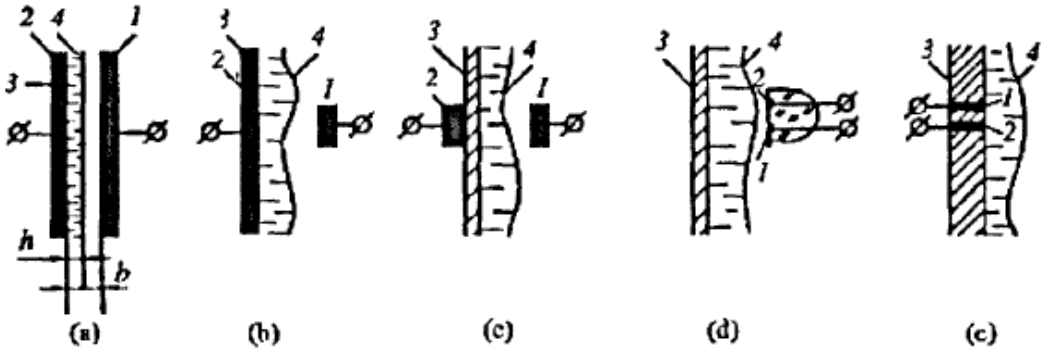


Figure 2.11: Different capacitive thickness sensors 1,2- first and second capacitor plate, 3-wall, 4-liquid film (Alekseenko et al., 1994)

The capacitance probe can measure the film thicknesses between 0.5 mm and 5 mm (Shedd and Newell, 1997). In order to measure the film thickness more accurately, electrode diameter should be as small as possible by taking in consideration signal to noise ratio. Determining the optimum diameter and its distance from the test surface is achieved by trial and error (Clark, 2002). It is critical to compensate for leakage currents in case electrodes are in contact with the test fluid (Shedd and Newell, 1997). Furthermore, it is crucial to shield the contacts and leads in order to eliminate lost capacitances and interference from other sources (Klausner et al., 1992). The accuracy of the technique is related to temperature change that affects the capacitance of the fluid. Hence, the sensor has to be calibrated at the same operating temperature (Jaworek and Krupa, 2004).

**Conductance Probes**

Conductance Probe is the most extensively used technique compared to other available techniques for measuring the film thickness. It works in a similar way as the capacitance probes where the difference in conductivity instead of capacitance between liquid and gas is used. Then, the liquid film thickness is related to the measured conductivity across a pair of probes in contact with the liquid film. This technique is suitable only for a conducting medium. The use of the conductance measurement had attracted the researchers including Hewitt and Roberts (1969), Conte and Azzopardi (2003), Belt (2007) and Zangana (2011) where the most of the research was done using an air/water system. There are three types of conductance probe in the industrial applications which have been used for film thickness measurement in pipes (Clark, 2002). These are flush

mounted, parallel wires and flush wire as schematically illustrated in Figure 2.12.

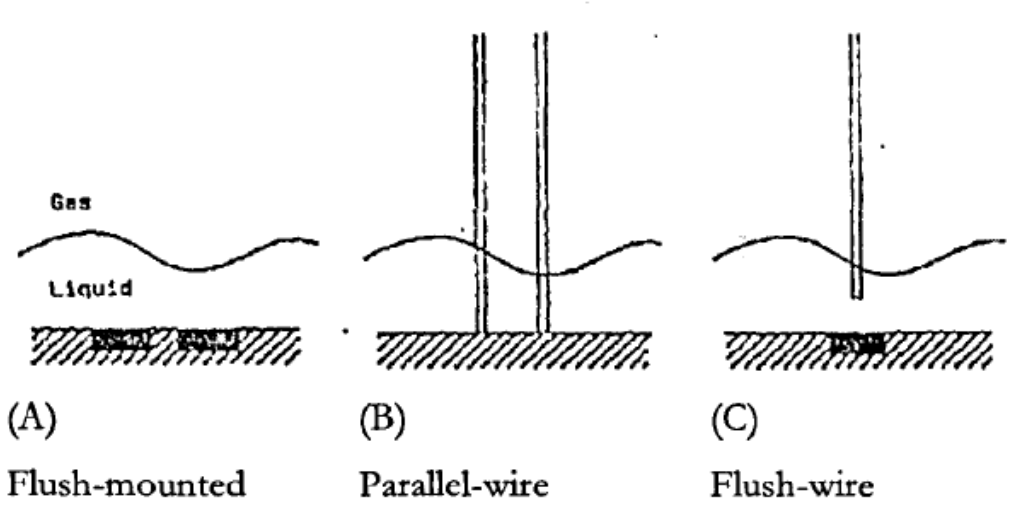


Figure 2.12: Schematic diagram of different conductance probe types (Clark, 2002)

Flush mounted conductance probes are non-intrusive and can measure thin film thickness up to 2 mm where it will saturate for the thicker film (Clark, 2002, Azzopardi, 2006). It has a non-linear relationship between the film thickness and output characteristics. The most popular and widely used flush mounted probe designs can be found in the literature are ring probes and concentric probes. Ring probe consists of a pair of metal ring electrodes separated by non-conducting material and flush mounted with the tube inner surface. They are only able to measure the average circumferential film thickness and unable to provide information about the film waviness. It was employed by Omebere-Iyari and Azzopardi (2007), Kaji and Azzopardi (2010) and Zangana (2011). Concentric probe (Figure 2.13) consists of a pin installed flush in the centre (d1) and separated by insulating material (d2) from the other electrode. The other electrode can be the pipe wall if it is metal or a concentric metal ring

surrounding the insulation material. It was used by different researchers in the past such as Azzopardi (1986),Wolf (1995) and Zhao et al. (2013).

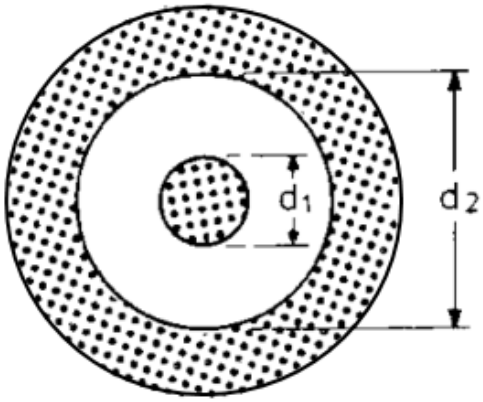


Figure 2.13: Schematic of concentric probe (Zhao et al., 2013)

In contrast, parallel wires conductance probes consist of two parallel thin wires stretched across a channel. They don't have saturation problem and can be used for the thicker film (Conte and Azzopardi, 2003, Azzopardi, 2006). It is intrusive but has a linear relationship between the film thickness and output characteristics. According to Karapantsios et al. (1989) and Conte and Azzopardi (2003), it is less reliable on thin liquid film measurement. Flush wire type is a combination of flush mounted and parallel wires which was used by Kang and Kim (1992). They claimed that their design has more accuracy and linearity over flush mounted and parallel wire probe. However, it is still intrusive.

**Radioactive Absorption**

There are different measurement techniques that are based on the Radiation Absorption which can be found in literature include neutron, gamma-ray and X-ray (Boyer et al., 2002). Most of these techniques are used to measure void fraction in two-phase flow based on radiation attenuation. These techniques consist of a radiation source emitter in one side of the test section and a radiation intensity detector on the other side after crossing the flow. The radiation is partially absorbed by the liquid film and the detected remaining radiation intensity is related to the film thickness measurement. The liquid film thickness can be calculated by applying (Clark, 2002, Tibiriçá et al., 2010):

$$\delta = -\frac{1}{\mu}\mathrm{Log}\left(\frac{\mathrm{i}}{\mathrm{i_o}}\right) \tag{2.49}$$

where $\delta$ is the thickness of the material, $\mu$ is the linear absorption coefficient of the material, $i$ is the emergent intensity, and $i_o$ is the incident intensity.

They can be utilized to measure film thickness where all the liquid between emitter and detector is in the form of a single film such as stratified flow. However, in annular flow the radiation crosses two films and liquid droplets entrained in gas phase. This limits the method to measure the line-averaged liquid fraction instead of local liquid film thicknesses (Clark, 2002, Tibiriçá et al., 2010). The locality of measurements is limited by the sizes of the radiation source since a narrow beam gives reliable data only when the continuous radiation is applied for a rather long period (Hewitt and Hall-Taylor, 1970). In addition, one of the main limitations of using these techniques is due the safety

aspects where other alternative techniques can achieve the required aim with less hazardous.

**Radioactive Emission**

Radioactive emission technique has been introduced for the first time by Jackson (1955) as shown in Figure 2.14. The measurement is based on the detection of the radiation from the radioactive substance dissolved in the flowing liquid. The radiation intensity of the localized film section is proportional to the film thickness. According to Collier and Hewitt (1964), there was no correction for the reduced contribution of the outer layers of the film compared to those closer to the detector which will affect the accuracy of the film thickness measurement in present of wavy interface (Clark, 2002). In addition, radiation is attenuated due to self-absorption in the liquid layer and accurate calibration is required (Hewitt and Hall-Taylor, 1970).

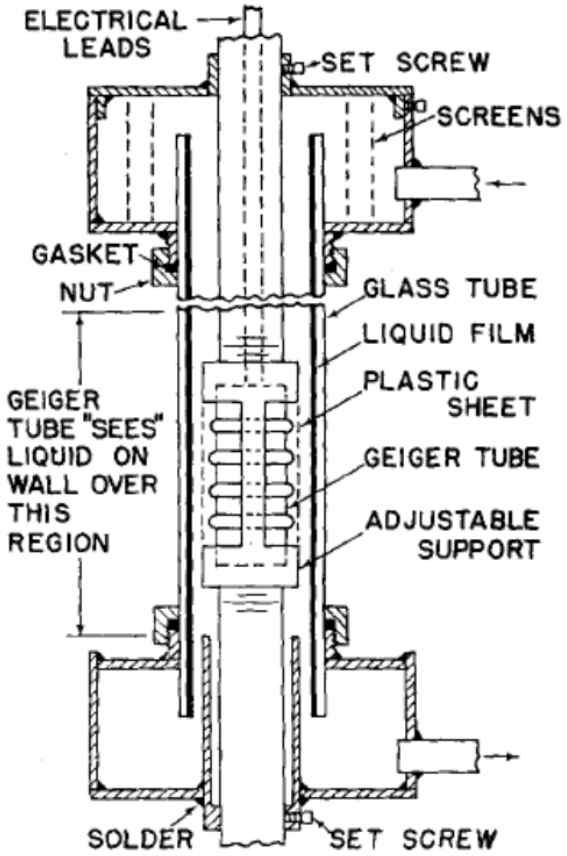


Figure 2.14: Radioactive Emission (Jackson, 1955)

**Ultrasonic Pulse-Echo Method:**

The ultrasonic Pulse echo technique has been applied by different researchers to measure the liquid film thickness including Park and Chun (1984), Lu et al. (1993) and Chen et al. (2005). It is based on that the ultrasound waves are transmitted and received by the same transducer. Then, the liquid film thickness is calculated by measuring the time differences between the transmitted and received signals with knowledge of the speed of sound in the liquid. This method will be further discussed in Chapter 5.

## 2.4.3. Point methods

Continuous or statistical information at a point in a liquid film can be obtained by the methods in this group. These methods have not been widely used as localised methods because of difficulty in implementation and results analysing. These methods include needle contact probe, hot wire probe and fiber-optic techniques.

**Needle contact Probe**

The needle contact probe is widely employed for film thickness measurement. It is used as a reference during validation or calibration of other devices due to its simplicity and applicability to measure any type and size of conducting liquid film flow (Shedd and Newell, 1997). The probe consists of a needle mounted on a movable rod which is coated with insulating material except for the tip. An electrode is mounted flush in the wall directly opposite the needle assembly so that when the needle tip touches the surface of the liquid film, a closed circuit is formed and current flows. Then, the distance between the needle point and the solid boundary is noted which represents the thickness of the film. A schematic for the typical needle contact probe arrangement is given in Figure 2.15 below:

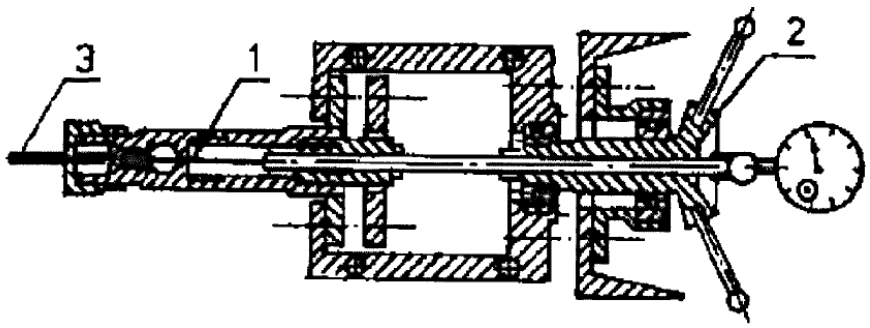


Figure 2.15: Typical needle contact probe used for film thickness measurement 1-Needle, 2- Driving mechanism, 3- Wall electrode (Hewitt, 1978).

Due to the wavy structure of the film surface, the needle may touch the film only erratically. Also, information about the instantaneous liquid film thickness cannot be obtained since only one depth is investigated at each needle setting. However, statistical information concerning the distribution of the instantaneous film thickness can be obtained from the analysis of the contact time and frequency. The method is simple but time-consuming (Azzopardi, 2006). In addition, it is intrusive where the needle tip penetrates the film interface. The measuring error of this method can be related to the problem of contact hysteresis where the liquid film may remain in the needle tip causing a delay break of contact with the liquid film (Hewitt and Hall-Taylor, 1970). Another source of error is the thermal expansion of the needle and mechanical positioning apparatus (Shedd and Newell, 1997).

**Hot-wire Probe:**

Hot-wire probe is based on the principle of the hot-wire anemometer which is used for velocity and wall shear stress measurements (Bruun, 1996). It works based on heat transfer effect where a very fine wire is electrically heated up by a constant current or maintained at a constant temperature above the ambient. When the wire touches the film surface, the wire's temperature and its resistance fall sharply due to the enhanced heat transfer capabilities of the liquid relative to air. The film thickness is related to the resistance of the wire. It has been used by ISHIGAI et al. (1972) where they have replaced the needle probe with hot-wire probe in order to remove the limitation of needle probe to conducted fluid and extend its application to liquids with low conductivities. However, this method still suffers from the same difficulties and limitation of needle probe. Lyu and

Mudawar (1991) used an alternative hot-wire approach where hot wire inserted into the gas-liquid interface and heated by a constant current. The film thickness is related to the voltage signal because the total electrical resistance depends on the length of wire immersed in the liquid. However, the measurement using this technique is not reliable because the heat transfer between the wire and liquid is also a function of the velocity of the film. In addition, the technique is intrusive.

**Fiber-Optic Techniques:**

The fiber optic techniques were introduced by Ohba et al. (1984) and later was further enhanced by Than et al. (1993) and Yu and Tso (1995). The technique is based on emitting a light by a laser to the liquid through the test section wall by a transmitting optical fiber, and receiving the light reflected from the liquid surface through other optical fibers which are flush mounted in the wall surface. The sensor head consists of a transmitting fiber as the light emitting source in the centre and six receiving fibers surrounding it which are joined tightly to each other as shown in Figure 2.16. Each receiving fiber has a photo-detector at its end which is connected to analysing electronics. The received light intensity has a different value corresponding to the position of the receiving fiber, and is dependent on both film thickness and the inclination angle to the surface with respect to the wall surface. Thus, the film thickness can be obtained by processing the outputs from the six photodetectors. This setup called multi-fiber optic which is suitable for film thickness measurement between 1-4 mm (Yu et al., 1996). However, Ohba et al. (1992) found that this sensor is unable to accurately measure liquid film thickness thinner than 1 mm. Therefore, they developed a new sensor called mono- fiber optic sensor identical to the multi-

fiber optic sensor but only consists of one fiber that acts as both emitter and receiver.

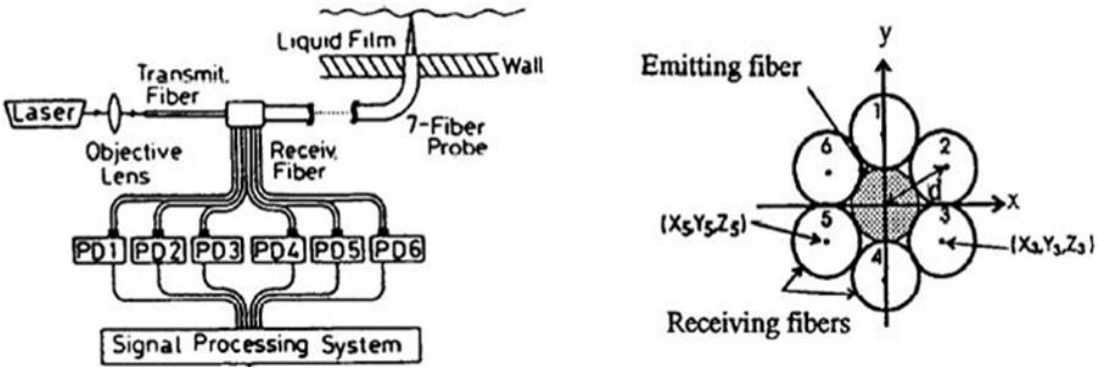


Figure 2.16: Schematic diagram of the fiber optic sensor and Arrangement of the multi-fiber sensor (Yu et al., 1996).

Yu and Tso (1995) developed a simulation software for both multi-fiber and mono-fiber studies. They concluded that the multi-fiber sensor is capable of measuring liquid film thickness between 1 – 4 mm and the mono-fiber sensor for liquid film thickness below 1mm. This conclusion is in agreement with findings by Ohba et al. (1984) and Ohba et al. (1992). Mono-fiber sensor allows the measurement of the film thickness where the inclination of the reflecting interface is zero (Yu and Tso, 1995). Therefore, it is very important to calibrate the sensor in order to evaluate the inclination angle and the attenuation effect within the liquid. The effect of bubbles and absorption in the liquid has not been considered (Perron et al., 2006). This technique requires transparent tube and permanent mounting of a fiber assembly in a test section (Tibiriçá et al., 2010).

### 2.4.4. Spatial methods

This group has been introduced by Clark in 2002 where multiple of point or localised measurements from the same type are used simultaneously in different areas of the film in order to build up a global picture of the film thickness structure of the area under study. These methods help to better understand liquid film structure, especially for the wavy interface by providing three-dimensional structures. However, the use of these methods means more cost compared to single measurement where there will be increased in resources in both implementation and analysis. An example of this group is Multi-pin Film Sensors (MPFS) which will be discussed in Section 3.3.2.1.

### 2.4.5. Conclusion

As discussed in Chapter 1, the silicone oil is used in the current study as a liquid phase which is non-conducting fluid. Therefore, the review was conducted to find a technique that can work on non-conducting medium, not intrusive and provide information about the film characteristics (i.e waves). Commonly available and widely used measurement techniques are based on the fluid electrical properties (conductance measurement) or require transparent geometry (optical measurement) or tracer chemicals (Absorption measurement). Even though the possibility of adding conductive chemicals exists, it is not favoured in most cases. Capacitance measurements were in development but require larger electrodes given the capacitance is in Pico-Farads for some of the oils used in the industry. Ultrasonic pulse echo technique has been selected where it can be applied even for non-transparent tubes and does not required additional

substance or conducting fluid. It is a non-intrusive and can be easily mounted on the pipe.

## 2.5. Shear Stress Measurement

Wall shear stress ($\tau_w$) is defined as the tangential force by the flowing fluid on a surface in contact with it. It plays a significant role in the prediction of the pressure drop measurement and the liquid film velocity profile in annular two phase flow. In order to understand the performance of a system, it is crucial to have knowledge about the drag made by the motion of fluid over a solid surface (Winter, 1977). The measurement of wall shear stress is a difficult parameter to be measured in fluid mechanics (Ayaz et al., 2013).

Wall shear stress is affected by the disturbance waves in the gas and the liquid film interface. Simultaneous measurement of wall shear stress using flush mounted hot film probe and liquid film thickness using conductance probe has been reported by Martin (1983), Hagiwara. Y (1988), Govan et al. (1989) and Zangana (2011). All have observed that the large disturbance wave's peak associated with the liquid film thickness also corresponds to a large peak in the wall shear stress.

### 2.5.1. Shear Stress Measurement Techniques

Various wall shear stress measurement techniques have been established in the last decades. They were classified into two main groups, direct and indirect measurements based on the measurement principle. Thorough reviews of the

available wall shear stress measurement techniques have been presented by Winter (1977), Hanratty and Campbell (1996), Naughton and Sheplak (2002), Sheplak et al. (2004) and Loureiro et al. (2010).

In the current study, these techniques for measuring the wall shear stress have been assessed based on the principle of measurement and their suitability in two-phase flow application as shown in Figure 2.17.

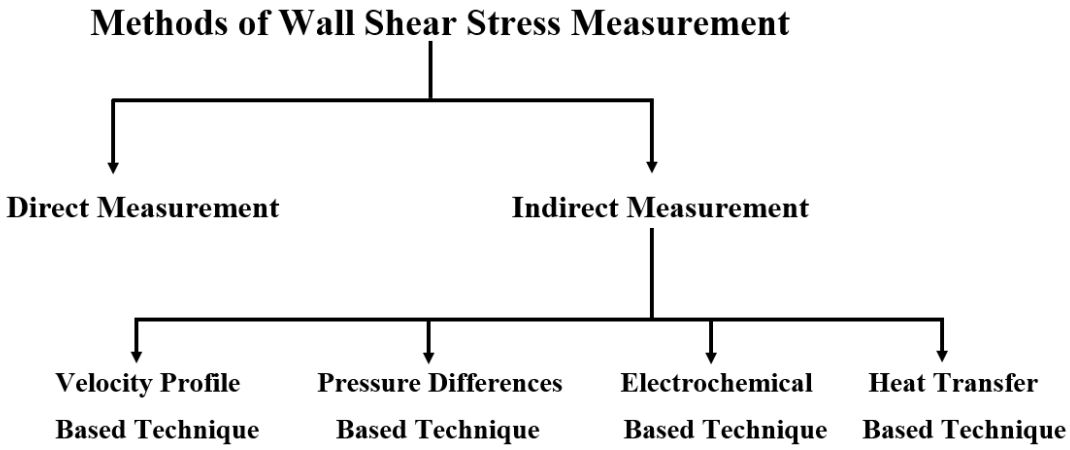


Figure 2.17: Classification of wall shear stress measurement techniques.

**Direct Measurement technique**

The conventional direct measurement technique for measuring the wall shear stress is based on mechanical movement of a flush mounted floating element due to the wall shear force applied on its surface as shown in Figure 2.18. The wall shear force measurement is made of the displacement of the element or of the force required to keep it at its original position. Then, the mean wall shear stress is calculated by knowing the wall shear force and the area of the element. More detail about the method and its limitation have been presented by  and Hanratty and Campbell (1996).

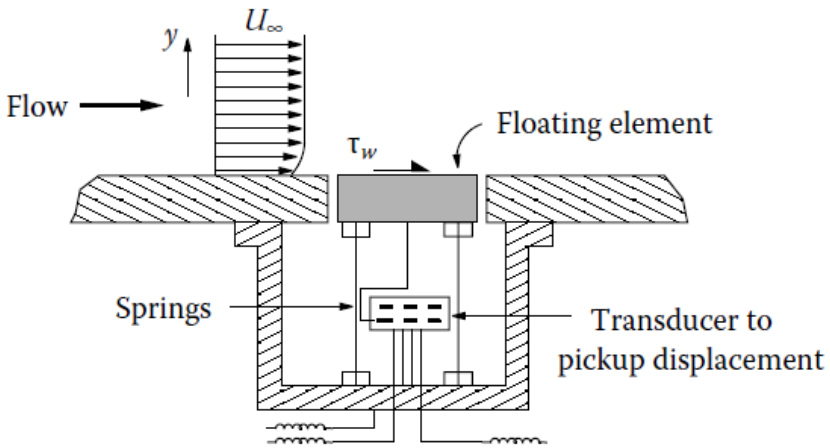


Figure 2.18: Schematic of Conventional Direct Measurement (Rathakrishnan, 2007).

The conventional technique limitations include relative low spatial and temporal resolution and sensitivity to floating element misalignment with the surface, surrounding clearance size, temperature variation and vibration. In addition, the gap around the floating element has to be very small in order to avoid any disturbance to the flow due to discontinuity at the surface.

In the recent decades, microelectromechanical system (MEMS) fabricated devices very thin (μm) compared to the conventional devices (mm) in order to overcome the limitations of the conventional devices as illustrated by Winter (1977). These devices work on the same principle described above (Sheplak et al., 2004). However, the MEMS devices still suffer from an error associated with pressure gradients, vibration inputs, and fabrication issues including the misalignment between the floating element and gap according to Etebari (2008).

In the two-phase flow, the direct technique has been rarely adopted due to the difficulty associated with manufacturing compared to the indirect techniques.

**Velocity Profile based technique**

Shear stress can be estimated through a relationship between shear stress and velocity profile. The velocity of the fluid that is flowing inside a straight tube is not equal at all points in the tube where the highest will be at the centre of the tube and then keep decreasing until it reaches close to zero near the tube wall. This velocity gradient is due to frictional forces in terms of fluid viscosity that are exerted between the adjacent layers of the flowing fluid and between the fluid and the walls of the tube. According to the no-slip condition, the velocity of the fluid at the boundary is zero, but at some height from the boundary, the flow velocity must equal of that of the fluid.

The relationship between the wall shear stress ($\tau_w$), liquid dynamic viscosity ($\mu_l$) and film velocity gradient or shear rate ($\frac{\partial u}{\partial y}$) is given by equation (2.50):

$$\tau_w = \mu_l \frac{\partial u}{\partial y} \tag{2.50}$$

This relationship is only true for all Newtonian fluid where dynamic viscosity is constant at all velocity gradients. However, in the case of non-Newtonian fluids where the dynamic viscosity depends on the shear rate and is not constant, this relationship is not applicable. In addition, the practical difficulty with Equation 2.48 is that the viscous sublayer of turbulent flow is very thin of the order of $\frac{v}{u_\tau}$ where $u_\tau$ = friction velocity = $u_\tau = \sqrt{\left(\frac{\tau_w}{\rho}\right)}$ and ν is kinematic viscosity. This makes $\frac{\partial u}{\partial y}$ has to be estimated from measurements made very close to the wall, typically at distances of less than of $\frac{5v}{u_\tau}$ which makes the measurement may be

subjected to significant and random errors appears as non-linear profile (Loureiro et al., 2010, Hutchins and Choi, 2002, Durst et al., 2004).

In the two-phase flow with thin liquid film makes this method more difficult and inappropriate due to difficulty in identifying the flowing boundary layer region and getting accurate velocity measurement using conventional instrumentation such as hot wire, Laser Doppler Velocimetry (LDV) and Particle Image Velocimetry (PIV) close to the wall (Salari and Tabar, 2011).

**Pressure Differences based technique**

The mean wall shear stress can be calculated by measuring the pressure drop across two points of fully developed turbulent flow in a pipe with the constant area by using the following relationship:

$$\tau_w = \frac{D\Delta P}{4l} - \rho_L g \qquad (2.51)$$

where ΔP is the pressure drop, D is pipe internal diameter, $\rho_L$ is liquid density and $l$ is the distance between the two tapping holes.

This relationship has been widely utilised for the calibration of other indirect wall shear stress measurement methods using single phase flow on a vertical pipe (Govan et al., 1989, Descamps et al., 2008, Zangana, 2011).

The popular techniques that have been used to estimate the mean wall shear stress from the pressure differences between two points, are Preston tube, Stanton gauge and sublayer fence as shown in Figure 2.19 (Hanratty and Campbell, 1996, Berca, 2007).

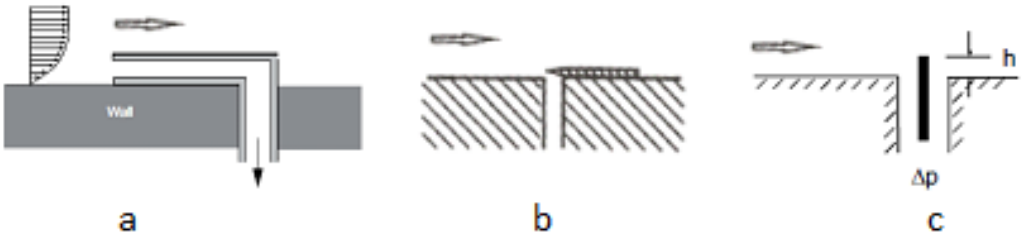


Figure 2.19: Schematic illustrations of (a) Preston tube, (b) Stanton gauge and (c) Sublayer fence (Berca, 2007).

Preston tube is the most popular than the other two which measures the mean wall shear stress ($\tau_w$) from the difference in pressure ($\Delta p$) between the pressure measured by the tube placed on the wall and the local static pressure measured by a nearby wall tap (Winter, 1977, Hanratty and Campbell, 1996, Loureiro et al., 2010). The following relationship suggested by Preston (1954) is used to calculate the wall shear stress:

$$\frac{\Delta p d^2}{\rho v^2} = F\left[\frac{\tau_w d^2}{\rho v^2}\right] \tag{2.52}$$

where d is the outside tube diameter, $\rho$ is the liquid density and $v$ is kinematic viscosity.

Stanton gauge measures the difference in pressure between the static pressure with/without the blade which is used to calculate the wall shear stress. However, there is no specific empirical expression could be used as it is very sensitive to geometrical particulars (Hanratty and Campbell, 1996). In addition, this method is affected by wall pressure fluctuations (Haritonidis, 1989). Sublayer fence relates the difference in pressure between upstream and downstream of the fence with the wall shear stress. It can be used with strong pressure gradient but its

accuracy is still unknown (Hanratty and Campbell, 1996). The tip of the blade must remain immersed within the viscous sublayer (Fernholz et al., 1996).

All the above techniques might introduce a disturbance to the flow even they are small in size (mm). In the two-phase flow with a thin film, it is difficult to identify the flowing boundary layer region and make the size of Preston tube, Stanton blade and the fence tip small to be immersed within the viscous sublayer. Therefore, in the two-phase flow, it is preferred to measure the pressure drop across two small holes on the surface separated by a known distance using a manometer or electronic differential pressure transmitter. However, this method is able to provide the mean wall shear by using Equation (2.14) that makes it suitable for the calibration of other indirect wall shear stress measurement methods.

**Electrochemical based technique**

The electrochemical technique is also known as Electrodiffusion method which consists of cathode and anode connected to the electric circuit as shown in Figure 2.20. Electrolytic solution is used as Redox system such as Potassium Ferricyanide, $\mathrm{Fe(CN)}_6^{-3}$ and Ferrocyanide, $\mathrm{Fe(CN)}_6^{-4}$ which is mixed with sodium hydroxide. $NaOH$. The application of the electrochemical technique in two phase flow has been attractive to many researchers including Cognet et al. (1984), Nakoryakov et al. (1984), Nakoryakov et al. (1986) and Zheng and Che (2007).

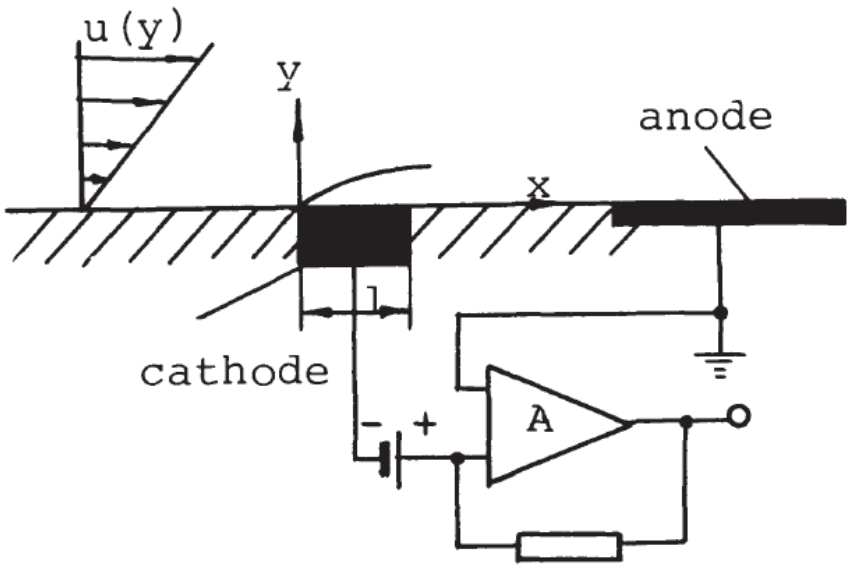


Figure 2.20: Schematic for Electrochemical method (Nakoryakov et al., 1984).

It has an advantage that its response is known theoretically, hence eliminating the need for calibration. Although this technique is used for measuring wall shear stress, it can be also used to measure velocity and void fraction of two-phase flows (Alekseenko et al., 1994). In the other hand, this technique is not suitable for the present of light and oxygen because they decompose the ferrocyanide ion to iron oxide, resulting in surfaces having an oxide film (Hanratty and Campbell, 1996). Therefore, this technique is not suitable for current work where the test facility using Perspex pipes and the air is used as a gas phase.

**Heat Transfer based technique**

Heat Transfer technique using a constant temperature anemometer has been widely used by researchers for measuring wall shear stress in turbulent flow. Hot-wire and flush mounted hot film probe are used to measure the wall shear

stress based on heat transfer. The hot-wire must be immersed in the viscous sublayer, hence the measurement of flow velocity is proportional to the wall shear stress as discussed in velocity profile based technique. In addition, hot-wire probes are thin and very fragile to be used with a liquid which makes them mainly used in gas flow (Bruun, 1996). Flush mounted hot film probe is the most popular especially in two-phase flow application due to present of liquid on the pipe wall in most of the two-phase flow regimes. It is non-intrusive and does not generate any disturbance to the flow. However, the thermal boundary layer that develops over film probe has to be within the viscous sublayer of the turbulent boundary layer. Many studies in two-phase flow in horizontal and vertical pipes has used a glue on flush mounted hot film probe from Dantec dynamics (Dantec 55R47) to measure the wall shear stress. These studies include Martin (1983), Govan et al. (1989), Descamps et al. (2008) and). More detail about the principle of measurement and calibration are discussed in Chapter 3.

### 2.5.2. Conclusion

The difficulties discussed above in the use of direct measurement, velocity profile, pressure difference in two phase flow make the electrochemical and heat transfer techniques preferable. Also, both techniques do not disturb the flow in two phase flow. As discussed above, the electrochemical technique is not suitable for the present of light and oxygen which is the case in the current experiment setup. Therefore, the heat transfer technique using flush mounting hot film probe is more attractive where it doesn't require adding any substance and has been used widely in two-phase application.

# CHAPTER 3

# EXPERIMENTAL ARRANGEMENTS

A number of experiments were carried out in developing a liquid film measurement technique using ultrasonic technique and also in studying annular flow regime. The experimental arrangements used are explained in details in this chapter. Two experimental test facilities were used in the current study. Both test facilities were constructed at the Department of Chemical and Environmental Engineering at the University of Nottingham. In section 3.1, the first test facility called a free falling liquid film annular flow test facility is described. This has a test section of 127mm internal diameter (ID) and length of 5 m. The second test facility called an upward vertical annular Flow Test Facility is described in section 3.2. This consists of a test section of 34.5mm internal diameter and length of 4 m. In section 3.3, the principle of measurement and calibration of the facilities instrumentations are described.

## 3.1. Free Falling Liquid Film Annular Flow Test Facility

### 3.1.1. Overview of the Experiment Test Facility

A schematic diagram of the free falling liquid film annular flow test facility is shown in Figure 3.1. The test facility is the same as that used by Abbas Hasan et al. (2016) as part of collaborative work. It has a test section made of acrylic resin (Perspex™) with 127 mm internal diameter (ID) and length of 5 m. Water was used as the working fluid where there was no gas flow. The test section is

connected to a storage tank that stores the water used. The water was pumped from the water tank using a centrifugal pump and controlled by a manual control valve and a bypass valve to deliver the desired liquid flow rate through a rotameter. The water flow rate was measured by the rotameter (MBP Industries Ltd) with an accuracy of ±5% of full scale. A liquid distributor at the top of the test section was used to ensure a uniform liquid film around the test section. Figure 3.2 shows the schematic design of the liquid distributor. Then, the water was fed back into the storage tank. Temperature and water conductivity were measured using a T-type thermocouple and TetraCon 325 Conductivity probe respectively. The experiments were performed at ambient temperature (≈20$^{o}$C) and atmospheric pressure. The water conductivity and the temperature were measured before and after each experiment.

The test facility was used to validate the measurement of an ultrasonic technique against a Multi Probe Film Sensor (MPFS). Both techniques were used to measure the liquid film thickness. The ultrasonic sensor and the MPFS were located at 320 cm (25.2D) and 350 cm (27.6D) from the bottom of liquid distributor respectively. The experiments were conducted at different liquid Reynolds numbers ($Re_L$) ranging from 618 to 1670. $Re_l$ is defined as:

$$Re_l = \frac{\rho_l u_{sl} \delta}{\mu_l} = \frac{\rho_l Q_l}{\pi D \mu_l} \tag{3.1}$$

$$u_{sl} = \frac{Q_l}{\pi D \delta} \tag{3.2}$$

where $\rho_l$ is liquid density, $u_{sl}$ is liquid superficial velocity, $Q_l$ is liquid volumetric flowrate, D is pipe internal diameter and $\mu_L$ is the dynamic liquid viscosity.

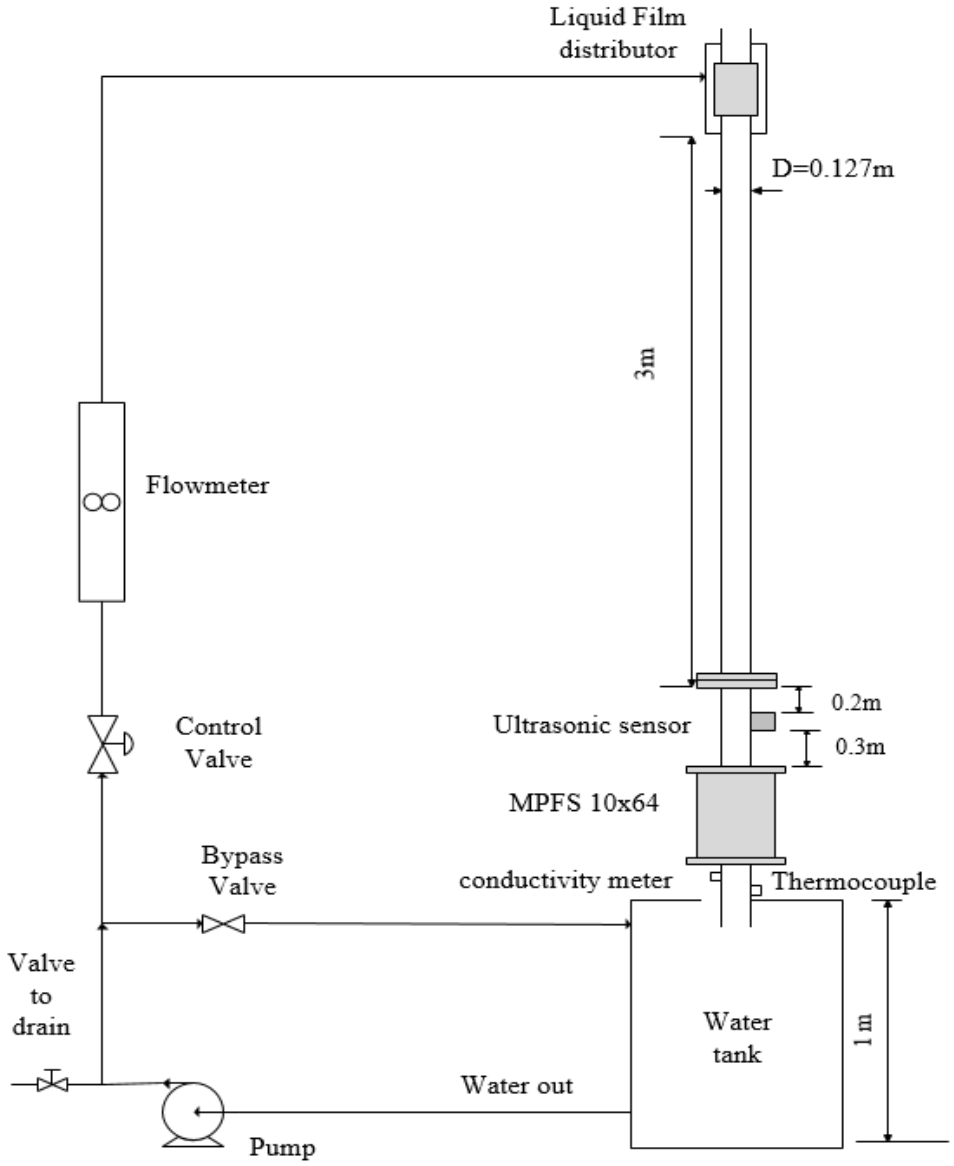


Figure 3.1: Schematic Diagram of the free falling liquid film annular flow test facility.

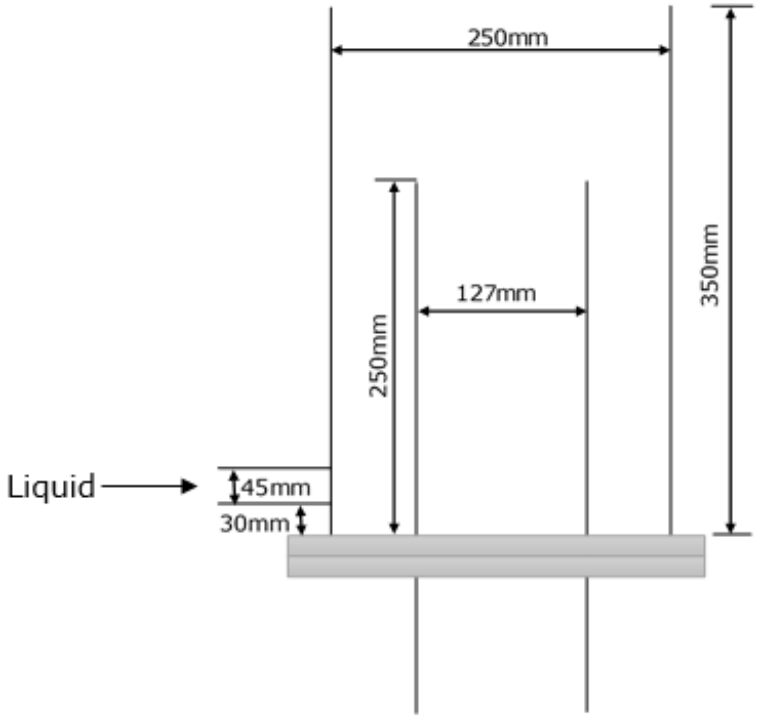


Figure 3.2: Schematic Diagram of the liquid distributor.

## 3.2. Upward Vertical Annular Flow Test Facility

### 3.2.1. Overview of the Experiment Test Facility

A schematic of the upward vertical annular flow test facility is shown in Figure 3.4. The test facility is similar to that used by Zhao et al. (2013) to study the behaviour and characteristics of the disturbance waves by the measurement of film thickness using an air/water system. Pipe diameter, injector, film thickness concentric probe and differential pressure transmitter were similar to the experimental arrangement used by Zhao et al. (2013). However, the length of the test section was modified to ensure that a fully developed annular flow is achieved. In addition, a wall shear stress was measured in the current study. The

test facility has a test section height of 4 m made of acrylic resin (Perspex™) with 34.5 mm inner diameter (ID). The liquid phase was stored in a storage tank with a capacity of 600 litres. The liquid was pumped from the storage tank using a centrifugal pump. The liquid flow rate was controlled by a manual control valve and a bypass valve to deliver the desired value through one of the three sets of rotameters based on the operating range. The air phase was supplied from the main header in the Lab. The air flow rate was controlled and adjusted by a manual control valve to deliver the desired value through one of the two sets of rotameters based on the operating range. Both liquid and gas flow rates were measured using calibrated rotameters (MBP Industries Ltd) with an accuracy of ±5% of full scale. The experiments were conducted for gas superficial velocity ranging from 17.83 m/s to 35.66 m/s and liquid superficial velocity ranging from 0.018 m/s to 0.089 m/s with water and from 0.018 m/s to 0.094 m/s with silicone oil both at atmospheric conditions. The selection of the gas and liquid operating range criteria will be discussed in Chapter 4. The air and liquid were injected using a conical injector system. It was designed to achieve an annular flow regime. It consists of an annular chamber to which the liquid is introduced and the inner wall has an angled inlet as shown in Figure 3.3. The liquid was injected from the side and the gas from the center to create a uniform liquid film around the boundary of the wall. The liquid was injected at four different injection points that allowed the liquid film to be introduced at the same rate. The airline was equipped with a non-return valve to prevent the flow of water into the gas rotameters. The air flow was allowed to develop by keeping a distance of 70 cm (20.3D) downstream the injector similar to the specification required in flow measurements.

The test facility is designed to measure pressure drop, film thickness and wall shear stress simultaneously. According to the investigation by Zhao et al. (2013), the liquid film reached the fully developed region at a distance of L/D = 20 upstream of the injector. However, in order to ensure the fully developed region is achieved, the measurements of the liquid film thickness and wall shear stress in the current study were made at a distance of L/D= 75 upstream of the injector. The liquid film thickness was measured using an ultrasonic technique and a concentric conductance probe. The wall shear stress was measured using a commercial glue-on flush mounted hot film probe (Dantec 55R47, Dantec dynamics Ltd). The two-phase pressure drop across the measurement test section and over an axial distance of 1.62 m between the two pressure tapings was measured using a differential pressure transducer (Remote seal Rosemount 3051 model). Four temperature sensors (T-type thermocouple, TC Direct Ltd) were used. Two of them were installed after gas and liquid flow meters. The other two were installed after the injector and close to the measurement section above the wall shear stress probe. The temperature sensor at the measurement section was mounted close to the inner wall of the tube to ensure small film thickness temperature is captured. The liquid temperature was maintained constant ($\approx 20^{o}$C) during the measurement by running the rig for two hours before taking any measurements. In addition, the liquid tank temperature was controlled using a cold tap water flowing in a coil inside the tank in order to stabilize the tank temperature. The stability of the liquid temperature was checked by comparing the time series data of the temperature sensors after the injector and close to the measurement section where the maximum average variation between them was less than $0.2^{o}$C. The air/liquid mixture was separated using a cyclone separator.

The air was vented to atmosphere while the liquid was fed back into the storage tank.

In order to achieve the aim and objectives of the current study, the experiments consist of two parts. Initially, water was used as a liquid phase and air as a gas phase in order to compare the results with the literature. This was essential to validate our measurement methodology and understand the relationship between film thickness, wall shear stress, and pressure drop. Secondly, the liquid phase was replaced with silicon oil (4.4cP) to study and develop better understanding about the relationship between the above three parameters (i.e. film thickness, wall shear stress, and pressure drop). In addition, this test facility was also used to validate the measurement of the ultrasonic technique against the concentric conductance probe for measuring liquid film thickness using an air/water system. The ultrasonic technique was then used to measure the liquid film thickness using an air/silicone oil system. During the experiments using the air/water system, the water was replaced with new clean water before starting the experiments. This was performed to avoid build-up of scale, algae. Also, when the rig was not in use, the tank was kept empty.

The properties of the fluids used are shown in Table 3.1.

| Fluid | Density ($kg/m^3$) | Viscosity (Pa.s) | Surface tension (N/m) |
|---|---|---|---|
| Air | 1.2 | $1.78 \times 10^{-5}$ (0.0178cP) | |
| Water | 998.2 | 0.001 (1cP) | 0.073 |
| Silicone Oil | 919 | 0.0044 (4.4cP) | 0.02 |

Table 3.1: Properties of the fluids at atmospheric pressure and temperature 20°C.

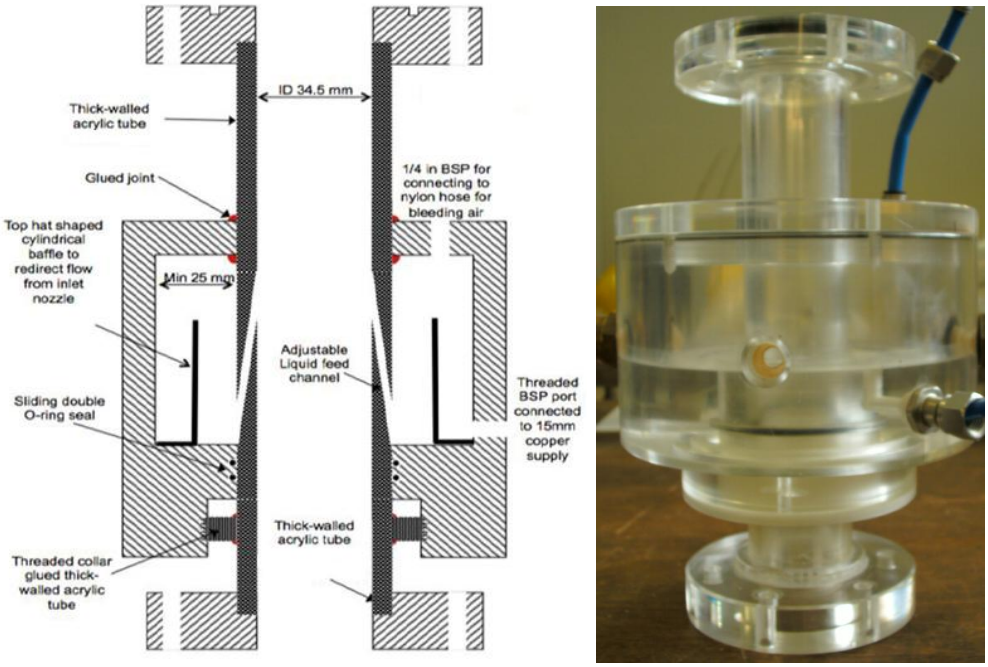


Figure 3.3: Schematic diagram (Zhao et al., 2013) and a photo of the liquid injector.

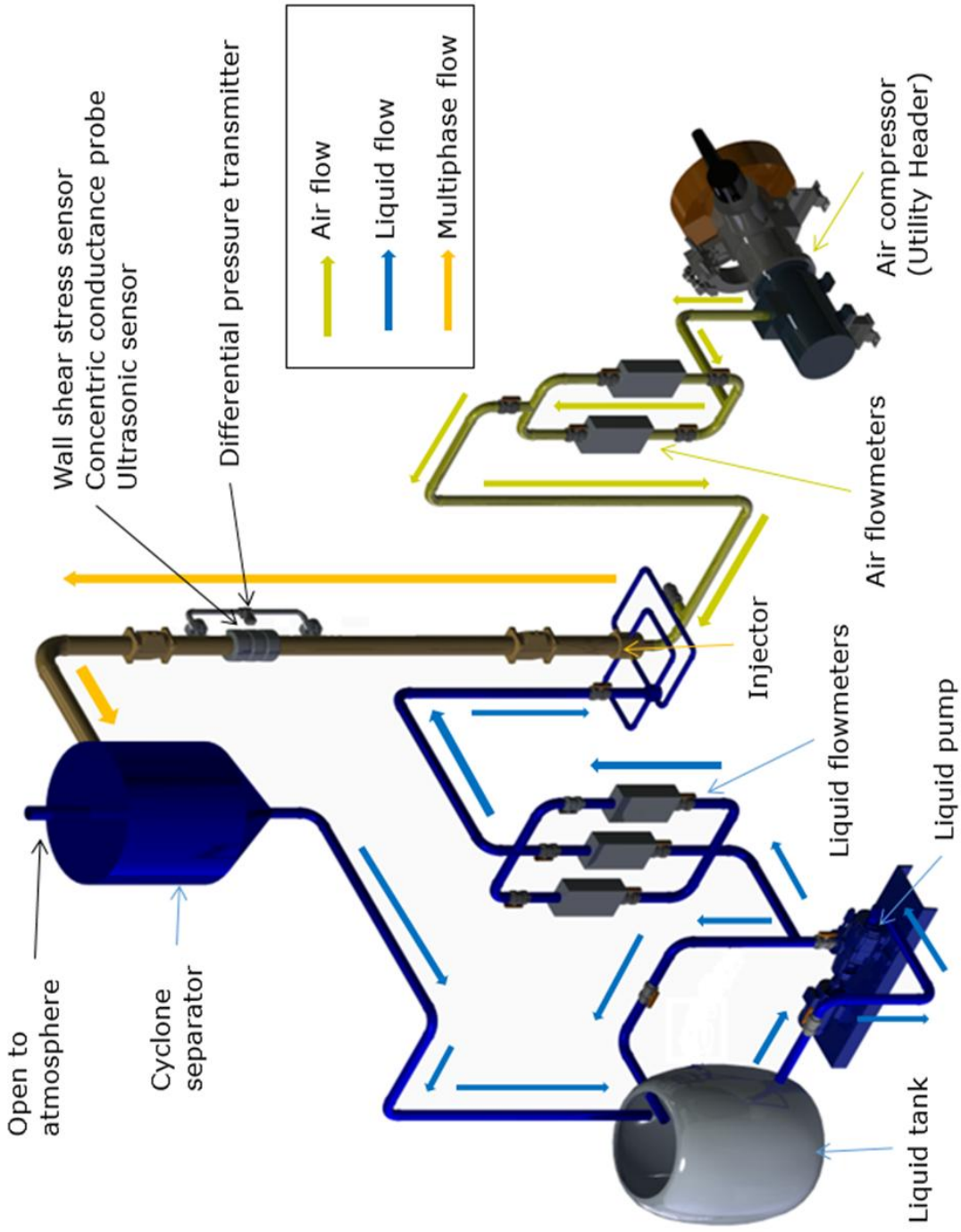


Figure 3.4: Schematic diagram of the upward vertical annular flow test facility.

## 3.3. Test Facilities Instrumentation

In this section, the instrumentation and their calibration procedure is discussed. Table 3.1 illustrated the specification of main instrumentation used in the test facility.

| Instrument | Manufacture | Model | Range | Uncertainty |
|---|---|---|---|---|
| Air flowmeters | MBP Industries Ltd | Rotameter | 0-500 and 500-5000 litres/min | ±5% |
| Liquid flowmeters | MBP Industries Ltd | Rotameter | 0-1, 0-10 and 0-100 litres/min | ±5% |
| Differential pressure | Rosemount | Remote seal Rosemount 3051 model | 0-22 kPa | ±0.25% |
| Temperature | TC Direct Ltd | T-type thermocouple | 0-100 $^{o}$C | ±1 $^{o}$C |
| Ultrasonic Transducer | Technisonic | IPM-0502-HR | 0.1-6mm | ±5%* |
| Multi Pin Film Sensor | Helmholtz-Zentrum Dresden-Rossendorf | - | 0-6mm | ±3.6%* |
| Concentric Probe | Imperial College | - | 0-3mm | ±2.4%* |
| Hot film shear stress | Dantec dynamics Ltd | Dantec 55R47 | - | ±5%** |

*Based on experimental data.

**Based on combined uncertainty of pressure drop and flowmeter.

Table 3.2: Details of the instruments used in the experiments.

### 3.3.1. Two phase Pressure Drop Measurement

The two-phase pressure drop across the test section and over an axial distance of 1.62 m between the two pressure tapings was measured using a differential pressure transducer (Remote seal Rosemount 3051 model) with a range of 0-22 kPa and an output voltage from 1 to 5V. The pressure drop measurements were used to develop a better understanding of its relationship with the wall shear stress and the film thickness in two-phase flow by measuring all the three parameters simultaneously. In addition, it was used to calibrate the hot film wall shear stress probe.

In the current study, the remote seal Rosemount differential pressure transducer was used which helps to prevent the induced of air bubbles in the pressure tapings. The remote seal system is a symmetrical system that utilizes equal diaphragm seals and capillary length on the high and low-pressure sides of the transmitter. Each capillary length is filled with the same amount of silicone fluid that helps to eliminate the seal temperature effect due to equal pressure on both sides of the transmitter diaphragm. Diaphragm seals are used to isolate the silicone fluid from the fluid in the tube. This differential pressure transmitter was used to measure the pressure drop of air/water and air/silicone oil systems.

### 3.3.1.1. Calibration of the differential pressure transmitter

The remote seal differential pressure transmitter was calibrated by varying the liquid level (H) in the test section in order to determine the output voltage for corresponding pressure difference at the transmitter. The high-pressure side (HP) of the transmitter was connected to the liquid and the low-pressure side (LP) was opened to the atmosphere. The test section was scaled from zero at HP side using a special scaled tape in order to know the liquid level (H). The corresponding output voltage from the transmitter was recorded simultaneously using LabVIEW as part of full loop calibration. A schematic diagram of the remote seal pressure transmitter is shown in Figure 3.5.

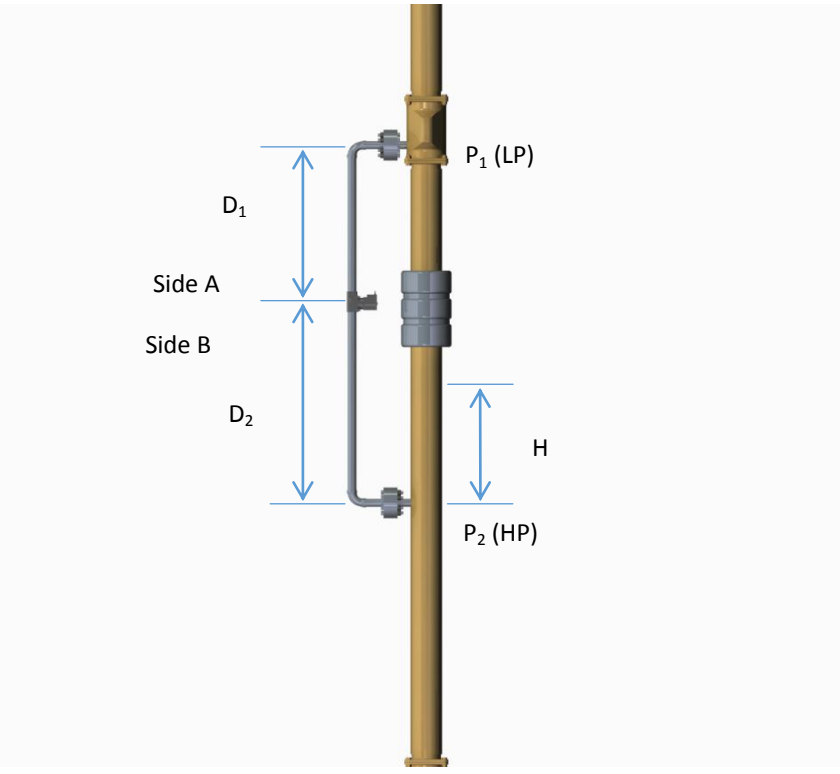


Figure 3.5: Schematic diagram of the remote seal differential pressure transmitter.

Applying a force balance across the transmitter between side A and side B, the pressure difference (ΔP) could be measured by the following relationship

$$\Delta P = P_B - P_A = (P_2 - P_1) - \rho_s g(D_2 + D_1) \quad (3.3)$$

where $P_1$ is the pressure at low side, $P_2$ is the pressure at the high side, $\rho_s$ is the silicone fluid density in the tapping line, g is the gravitational acceleration, $D_1$ is the height between $P_1$ tapping and transmitter and $D_2$ is the height between $P_2$ tapping and transmitter.

The $P_2$ at high side (HP) can be obtained by measuring the height of liquid level (H) with knowledge of the liquid density ($\rho_l$) and keeping the $P_1$ open to the atmosphere:

$$P_2 = \rho_l g H \quad (3.4)$$

As can be observed from equation (3.3), there is a gravitational term arising from the difference in height between the pressure tapping points due to the silicone fluid in the tapping lines. In the vertical system, it is necessary to deduct this gravitational term from the measured pressure drop in order to obtain the true pressure drop across the two tapings.

The same calibration procedure of differential pressure transmitter was followed for air/water and air/silicone oil systems. The calibration was repeated three times for each system where all the repeated runs fall in the same curve with a maximum standard deviation of 0.014 kPa. The relationship between the output voltage and the differential pressure is linear and the calibration curves of both systems are shown in Figure 3.6 and 3.7.

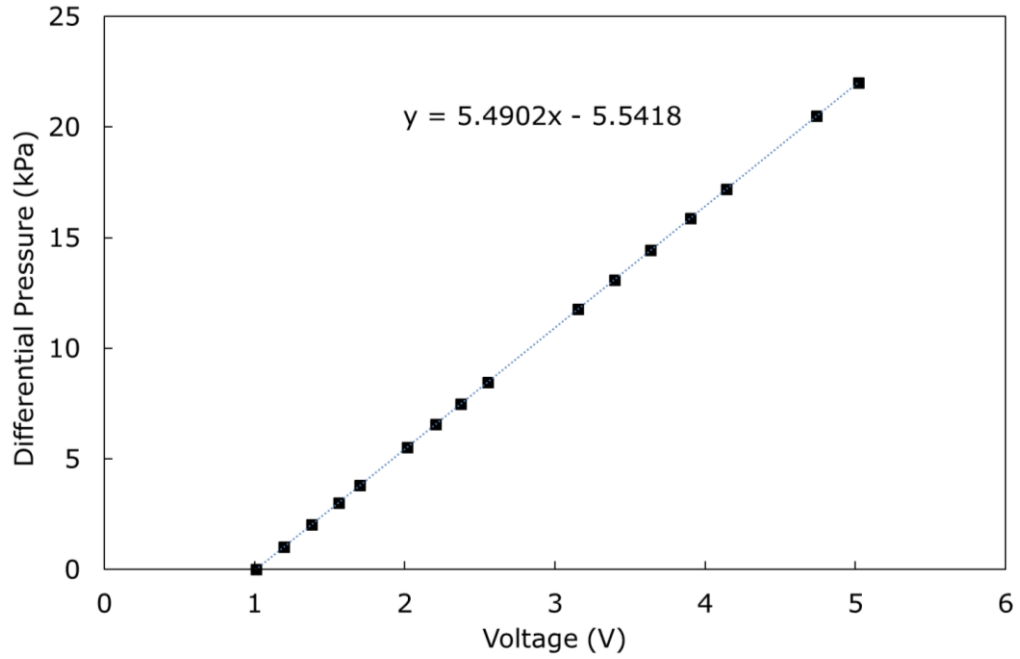


Figure 3.6: Calibration curve of DP transmitter for an air/water system

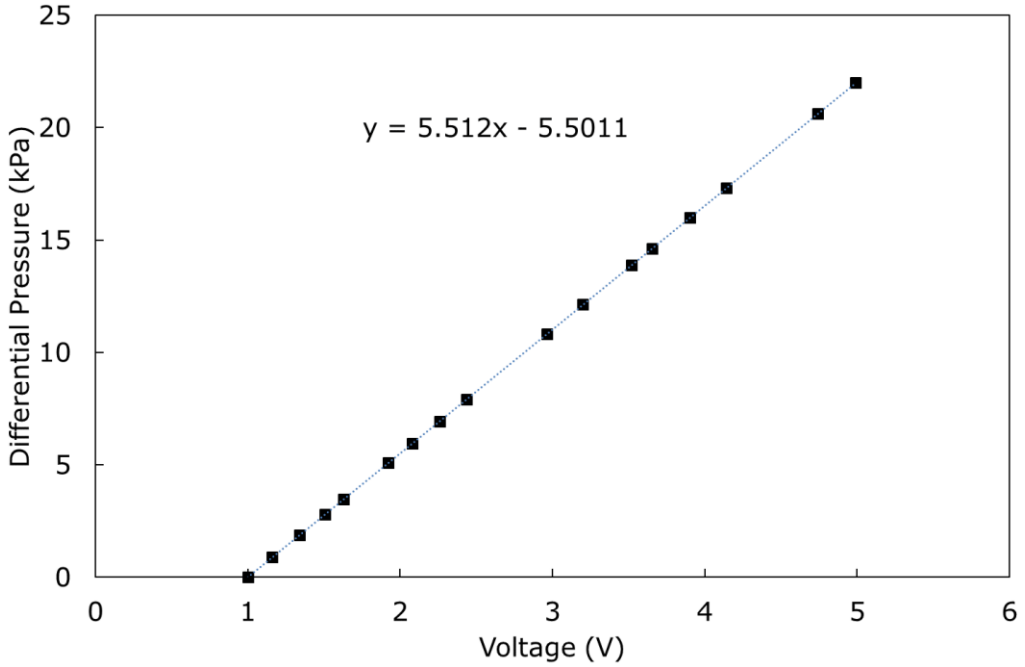


Figure 3.7: Calibration curve of DP transmitter for an air/silicone oil system

### 3.3.1.2. Single-phase Pressure Drop Measurements

In order to develop confidence about the two-phase pressure drop measurements, the single-phase pressure drop measurements using water were validated over the same measurement setup at 1.62m difference between the two pressure tapings in the rig. The single-phase measurements were compared with the calculated values for a smooth pipe using Darcy-Weisbach equation (Equation 3.5).

$$\frac{\Delta p}{L} = f_D . \frac{\rho_l}{2} . \frac{U_{sl}^2}{d_o} \tag{3.5}$$

where $\frac{\Delta p}{L}$ is the frictional pressure loss per unit length, $\rho_l$ is the liquid density of the fluid, $d_o$ is the pipe internal diameter, $U_{sl}$ is the liquid superficial velocity and $f_D$ is the Darcy friction factor.

The Darcy friction factor, $f_D$ for the turbulent flow was found using Moody Diagram, Colebrook-White equation, and Blasius equation. There are large number of equations available in the literature to calculate Darcy-Weisbach friction factor for turbulent flow. The above three were selected as they are the most well-known and used.

The Darcy-Weisbach friction factor for the turbulent flow was measured from Moody Diagram. The Colebrook-White equation (Equation 3.6) is

$$\frac{1}{\sqrt{f_D}} = -2.0 \log_{10} \left( \frac{\frac{\epsilon}{d_o}}{3.7} + \frac{2.51}{Re\sqrt{f_D}} \right) \tag{3.6}$$

where $\epsilon$ is the relative pipe roughness (0.0025) and $Re$ is the Liquid Reynolds number $\mathrm{Re} = \frac{\rho_l U_l d_o}{\mu_l}$ ($\mu_l$ is the liquid viscosity).

The Blasius equation (Equation 3.7) is

$$f = \frac{0.079}{\mathrm{Re}^{0.25}} \tag{3.7}$$

The Darcy friction factor was calculated by multiplying the friction factor calculated by Blasius equation by 4 because the Blasius equation is used to calculate the Fanning friction factor which equals one-quarter of the Darcy friction factor. The total single phase pressure drop was calculated by adding the gravitational pressure drop ($\rho_l gL$) to the frictional pressure drop calculated by using Darcy-Weisbach equation (Equation 3.5).

The single-phase pressure drop measurements were performed using water and repeated three times. There was a good agreement between the measured pressure drop and the calculated pressure drop using Moody Diagram, Colebrook-White equation, and the Blasius equation as shown in Figure 3.8. The uncertainty of the pressure drop measurement is affected by the accuracy of the flow measurement which is +/-5% of full scale. This means the uncertainty at the low velocity is higher than the uncertainty at maximum velocity. However, the overall relative error of pressure drop between the measured and calculated is within +/-0.21%. For example, the error at the maximum point between measured and calculated using Colebrook-White equation will be reduced from 0.16% to 0.03% if the liquid flow rate is taken as 1.14 m/s instead of 1.15 m/s.

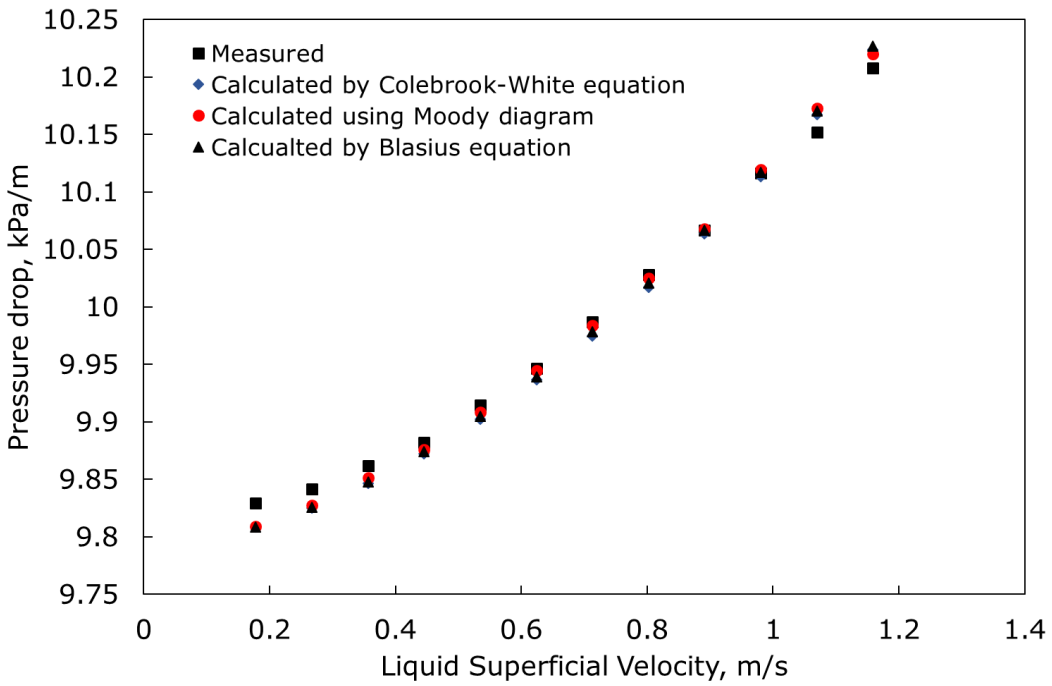


Figure 3.8: Single phase pressure drop using water comparison with pressure drop calculated by using Moody Diagram, Colebrook-White equation, and Blasius equation.

### 3.3.2. Liquid Film Thickness Measurement

In the current study, Multi Pin Film Sensor (MPFS), concentric probe and ultrasonic sensor were used to measure the instantaneous and averaged liquid film thicknesses. The Multi Pin Film Sensor (MPFS) and concentric probe were used to measure the liquid film thickness of an air/water system on the free falling liquid film annular flow test facility and the upward vertical annular flow test facility respectively. In addition, both techniques were used to evaluate the performance of ultrasonic technique as part of the evaluation methods in order to use the ultrasonic technique to measure the liquid film thickness of an air/silicone oil system in the upward vertical annular flow test facility. Both the

Multi Pin Film Sensor (MPFS) and concentric probe are based on conductance measurements and required a liquid that is electrically conducting. They were non-intrusive and flush mounted with the inner pipe wall on a separate flange. The ultrasonic technique is based on acoustic measurement and can be employed on conducting and non-conducting liquid. It is non-intrusive and detached to the outside wall of the test section using a special clamp flange to hold the transducer.

Next, MPFS and concentric probe measuring principle and their calibration are described below where the ultrasonic technique and the validation methods are discussed in Chapter 5.

#### 3.3.2.1. Multi Pin Film Sensor (MPFS)

The Multi Pin Film Sensor (MPFS) is based on measurements of the electrical conductance between two electrodes in contact with the liquid film. The MPFS measurements are similar to other conductance measurement techniques that have been used in literature include Zabaras et al. (1986), Fore and Dukler (1995), Conte (2000) and Zangana (2011). The main difference between the MPFS and the other measurement techniques in literature is that the MPFS is capable to measure the instantaneous film thickness at 10 axial positions simultaneously whereas the one in literature has been used to measure the instantaneous film thickness at only one axial position. The MPFS consists of 10 measurement locations in the axial direction times 64 measurement locations in the circumferential direction as shown in Figure 3.9. This means there are 640 measurements points. The ultrasonic measurement was compared with one of

these 64 measurements in the first axial location that is aligned with the ultrasonic transducer. The first MPFS design was used by Belt (2007) where 32 measurement locations in the circumferential direction were used instead of 64 measurement locations. The main difference is due to the difference in the pipe diameter used by Belt (2007) which was 50 mm compared to the current pipe diameter of 127 mm. Additional details about MPFS can be found in Belt (2007) and Abbas Hasan et al. (2016) who have employed this technique.

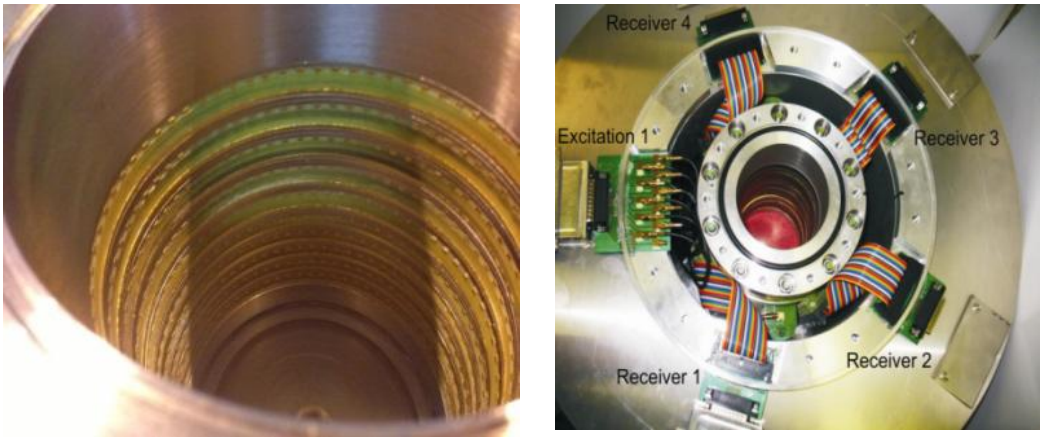


(a) (b)

Figure 3.9: Multi Pin Film Sensor (MPFS), Inner (a) and electronic connections (b)

### 3.3.2.2. Concentric Probe

The concentric probe operates by relating the film thickness to conductance across the two electrodes. The concentric probe works on the same principle as MPFS but it was designed to measure the instantaneous film thickness at only four circumferential positions in one axial direction separated by $90^{o}$ angle. The probes were designed and constructed by Zhao et al. (2013) and used to measure the film thickness with pipe diameter 34.5mm. This is similar to the current

experiment arrangement as part of the collaborative work with the Imperial College. The concentric probe in Figure 3.10 consists of the central pin with a diameter (d1) of 3.2 mm and the outer ring with an internal diameter (d2) of 13.2 mm and an outer diameter (d3) of 13.4 mm. The probe was installed flush with inner surface of a separate flange. More details about the design in terms of dimensions specification and precautions can be found in Zhao (2014). The concentric probe was used by different researchers in the past such as Azzopardi (1986) and Wolf (1995). There are four concentric probes but in the current experiment, the ultrasonic technique was compared with one probe where both of them were aligned and separated by 70mm due to flange arrangement.

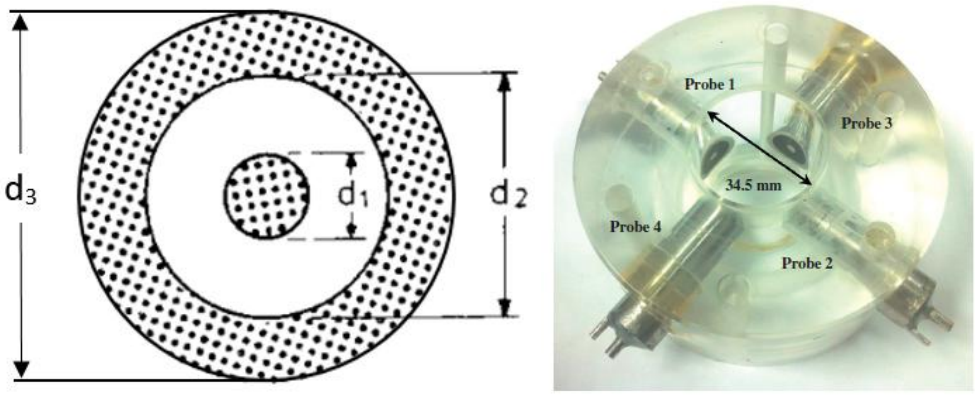


Figure 3.10: Schematic and arrangement of concentric probes (Zhao et al. (2013))

### 3.3.2.3. Calibration Procedure of MPFS and Concentric probes

The MPFS and the concentric probe were all calibrated using the same method. They were calibrated by inserting different known diameters of non-conducting solid rods (PVC) inside the sensor in which the remaining annulus was filled with water under test. The water simulates a film of known thickness that can be related to the measured probe output voltage. These rods were machined very carefully with accuracy better than 10μm. The calibration was repeated three times. In order to ensure the annulus gap represented the expected film thickness, the rod was centered at the bottom using a base block and at the top using a plastic insert guide. The calibration setup of the concentric probe is shown in Figure 3.11. More details about the calibration of the MPFS can be found in Abbas Hasan et al. (2016).

The calibration of the four probes was performed simultaneously where the electronic box is capable to drive five probes at the same time. The electronic circuit was designed and used by Conte (2000). It was also used by Zangana (2011) to measure the film thickness using pin probes. The probes were supplied by 10 kHz alternating current. The signals from the probe were transferred to a buffer amplifier and a low-pass filter before sending them to the data acquisition system. The calibration of the concentric probe was repeated three times as shown in Figure 3.12 for probe 1. The maximum standard deviation between repeated runs was 0.07 volt. An example of the calibration curve of a measuring receiver of MPFS which relates the output current (in Analogue-to-digital converter, ADC unit) with the liquid film thickness is shown in Figure 3.13.

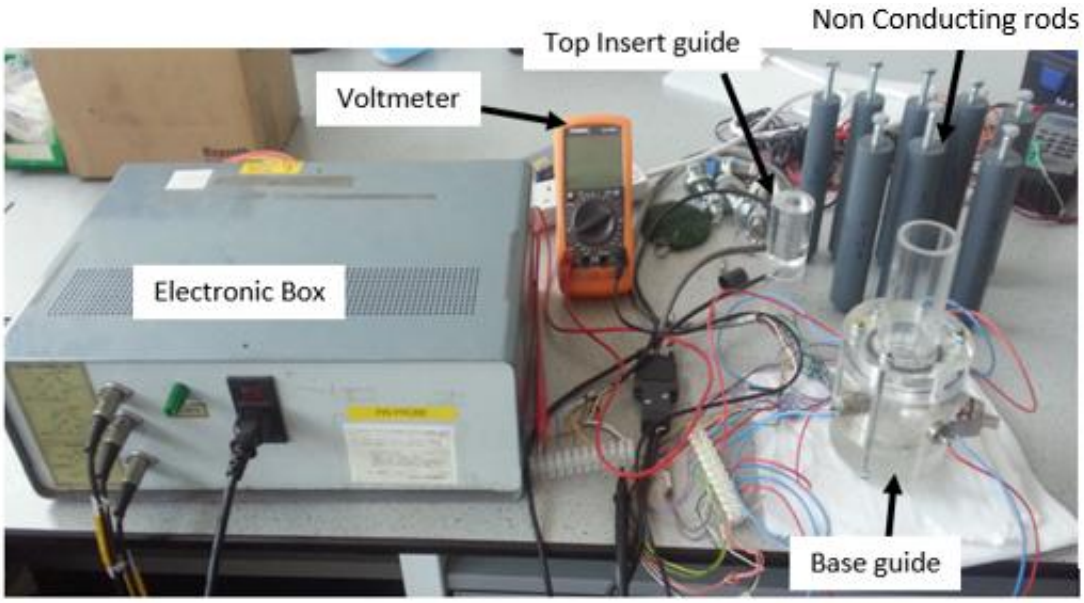


Figure 3.11: Calibration setup of the concentric probes.

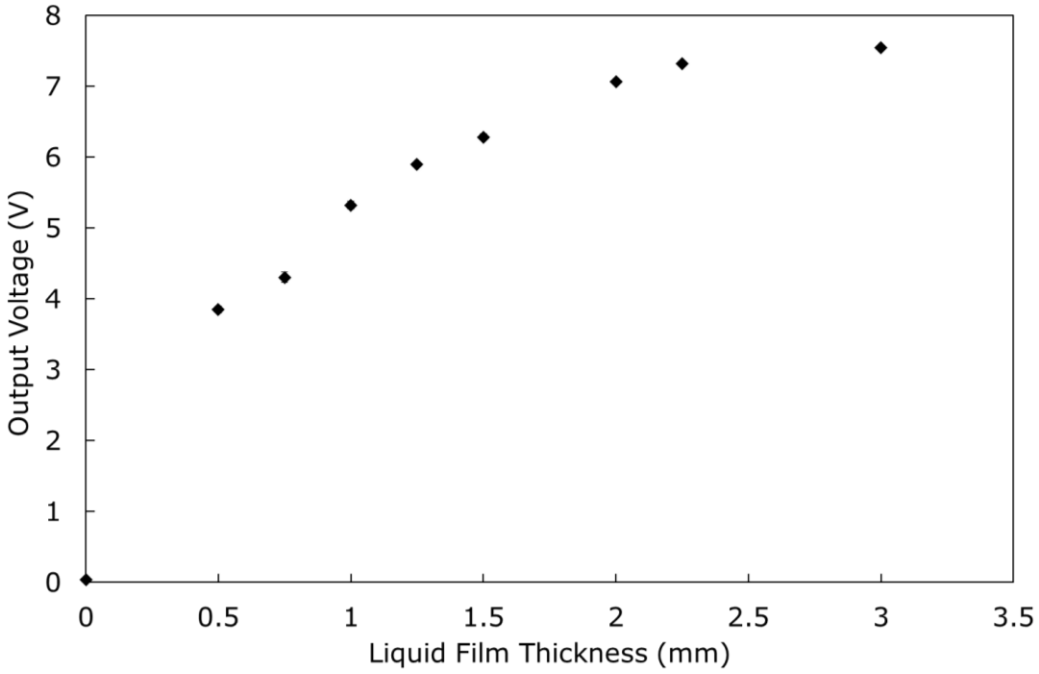


Figure 3.12: Calibration curve of the concentric probe 1. The plot shows the voltage measurements for three repetitions with maximum standard deviation between them was 0.07 volt.

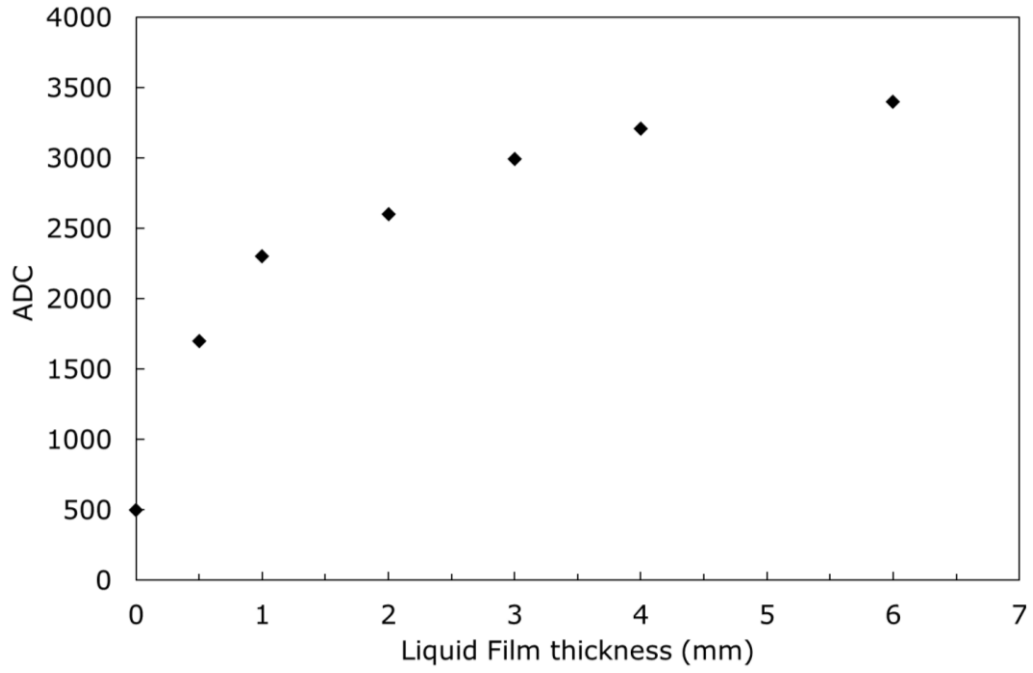


Figure 3.13: Calibration curve of the MPFS (Abbas Hasan et al., 2016).

### 3.3.3. Wall Shear Stress Measurement

Wall shear stress was measured using a commercial glue-on flush mounted hot film probe from Dantec dynamics (Dantec 55R47) based on the evaluation outcome in Chapter 2. All the wall shear stress measurements were conducted in the fully developed annular flow region above the flow reversal region as discussed in Section 3.2.1 and Chapter 4. The measuring principle and calibration procedure are discussed in the following subsections.

### 3.3.3.1. Principle of operation of hot film probe

Wall shear stress ($\tau_w$) is measured using a small, electrically heated probe to a constant temperature and mounted flush with the inner diameter of the pipe. The wall shear stress is related to the measuring voltage (V) generated by a constant temperature anemometer that senses the changes in the heat transfer from the heated probe exposed to fluid motion. This relationship is described by equation (3.8) which has been used by researchers utilising flush mounted hot film probes in two-phase flow e.g., Martin (1983), Whalley and McQuillan (1985), Govan et al. (1989), Wolf (1995) and Zangana (2011).

$$V^2 = A + B\tau_w^{1/3} \tag{3.8}$$

where A and B are constants which are related to the physical properties of the fluid near the probe and the geometry of the probe making probe calibration essential (Martin, 1983, Boyer et al., 2002).

The above relationship in Equation 3.8 is valid when the thermal boundary layer thickness ($\delta_T$) is smaller than the laminar sublayer of the momentum boundary layer. The thermal boundary layer thickness ($\delta_T$) of the hot film probe can be calculated using the following equation 3.9 (Martin, 1983):

$$\delta_T = \frac{k}{h} = 1.86\left(\frac{\mu\alpha x}{\tau_w}\right)^{1/3} \tag{3.9}$$

where k is the thermal conductivity of the liquid, h is the heat transfer coefficient from heated wall to the fluid, μ is the liquid viscosity, α is the thermal diffusivity of the liquid, x is the width of the probe and $\tau_w$ is wall shear stress.

Martin (1983) and Zangana (2011) showed that if the wall shear stress is less than 100 Pa, the thermal boundary layer will be smaller than the laminar sublayer of the momentum boundary layer for hot film probes with widths 0.1 mm and 0.2mm. There is another limitation of using this relationship in the two-phase flow where the thermal boundary layer thickness ($\delta_T$) should not exceed the liquid film thickness. In the current study, the thermal boundary layer is much lower than the minimum liquid film thicknesses (0.1mm). The hot film probe width used in the current experiment was 0.1 mm. The thermal boundary layer at minimum wall shear stress of 6 Pa is 0.023 mm with water and 0.031 mm with silicone oil. The thermal boundary layer at maximum wall shear stress of 25 Pa is 0.014 mm with water and 0.021 mm with silicone oil.

The anemometer is used to keep the probe temperature constant. A Wheatstone bridge is the main component of the anemometer circuit where the wall shear stress probe is connected to one of its arms as shown in Figure 3.14. Its operation relies on the variation of the electrical resistance of the probe material with temperature. When the velocity of the fluid passing over the probe increases, the probe temperature hence its resistance fall. This generates imbalance to the bridge (Equation 3.10). This is sensed by the servo amplifier which signals the current source to increase its output voltage to reheat the probe in order to rebalance the bridge. The increase of the voltage indicates the increase of the heat transfer and the wall shear stress. This operation occurs instantaneously which means any variation in probe resistance will be captured, hence wall shear stress (Hanratty and Campbell, 1996).

$$\frac{R_{var}}{R_1} = \frac{R_c + R_{ps} + R}{R_{int}} \tag{3.10}$$

where $R_{var}$ is the variable resistance in the bridge, $R_1$ and $R_{int}$ are the internal resistances in the bridge, $R_c$ is the resistance of the cable to the hot film probe, $R_{ps}$ is the resistance of the probe support and R or $R_w$ is the resistance of the probe at its operating temperature.

As the probe temperature hence its resistance has to be kept constant by the anemometer, an overheating ratio (a) needs to be defined. The overheating ratio should be selected where the probe temperature has to be higher than the bulk temperature that makes the probe less sensitive to the variation in the bulk temperature and prevent bubble formation on the probe. The overheating ratio (a) can be calculated by using the following relationship:

$$a = \frac{R_w - R_{ref}}{R_{ref}} = \alpha_{ref}(T_w - T_{ref}) \tag{3.11}$$

where $R_w$ is the resistance of the probe at its operating temperature $T_w$, $R_{ref}$ is the sensor resistance at reference temperature $T_{ref}$ and $\alpha_{ref}$ is the sensor temperature coefficient of resistance at $T_{ref}$.

In the current study, MiniCTA Anemometer made by Dantec Electronics Ltd was used as a constant-temperature anemometer and the operating manual is provided in Appendix 1.

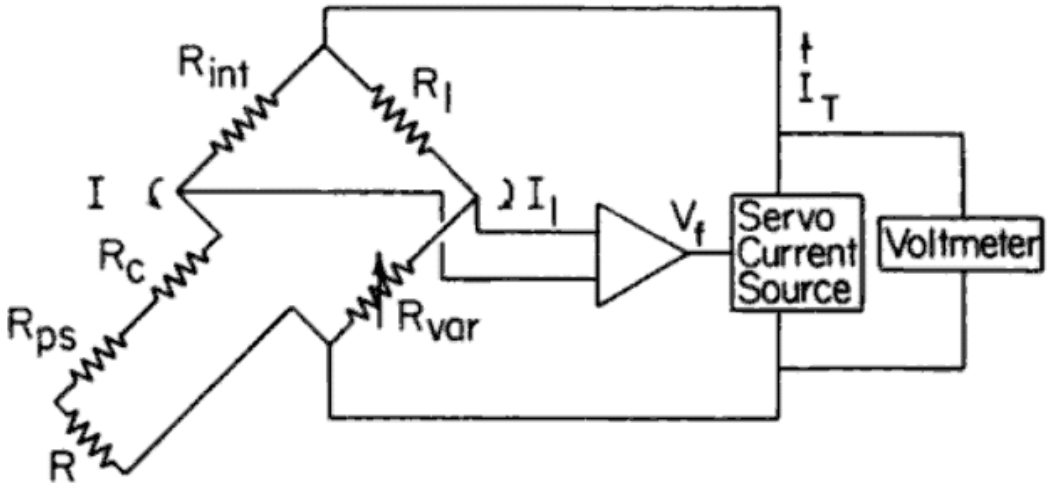


Figure 3.14: The electrical circuit of a constant-temperature anemometer (Hanratty and Campbell, 1996).

### 3.3.3.2. Temperature correction

The probe temperature is affected by liquid velocity and liquid bulk temperature. An increase in the bulk temperature would make the anemometer circuit believe that the fluid slowed down since less heat was transferred. Therefore, an effort was made to make the bulk temperature constant when obtaining the measurements by controlling the storage tank temperature as discussed in Section 3.2.1. All the measurements were recorded at the calibration temperature by allowing enough time for the temperature to reach the same calibration temperature. Before the calibration and measurements, the flowing rig temperature was allowed to stabilize by running the rig for a period of time (around 2 hours). When the gas or liquid flow rate changed, the temperature was allowed to stabilize before recording the data. In addition, the bulk temperature close to the hot film probe was measured using T-type thermocouple for

temperature correction as there was a small temperature variation within ±0.7$^{o}$C during the measurements over the full range of gas flow rate at fixed liquid flow rate. The following correction relationship recommended by the MiniCTA Anemometer manufacturers was used:

$$E_{corr} = \left(\frac{T_w - T_{ref}}{T_w - T_{acq}}\right)^{0.5} . E_{acq} \quad (3.12)$$

where $E_{corr}$ is the corrected voltage, $E_{acq}$ is the measured voltage, $T_w$ is the operating temperature of the sensor, $T_{ref}$ is the reference temperature and $T_{acq}$ is the acquisition of actual flow temperature.

### 3.3.3.3. Calibration of the hot film wall shear stress probe

In order to find the constant A and B in equation 3.8, the hot film probe has to be calibrated. The probe has to be calibrated in situ on the rig where the measurements are to be taken, as these constants are related to the physical properties of the fluid near the probe and the geometry of the probe. In addition, the probe is sensitive to the change in position (Bruun, 1995).

Previous researchers in two-phase flow applications have calibrated the hot film probe using the differential pressure measurement in single phase flow or in two-phase flow. Single phase flow calibration was widely employed by different researchers such as Martin (1983), Whalley and McQuillan (1985), Shaha (1999), Descamps et al. (2008) and Zangana (2011). The two-phase flow calibration was used by researchers including Owen (1986), Govan et al. (1989) and Wolf (1995). In the present study, the two phase calibration was used because the two-phase annular flow wall shear stress is greater than the single

phase wall shear stress according to the measurements completed by the above researchers. This means that the single phase calibration requires very large liquid flow rates and the current test facility can not deliver these large flow rates. The two phase calibration has to be performed at low liquid flow rate where there is no entrainment. This was estimated by defining the critical liquid Reynolds number ($Re_{LFC}$) using Owen and Hewit (1986) correlation:

$$Re_{LFC} = \exp\left[5.8405 + 0.4249\frac{\mu_g}{\mu_l}\sqrt{\frac{\rho_l}{\rho_g}}\right] \tag{3.13}$$

where $\mu_l$ and $\mu_g$ is the liquid and gas dynamic viscosities, and $\rho_g$ and $\rho_l$ are gas and liquid densities.

The wall shear stress ($\tau_w$) was calculated from the measurement of two phase pressure drop $\left(\frac{dp}{dz}\right)_{tot}$ using the following relationship:

$$\left(\frac{dp}{dz}\right)_{tot} = \frac{4\tau_w}{d} + g\left[\rho_g\varepsilon_g + (1-\varepsilon_g)\rho_l\right] \tag{3.14}$$

where d is pipe diameter, $\varepsilon_g$ is the void fraction, g is the acceleration due to gravity. The void fraction ($\varepsilon_g$) was calculated from the film thickness measurement ($\delta$) by the following equation:

$$\varepsilon_g = \left(1 - \frac{2\delta}{d}\right)^2 \tag{3.15}$$

The cubic root of the calculated wall shear stress at different gas flow rates was plotted against the square of the anemometer output voltage in order to obtain the value of the constant A and B in equation (3.8). The calibration curve of the probe for water and silicone oil are shown in Figure 3.15 and Figure 3.16 respectively.

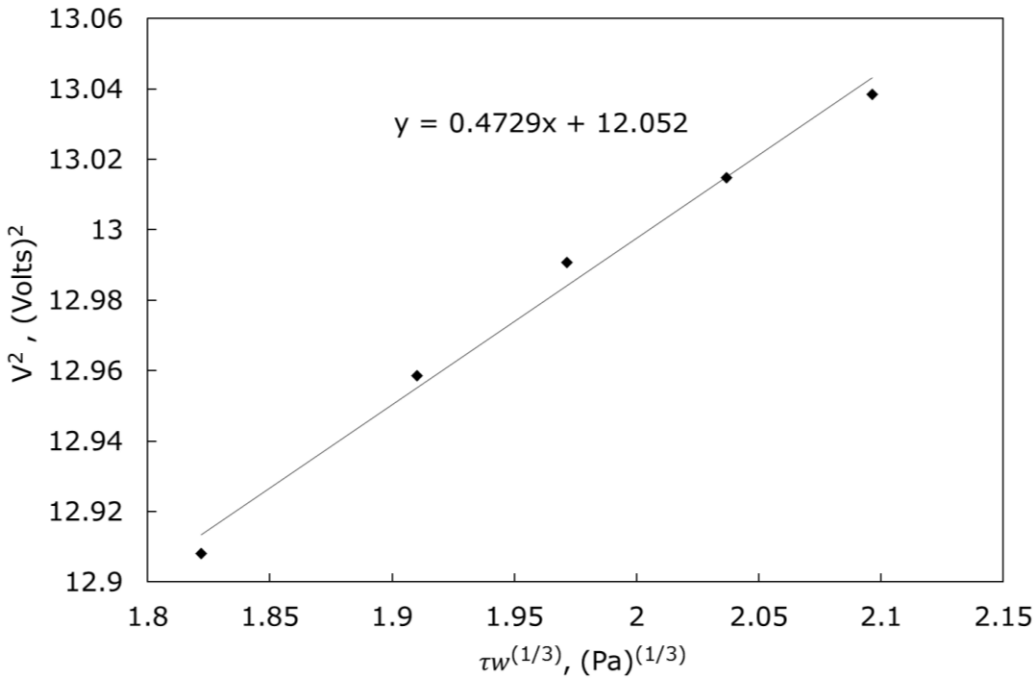


Figure 3.15: Two phase calibration curve of the wall shear stress hot film probe using an air/water system.

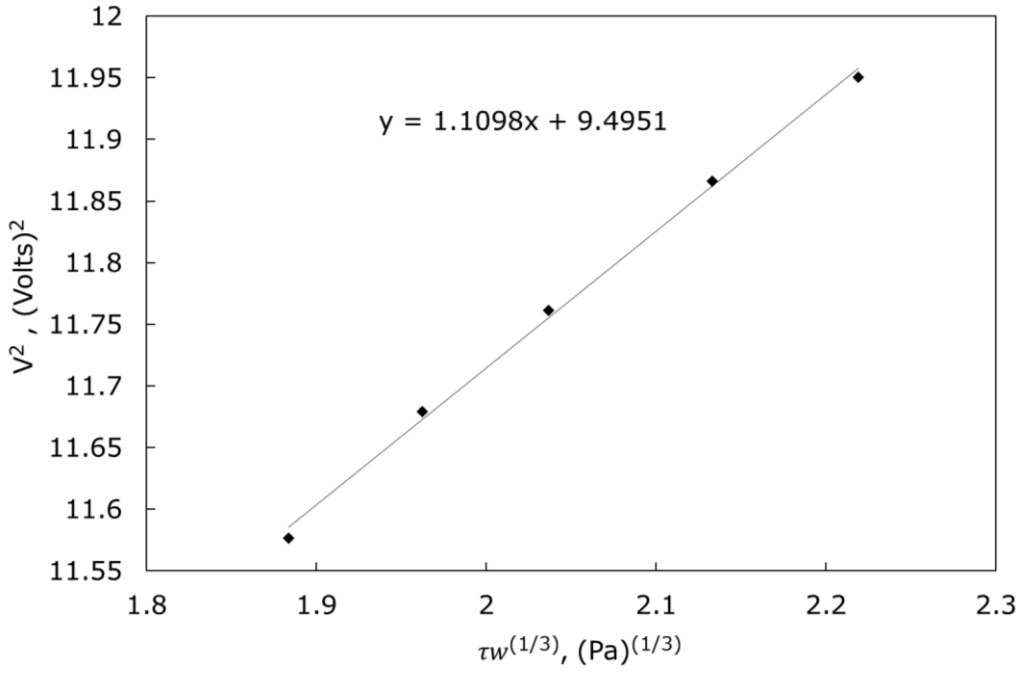


Figure 3.16: Two phase calibration curve of the wall shear stress hot film probe using an air/silicone oil system.

#### 3.3.3.4. Hot film probe (Dantec 55R47)

In the current study, the wall shear stress was measured using the commercial glue on hot film probe (Dantec 55R47) supplied by Dantec Electronics Ltd. The probe is made of a thin nickel film (0.1 mm x 0.9 mm) deposited on a 0.05 mm thick polyamide foil and coated with a 0.5 μm of quartz for protection against electrolytic attack. The electrical connection is made of a gold plated area where copper wires (0.1 mm thick) are soldered onto it and used to connect the probe to the anemometer. A special Perspex plug and a separate flange were designed and fabricated to ensure the probe installed tight and flush with surface and allowed easy removal for checking. The probe was glued into the Perspex plug face that had the same curvature as the pipe with Loctite glue. The probe wires were fed through a pair of holes in the plug which were sealed with the Perspex glue (Tensol cement) to prevent any leakage. Then, the plug was inserted into the prepared flange until the probe surface was aligned flushed with the tube wall by using two bolted screws. The plug was sealed and made leak tight by using an O-ring. Two other bolted screws were used to guide and help on removing the plug out from the flange after removing the first two. Probe wires were soldered and connected to BNC plug which was used to connect MiniCTA cable. The hot film probe installed on the plug is shown in Figure 3.17.

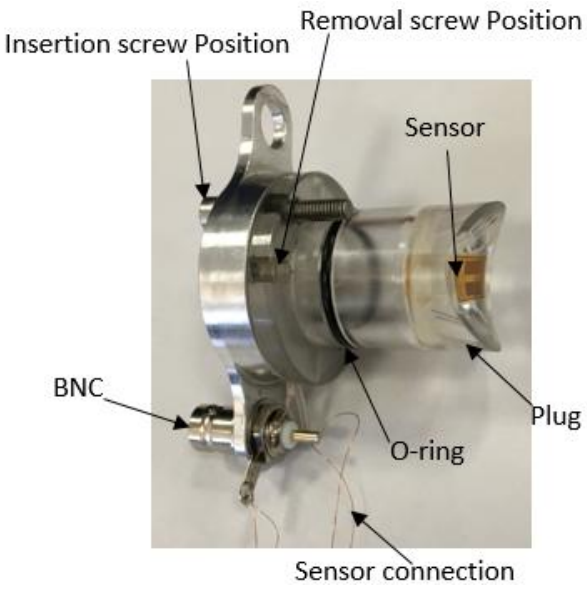


Figure 3.17: Hot film probe (Dantec 55R47) installed on the plug.

### 3.3.4. Thermocouple

The temperature measurement was one of the most important measurements in current study especially the temperature measurement close to the measurement section. It was used for temperature compensation for the hot film probe and the liquid speed of sound calculation for the ultrasonic technique. Four temperature sensors (T-type thermocouple, TC Direct Ltd) were used. Two of them were installed after gas and liquid flow meters and the other two were installed after the injector and close to the measurement section. Calibration of these thermocouples was performed using ice and water at different temperatures up to 100$^{o}$C. The thermocouple was connected to a temperature transmitter (RS component Ltd) which converts the thermocouple voltage measurement (mV) to an output voltage (1-5V). The temperature transmitter has zero and span functions that can adjust the zero temperature to 1V and 100$^{o}$C to 5V. The measured output voltage of the thermocouple using voltmeter was related to the

measured temperature using a digital thermometer (E.T.I. Ltd) with an accuracy of $\pm 1^{o}$C. All the measurements were taken simultaneously and the calibration curve was obtained after adjusting zero and span until repeated measurement obtained as shown in Figure 3.18.

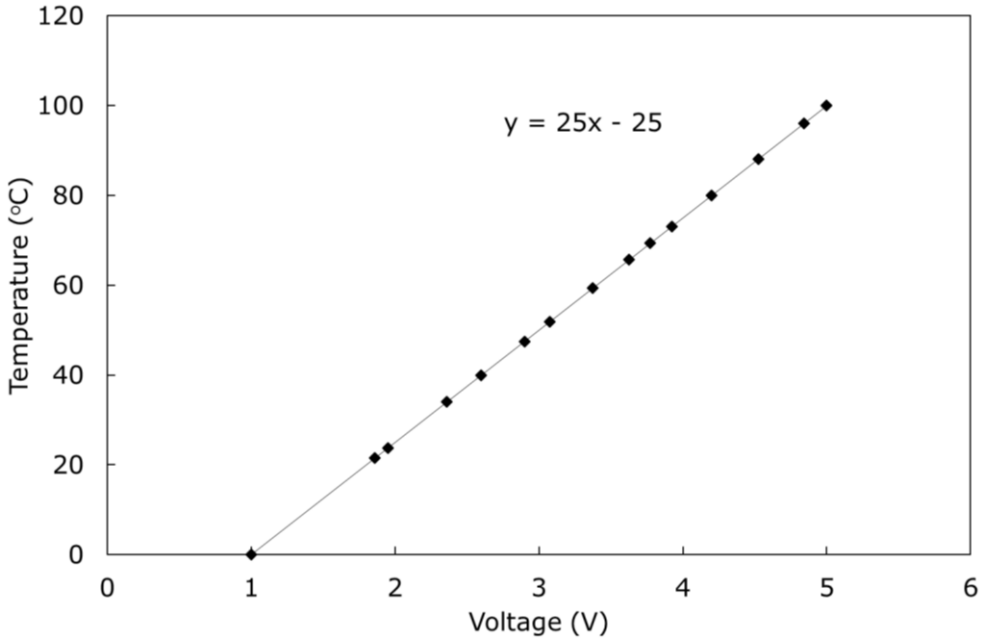


Figure 3.18: Thermocouple calibration curve.

### 3.3.5. Data Acquisition

In the current study, LabView (National Instruments, version 2013) was used as a data acquisition (DAQ) system. It acts as an interface between the measurement sensors and the computer where the sensor signals were converted by inserting the calibration curve equation to the physical values of the corresponding measurements. The data sampling rate for the present study was 500Hz for duration of 30 seconds. The sampling rate was selected to match with the maximum sampling rate by the ultrasonic sensor. All of the measurement were recorded simultaneously and saved as Excel files.

# CHAPTER 4

# TWO-PHASE PRESSURE DROP MEASUREMENTS

The importance of pressure drop measurement in equipment and pipeline design of two-phase systems has attracted researchers, as an example, it governs the pumping requirement to move the fluids. Most of previous studies were conducted using an air/water system to find the relationship between pressure drop, film thickness and wall shear stress. The aim of the current study is to understand the relationship between the three parameters and test existing correlations using an air/silicone oil system. Therefore, the two-phase pressure drop across the test section (34.5mm inner diameter) and over an axial distance of 1.62 m between the two pressure tapings was measured using differential pressure transducer (Remote seal Rosemount 3051 model). The two-phase pressure drop measurements were conducted for air/water and air/silicone oil systems between gas superficial velocities ranging from 17.83 m/s to 35.66 m/s, and liquid superficial velocities ranging from 0.018 m/s to 0.089 m/s with water, and from 0.018 m/s to 0.094 m/s with silicone oil.

In this chapter, the experimental results of the two phase pressure drop for air/water and air/silicone oil systems are presented. In Section 4.1, the method for identifying the annular flow regime and ensuring the liquid film is moving in an upwards direction is discussed. Section 4.2 discusses the effect of gas and liquid superficial velocity on two-phase pressure drop. The effect of viscosity

and surface tension are presented in Section 4.3. Finally, prediction correlations for two-phase pressure drop are evaluated against measured two-phase pressure drop in Section 4.4.

## 4.1. Annular Flow Regime Identification

The current study is focused on the vertical upward annular flow regime. Therefore, it is important in the current experiments to ensure that the annular flow regime is achieved and the liquid film is moving in an upwards direction. One of the main important criteria is to define a minimum gas superficial velocity in order to ensure there is no flow reversal where all the liquid film is moving in the upwards direction (Hewitt et al., 1965). Most of the previous researchers such as Owen (1986), Govan et al. (1989) and Wolf (1995), Zangana (2011) and Zhao (2014) have used Wallis parameter ($U_g^*$) to define the point where there is no flow reversal by the relationship between pressure drop and dimensionless gas superficial velocity as defined by Wallis (1962). The dimensionless gas superficial velocity ($U_g^*$) is expressed by Equation 4.1:

$$U_g^* = U_{sg}\left(\frac{\rho_g}{gD(\rho_l-\rho_g)}\right)^{0.5} > 1 \qquad (4.1)$$

where $U_{sg}$ is the gas superficial velocity, $\rho_l$ and $\rho_g$ are the liquid and gas density respectively, D is the pipe internal diameter and g is the gravitational acceleration.

According to Hewitt and Hall-Taylor (1970), the minimum pressure gradient is defined as the point where the annular flow exists and this is related to the Wallis parameter ($U_g^*$). They indicated that the minimum pressure gradient point will depend on the method of injection in which the annular flow may exist at a gas flowrate down to a $U_g^*$ value of 0.8 and is possible for even lower. In addition, the above researchers have used another parameter called Kutateladze number, $Ku_g$ (Equation 4.2). The Kutateladze number ($Ku_g$) is used to ensure the gas velocity is sufficient to suspend the entrained droplets (Taitel et al., 1980). The annular flow exists when the $Ku_g$ is greater than 3.2.

$$Ku_g = U_{sg}\left(\frac{\rho_g^2}{g\sigma(\rho_l-\rho_g)}\right)^{0.25} > 3.2 \qquad (4.2)$$

where σ is the surface tension.

As can be seen in Figure 4.1 for the air/water system and Figure 4.2 for the air/silicone oil system, the minimum pressure gradient happens below the Kutateladze number and Wallis parameter for both systems. The minimum pressure gradient occurs at $U_g^*$= 0.532 and $Ku_g$ = 1.89 for the air/water system and at $U_g^*$=0.555 and $Ku_g$= 2.67 for the air/silicone oil system. These findings support the statement about the effect of the injection method on the minimum pressure gradient point. In the current study, a conical injector was used compared to a porous wall injection method used by Wallis (1962). In addition, the gas superficial velocity to meet Kutateladze number and Wallis parameter is lower for the air/silicone oil system compared to the air/water system. This means that the annular flow exists at lower gas superficial velocity for the air/silicone oil system compared to the air/water system. This highlights the

effect of the liquid properties such as surface tension. However, to ensure there is no flow reversal and the annular flow exists, the minimum gas flow rate considered in this study is at $U_g^* > 1$. Therefore, the annular flow regime exists between a gas superficial velocity ranging from 17.83 m/s to 35.66 m/s and liquid superficial velocity ranging from 0.018m/s to 0.089m/s with water and from 0.018m/s to 0.094m/s with silicone oil. The experiment ranges of gas and liquid superficial velocities for both systems based on above criteria were plotted on Taitel et al. (1980) flow pattern map for a 50mm pipe diameter (Figure 4.3). The experiment ranges of both systems are close to each other, therefore same points assume for both systems. Even though Taitel et al. (1980) flow map was developed for the air/water system, the range considered to ensure annular flow exists for air/silicone oil system shows a good agreement.

As can be observed from the Figures 4.1 and 4.2 for both air/water and air/silicone oil systems respectively, the maximum gas flow rate is not the same for all liquid flow rates because a liquid dry out was observed at the injector above the maximum plotted point where the liquid was completely removed. In Figure 4.2, the time-averaged pressure drop of the air/silicone oil system at a liquid superficial velocity of 0.018 m/s is zero due to the gas flow only and the liquid superficial velocity was not enough to lift the liquid.

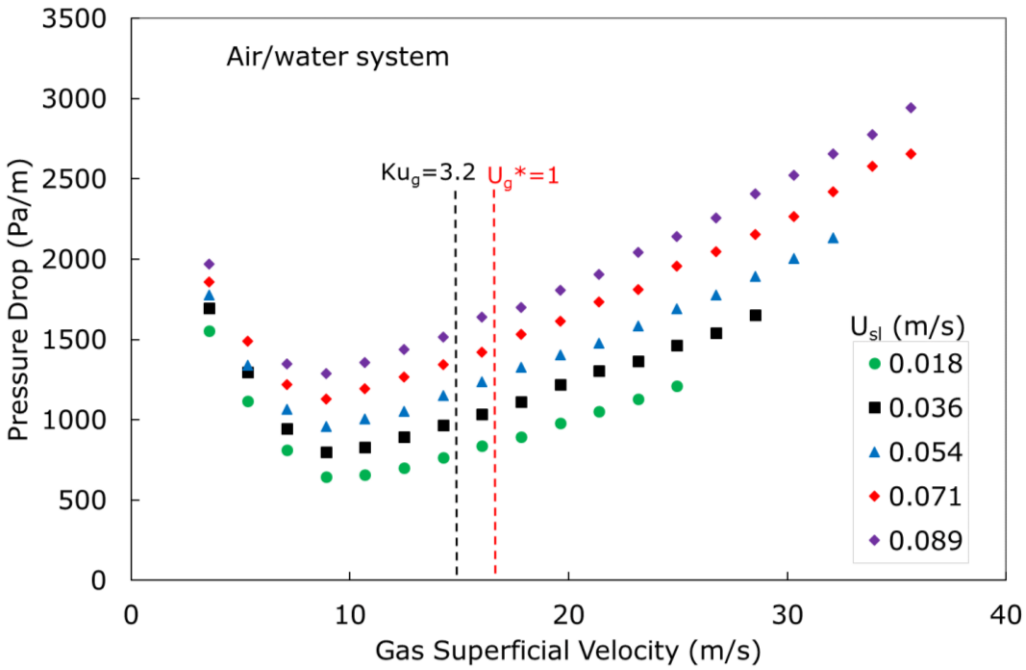


Figure 4.1: Two-phase Pressure drop measurement of an air/water system.

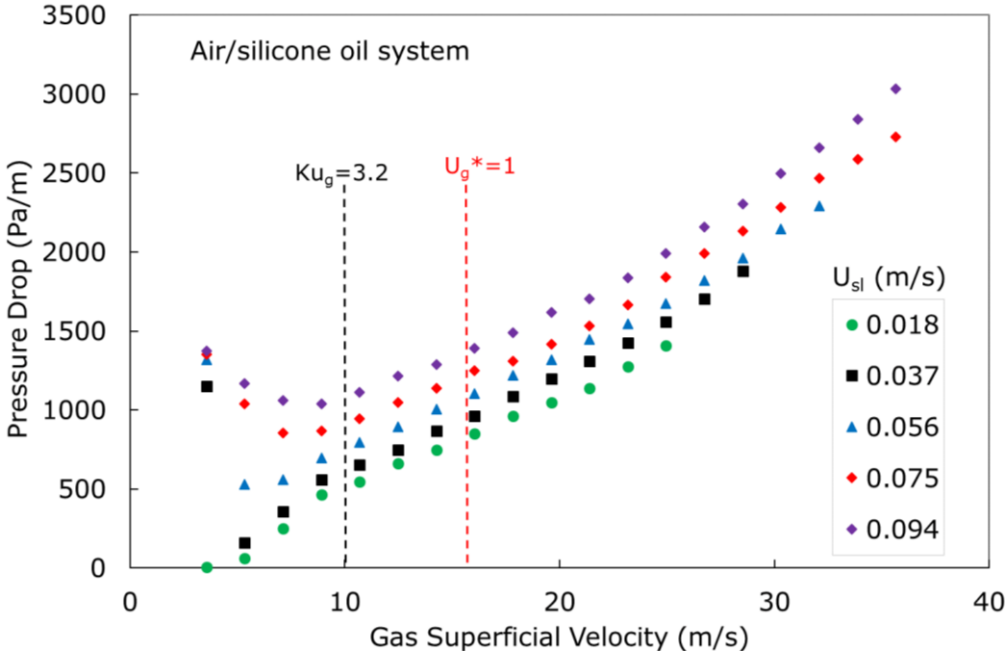


Figure 4.2: Two-phase Pressure drop measurement of an air/silicone oil system.

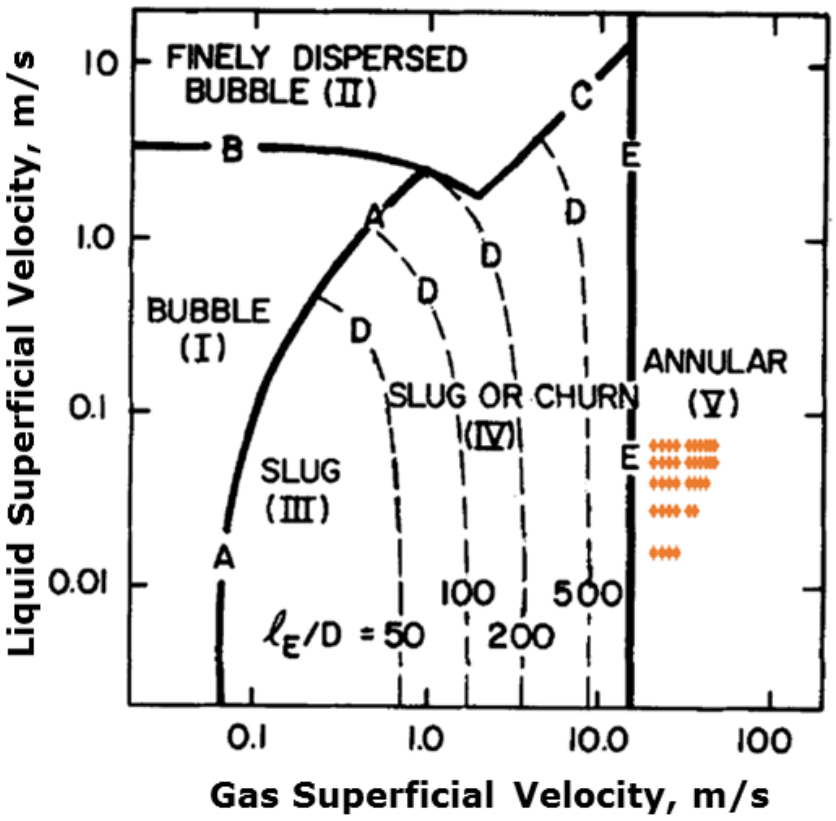


Figure 4.3: Experiment ranges for air/water and air/silicone oil systems plotted on Taitel et al. (1980) flow pattern map. The experimental ranges of both systems are close to each other, therefore same points assumed for both systems.

## 4.2. Effect of gas and liquid superficial velocity on two-phase pressure drop

Both gas and liquid superficial velocities have an impact on the total pressure drop. Owen (1986) used them to identify the flow regime by relating the dimensionless gas velocity ($U_g^*$) to a dimensionless pressure drop at fixed liquid mass flux as illustrated in the example in Figure 4.4.

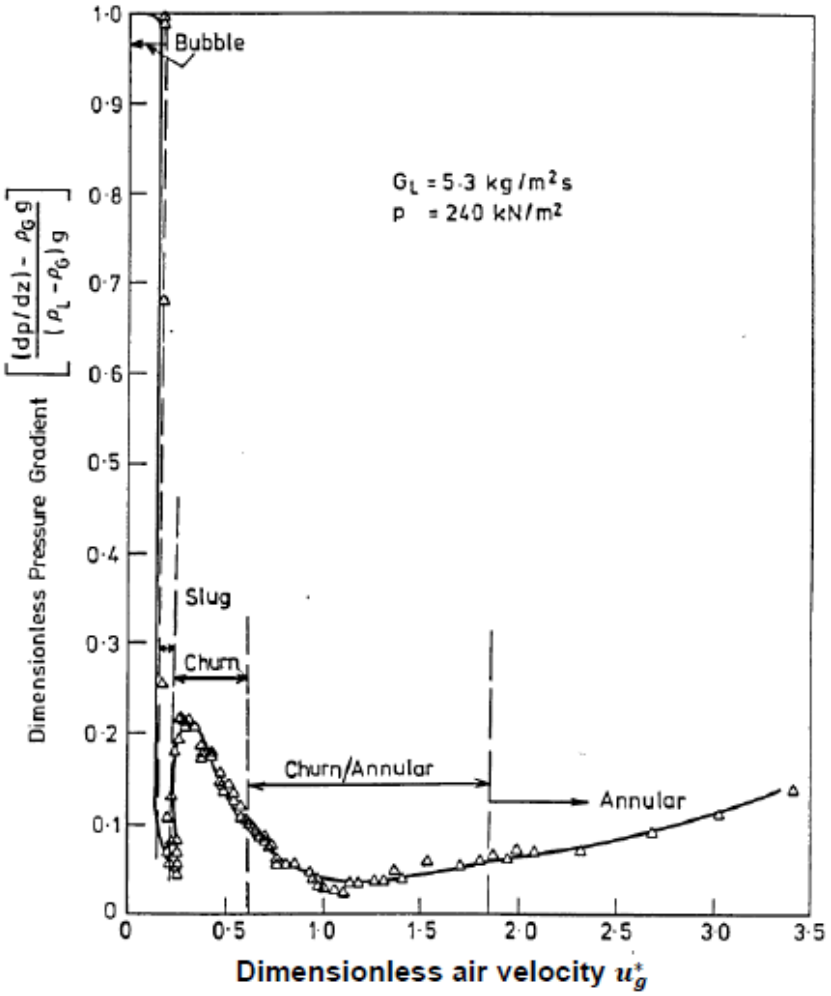


Figure 4.4: Flow regime map using pressure drop measurements at different gas flow rates and low liquid flow rate (Owen, 1986).

As discussed in section 4.1, for the air/water system the annular flow exists between gas superficial velocities ranging from 17.83 m/s to 35.66 m/s and water superficial velocities ranging from 0.018 m/s to 0.089 m/s. Figure 4.1 shows the influence of the gas and liquid superficial velocity on the time-averaged total pressure drop for the air/water system. The time- averaged total pressure drop of vertical upward annular flow increases with increasing the gas and liquid superficial velocities. A similar trend in vertical upward annular flow were reported by other researchers such as Martin (1983), Fore and Dukler (1995), Belt et al. (2010), Zhao (2014) and Pan et al. (2015b).

One of the characteristics of annular flow is the presence of disturbance waves at the liquid film/gas core interface. They are responsible for liquid droplet entrainment into the gas core (Azzopardi, 1997, Barbosa et al., 2002). The amount of entrainment rate is affected by the increase of gas and liquid superficial velocities. As the liquid superficial velocity increases, the disturbance waves appear that generate droplets entrained into the gas core. However, the increase of gas superficial velocity has more impact as it increases the interfacial shear force on the liquid film/gas core interface that leads to increase the entrainment rate. Fore and Dukler (1995) stated that the entrainment and deposition in the gas-liquid upward annular flow account for 20% of the pressure gradient. This finding was supported by Pan et al. (2015b) who indicated that the entrainment and deposition of droplets and gas eddy can account for approximately 14.5% of the pressure gradient.

For the air/silicone oil system, the annular flow regime exists between a gas superficial velocity ranging from 17.83 m/s to 35.66 m/s and liquid superficial velocity ranging from 0.018 m/s to 0.094 m/s with silicone oil. From Figure 4.2, the time-averaged total pressure drop of air/silicone oil system increases with increasing the gas and liquid superficial velocities. The increase of time-averaged total pressure drop of air/silicone oil system shows a similar trend to the increase of time-averaged total pressure drop of air/water system with increasing the gas and liquid superficial velocities. These results indicate that the effect of gas and liquid superficial velocities on time-averaged total pressure drop for both systems exhibit same behaviour even with changing the liquid properties. The influence of the liquid properties (i.e viscosity and surface tension) on time–averaged total pressure will be discussed in Section 4.3.

As mentioned above the droplet entrainments contribute to the pressure drop. Therefore, the prediction of the droplet entrainments rate ($\dot{m}_{le}$) is important. In the current study, the entrainment rate ($\dot{m}_{le}$) at each flow rate was calculated using Al-Sarkhi et al. (2012) entrainment correlation. Four entrainment correlations were evaluated that were widely used in literature. These correlations are Oliemans et al. (1986), Ishii and Mishima (1989), Sawant et al. (2008) and recently Al-Sarkhi et al. (2012) as discussed in Chapter 2. The last three correlations show almost the same results for air/water system as shown in Figure 4.5. Both Sawant et al. (2008) and Al-Sarkhi et al. (2012) correlations achieved similar results in predicting entrainment when the air/silicone oil system was used as shown in Figure 4.6. However, all four correlations were developed using the air/water system and their accuracy to predict the entrainment with the air/silicone oil cannot be assessed where further work is

still required by measuring the entrainment rate of different surface tension and viscosity using same entrainment measurement technique. Sawant et al. (2008) correlation was derived as an improvement to Ishii and Mishima (1989) correlation and Al-Sarkhi et al. (2012) was developed as an improvement to Sawant et al. (2008). Therefore, Al-Sarkhi et al. (2012) correlation was selected as it showed an improvement in predicting the entrainment compared to Sawant et al. (2008) correlation.

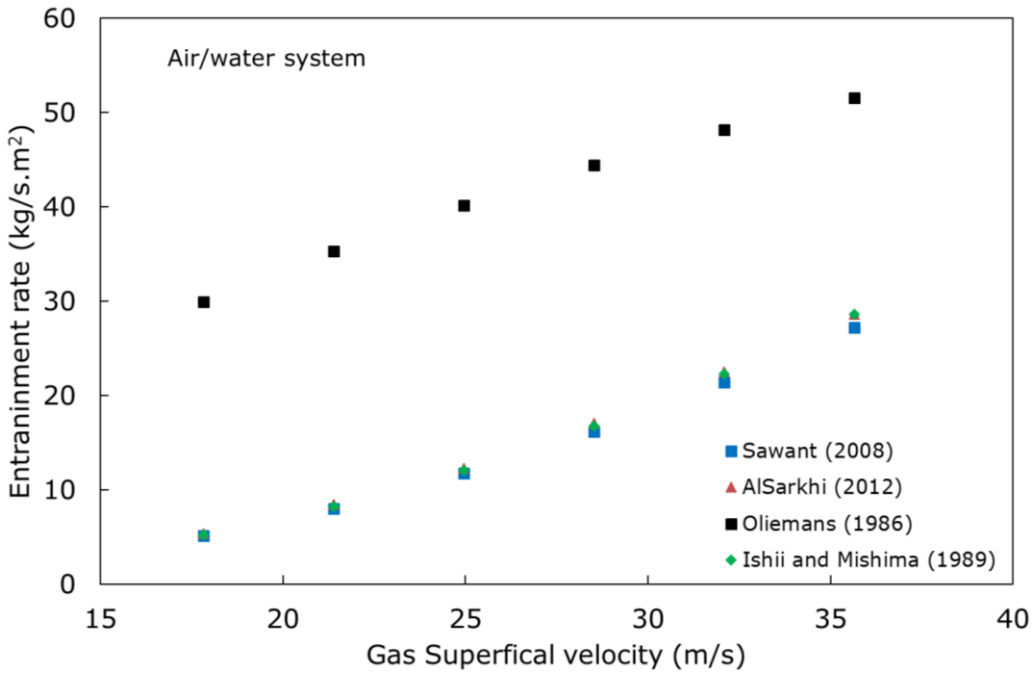


Figure 4.5: Comparison of entrainment correlations at different gas superficial velocities and liquid superficial velocity of 0.089 m/s for air/water system.

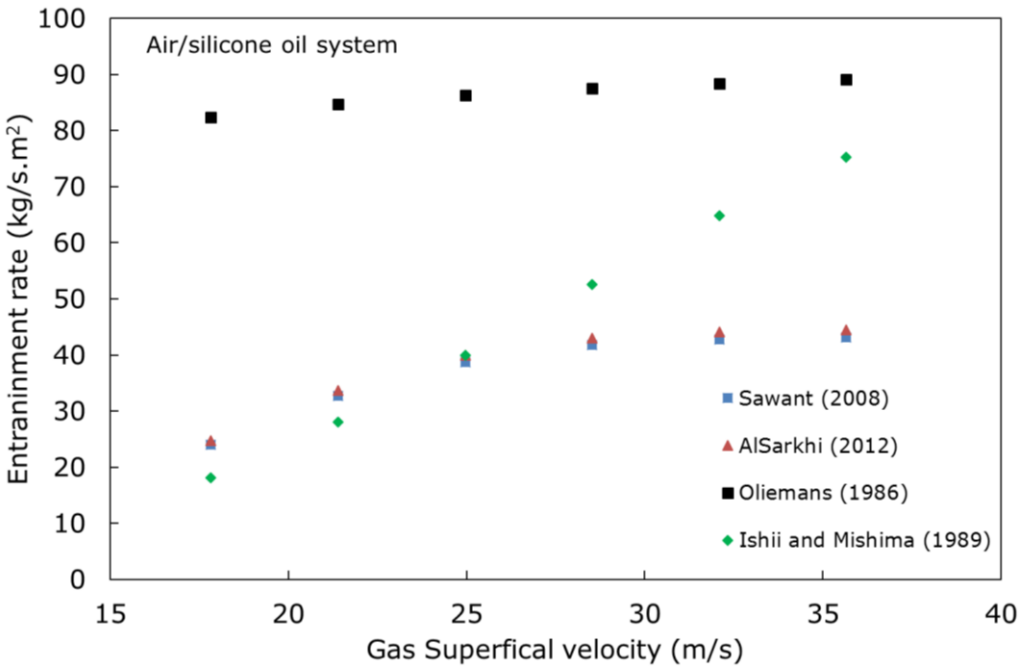


Figure 4.6: Comparison of entrainment correlations at different gas superficial velocities and liquid superficial velocity of 0.089 m/s for air/silicone oil system.

According to Sawant et al. (2008), the entrainment process can be divided into three regions based on the experimental entrainment fraction measurements at different liquid Reynolds numbers as shown in Figure 4.7. In Figure 4.7, the entrainment fraction is plotted against the modified Weber number (Equation 2.9) of Ishii and Mishima (1989) to power of 1.25 and the liquid Reynolds number (Equation 2.5) is considered constant. The first region (O-A) depends only on the Weber number and the second region (A-B) depends on both Weber and liquid Reynolds numbers. The third region depends only on the liquid Reynolds number.

$$\mathrm{Re}_{sl} = \frac{\rho_l U_{sl} D}{\mu_l} \tag{2.5}$$

$$\mathrm{We} = \frac{\rho_g U_{sg}^2 D}{\sigma}\left(\frac{\rho_l - \rho_g}{\rho_g}\right)^{1/4} \tag{2.9}$$

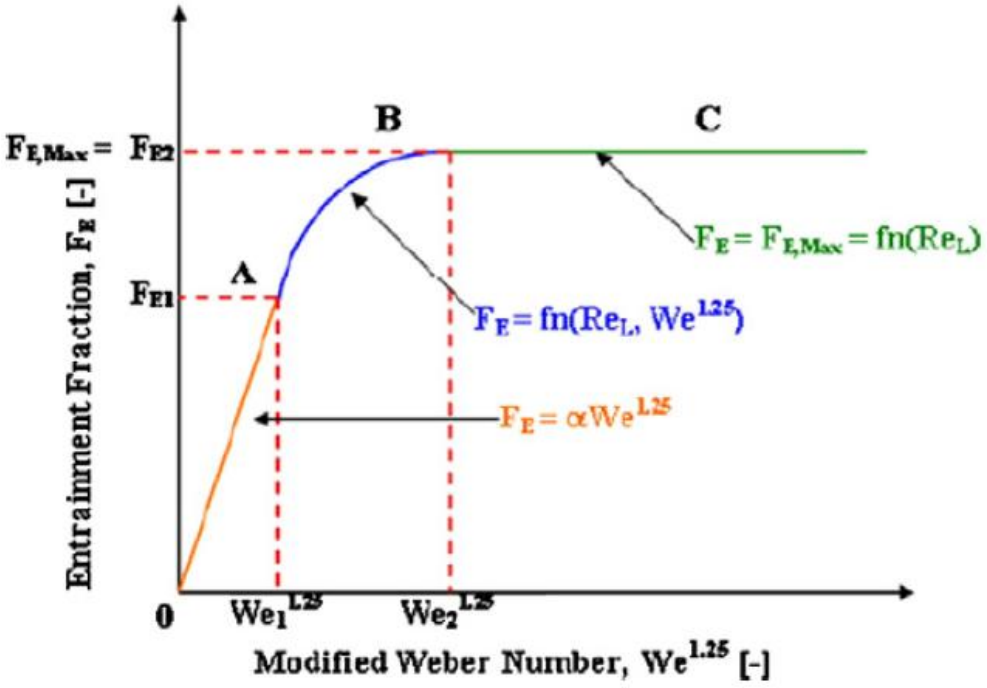


Figure 4.7: Entrainment process (Sawant et al., 2008).

Figure 4.8 and Figure 4.9 show the calculated entrainment rate of air/water system and air/silicone oil system respectively using Al-Sarkhi et al. (2012) correlation. In general, the calculated entrainment rate increases with increasing gas and liquid superficial velocity for air/water and air/silicone oil systems respectively. The entrainment rate was compared based on entrained mass flux rather than the entrained fraction as it helps to show the magnitude of droplet entrainment.

Based on the Sawant et al. (2008) entrainment process, the calculated entrainment rate of air/water and air/silicone oil systems are analysed. The calculated entrainment rate by Al-Sarkhi et al. (2012) correlation is based on the relationship between the Weber number and Reynolds number as per Sawant et al. (2008) entrainment process (Figure 4.7). The effect of surface tension appears in the Weber number where the effect of the viscosity appears in the Reynolds number. In the case of air/water system (Figure 4.8), the calculated entrainment rate at a gas superficial velocity up to 25 m/s is dependent only on the Weber number and hence surface tension. At gas superficial velocity above 25 m/s, the calculated entrainment rate is dependent on the Weber number (Surface tension) and Reynolds number (Viscosity). In the case of air/silicone oil system (Figure 4.9), the calculated entrainment rate is dependent on the Weber number (Surface tension) and Reynolds number (Viscosity) at a gas superficial velocity up to 25 m/s. At gas superficial velocity above 25 m/s, the calculated entrainment rate is dependent only on the Reynolds number (Viscosity). However, the accuracy of the calculated entrainment rate of air/silicone oil is unknown and should be taken into consideration as the correlation is not yet proven with low surface tension and high viscosity compared to water properties.

The effect of surface tension and viscosity on entrainment rate are demonstrated in Figure 4.10. From Figure 4.10, when the surface tension is constant, there is no much effect of changing the viscosity on the calculated entrainment rate. This can be observed where the calculated entrainment rate at Weber number less than 17000 is not affected when the viscosity is changed from 0.001cP to 0.0044 cP and the surface tension remains constant at 0.073 N/m (Region O-A). In contrast, when the surface tension is changed from 0.073 N/m to 0.02 N/m and

the viscosity remains constant at 0.001 cP or 0.0044 cP, the calculated entrainment rate is much higher compared to the calculated entrainment rate at high surface tension. This can be noticed where the calculated entrainment rate at Weber number greater than 17000 increased. However, the calculated entrainment rate at low viscosity (0.001cP) and low surface tension (0.02 N/m) is higher than the calculated entrainment rate at high viscosity (0.0044cP) and low surface tension (0.02 N/m). The effect of viscosity at high Weber number above 80000 is higher on the calculated entrainment rate (Region B-C) as shown in Figure 4.10.Therefore, the difference in the calculated entrainment rate between air/water and air/silicone oil systems is mainly because of the change of surface tension and viscosity.

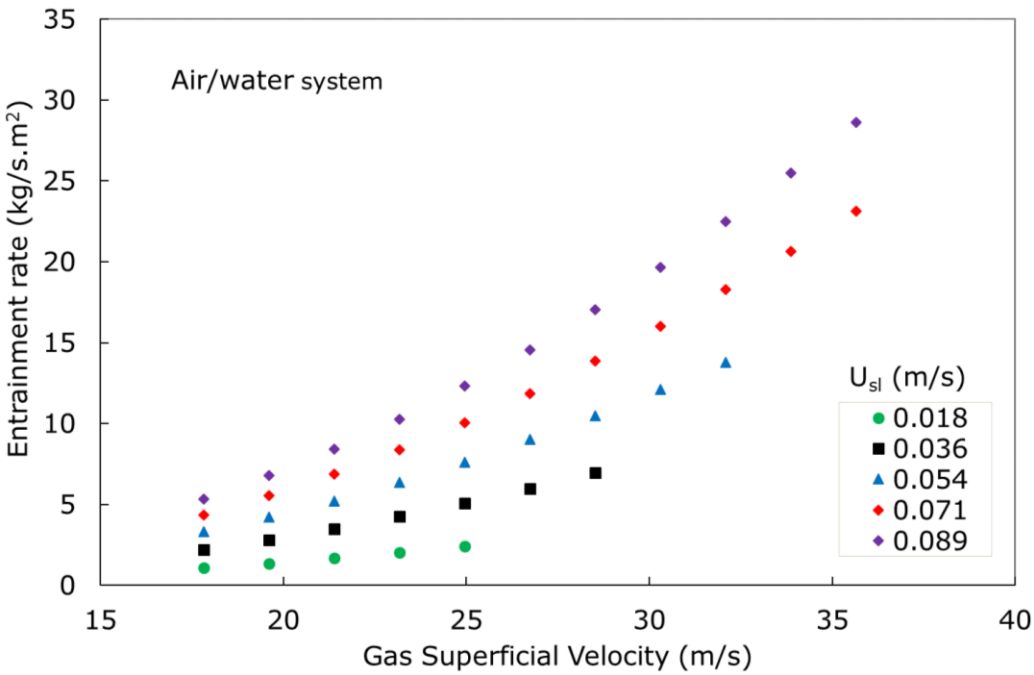


Figure 4.8: Effect of gas superficial velocity on the calculated entrainment rate of air/water system.

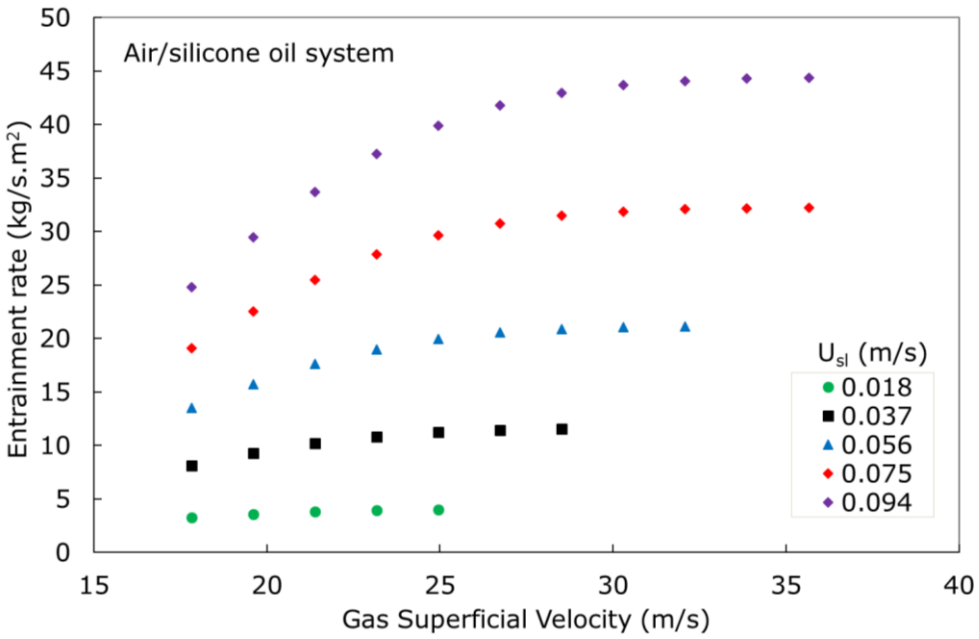


Figure 4.9: Effect of gas superficial velocity on the calculated entrainment rate of air/silicone oil system.

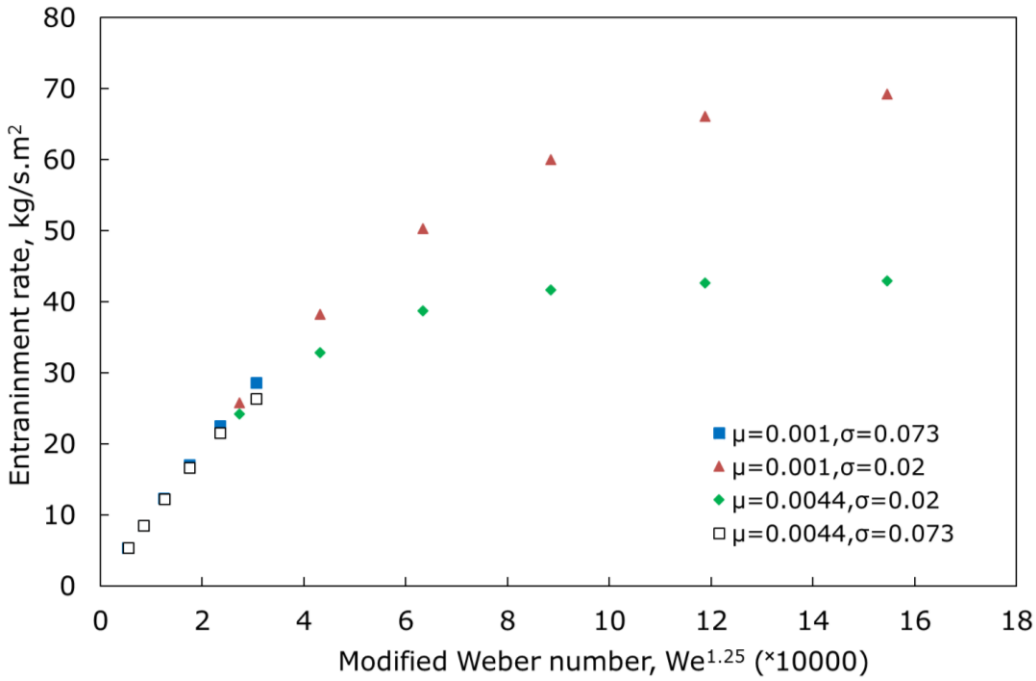


Figure 4.10: Effect of surface tension and viscosity on the calculated entrainment rate at different gas superficial velocities ranging from 17.83 m/s to 35.66 m/s and liquid superficial velocity at 0.089 m/s.

## 4.3. Effect of viscosity and surface tension on two-phase pressure drop

As discussed in section 4.1, the annular flow exists at lower gas superficial velocity for the air/silicone oil system compared to the air/water system due to the influence of the surface tension. This was observed where the gas superficial velocity to meet Kutateladze number and Wallis parameter is lower for the air/silicone oil system compared to the air/water system. In addition, the influence of the viscosity was reported by Taitel et al. (1980), Schmidt et al. (2008) and Alamu (2010) where the liquid viscosity causes a shift to the transition boundaries on the flow pattern map. The effect of viscosity and surface tension on pressure drop was analysed by comparing the results of pressure drop using air/water and air/silicone oil systems. An example is shown in Figure 4.11 at the water and silicone oil superficial velocity of 0.071m/s and 0.075m/s respectively. From Figure 4.11, it is clear that the pressure drop of the air/silicone oil system for gas superficial velocity up to 28.52 m/s is lower than the pressure drop of the air/water system. The pressure drop of the air/silicone oil system intercepts and then exceeds the pressure drop of the air/water system at a point where the gas superficial velocity reached 30.31m/s. This intercept point increases when the liquid superficial increases. Based on the calculated entrainment rate, it was observed that the intercept point of the pressure drop occured when the entrained mass flux of water is approximately half the entrained mass flux of silicone oil as shown in Figure 4.11. This highlights the effect of the entrainment on the pressure drop as mentioned in section 4.2. As indicated in Section 4.2, the accuracy of calculated entrainment rate of

air/silicone oil is unknown. Therefore, the ratio between the calcualted entrainment rate of both systems to find the intercept point required to be confirmed in the future by measuring the entrainment rate of both systems using same entrainment measurement technique.

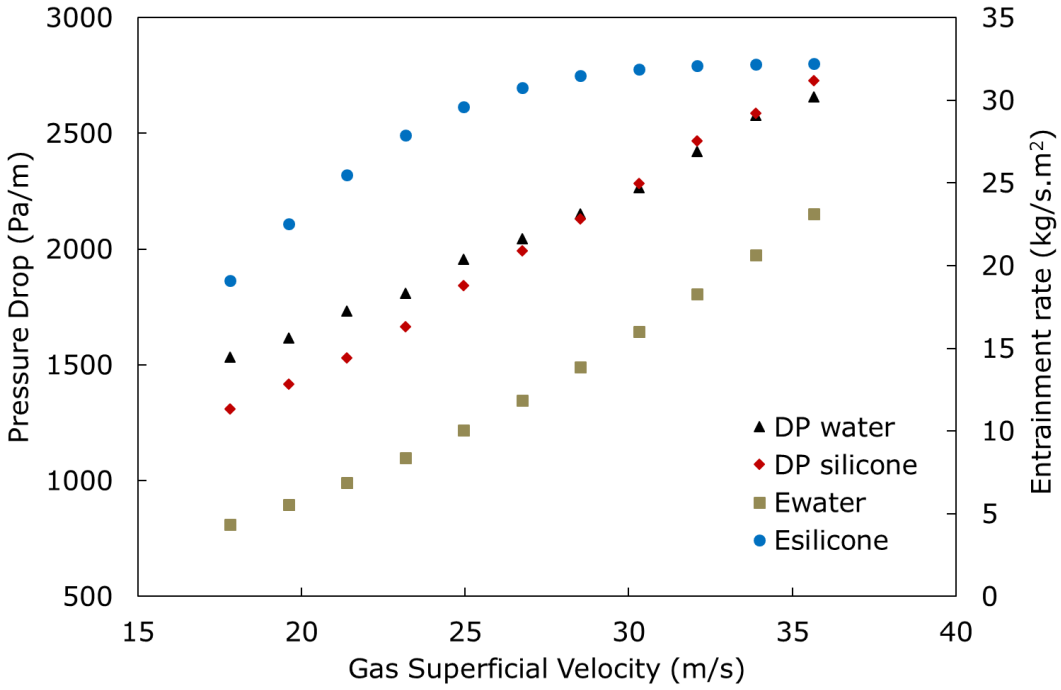


Figure 4.11: Effect of viscosity and surface tension on pressure drop (DP) and entrainment rate (E) at water and silicone oil superficial velocity of 0.071m/s and 0.075m/s respectively.

The intercept between the measured pressure drop of air/water and air/silicone oil systems could be related to the effect of frictional pressure drop and hence wall and interfacial shear stresses. In the annular two-phase flow, the frictional pressure drop is dominant compared to gravitational pressure drop. The frictional pressure drop is affected by the wall shear stress ($\tau_w$) and the interfacial shear stress ($\tau_i$) (Henstock and Hanratty, 1976, Owen, 1986, Hanratty, 2013, Pan et al., 2015b, Aliyu et al., 2017). The wall shear stress is influenced by

the liquid viscosity and liquid superficial velocity while the interfacial shear stress is affected by disturbance wave height, liquid viscosity, droplet entrainment and gas core and liquid superficial velocity (Fukano and Furukawa, 1998, Pan et al., 2015b, Aliyu et al., 2017).

In the current study, the wall shear stress with the air/silicone oil system is higher than the wall shear stress with the air/water system as will be discussed in Chapter 6. The difference in the wall shear stress between air/water system and air/silicone oil systems is small at low gas superficial velocity and keep increasing with increasing gas superficial velocity. On the other hand, the calculated interfacial shear stress ($\tau_i$) of the air/silicone oil system is lower than the calculated interfacial shear stress of the air/water system as shown in Figure 4.12. The interfacial shear stress ($\tau_i$) was calculated using the correlation proposed by Pan et al. (2015b) (Equations 4.3) as it was derived considering the effect of disturbance waves, gas and liquid viscosity and gas core and liquid superficial velocity. Most of the available correlations for interfacial shear stress were developed as a modification of the interfacial friction factor proposed by Wallis (1969). These correlations treated the liquid film as pipe wall roughness and did not take into consideration the characteristics of the liquid film (i.e disturbance waves) (Pan et al., 2015b). Pan et al. (2015b) correlation is in the form of liquid ($Re_f$) and gas ($Re_g$) Reynolds number as shown below:

$$C_{fs} = 33.6\, Re_g^{-0.91} Re_f^{0.30} \cong \frac{\tau_i}{\rho_g U_{sg}^2} \tag{4.3}$$

where $C_{fs}$ is the non-dimensional pressure drop originating from the interfacial shear stress (Pan et al., 2015b).

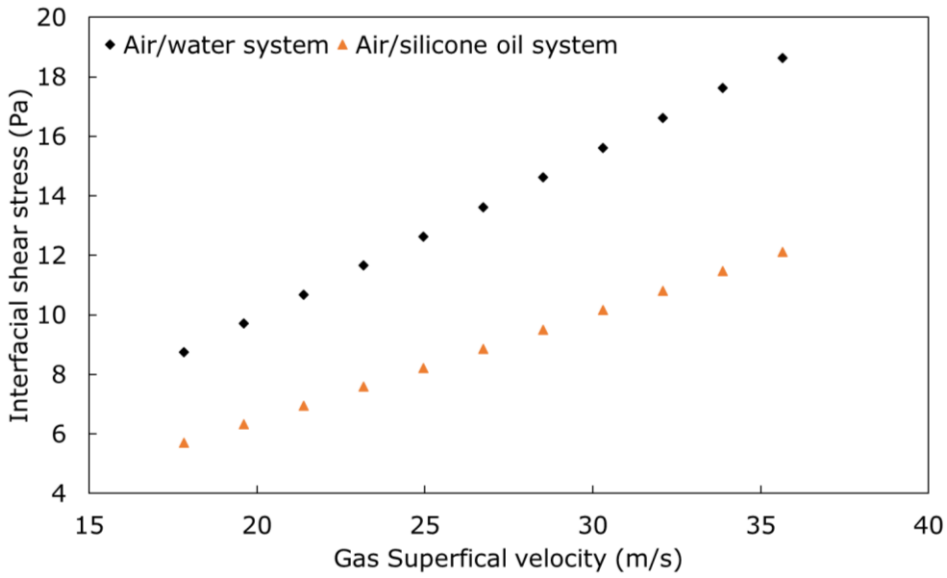


Figure 4.12: The calculated interfacial shear stress using Pan et al. (2015b) correlation at different gas superficial velocities and water and silicone oil superficial velocity of 0.071m/s and 0.075m/s respectively.

As discussed previously, the calculated entrainment rate of the air/silicone oil system is higher than with the air/water system. The entrainment rate is related to the force balance between the interfacial shear force and surface tension force. This force balance is normally expressed by using a Weber number (We) (Equation 2.9).

The low interfacial shear stress with air/silicone oil system could be related to the low surface tension. As will be shown in Section 4.4.2, the two-phase pressure drop of both system is well predicted by using the characteristics shear stress suggested by Henstock and Hanratty (1976). Therefore, the pressure drop with air/silicone oil system is lower at low superficial velocity until the difference in the shear stress between air/silicone oil and air/water systems is enough to make the pressure drop with the air/silicone oil system higher than the pressure drop with the air/water system.

## 4.4. Prediction of total pressure drop in vertical two-phase flow

### 4.4.1. Two-phase pressure drop prediction using empirical correlations

There are many correlations in the literature which were developed to predict the pressure drop in two-phase flow as per Hewitt (1982) and Azzopardi (2006). These correlations are accurate only near the development conditions (Fore and Dukler, 1995, Wang et al., 2004). The current measured pressure drop results for both air/water and air/silicone oil systems were compared with the most well-known correlations as described by Azzopardi (2006). The two-phase pressure drop is calculated using homogeneous flow model and separated flow model as discussed in Chapter 2. In the separated flow model, the frictional pressure drop was calculated using Chisholm (1967), Friedel (1979) and Beggs and Brill (1973) correlations. The overall pressure drop is calculated from the sum of the frictional pressure drop which is calculated by the correlations and the gravitational pressure drop. The acceleration pressure drop is neglected because it is assumed that the system is at equilibrium.

The comparison between the meausred and predicted pressure drop for air/water and air/silicone oil systems within ±50% deviation margin are shown in Figure 4.13 and Figure 4.14.

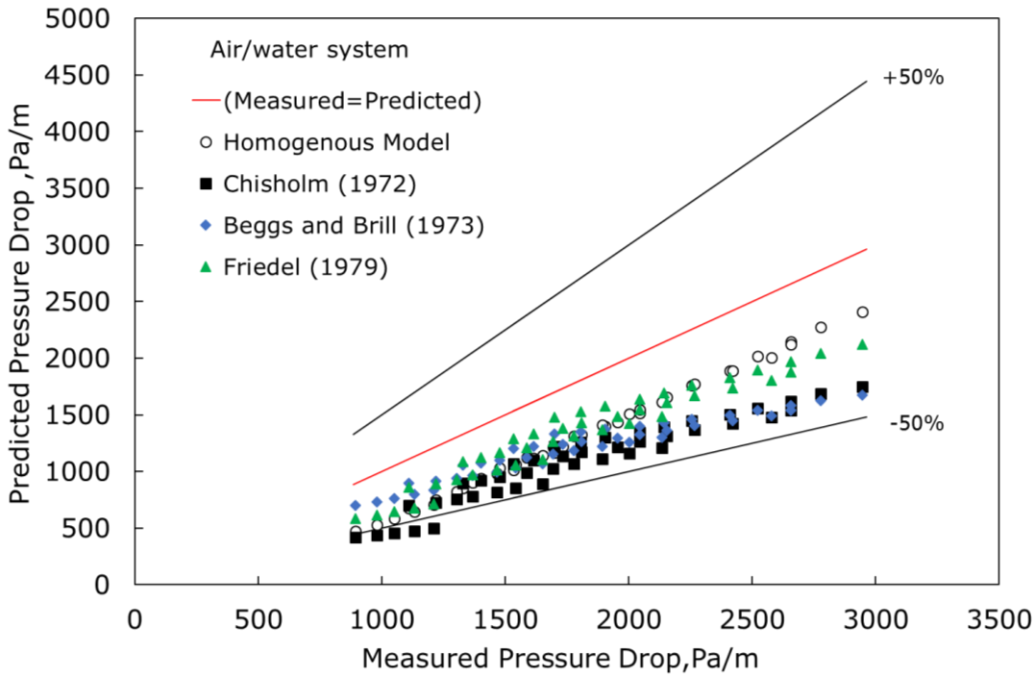


Figure 4.13: Comparison between the measured and predicted pressure drop for the air/water system within ±50% deviation margin.

The comparison of the measured pressure drop for the air/water system with predictive correlations (Figure 4.13) shows that all of the correlations were under-predicted the pressure drop. The homogeneous model and Friedel (1979) correlation could predict the trend behaviour better than Chisholm (1967) and Beggs and Brill (1973) correlations. The Beggs and Brill (1973) was the best at low-pressure drop where the homogeneous model was the best at high-pressure drop among other correlations.

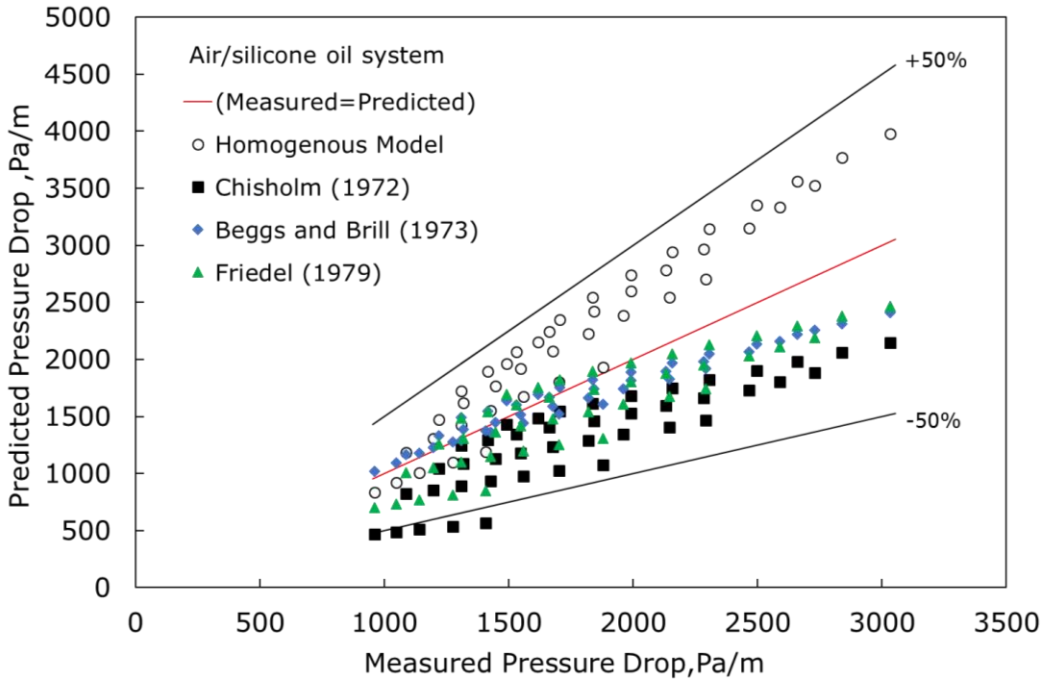


Figure 4.14: Comparison between the measured and predicted pressure drop for the air/silicone oil system within ±50% deviation margin.

The predictive correlations of pressure drop could predict the pressure drop of the air/silicone oil system better than the air/water system as shown in Figure 4.14. The Beggs and Brill (1973) correlation was the best compared to other correlations.

The discrepancy between the predicted pressure drop by different correlation and the measured pressure drop is not surprising and expected where most previous researchers achieved similar results with ±50% deviation or even higher (Martin, 1983, Owen, 1986, Zangana, 2011). This discrepancy could be related to many factors. Hewitt (1982) and Owen (1986), for example, stated that none of the general correlations for two-phase pressure drop is accurate. They attributed this to entrance effects and the inherent inaccuracy of the data used for making the

correlations. In addition, there are other factors that could contribute and influence the accuracy of pressure drop prediction. These factors include pipe diameter, operating pressure, development region from the injector and operating flow rates. Moreover, these correlations are not taking into consideration the effect of the entrainment which has a significant impact on pressure drop as reported by Fore and Dukler (1995) and Pan et al. (2015b). Most of these correlations do not consider the effect of the characteristics of the interface (e.g disturbance waves) on pressure drop (Wang et al., 2004).

### 4.4.2. Two-phase pressure drop prediction using shear stress

As discussed in Section 4.3, the frictional pressure drop is affected by the wall shear stress and interfacial shear stress. The frictional pressure drop $\left(\frac{dp}{dl}\right)_f$ could be also calculated from shear stress using:

$$\left(\frac{dp}{dl}\right)_f = \frac{4\tau}{D} \tag{4.4}$$

where $\tau$ is either the wall shear stress ($\tau_w$) or the characteristic shear stress ($\tau_c$)

Henstock and Hanratty (1976) used a characteristic shear stress for thin film by using the following expression (Equation 4.5):

$$\tau_c = \frac{2}{3}\tau_w + \frac{1}{3}\tau_i \tag{4.5}$$

Owen and Hewitt (1985) showed that the film velocity profile could be represented by the Universal Velocity Profile if the Henstock and Hanratty (1976) characteristic shear stress was used (Owen, 1986). In the current study,

the measured shear stress and the characteristic shear stress were used to calculate the frictional pressure, and hence the total pressure drop. The interfacial shear stress was estimated using the correlation proposed (Equation 4.4) by Pan et al. (2015b). Figure 4.15 shows the comparison between the measured total pressure drop and the calculated total pressure drop for air/water system using both the wall shear stress and the characteristic shear stress. As can be seen, there is no much variation between the total pressure drop using the wall shear stress and the characteristic shear stress. This finding is similar to that reported by Henstock and Hanratty (1976) and the assumption by Hewitt (1982) that $\tau_w \approx \tau_i$. Both methods were able to predict the total pressure drop of air/water system within ±10%.

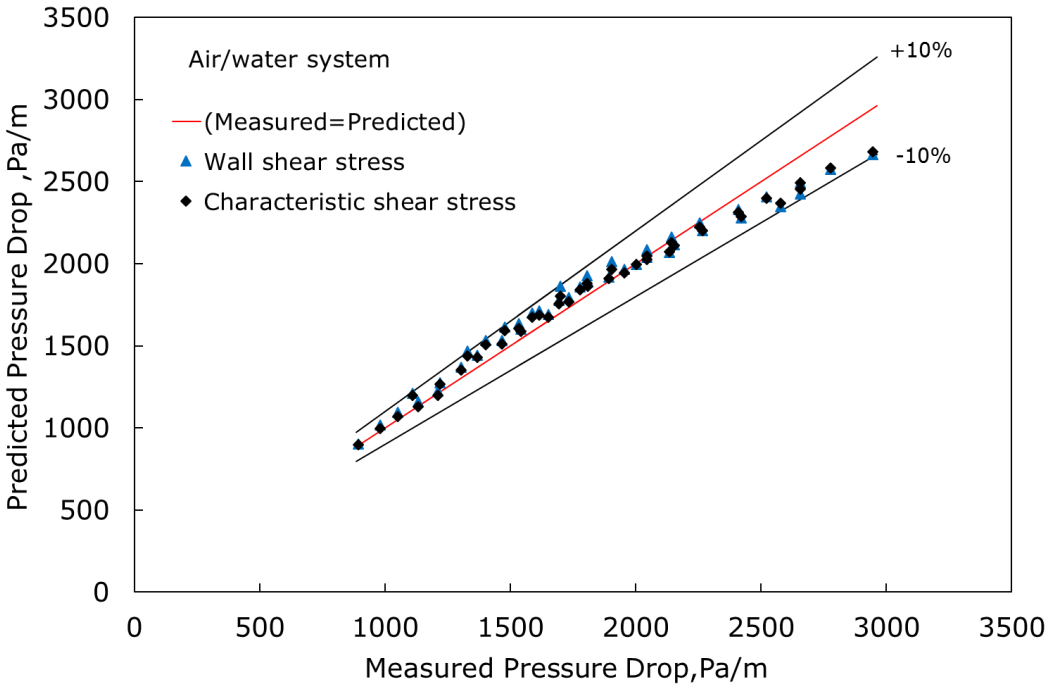


Figure 4.15: Comparison of the measured total pressure drop with the values calculated using measured wall shear stress and characteristic shear stress for the air/water system

The comparison between the measured total pressure drop and the calculated total pressure drop for air/silicone oil system using both the wall shear stress and the characteristic shear stress is shown in Figure 4.16. The wall shear stress was over predicting the total pressure drop within ±30%. However, the characteristic shear stress shows better prediction than wall shear stress within ±15%. The variation was calculated using relative error:

$$\text{Relative error } (\%) = \left[\frac{(\text{DP}_{\text{Pred}} - \text{DP}_{\text{Exp}})}{\text{DP}_{\text{Exp}}}\right] \times 100\% \qquad (4.6)$$

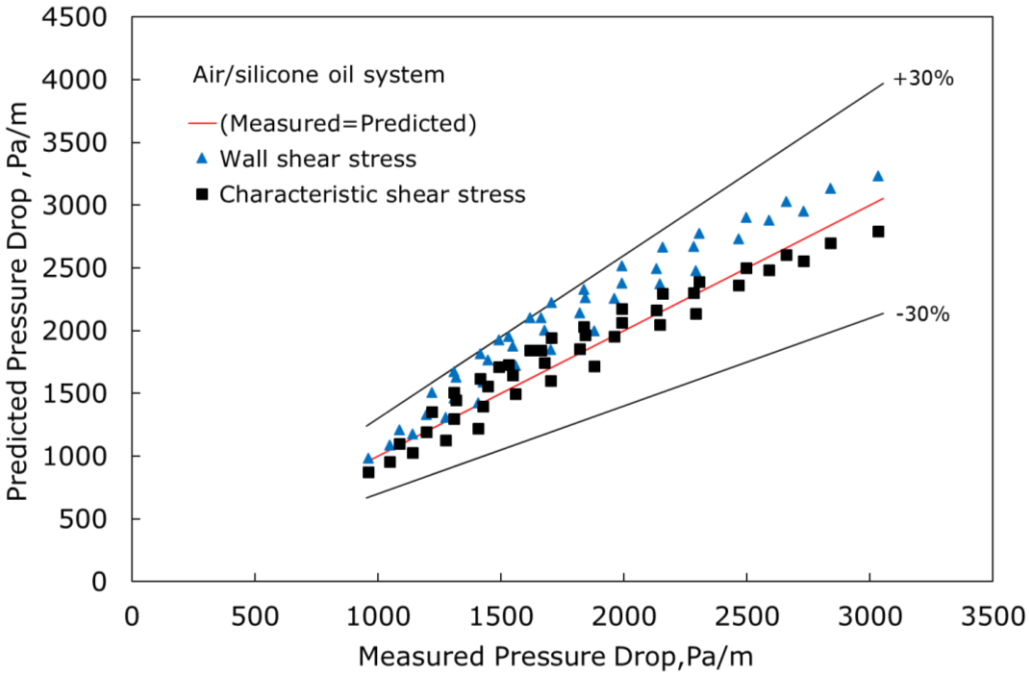


Figure 4.16: Comparison of the measured total pressure drop with the values calculated using measured wall shear stress and characteristic shear stress for the air/silicone oil system

## 4.5. Summary

The two-phase pressure drop results were analysed for air/water and air/silicone oil systems at gas superficial velocity ranging from 17.83 m/s to 35.66 m/s, and liquid superficial velocity ranging from 0.018m/s to 0.089m/s with water, and from 0.019m/s to 0.094m/s with silicone oil. From the results and discussion, the following could be summarised:

- The existence of Annular flow regime in the current experiments was identified by meeting Wallis parameter ($U_g^*$) and Kutateladze number ($Ku_g$) criteria.

- The average (mean) total pressure drop increases with increasing the gas and liquid superficial velocity for both air/water and air/silicone oil systems.

- The total pressure drop of air/silicone oil system exhibits similar trend profile to the one obtained for the air/water system regardless of the liquid physical properties.

- The change of viscosity and surface tension of the liquid phase has an impact on the total pressure drop where total pressure drop of air/silicone oil system is lower at low gas superficial velocity. Then, it keeps increase with increasing gas superficial velocity until it becomes greater than the total pressure drop of air/water system. The intercept point where the total pressure drop of air/silicone oil system exceeds that of air/water system, increases with increasing the liquid superficial velocities.

- The droplet entrainment rate was calculated using Al-Sarkhi et al. (2012) correlation based on the comparison with some of existing correlations. The calculated entrainment rate of air/silicone oil system was higher compared to the calculated entrainment rate of air/water system. The difference in the calculated entrainment rate between both systems was related to the influence of viscosity and surface tension based on entrainment process method suggested by Sawant et al. (2008).

- The interfacial shear stress was calculated using Pan et al. (2015b) correlation as it considers the characteristics of liquid film compared to existing correlations that deals with liquid as a type of pipe roughness. The calculated interfacial shear stress of air/silicone oil system was lower than that of air/water system.

- The total pressure drop was predicted using different existing empirical correlations. Most of these correlations were under predict the total pressure drop for both air/water and air/silicone oil systems within ±50% relative deviation.

- The total pressure drop was also predicted based on the calculated frictional pressure drop from the shear stress. Wall shear stress and characteristics shear stress suggest by Henstock and Hanratty (1976) were used. Both shear stresses were able to predict the total pressure drop of both systems. The calculated total pressure drop using both shear stresses were predicted within ±10% relative deviation for the air/water system and within ±30% for the air/silicone oil system.

# CHAPTER 5

# LIQUID FILM THICKNESS MEASUREMENTS

As discussed in Chapter 1, the current study focuses on finding the relationship between pressure drop, liquid film thickness and wall shear stress in an air/silicone oil system. The liquid film thickness is associated with waves (i.e disturbance waves) that affect both pressure drop and wall shear stress. The liquid film thickness measurement is crucial to study the behaviour of the gas and liquid film interface with a variation of gas and liquid superficial velocities. There is still a lack of experimental data on the effect of changing the physical properties of the liquid on the liquid film thickness and hence validation of the existing liquid film thickness correlations. In the current study, finding a liquid film thickness measurement technique which can operate with silicone oil is an important ambition. Most of the popular and widely used techniques were developed using water.

In this chapter, the development of liquid film thickness measurement using the ultrasonic technique and the experimental results of the liquid film thickness for air/water and air/silicone oil systems are discussed. In Section 5.1, the development of the ultrasonic technique for measuring the liquid film thickness and the validation processes are presented. Section 5.2 discusses the effect of gas and liquid superficial velocity on liquid film thickness measurements. The effect of viscosity and surface tension on liquid film thickness measurements are

presented in Section 5.3. Finally, prediction correlations for liquid film thickness are compared with the measured liquid film thickness in Section 5.4.

## 5.1. Development of liquid film thickness measurement using ultrasonic technique

As discussed in Chapter 2, several techniques have been developed for liquid film thickness measurement in two-phase flow. Clark (2002) had reviewed these measurement techniques and found that different techniques encountered difficulties in recording accurate measurements when the film thickness was less than 10 mm. Commonly available and widely used measurement techniques are based on the fluid electrical properties (conductance measurement (Kang and Kim, 1992) or require transparent geometry (optical measurement (Yu et al., 1996) or tracer chemicals (fluorescence measurement (Ng et al., 2009)). Many of the liquid film measurement techniques have been developed using water as a liquid phase by exploiting the advantage of its electrical properties (i.e conductivity). Therefore, the development of techniques that do not depend on the electrical characteristics of the liquid and can operate with a non-conducting medium such as oil are required. In this present study, silicon oil was used as the liquid phase as its physical properties resemble typical process liquids used in the oil and gas industry. This is an electrically non-conducting fluid.

In the present work, an ultrasonic pulse echo technique has been applied to measure the liquid film thickness where the signal is transmitted and received by the same transducer. It is a non-intrusive measurement technique that can easily be attached to different locations on the pipe and operates on opaque materials such as PVC and metals. The capability of the ultrasonic technique for measuring liquid film thicknesses in the range of 0.1 to 6 mm was examined for static films (on bench top experiments) as well as for films in annular flow in a cylindrical pipe. A frequency domain method was used for film thicknesses <0.5 mm and the time of flight method was utilised for film thickness >0.5 mm. A new processing method called baseline removal method is proposed for film thickness <0.5 mm. The ultrasonic measurements were compared with a Multi Pin Film Sensor (MPFS) and a concentric conductance probe in both a downward and upward vertical flow rig using an air/water system to assess the accuracy and the applicability to dynamic films.

### 5.1.1. Application of Ultrasonic Pulse Echo measurement

Ultrasound measurements have been employed in many applications which cover different disciplines such as engineering, physics, and medicine. Ultrasound is a branch of acoustics with waves propagates at a frequency greater than 20 kHz, this is the upper limit of the human hearing (Cheeke, 2002). They are oscillations of pressure and require a medium to propagate through. Figure 5.1 shows the frequency spectrum ranges for various ultrasonic processes.

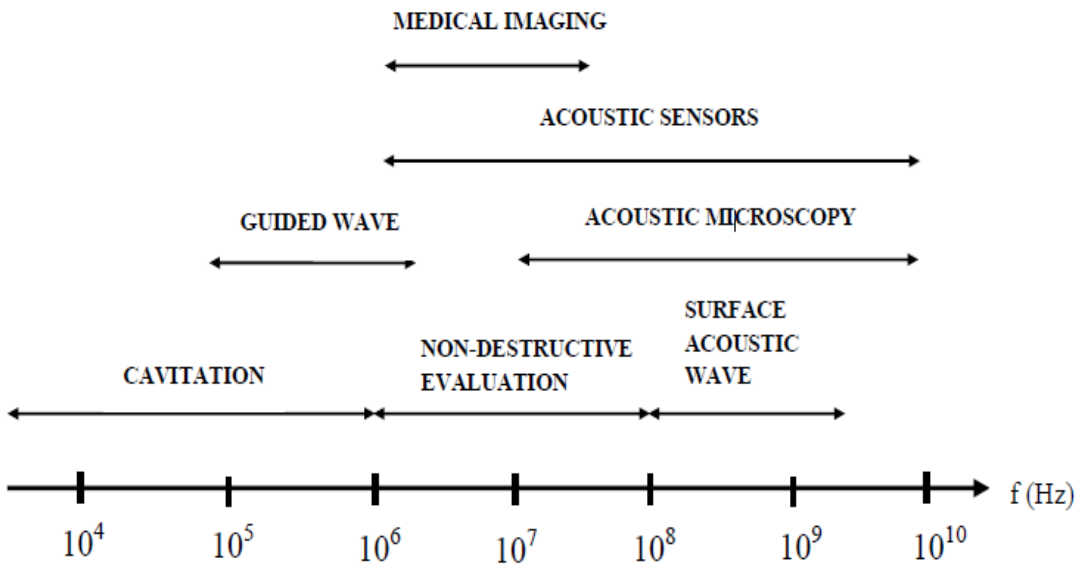


Figure 5.1: Frequency spectrum ranges for various ultrasonic processes (Cheeke, 2002).

The ultrasonic pulse echo technique has been used by Park and Chun (1984) to investigate the effects of wall thickness, wall material, and ultrasonic frequency on liquid film thickness measurements. They have also compared the technique against theoretical calculations using a static film on plate and tube test sections. They concluded that the ultrasonic pulse echo technique can be used when the tube wall thickness ($\delta_w$) is greater than the minimum given by Equation (5.1) because they found that the reflected signals are superimposed when the wall thickness is less than this limit.

$$\delta_{w,min} \geq \frac{Nc_w}{2f} \tag{5.1}$$

where N is the number of cycles in one ultrasonic pulse, $c_w$ is the speed of ultrasonic wave in the wall material and f is the frequency of ultrasonic wave.

They have also concluded that the acoustic impedance mismatch between the wall material and the liquid film is low enough to allow the signals to be transmitted into the liquid film, hence the reflected peak from the liquid film/air interface remains distinguishable. Lu et al. (1993) measured condensate film thicknesses using an ultrasonic pulse echo technique in a horizontal rectangular test section. They indicated that the ultrasonic method for measuring wavy film could be improved by increasing the data acquisition rate (frame/second). Serizawa et al. (1994) evaluated an ultrasonic measurement technique against a laser displacement gauge and impedance probe in stratified flow over a horizontal plate test section. They found an excellent agreement between the three measurement techniques. However, they indicated that the ultrasonic measurement has poor detection sensitivity due to the varying angle of the reflection interface. Chen et al. (2005) used the ultrasonic measurements to monitor the dynamic behaviour of condensing and non-condensing fluid films. They have proposed a new data processing method based on spectral analysis using a Fourier Transform method to measure film thicknesses from 50 to 750μm. Ultrasonic techniques have also been employed in two-phase flow by many of researchers to identify the flow regimes include Wada et al. (2006), Masala et al. (2007), Murai et al. (2010), Baba Musa and Yueng (2016) and Fachun et al. (2016). However, most of the research was performed using ultrasonic techniques to measure liquid film thicknesses greater than 1mm and to identify the flow regimes on a horizontal pipe using an air/water system.

## 5.1.2. Ultrasonic Theory

Ultrasonic techniques operate by transmitting low amplitude, high-frequency acoustic waves through the system under investigation (Watson, 2015). Ultrasonic waves assume different wave types based on the medium through which they can propagate. These wave types are longitudinal, shear, surface (Rayleigh) and plate (Lamb). However, the longitudinal wave type only exists in fluids due to their densities being too low to support shear waves and no solid boundaries for surface or plate waves (Watson, 2015). Therefore, the only waves discussed in the current study are the longitudinal waves where the particle motion of the medium is in the same direction of the propagation of the wave. These waves are also known as compressional waves which are sinusoidal in nature. The characteristic parameters of the wave include the wavelength ($\lambda$) and the period ($T$) of a complete wave cycle with respect to time or distance are shown in Figure 5.2.

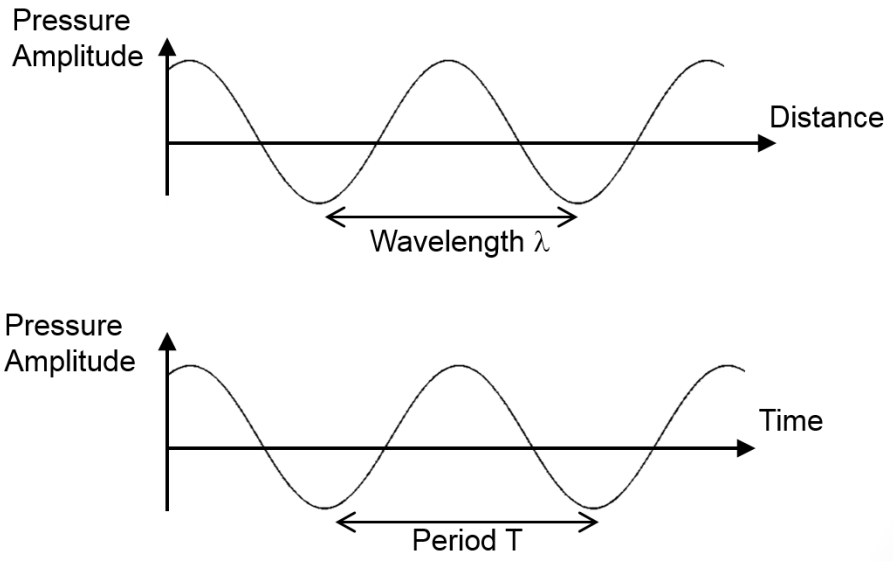


Figure 5.2: Characteristics of an acoustic wave- the wavelength ($\lambda$) and the period ($T$) of a complete wave cycle.

The wave frequency (f ) is related to the period (T) of the complete cycle by the following equation (5.2):

$$f = \frac{1}{T} \tag{5.2}$$

where the frequency is measured in Hertz (Hz or $s^{-1}$) and the period (T) of the complete cycle is measured in seconds (s).

The wavelength (λ) is related to the frequency (f ), the speed of sound (c) and the period (T) by using equation (5.3):

$$\lambda = \frac{c}{f} = cT \tag{5.3}$$

where the speed of sound (c) is measured in meter/seconds (m/s) and the wavelength (λ) is measured in meters (m). The wavelength depends on the frequency where the relationship between them is inversely proportional. The frequency of the propagating wave is governed by the transducer that can be selected based on the measurement required.

The speed of sound (c) at which the wave propagates in the medium is a function of the medium density (ρ) and adiabatic compressibility (k) or adiabatic bulk modules (B) which is given by equation (5.4) (Wood, 1941):

$$c = \frac{1}{\sqrt{k\rho}} = \sqrt{\frac{B}{\rho}} \tag{5.4}$$

The speed of sound is affected by changes in the medium properties which are temperature dependent. Therefore, it is important to understand and know the effect of the temperature on the medium. In addition, the temperature fluctuation

should be monitored where acoustic measurements are being made in order to correct its effect on the speed of sound. More details about how the speed of sound of the medium is measured can be found in Povey (1997).

#### 5.1.2.1. Wave Propagation at an interface between two mediums

When an ultrasonic wave propagates through the perpendicular interface of two mediums, part of the incident wave will be reflected back at the same velocity as the incident wave as shown in Figure (5.3). The other part will be transmitted into the second medium but at different velocity. The pressure reflection (*R*) and transmission (T) coefficients are used to determine the amplitudes of the transmitted and reflected waves, as well as the phase of the reflected wave. These coefficients are functions of the acoustic impedances of both mediums. The acoustic impedance of a medium (Z) is a function of density (ρ) and speed of sound (c) of the medium and can be defined as shown in equation (5.5):

$$Z = \rho c \tag{5.5}$$

The pressure reflection (R) and transmission coefficients (T) for a wave propagating through an interface at normal incidence are given by equations (5.6) and (5.7) respectively (Challis et al., 1998, Watson, 2015):

$$R = \frac{Z_2 - Z_1}{Z_2 + Z_1} \tag{5.6}$$

$$T = \frac{2Z_2}{Z_2 + Z_1} \tag{5.7}$$

where $Z_1$ and $Z_2$ are the acoustic impedance of medium1 and medium2 respectively.

The reflection equation indicates that the reflection increases when the impedance mismatch increases. However, the reflection coefficient (R) is a function of the incident angle θ, and the reflected waves can change significantly with θ.

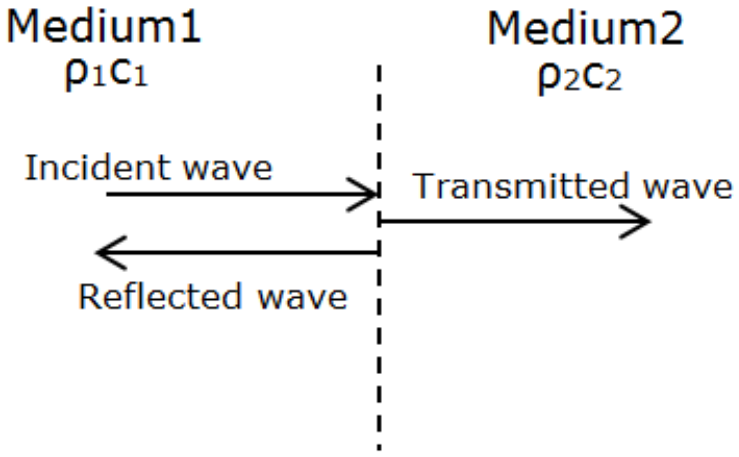


Figure 5.3: Wave propagation at the interface of two mediums.

### 5.1.3. Principle of Ultrasonic Pulse Echo

Ultrasonic pulse echo technique can be used to calculate distances by measuring the time differences between transmitted and reflected pulses and knowledge of the speed of sound in the medium. This can be better demonstrated by studying a system consisting of three different layers as shown in Figure 5.4. These three layers are a solid wall, a liquid film and air where an ultrasonic transducer is attached to the solid wall. When an ultrasonic pulse is transmitted from the transducer, it will be partly reflected at the solid wall/liquid interface and received back by the same transducer as shown in Figure 5.4. The other part of the pulse will be transmitted through the liquid and then reflected back from the

liquid film/air interface to the transducer. The time of flight (Δt) of the ultrasonic wave through the liquid film can be determined by recording the time difference between the first reflected pulse at the solid wall/liquid film interface and the first reflected pulse at liquid film/air interface. The liquid film thickness (δ) as shown in Figure 5.5 can then be calculated from the measurement of the time of flight using the following equation (5.8):

$$\delta = \frac{C_L \Delta t}{2} \tag{5.8}$$

where $C_L$ is the ultrasonic wave speed of sound in the liquid phase. This method is called the Time of Flight method (ToF).

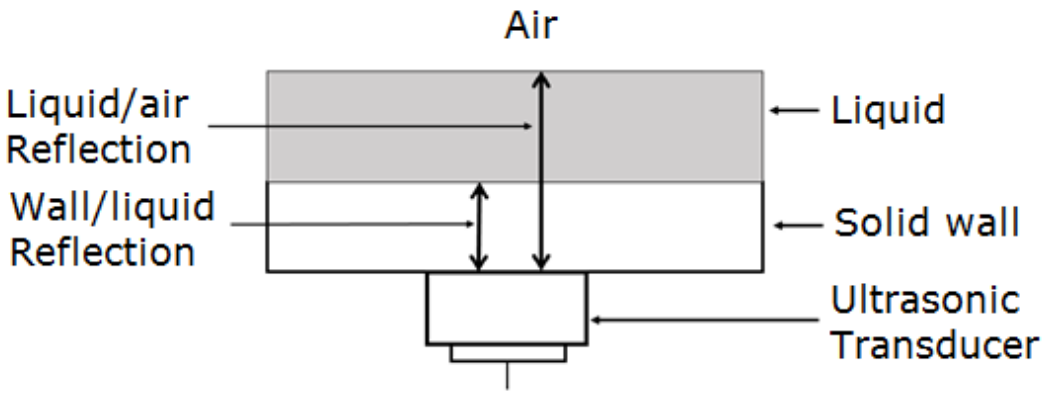


Figure 5.4: Schematic of pulse echo technique showing the two reflections of the ultrasonic pulse in a system consisting of three different layers (solid wall, liquid film and air).

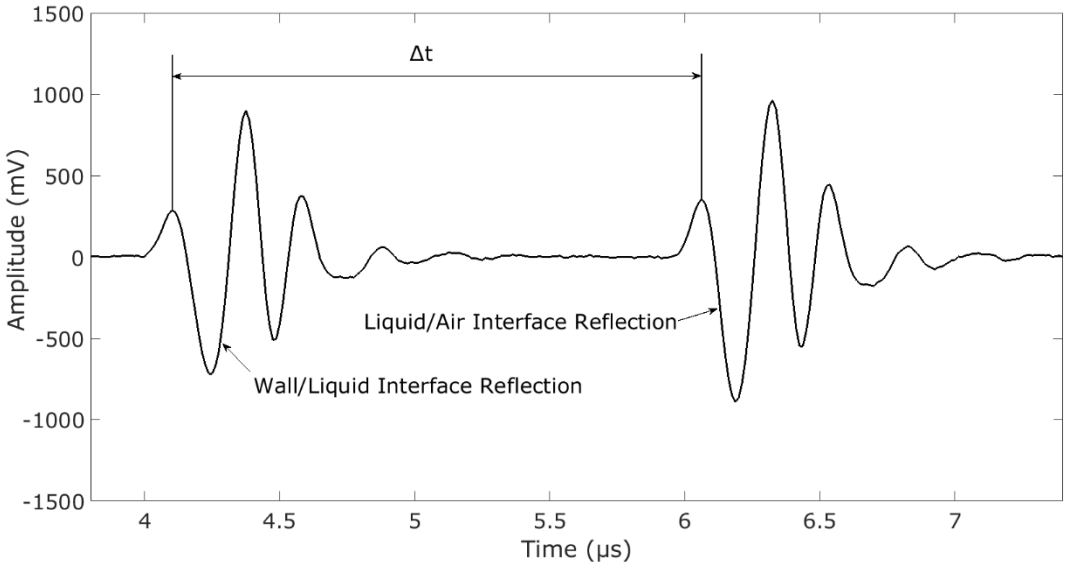


Figure 5.5: Ultrasonic Reflected Signal showing the two reflections of the ultrasonic pulse and the time difference between them.

Care must be taken to ensure the correct reflected pulse is used for calculations. Acoustic reverberations exist within the solid wall, but the liquid/air interface can be identified by varying the thickness of liquid layer. The time of flight method can only be used when the two reflected signals do not overlap in time. Therefore, the time of flight is useful for films having a thickness greater than half the pulse wavelength multiplied by the number of cycles in the pulse. This is approximately 0.45 mm for a water film while using a 5 MHz transducer with three cycles in the pulse. For a thin film thickness, less than 0.5mm, a frequency domain method developed by Chen et al. (2005) was used. The thin liquid film thickness was calculated using the following equation (5.9):

$$\delta = \frac{C_L}{4f_0} \tag{5.9}$$

where $f_0$ is the lowest frequency in the spectral data. As this cannot often be detected $f_0$ is taken as half of the average interval distance between each pair of adjacent spectral peaks. The method of Chen et al. (2005) requires numerous signal processing steps to calculate $f_0$ . First, a baseline signal is subtracted from the received signals. The baseline signal is a signal recorded from a film with infinite thickness. This contains only a single reflection from the wall/liquid interface which is located at the same position for all measurements made during the experiments. The remaining signal is then multiplied by a "flat top" window function. This was performed by a point-by-point multiplication. The center half of the signal was multiplied by one while both the beginning and end quarters were multiplied by coefficients which taper from one at the center to zero at the ends. The flat top function was used to improve the signal to noise ratio. The next step required the signals to be zero padded to ensure they contained a number of samples which is a power of two. This was performed to improve the efficiency of the following step which was to calculate the Fast Fourier Transform (FFT) of the signals. The FFT creates a power density spectrum, and the frequencies of the main spectral peaks were identified. The interval between each pair of adjacent spectral peaks was calculated and all intervals in a given spectrum were averaged. The average interval was divided by two to get $f_0$, which was then used to calculate the layer thickness using Equation (5.9). An example of an overlapped waveform signal (a) and frequency spectrum after applying the frequency method (b) for a 0.2 mm liquid film thickness is shown in Figure 5.6 (a and b). From Figure 5.6 (a), it is difficult to distinguish between the reflected signals from the wall/liquid interface and liquid/air interface where both reflected signals are overlapped. Figure 5.6 (b) shows the frequency

spectrum of waveform signals after applying the frequency method where three main frequency spectrum peaks are obtained.

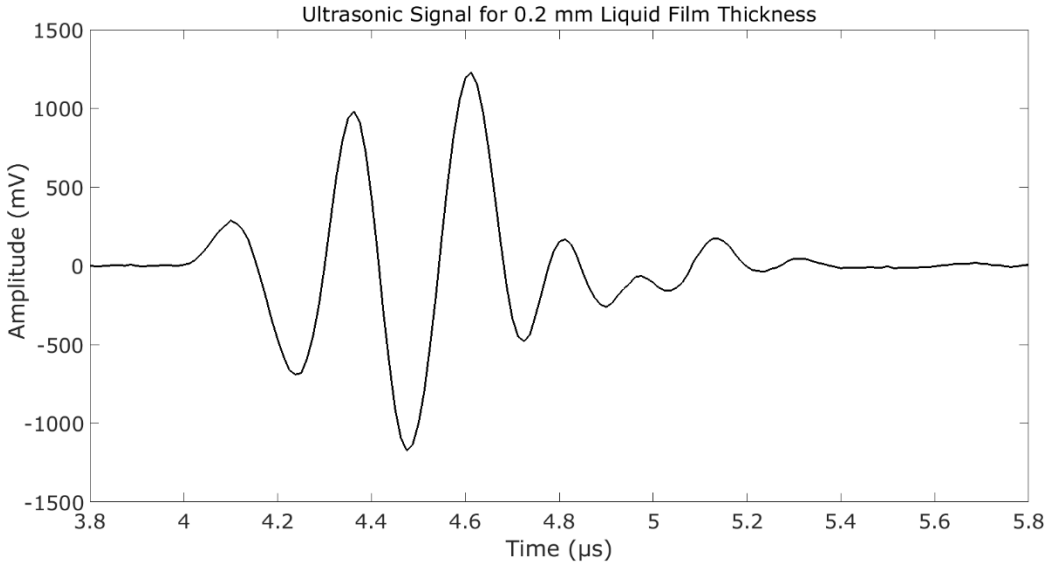


(a)

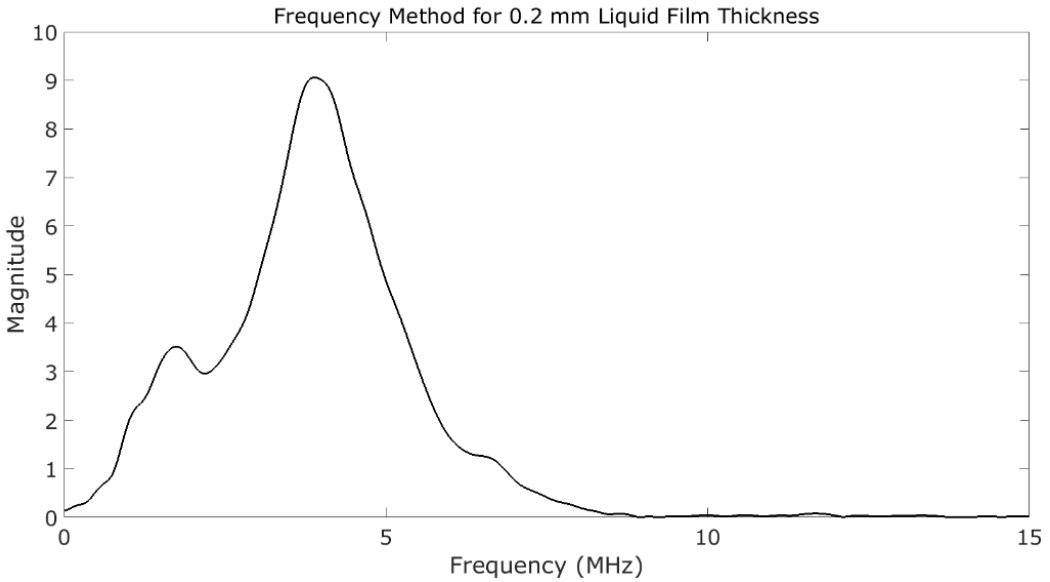


(b)

Figure 5.6: Original overlapped reflected waveform signal (a) and frequency spectrum after applying frequency method (b) for a 0.2 mm liquid film thickness

In the current study, a new processing method called the baseline removal method is proposed in addition to the above methods. It was developed for scenarios where the transmitted and reflected signals are overlapped in time. As described above, the measurement is based on identifying the reflected signals from the wall/liquid interface and the liquid/air interface. When the reflected signal from the wall/liquid interface is removed using the baseline, the remaining reflected signal will be from the liquid/air interface. Then, the time of flight method (Equation (5.8)) can be used to calculate the difference between the first peak from the wall/liquid interface and the first peak from the remaining waveform after removing the baseline. This processing method is evaluated by comparing the results with the frequency method using static measurements and the results from a concentric probe (Zhao et al., 2013) on the upward vertical annular flow test facility.

### 5.1.4. Baseline removal method

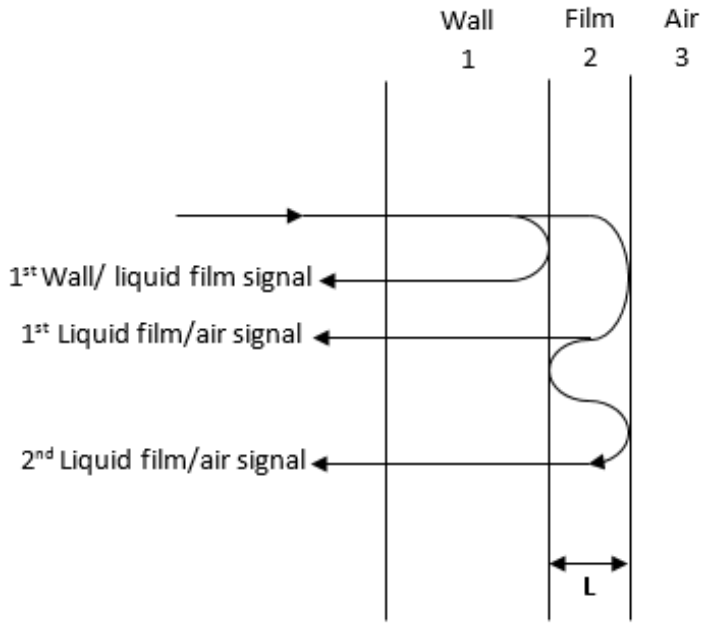


Figure 5.7: Diagram of the expected ultrasound wave paths for the three layers, a solid wall, a liquid film and air (Challis et al., 1998).

The measurement of the film thickness using a Time of Flight method by Equation (5.8) depends on identifying the first wall/liquid film reflected signal and the first liquid film/air reflected signal. When the liquid film is less than 0.5mm, the first liquid film/air reflected signal will overlap in time with the first wall/ liquid film reflected signal. This makes the two reflected signals interfere with each other and results a new reflected signal. However, there is a time difference between the two reflected signals where the first wall/liquid film reflected signal will always arrive before the first liquid film/air reflected signal even if they are overlapped by a factor of time required for the wave to propagate through the liquid film and reflect from the liquid film/air interface as shown in Figure 5.7. From Figure 5.7, the first wall/liquid film reflected signal arrives after the wave propagates through the wall and reflects from the

wall/liquid interface. In contrast, the first liquid film/air reflected signal arrives after the wave propagates through the wall and the liquid film and reflects from the liquid film/air interface. Therefore, the difference between the two reflected signals is the time taken by the wave to propagate through the liquid film twice. As an example, if the minimum liquid film thickness (L) is 0.1mm, this means the time difference between the two reflected signals will be equal to the time required for 0.2mm (2L). This can be demonstrated from the example given in Figure 5.8 which shows two different silicone oil film thickness waveforms (0.5mm (Blue line) and 0.6mm (Red line)). This is a 0.1mm different of film thickness between the two waveforms. In Figure 5.8, the amplitude of the two waveforms is plotted against the time in the same figure. It can be observed that there is a time difference between the two measurement points by the approximate time interval of 2L which is equal to 0.213μs.

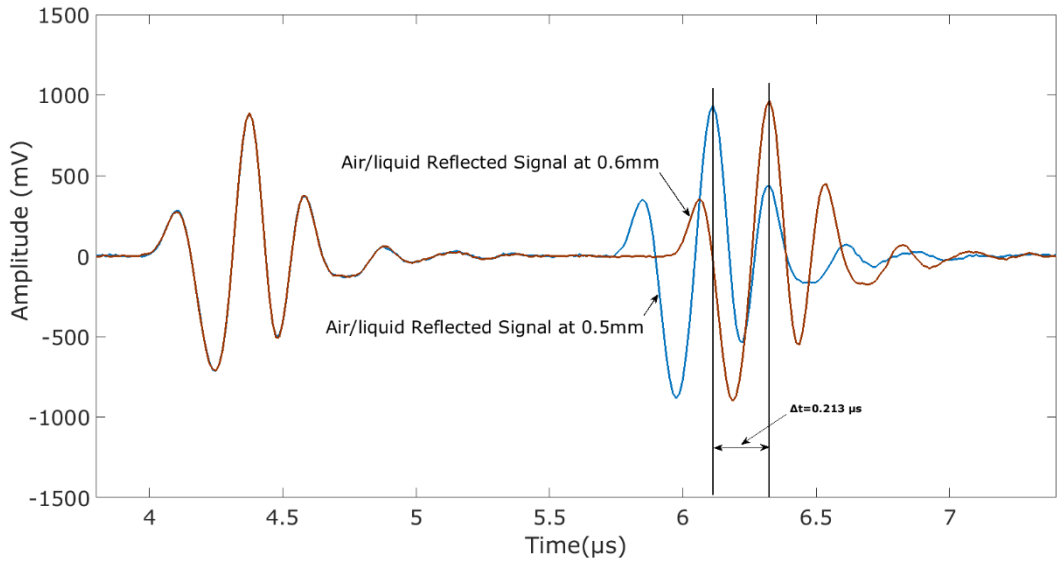


Figure 5.8: Two measurement waveforms with 0.1 mm different liquid film thickness. The first wall/liquid film signal is identical for both two measurement waveforms (0.5mm (Blue line) and 0.6mm (Red line)).

The first reflected wall/liquid film signal is always the same in terms of amplitude and location for all measurement waveforms across the measurement recording time. This was observed by plotting different measurement waveforms over each other as shown in Figure 5.8. However, in order to achieve this, the wall and liquid temperature should not be varying across the measurement recording time. In addition, the transducer position should be kept fixed and vibrations within the test section should be avoided.

As discussed and demonstrated from Figure 5.8, the time required by the waveform to propagate through a 0.1mm liquid film thickness is 0.213μs. In addition, the first wall/liquid reflected signal across the measurement time is identical for all the measurements. In order to evaluate the baseline removal method, Figure 5.9 shows an example of the baseline removal method for a silicone oil film thickness of 0.1 mm. In Figure 5.9, the amplitude of three signals is plotted in the same figure with respect to time. The three signals are original unprocessed overlapped signal (Red line), Baseline signal (Black line) and signal after subtracting the baseline signal (Blue line). As discussed at the end of section 5.1.3, the baseline removal method is based on subtracting the baseline signal from any overlapped signals to identify the first reflected liquid/air signal. Then, the time of flight through the film was calculated by measuring the time difference between the first peak from the wall/liquid interface from the baseline signal and the first peak from the remaining reflected peak after removing the baseline. Then, the film thickness was calculated using equation (5.8). From Figure 5.9, it can be observed that the time difference between the two reflected signals is 0.213 μs which is the same as demonstrated in Figure 5.8. The second observation is the identified first liquid film/air signal

consists of three cycles similar to the liquid film/air reflected signal from the thicker film as shown in Figure 5.8.

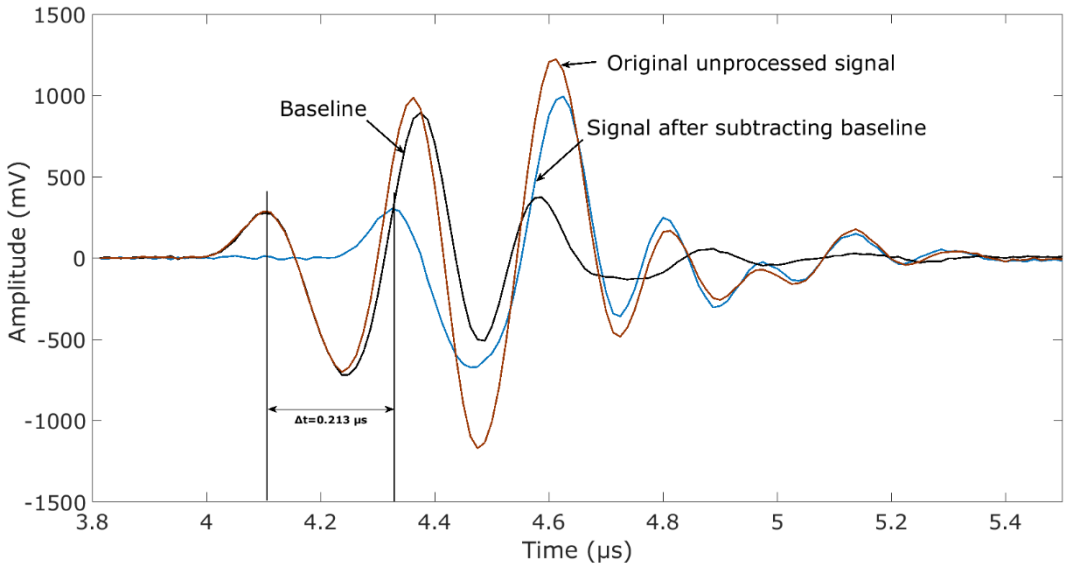


Figure 5.9: Ultrasound signals illustrating the baseline removal method for a film thickness of 0.1 mm. Original unprocessed signal (Red line), Baseline (Black line) and Signal after subtracting baseline (Blue line).

### 5.1.5. Ultrasonic Validation for film thickness measurement

The ultrasonic pulse-echo technique was validated using static and dynamic measurements. In the static measurements, the ultrasonic technique was validated using a benchtop experiment using water and silicone oil (4.4 cP). The ultrasonic technique was also validated against two other well-known measurement techniques based on conductance measurements using an air/water system under dynamic conditions. Each method of validation will be discussed in detail in the following subsections.

#### 5.1.5.1. Static measurement setup

The ultrasonic technique was validated using silicone oil (4.4 cP) as shown in the schematic diagram in Figure 5.10. The validation was for static conditions with film thicknesses between 0.1 mm and 6 mm. A cylindrical test section made of acrylic resin Perspex (Internal Diameter = 24.8 mm, wall thickness=5 mm and Height= 20 mm) was used. A Technisonic transducer model IPM-0502-HR 5MHz was used for these experiments. This was located in the centre of the bottom external surface of the test section. The diameter of the test section was measured using a digital caliper with an accuracy of +/-0.01 mm, and the volume was measured using a Gilson's Pipetman Classic with an accuracy of +/-2 µL. In the current study, a US-KEY (Lecoeur Electronique) was used as the transmitter, receiver, and digitiser. This was operated via LabVIEW. The received signals were recorded and processed using MATLAB to calculate the film thicknesses. The US-KEY is light, easy to install and does not require a separate power supply. The thickness of the film measured by the ultrasonic technique was compared with those calculated theoretically using equation (5.10):

$$\delta_{th} = \frac{V}{A} \tag{5.10}$$

where $\delta_{th}$ is theoretical liquid film thickness, V is the volume and A is the cross-sectional area.

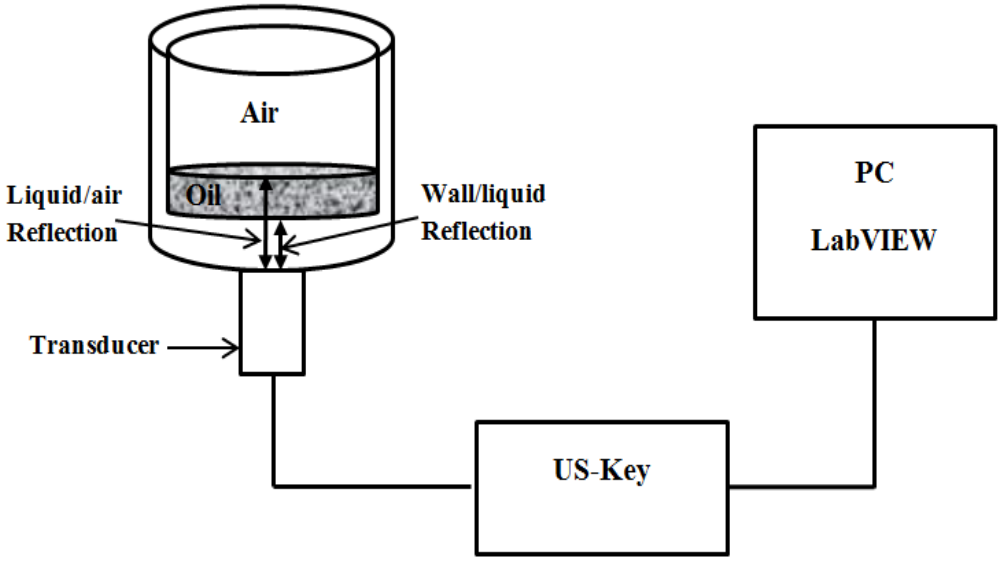


Figure 5.10: Schematic Diagram of the static experiment using a cylindrical test section.

The film thickness measurement using the US-KEY (Setup2) was validated and compared with the conventional setup (Setup1) as shown in Figure 5.11. In the conventional setup, an Ultrasonic Pulser Receiver (UPR) was used as a transmitter and receiver with an oscilloscope as a digitiser. Both setups achieved the same results with an absolute error in film thickness measurement within ±0.0004 mm as shown in Figure 5.12.

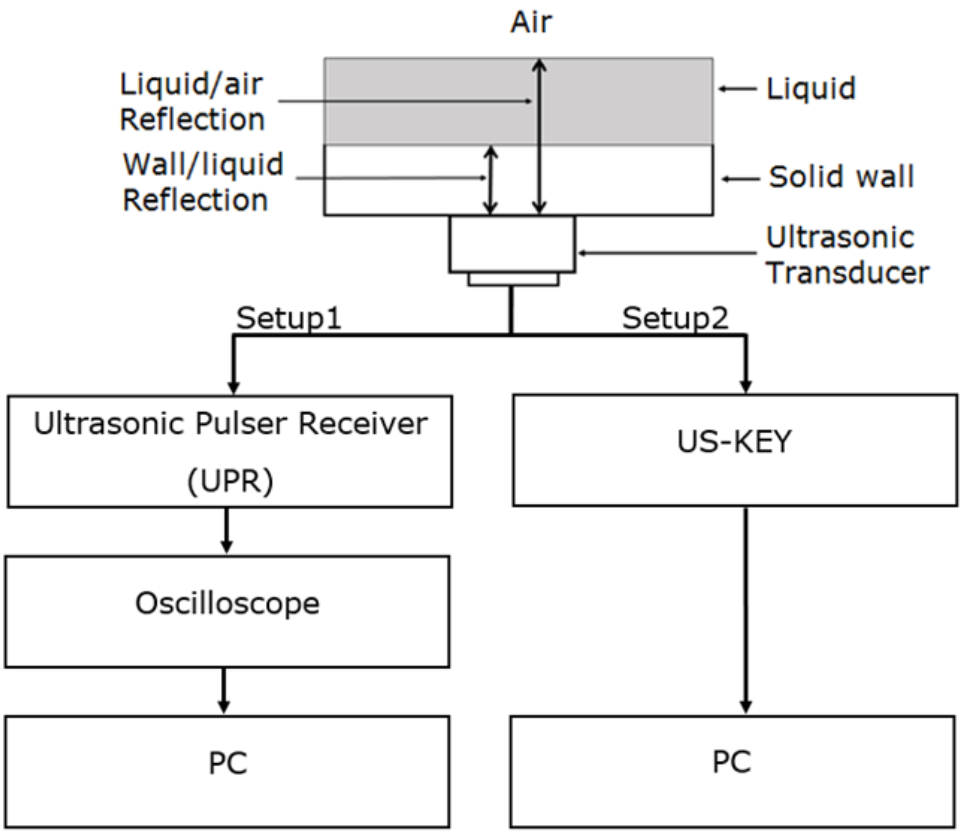


Figure 5.11: Ultrasonic measurement setups

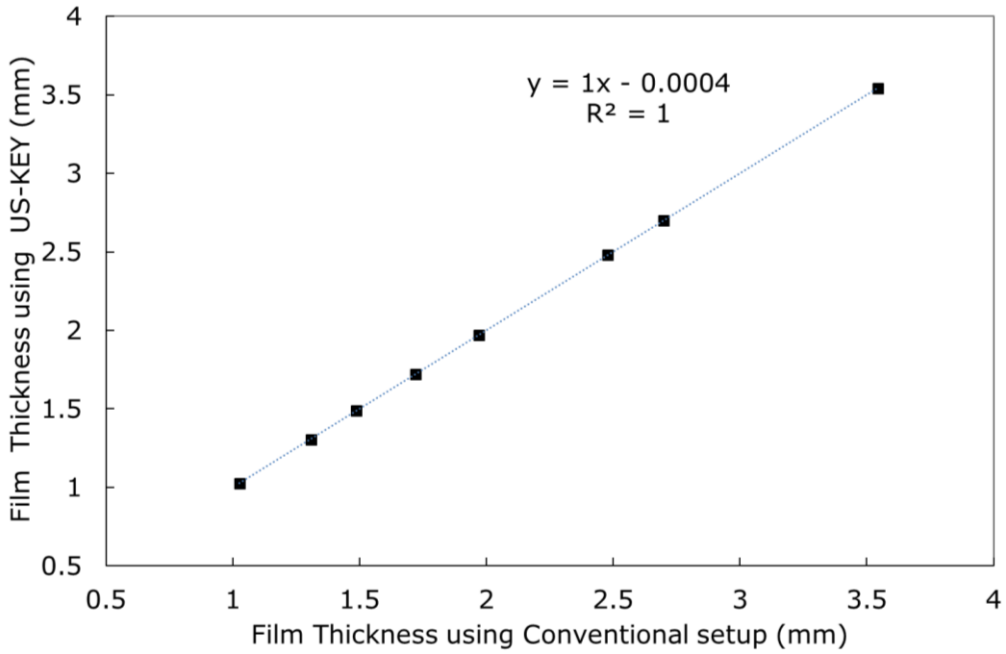


Figure 5.12: Comparison results between Ultrasonic measurement setups.

Silicon oil with 4.4 cP viscosity was used as it is the same liquid that will be used in the upward annular flow test facility and can generate film thicknesses less than 1 mm. It was difficult to generate thin films less than 1 mm using water due to surface tension effects. The speed of sound of the silicone oil at temperatures ranging between 10 and 45°$C$ at atmospheric pressure was measured using a TF instruments RESOSCAN as shown in Figure 5.13. Figure 5.13 shows the relationship between the silicone oil speed of sound and the temperature. These measurements were required to account for any temperature effects on the liquid film thickness measurements that is expected in the current experiments. The measurement of silicone oil speed of sound was repeated three times during heating and cooling and the maximum speed of sound coefficient of variation was within 0.02%. The coefficient of variation is defined as the ratio of the standard deviation to the mean. The silicone oil speed of sound can be calculated using the following equation (5.11) based on repeated measurements obtained using the TF instruments RESOSCAN.

$$C_L = 1.0472 \times 10^3 - 3.2691T + 4.2 \times 10^{-3}T^2 \quad (5.11)$$

where T is the temperature in degrees Celsius. This equation is valid for temperature range 10-45$^{o}$C at atmospheric pressure.

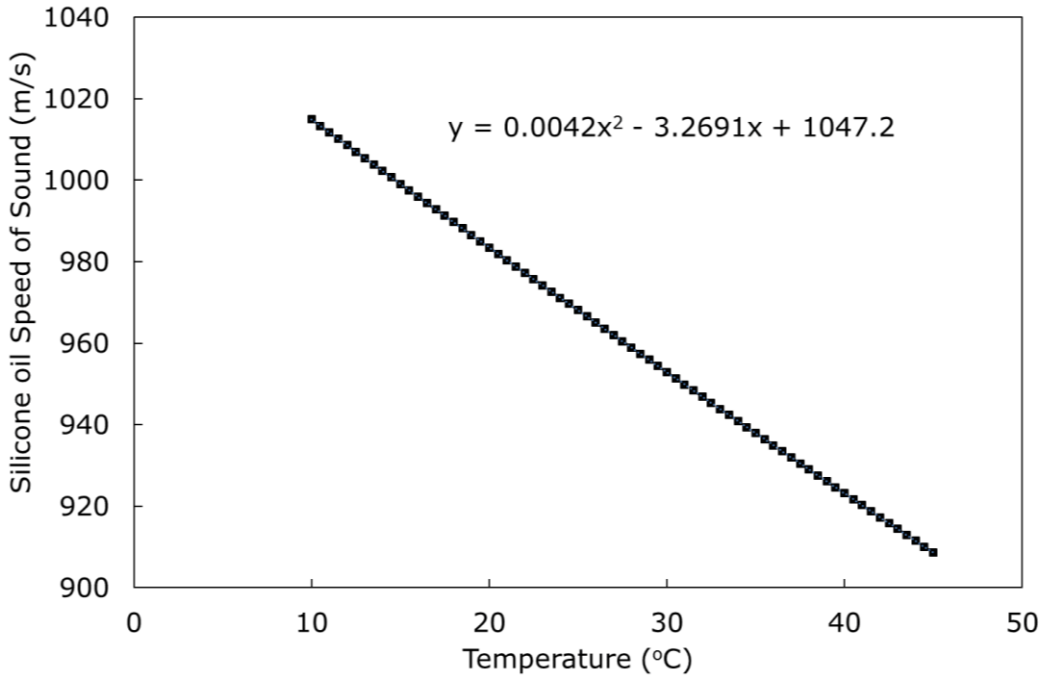


Figure 5.13: Speed of Sound of silicone oil (4.4 cP) for temperature range 10-45$^{o}$C at atmospheric pressure.

The RESOSCAN measurement was validated by measuring the speed of sound of distilled water for temperature range 10-45$^{o}$C at atmospheric pressure and comparing with those available in the literature (Equation 5.12) as shown in Figure 5.14. The relative deviation between RESOSCAN and Equation 5.12 was ±0.04%. The speed of sound of distilled water (Figure 5.14) at a known temperature for the experiments was calculated using equation (5.12) (Bilaniuk and Wong, 1993).

$$C_L = 1.40238677 \times 10^3 + 5.03798765T - 5.80980033 \times 10^{-2}T^2 + 3.34296650 \times 10^{-4}T^3 - 1.47936902 \times 10^{-6}T^4 + 3.14893508 \times 10^{-9}T^5 \quad (5.12)$$

where T is the temperature in degrees Celsius. This equation is valid for temperature range 0-100$^{o}$C at atmospheric pressure.

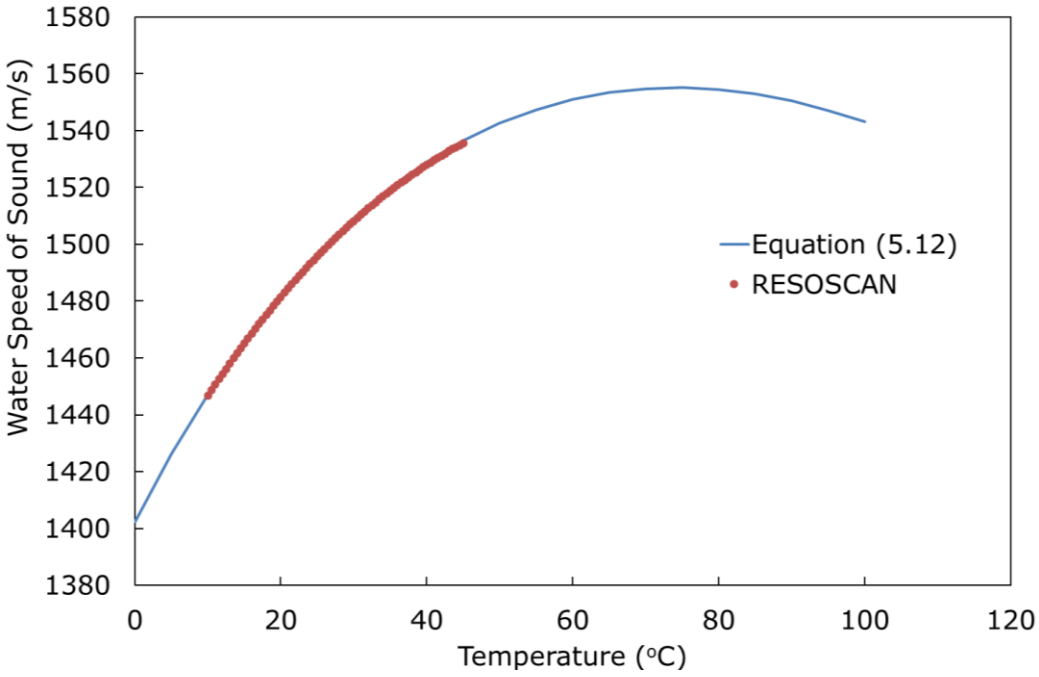


Figure 5.14: Comparison of water speed of sound measurement using RESOSCAN with literature Bilaniuk and Wong (1993) equation).

Distilled water was also used to validate the film thickness measurements with a different test rig using a rectangular tank made of acrylic resin Perspex (width= 110 mm, length = 200 mm, wall thickness=5 mm and Height= 50 mm). The US-KEY and a Technisonic transducer model IPM-0102-HR 1MHz were used. The same method of validation with silicone oil was followed with distilled water. This was used to validate the ultrasonic technique for film thickness greater than 2 mm up to 6 mm and was also capable of investigating the effect of inclination angle (incident wave angle) on measurement capability. The ultrasonic measurement is affected by the incident wave angle where it has poor detection sensitivity due to the varying angle of the reflection interface according to

Serizawa et al. (1994). The angle was adjusted by lowering the test rig from one side. This angle was measured using a clinometer digital measurement. The other end of the test rig was fixed with a pivot joint where the test rig could be easily tilted. These experiments were performed on a film with a 6mm thickness. The effect of inclination angle will be discussed in section 5.1.5.3.

#### 5.1.5.2. Static measurement results

Figure 5.15 and Figure 5.16 show the comparisons of the mean film thicknesses of silicone oil and water obtained by the ultrasonic methods and theoretical calculations (Equation 5.10). For both experiments, the test was repeated three times to understand variability at temperature $20^{o}C \pm 0.2^{o}C$. The maximum standard deviation error of the mean at each measurement point between repeated tests was 0.03 mm for both fluids. The time of Flight method was used for film thicknesses greater than 0.5 mm. Both frequency and baseline removal methods were used for film thicknesses less than 0.5 mm. The standard deviation error was calculated by dividing the standard deviation by the square root of number of repeated points.

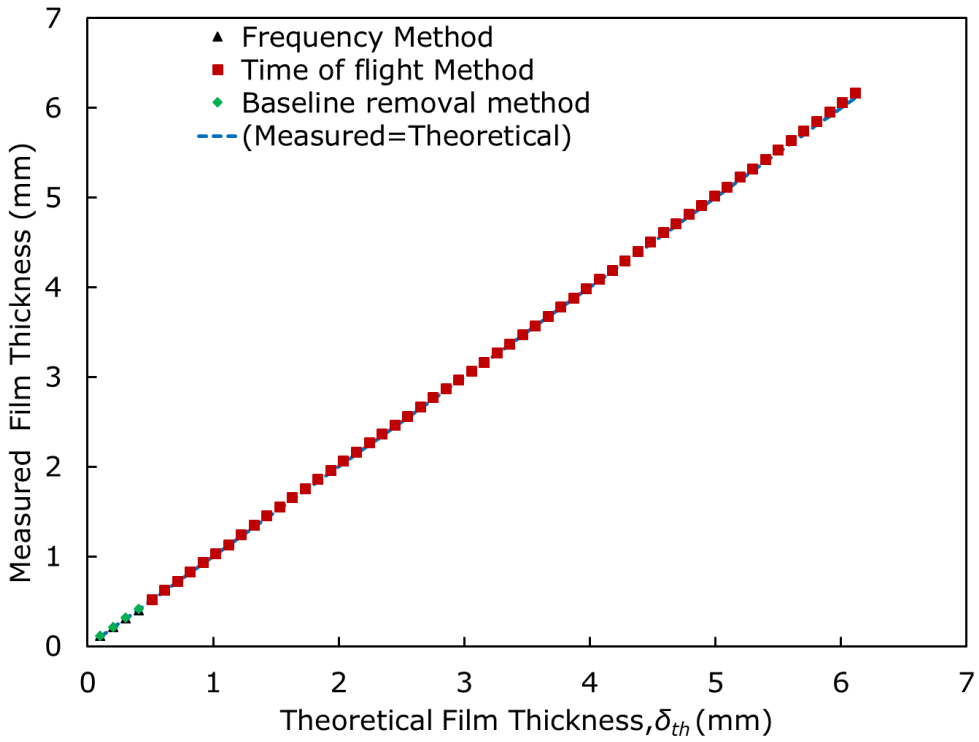


Figure 5.15: Ultrasonic pulse echo validation results for different processing methods against theoretical calculations (Equation 5.10) using silicone oil with maximum standard deviation error of 0.03 mm.

From Figure 5.15, the ultrasonic technique shows good agreement with the theoretical results (Equation 5.10). The comparison of the mean film thicknesses of water obtained by the ultrasonic technique and theoretical calculation (Equation 5.10) are shown in Figure 5.16. The measured values in Figure 5.16 for thinner films (2mm and 3mm) are slightly deviated from the calculated value by maximum relative deviation of 2% due to an error in volume, the speed of sound and temperature measurements in laboratory conditions. However, it should be noted that there is a better agreement when the film thickness increases. This is due to the improved accuracy of the volume measurements of

the liquid. In general, the ultrasonic results show good agreement with values obtained theoretically (Equation 5.10) taking potential measurement errors into account.

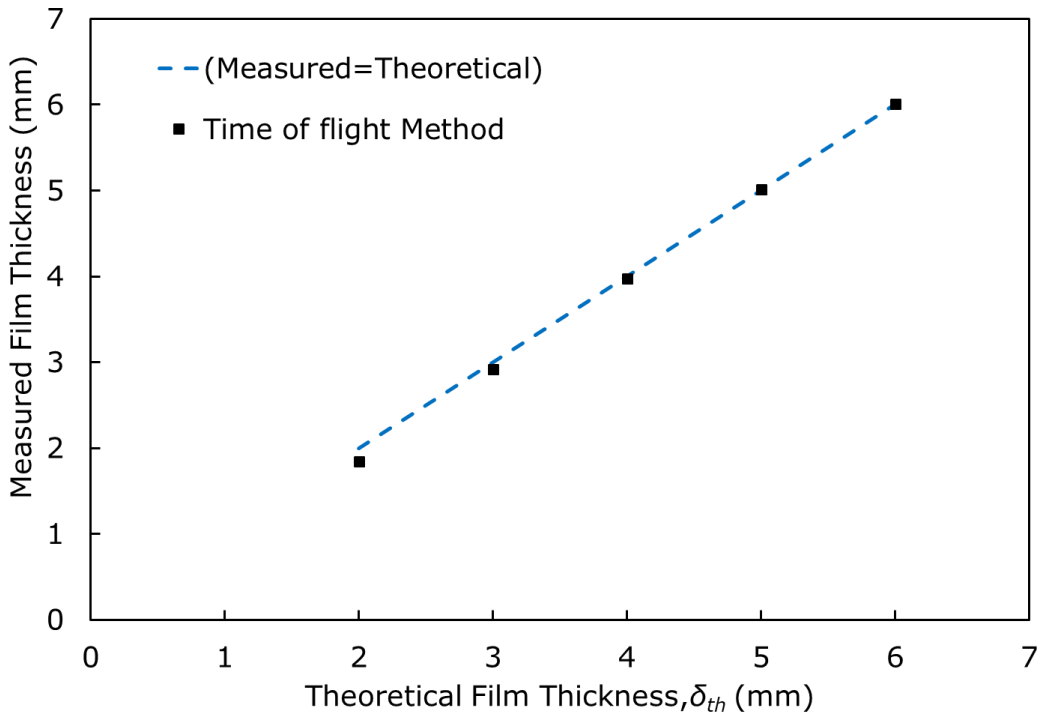


Figure 5.16: Ultrasonic pulse echo validation results for the time of flight method against theoretical calculations (Equation 5.10) using water with maximum standard deviation error of 0.03mm.

The film thickness measurements between 0.1 mm and 0.5 mm were calculated using the frequency domain and baseline removal methods. Figure 5.17 shows the results of film thickness measurement from the frequency domain and baseline removal methods against the film thickness measurement from theoretical calculations (Equation 5.10). Both processing methods showed good agreement. However, the baseline removal method requires less computational processing compared to the frequency method as discussed in Section 5.1.3.

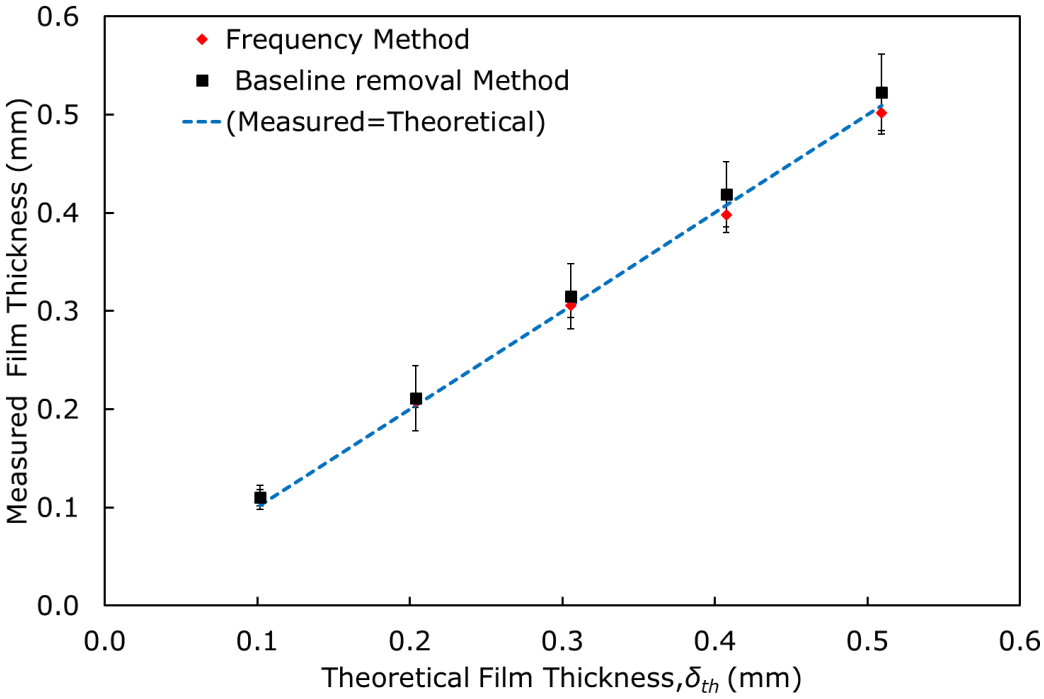


Figure 5.17: Ultrasonic pulse echo validation results in silicone oil for the frequency domain and baseline removal methods. These are compared to theoretical calculations (Equation 5.10) based on the volume of fluid added.

### 5.1.5.3. Effect of Inclination Angle on Ultrasonic Measurement

As discussed before, the reflected waves are affected by the angle of the incident waves which was highlighted as a problem by Serizawa et al. (1994). Therefore, the effect of the variation of the incident wave angle (inclination) was investigated up to 4 degrees. This angle was the upper limit because the liquid was completely removed from the sensor above 4 degrees. This was performed using the rectangular test rig at a 6mm liquid film thickness and a 1 MHz transducer instead of 5 MHz. The detection of the reflected signal from the liquid film/air interface depends on the transducer diameter according to Serizawa et al. (1994) and both transducers used in this work have the same

diameter. A wider transducer diameter will capture more reflected signal compared to a narrow transducer diameter. Figure 5.18 shows that the amplitude of the reflected signal decreased as the inclination angle increased because some of the reflected signals are not received by the transducer. It was also observed that as the inclination angle increased, the measured time of flight reduced affecting the film thickness measurements. This is in agreement with the observations of Serizawa et al. (1994). Serizawa et al. (1994) used an inclined solid surface placed in water to simulate the reflection interface. In the current study, the effects of inclination angle will be less as the liquid film thickness is thin and less than 1mm and the transducer will be able to capture most of the reflected signals.

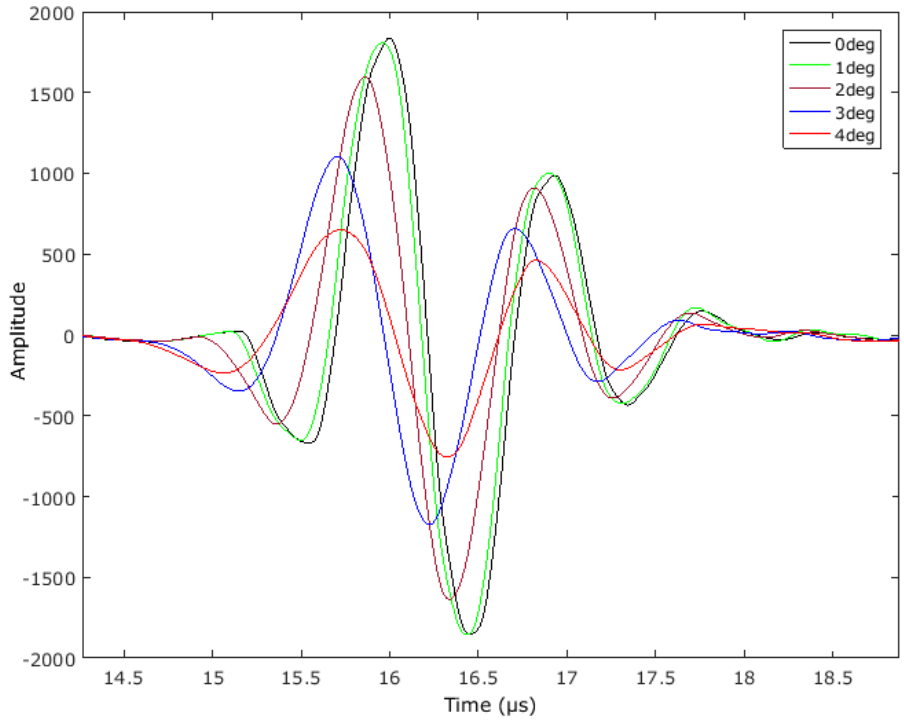


Figure 5.18: Effects of inclination angle on the captured ultrasonic signal. The decreasing amplitude of the captured signal with the increasing inclination angle is clearly shown.

### 5.1.5.4. Dynamic measurement setup

The capability of the ultrasonic pulse echo technique to measure film thicknesses in the flowing test facilities was evaluated by comparing its output signal with other measurement techniques. It was evaluated against a Multi Pin Film Sensor (MPFS) using the falling film annular flow test facility (Figure 3.1) at different liquid Reynolds numbers ($Re_l$) ranging from 618 to 1670. $Re_l$ is defined as:

$$Re_l = \frac{\rho_l u_{sl} \delta}{\mu_l} = \frac{\rho_l Q_l}{\pi D \mu_l} \tag{3.1}$$

$$u_{sl} = \frac{Q_l}{\pi D \delta} \tag{3.2}$$

where $\rho_l$ is liquid density, $u_{sl}$ is liquid superficial velocity, $Q_l$ is liquid volumetric flowrate, D is pipe internal diameter and $\mu_L$ is the dynamic liquid viscosity. The length scale used to calculate the liquid Reynolds number is the mean liquid film thickness. It was also evaluated against a concentric conductance probe on the upward vertical annular flow test facility (Figure 3.4). The experiments were conducted for gas superficial velocity ranges from 17.83 m/s to 35.66 m/s and liquid superficial velocity 0.089 m/s with water at atmospheric conditions. The test facilities and the measurement techniques with their calibration were described in Chapter 3.

### 5.1.5.5. Dynamic measurement results

*Falling films*

During the falling film annular flow experiments using water, the film thickness measurements were in agreement between the ultrasonic technique and the Multi Pin Film Sensor (MPFS) at different liquid Reynolds numbers. Both measurement techniques were able to measure the variation in the liquid film thickness as shown in Figures 5.19 and 5.20. Figures 5.19 and 5.20 show the instantaneous measurement of the liquid film thickness at liquid Reynolds number 618 using ultrasonic and MPFS techniques respectively. There is a spatial separation of 300 mm between the two sensors.

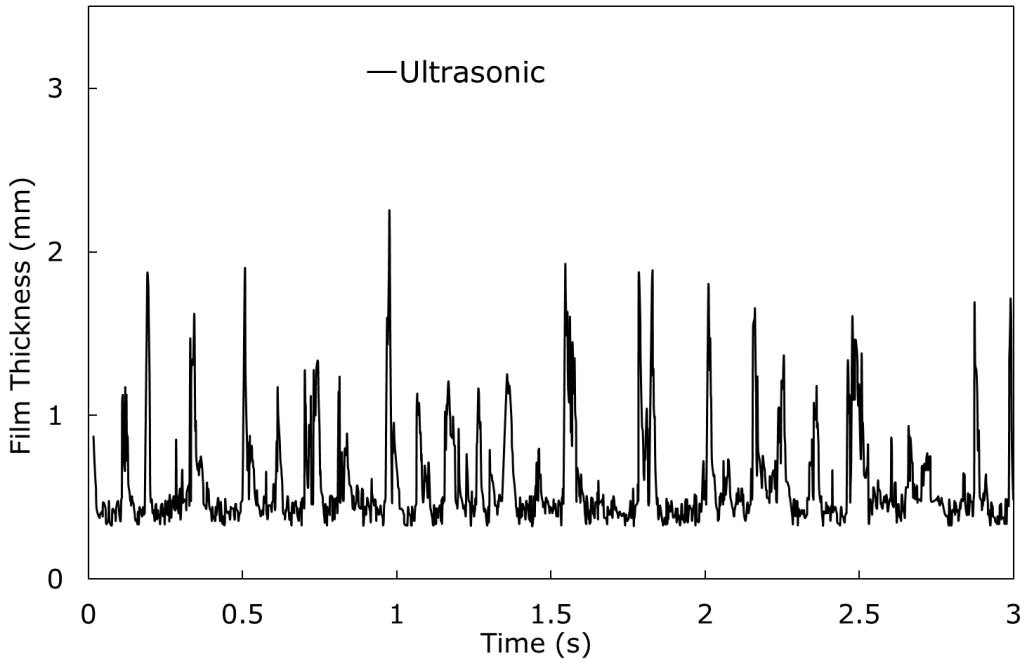


Figure 5.19: Instantaneous variation of the film thickness using Ultrasonic technique at liquid Reynolds number 618.

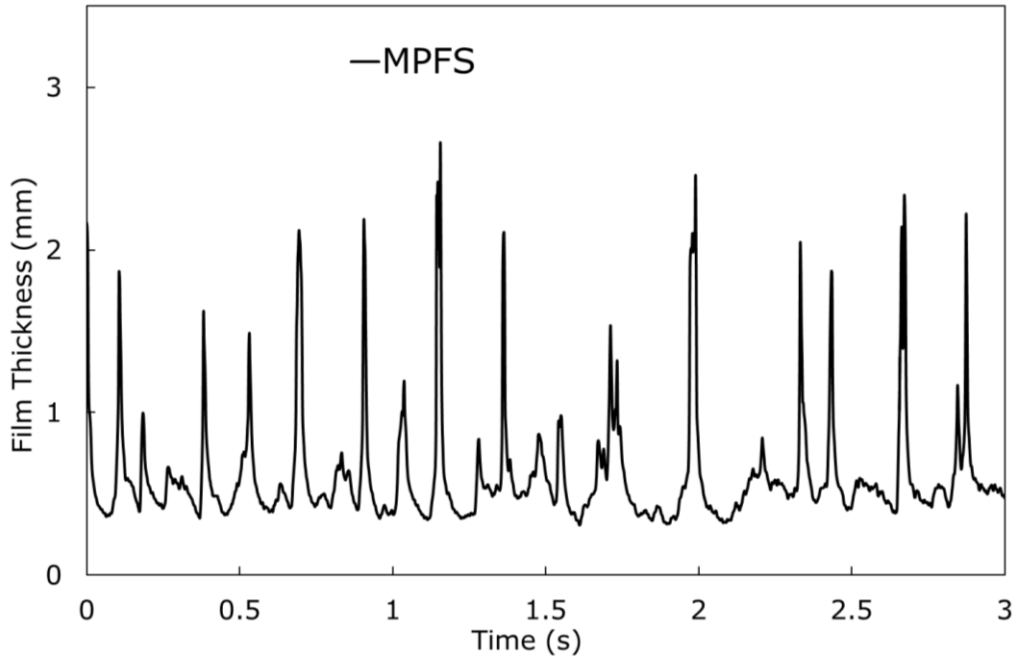


Figure 5.20: Instantaneous variation of the film thickness using MPFS at liquid Reynolds number 618.

The film thickness measurements of both techniques were statistically analysed using Power Spectral Density (PSD). The Power Spectral Density (PSD) was obtained using Welch's method in the MATLAB software. In the Welch's method, the time series signal is divided into small overlapping segments where spectrum analysis using a FFT is computed for each segment. Then, the averaging spectral estimate for all segments is obtained. In the current analysis, the length of each segment is 500 with 50% overlap between them. The power spectral density of both techniques for different Reynolds numbers ranged from 618 to 1670 are shown in Figure 5.21. Both techniques were able to measure the variation of the film thickness frequency and agreed with each other. The film thickness exhibits a frequency ranging from 5 Hz to 8 Hz and generally increased with increasing the liquid Reynolds number.

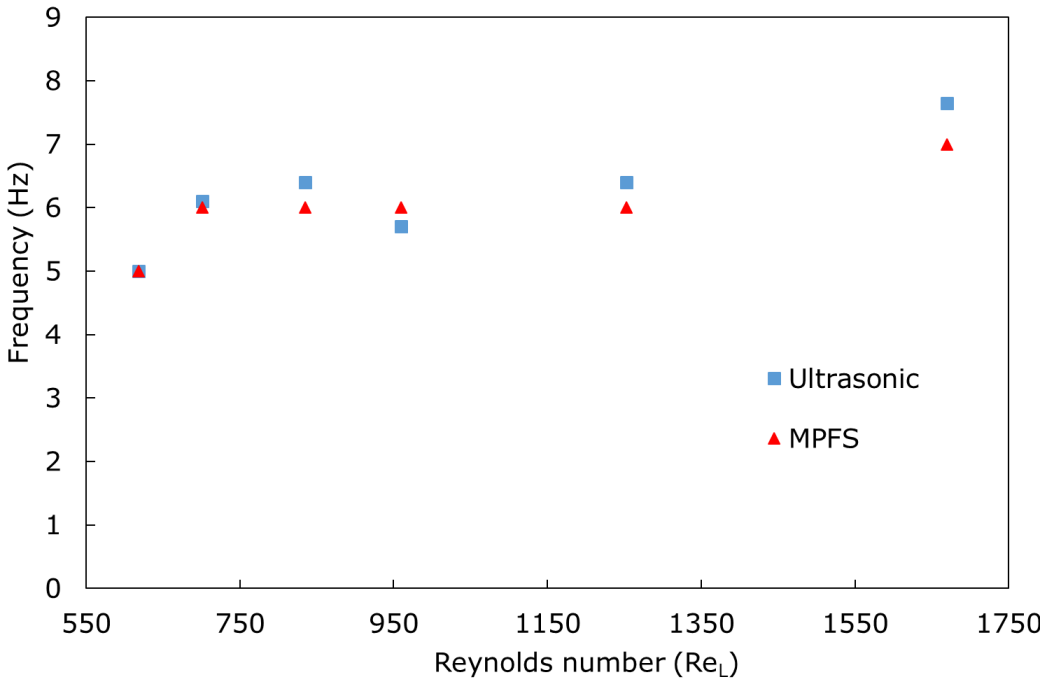


Figure 5.21: Power Spectral Density (PSD) of the film thickness measurements using MPFS and ultrasonic techniques at different liquid Reynolds numbers.

Applying the frequency domain method in wavy films is challenging and results in many spectral peaks requiring significant post processing and leading to unreliable results as indicated in Figure 5.22. This was checked by comparing the time of flight results at film thickness equal to 0.5 mm with the results obtained by the frequency domain method. The frequency domain method gives a higher value which was 0.8 mm. Further development is required to enhance the capabilities of the frequency domain method to operate on wavy films. The data obtained by the frequency domain method was rejected in the current comparisons between the ultrasonic technique and the MPFS. Instead, the baseline removal and time of flight methods were used in calculating the instantaneous film thickness.

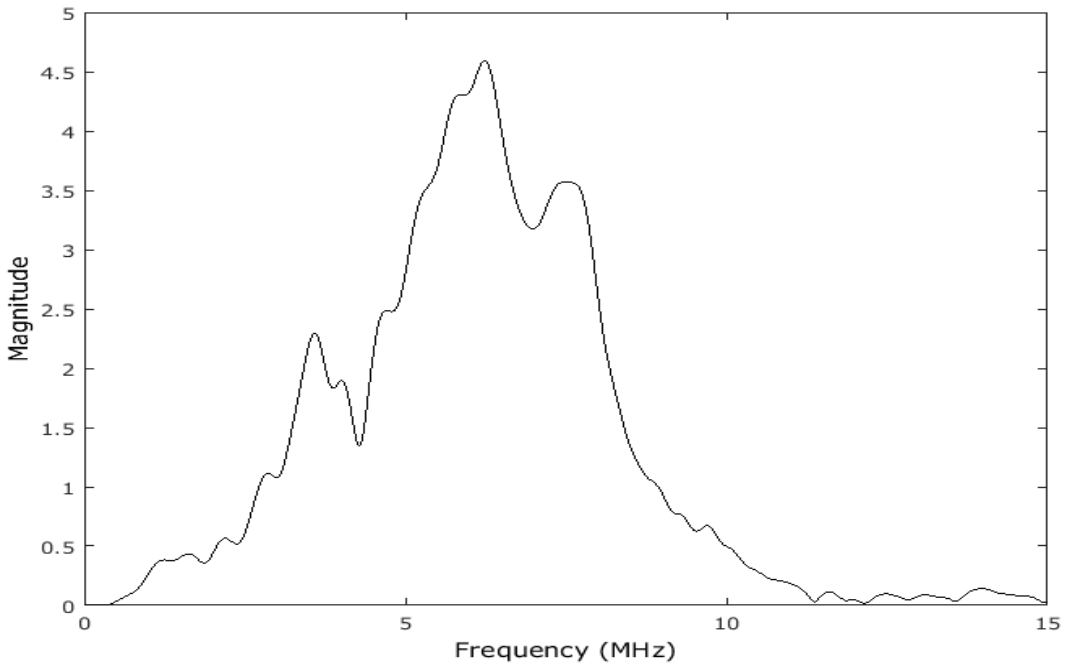


Figure 5.22: Spectrum Wavy Signal results after applying the frequency method where many spectral peaks are appearing.

In terms of the mean film thickness, the data obtained by the ultrasonic measurements showed good agreement with the Multi Pin Film Sensor (MPFS) with a relative deviation less than ±5% between them. This highlights the potential of the technique as shown in Figure 5.23. Figure 5.23 shows the comparison of mean liquid film thickness measurements between the MPFS and the ultrasonic measurements at different liquid Reynolds numbers. Both techniques show the expected trend where the measured film thickness increased as the liquid Reynolds number increased.

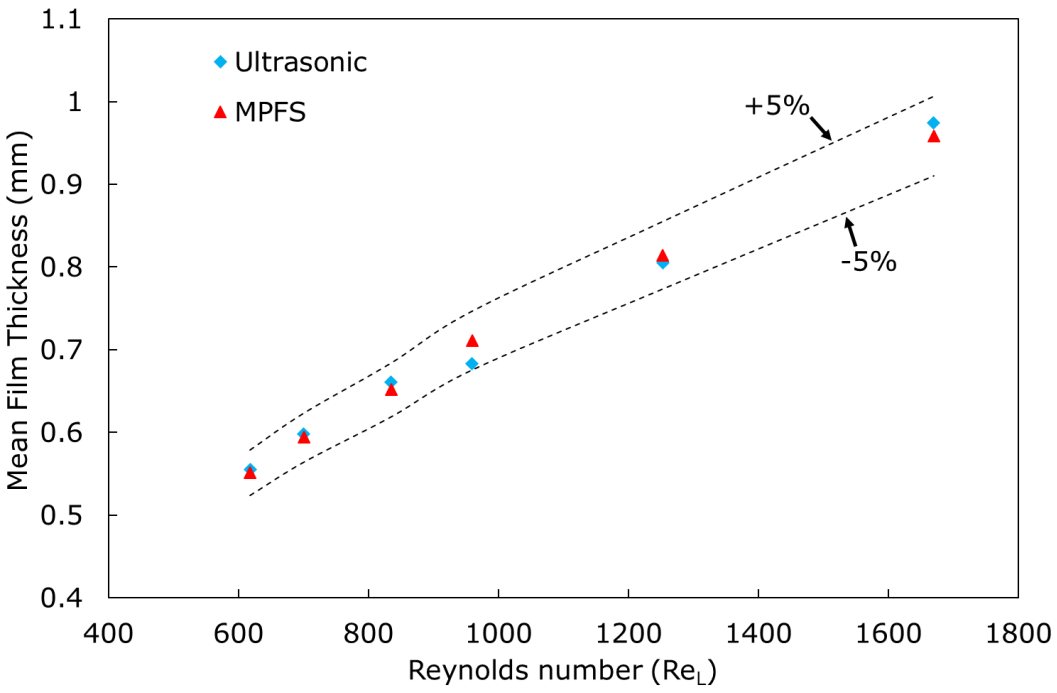


Figure 5.23: Mean film thickness between Ultrasonic and MPFS using water with a relative deviation less than ±5% between them.

*Upward annular flow*

In the upward vertical annular flow experiments, the time series measurements of film thickness by the ultrasonic technique showed similar trends to that measured by the concentric conductance probe (Described in Chapter 3) for the same experimental parameters. Both measurements techniques were able to measure the variation in the liquid film thickness as shown in Figures 5.24 and 5.25. Figures 5.24 and 5.25 show the capability of both techniques to measure the instantaneous film thickness in upward vertical annular flow at a liquid superficial velocity of 0.089m/s and gas superficial velocity of 35.66 m/s. There is a spatial separation of 70 mm between the two sensors. The film thickness measurements recorded using the ultrasonic technique were calculated using the

baseline removal and time of flight methods. This was performed to check the capability of baseline removal method for measuring film thicknesses less than 0.5 mm on a flowing test facility.

The power spectral density of both techniques at a liquid superficial velocity of 0.089 m/s and different gas superficial velocities ranging from 17.83 to 35.66 m/s are shown in Figure 5.26. Both techniques were able to measure the variation of the film thickness frequency and agreed with each other. The film thickness frequency increases with increasing gas superficial velocities which varies from 7 Hz to 18 Hz.

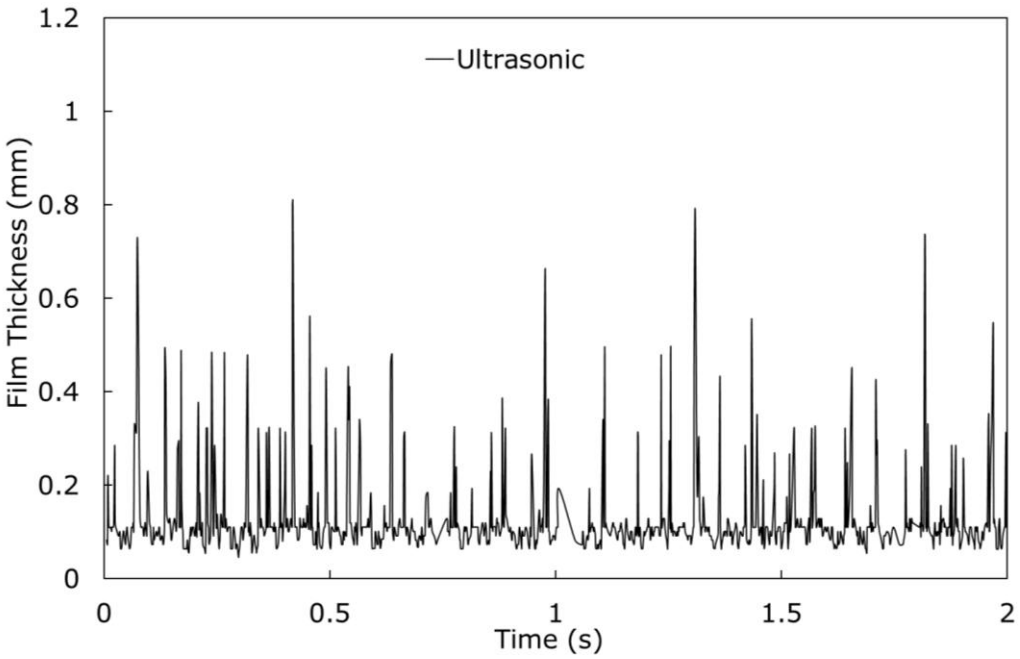


Figure 5.24: Instantaneous variation of the film thickness using the ultrasonic technique at water and gas superficial velocities of 0.089 m/s and 35.66 m/s respectively.

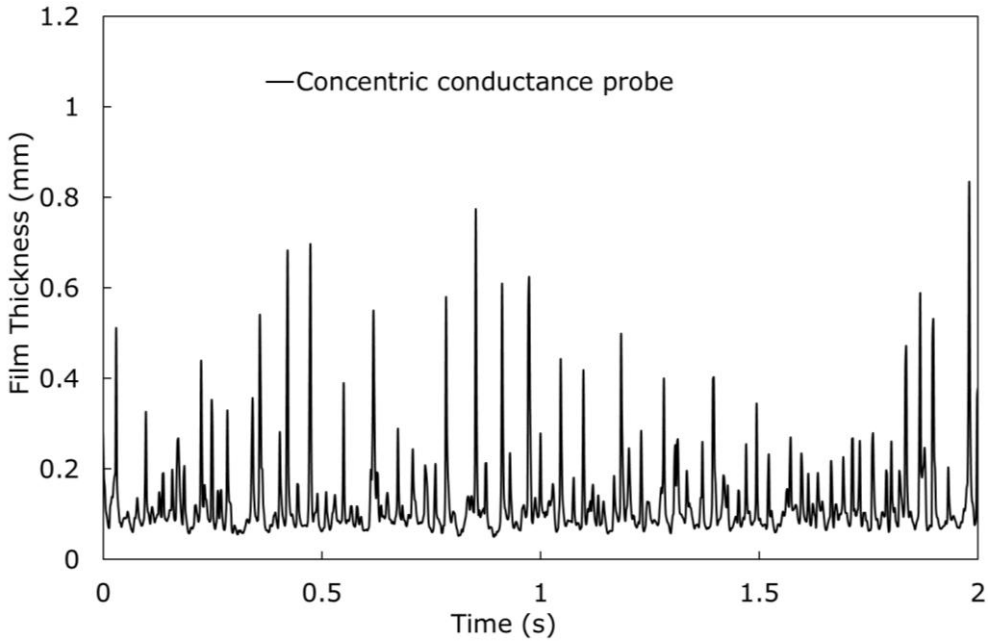


Figure 5.25: Instantaneous variation of the film thickness using the concentric conductance probe at water and gas superficial velocities of 0.089 m/s and 35.66 m/s respectively.

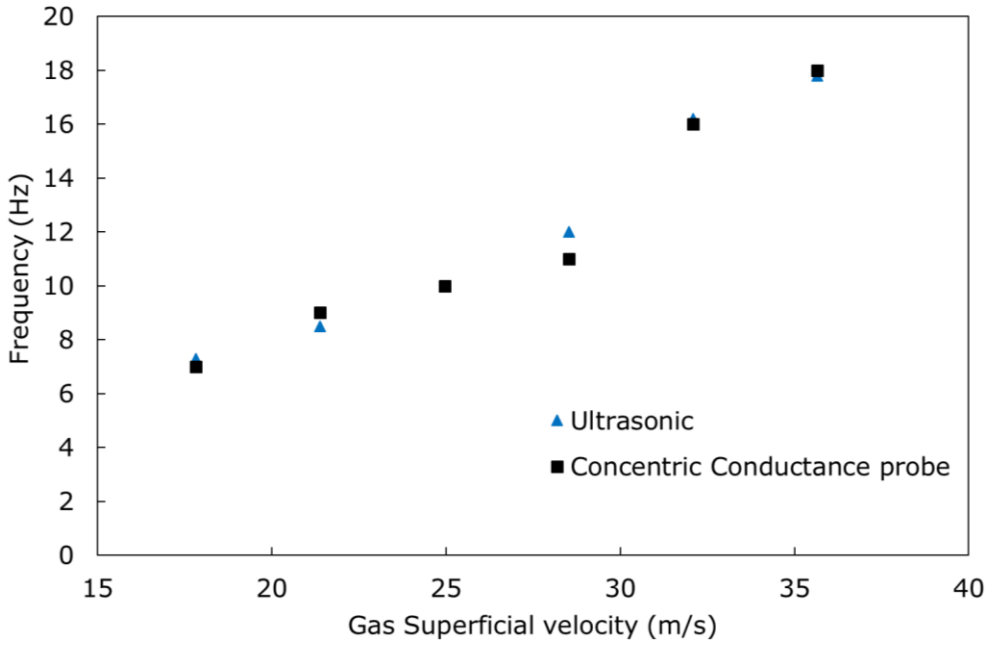


Figure 5.26: Power Spectral Density (PSD) of the film thickness measurements using the concentric probe and ultrasonic technique at different gas superficial velocities and water superficial velocity of 0.089 m/s.

The ultrasonic technique and concentric conductance probe technique also showed excellent agreement in term of the mean film thickness measurement with a relative deviation less than ±5% between them. Both techniques showed the expected trend where the measured film thickness decreased as the gas superficial velocity increased at fixed liquid superficial velocity (Figure 5.27).

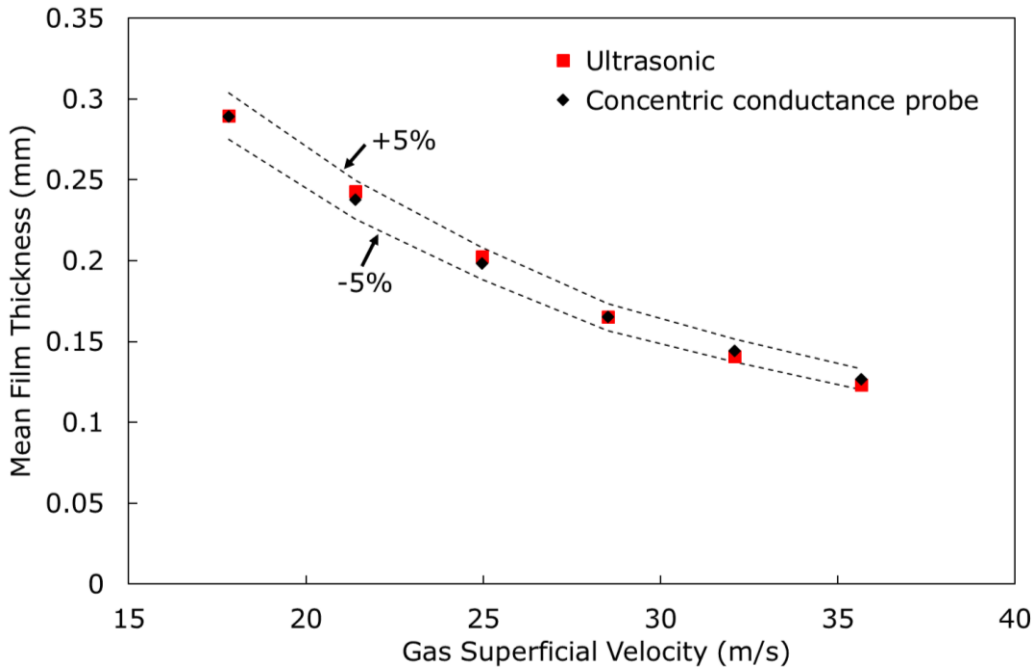


Figure 5.27: Mean film thicknesses measured using ultrasonic and concentric conductance techniques at water superficial velocity of 0.089 m/s with a relative deviation less than ±5% between them.

Both static and dynamic measurements show the capabilities of the ultrasonic technique for measuring thin film thicknesses using different signal processing methods. It also highlights the capability of the baseline removal method for measuring the film thickness when the reflected signals were overlapped in time. Increasing the data acquisition rate can improve the temporal resolution of measured film thicknesses. More data points will allow a more accurate calculation of the mean film thickness. Hence, characteristics of the instantaneous liquid film could be better identified in the flowing test facility. The current ultrasonic measuring system has a data acquisition rate of 500 Hz, (500 frames/s). It is higher than other systems used by previous researchers including Park and Chun (1984), Lu et al. (1993), Serizawa et al. (1994) and Chen et al. (2005).

## 5.2. Effect of gas and liquid superficial velocity on liquid film thickness

The mean liquid film thickness is influenced by gas and liquid superficial velocities as shown in Figure 5.28 for an air/water system using the upward vertical annular flow test facility. The mean liquid film thickness increases with increasing the liquid superficial velocity due to an increase in the liquid volume. On the other hand, the mean liquid film thickness decreases with increasing the gas superficial velocity due to the increase of interfacial shear force and hence the entrainment rate (Sawant et al., 2008). This observation was also reported by previous researchers such as Fukano and Furukawa (1998), Belt et al. (2010), Zhao et al. (2013). Ju et al. (2015) reported that the liquid film thickness is

affected by the ratio of inertia force and surface tension of both gas and liquid through the Weber number. Hence this effect is related to the entrainment rate which is influenced by these forces as discussed in Chapter 4.

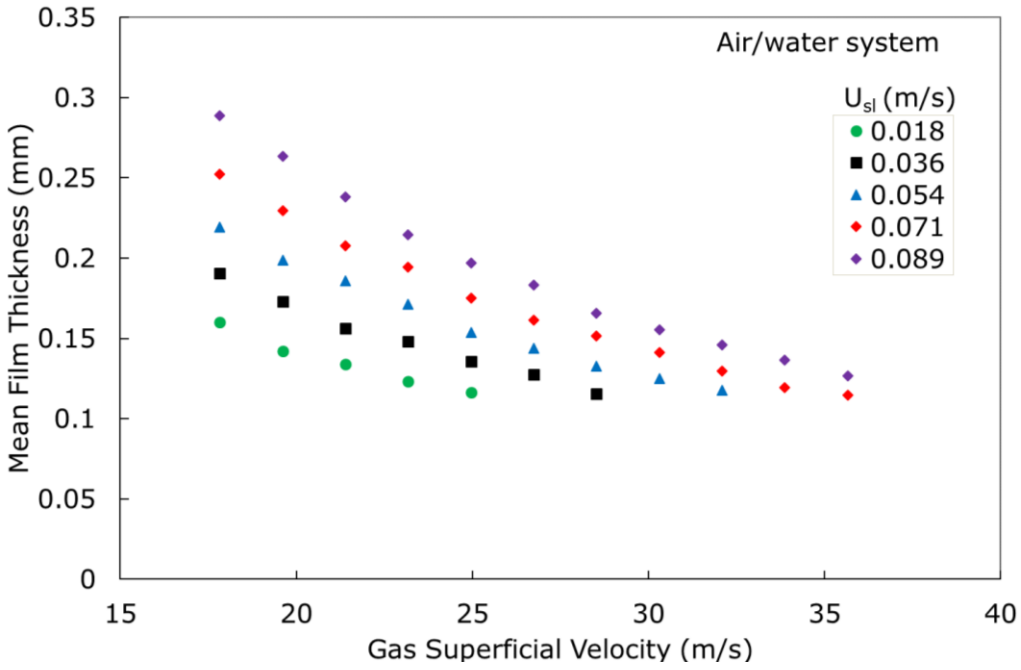


Figure 5.28: Effect of gas and liquid superficial velocity on the mean film thickness of air/water system.

In addition, the increase of the gas superficial velocity leads to the reduction in the disturbance wave height as shown in Figure 5.29 for a water superficial velocity of 0.089 m/s and gas superficial velocity of 17.83 m/s and 35.66 m/s. Sawant et al. (2008) and Pan et al. (2015a) presented similar behaviour.

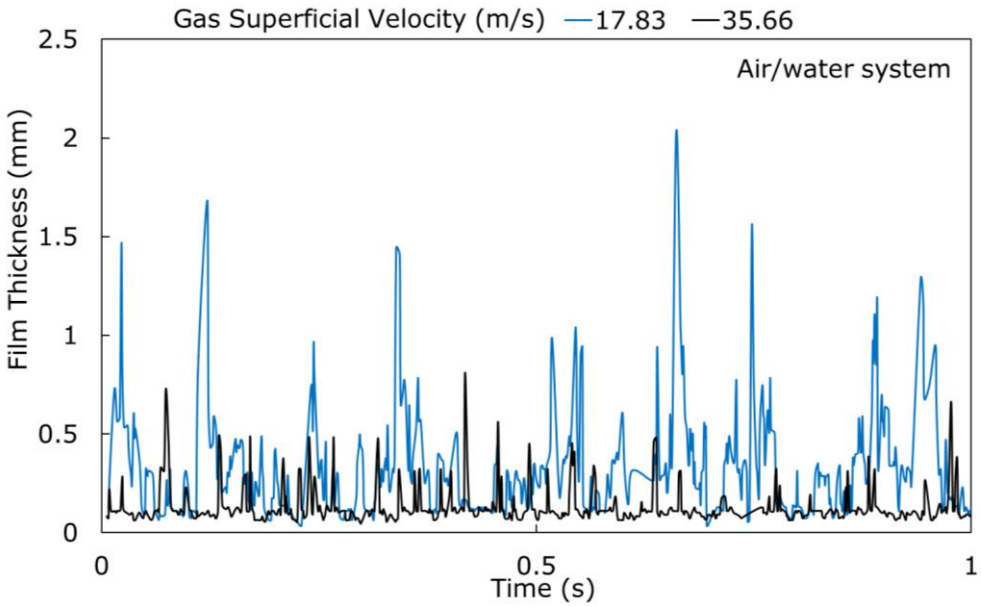


Figure 5.29: Effect of gas superficial velocity on the disturbance wave height of an air/water system for a water superficial velocity 0.089 m/s and gas superficial velocity of 17.83 m/s and 35.66 m/s.

The previous researchers related the reduction of the liquid film thickness to the increase of entrainment rate, and when the entrainment rate reaches nearly steady state, there will be less effect on the film thickness (Sawant et al., 2008, Al-Sarkhi et al., 2012). On the other hand, the effect of the increase in the entrainment rate could be related to the reduction in the disturbance wave height due to the increase of the interfacial shear force on the air/liquid interface and making the interface smooth as the gas superficial velocity increases. This indicates that the mean liquid film thickness decreases as the disturbance wave height decreases. When the interface becomes smooth, there will be no further reduction in the mean film thickness, and the entrainment rate reaches steady state.

The air/silicone oil system shows similar behaviour to the air/water system when the gas and liquid superficial velocity increases as shown in Figure 5.30. The mean film thickness of silicone oil decreases with increasing gas superficial velocities and rises with increasing liquid superficial velocities. Also, the increase of the gas superficial velocity leads to the reduction in the disturbance wave height as shown in Figure 5.31 at a silicone oil superficial velocity of 0.094 m/s and gas superficial velocity of 17.83 m/s and 35.66 m/s. This indicates that the liquid film thickness of the air/silicone oil system behaves similar to that observed in the air/water system with changing the gas and liquid superficial velocities regardless of different liquid properties.

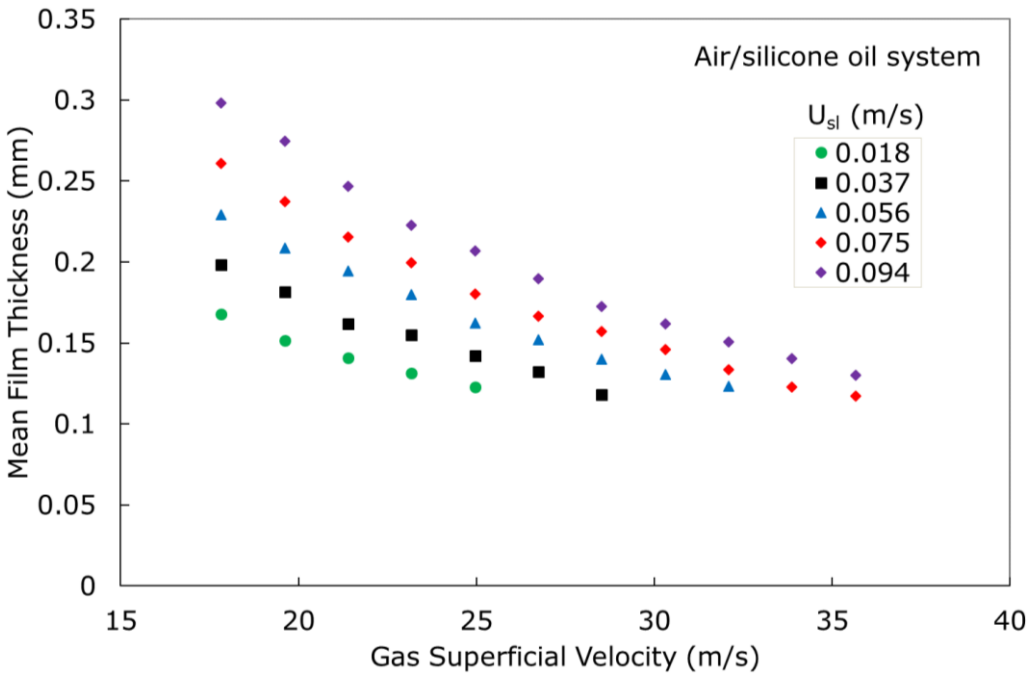


Figure 5.30: Effect of gas and liquid superficial velocity on the mean film thickness of air/silicone oil system.

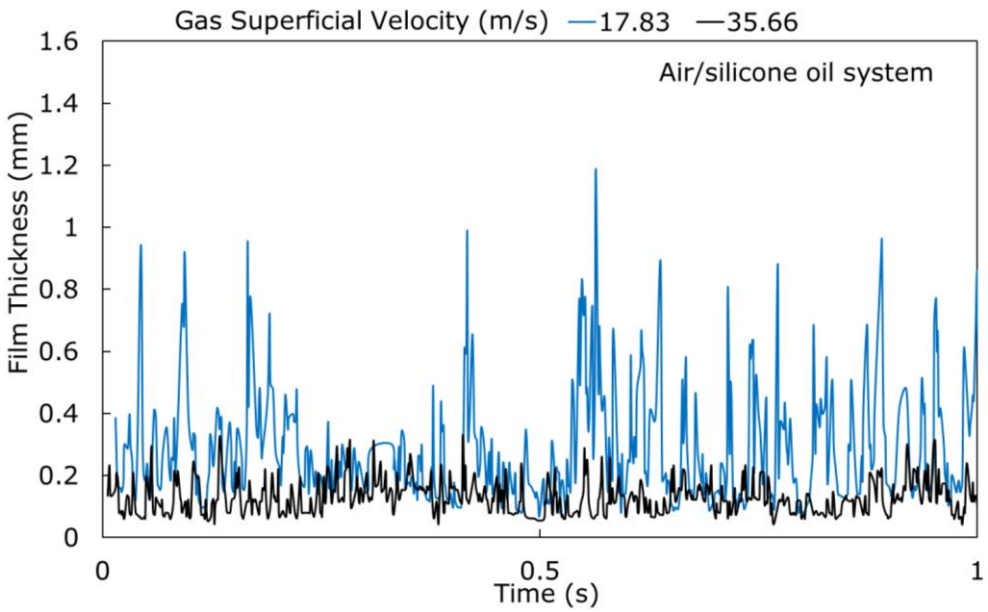


Figure 5.31: Effect of gas superficial velocity on the disturbance wave height of an air/silicone oil system for a silicone oil superficial velocity of 0.094 m/s and gas superficial velocity of 17.83 m/s and 35.66 m/s.

## 5.3. Effect of viscosity and surface tension on liquid film

Figure 5.32 shows the comparison between the mean liquid film thickness for an air/water system and an air/silicone oil system respectively for different liquid superficial velocities. When comparing the results from the air/water system with the air/silicone oil system, there is a slight difference between the two systems which is within the accuracy of the measurement of ±5% as per the comparison between the ultrasonic measurement and the conductance measurement by concentric probe and MPFS. According to the study by Fukano and Furukawa (1998), the liquid film thickness increases as the liquid viscosity increases and the mean liquid film thickness decreases asymptotically when the

gas superficial velocity increases regardless of the magnitude of viscosity and liquid superficial velocity. However, the surface tension in their study was close to the water surface tension where its effect was negligible.

The difference between the mean film thickness of the air/water system and the air/silicone oil system keeps reducing as the gas superficial velocity increases until it is almost the same and close to each other. This difference could be related to the increase in the entrainment rate as shown and discussed in chapter 4.

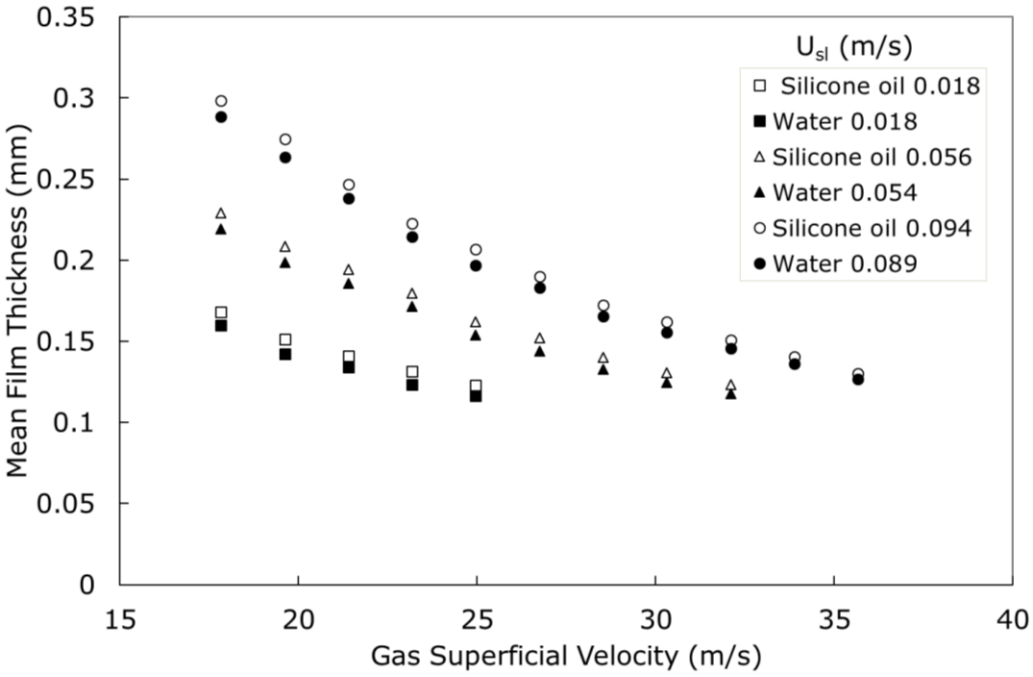


Figure 5.32: Effect of viscosity and surface tension on mean film thickness at water superficial velocity of 0.018m/s, 0.054m/s and 0.089m/s and silicone oil superficial velocity of 0.018m/s, 0.056m/s and 0.094m/s.

## 5.4. Prediction of the mean liquid film thickness

The importance of the liquid film thickness and its effect on the pressure drop and interfacial shear stress in annular two-phase flow is reflected in a large number of correlations to predict it in the literature. The liquid film thickness correlations suffer from the same issues as other predicting correlations for pressure drop as discussed in Chapter 4. Berna et al. (2014), Ju et al. (2015) and Pan et al. (2015a) have evaluated some of the available correlations, and they concluded that these correlations have large relative errors or are limited to the range of the experimental data used to develop them. They have proposed new correlations to predict the liquid film thickness.

The mean liquid film thickness results using the upward annular flow test facility were compared with some of the existing correlations. These correlations were the one summarised by Azzopardi (2006) and the new correlations proposed by Berna et al. (2014), Ju et al. (2015) and Pan et al. (2015a) as shown in Table 5.1. The selection was based on those most widely used or ones incorporating the effects of viscosity and surface tension.

| Reference | Correlation |
|---|---|
| Ambrosini (Azzopardi, 2006, Berna et al., 2014) | $\delta_l^+ = \frac{\rho_l \delta u^*}{\mu_l} = \begin{cases} 0.34 Re_{lf}^{0.6} & Re_{lf} \leq 1000 \\ 0.0512 Re_{lf}^{0.875} & Re_{lf} > 1000 \end{cases}$ <br> $u^* = \sqrt{\frac{\tau_i}{\rho_l}}$, $Re_{lf} = (1-E)Re_l$, $Re_l = \frac{\rho_l U_l D}{\mu_l}$ |
| Fukano and Furukawa (Fukano and Furukawa, 1998) | $\frac{\delta}{D} = 0.0594 \exp\left(-0.34 Fr_g^{0.25} Re_l^{0.19} x^{0.6}\right)$ <br> $Fr_g = \frac{U_{gs}}{\sqrt{gD}}$, $x = \frac{U_{gs}\rho_g}{U_{gs}\rho_g + U_{ls}\rho_l}$ |
| Kosky and Staub (1971) (Azzopardi, 2006) | $\delta_l^+ = \frac{\rho_l \delta u^*}{\mu_l} = \begin{cases} 0.707 Re_{lf}^{0.5} & Re_{lf} \leq 50 \\ 0.6323 Re_{lf}^{0.5286} & 50 < Re_{lf} \leq 1483 \\ 0.0504 Re_{lf}^{0.875} & Re_{lf} > 1483 \end{cases}$ |
| Henstock (Henstock and Hanratty, 1976) | $\frac{\delta}{D} = \frac{6.59F}{(1+1400F)^{0.5}}$, $F = \frac{1}{\sqrt{2} Re_g^{0.4}} \frac{Re_f^{0.5}}{Re_g^{0.5}} \frac{\mu_f}{\mu_g} \frac{\rho_g^{0.5}}{\rho_f^{0.5}}$ |
| Berna (Berna et al., 2014) | $\frac{\delta}{D} = 7.165 Re_g^{-1.07} Re_l^{0.48} \left(\frac{Fr_g}{Fr_l}\right)^{0.24}$, $Fr_l = \frac{U_{ls}}{\sqrt{gD}}$ |
| Pan (Pan et al., 2015a) | $\frac{\delta}{D} = 2.03 Re_l^{0.15} Re_g^{-0.6}$, $Re_g = \frac{\rho_g U_{gs} D}{\mu_g}$ |
| Ju (Ju et al., 2015) | $\frac{\delta}{\delta_{max}} = \tanh\left(14.22 We_l^{0.24} We_g''^{-0.47} N_{\mu_l}^{0.21}\right)$ <br> $\delta_{max} = 0.071D, We_g'' = \frac{\rho_g U_{gs}^2 D}{\sigma}\left(\frac{(\rho_l - \rho_g)}{\rho_g}\right)^{1/4}$ <br> $N_{\mu_l} = \frac{\mu_l}{\sqrt{\rho_l \sigma \sqrt{\frac{\sigma}{g(\rho_l - \rho_g)}}}}$, $We_l = \frac{\rho_l U_{ls}^2 D}{\sigma}$ |

Table 5.1: Summary of the correlations for predicting the liquid film thickness

Figure 5.33 and Figure 5.34 show the comparison of measured liquid film thickness with predicted correlations for different gas superficial velocity and liquid superficial velocity of 0.089m/s for an air/water system and 0.094 m/s for an air/silicone oil system. As observed from Figure 5.33 and Figure 5.34 for air/water and air silicone oil systems, none of the correlations was able to predict the liquid film thickness, and most of them over predicted. This finding is not surprising and similar to the finding by Berna et al. (2014), Ju et al. (2015) and Pan et al. (2015a) where most of the correlations they evaluated were over predicting. In addition, none of them agrees with each other, and all of them show the same trend profile where the film thickness decreases as the gas superficial velocity increases. An example of the results obtained for the correlations evaluated by Berna et al. (2014) is shown in Figure 5.35. From Figure 5.35, it is clear that none of the correlations was able to predict the measured liquid film.

All of the correlations have used constants which were based on their experiment results and a trial and error basis. As an example, Fukano and Furukawa (1998) stated that their correlation was based on trial and error. These constants might be the cause of the variation between the correlations. Most of these correlations have been modified by other researchers and resulted in them proposing new correlations. Azzopardi (2006) indicated that the need for physical constants derived from experimental data should be minimised.

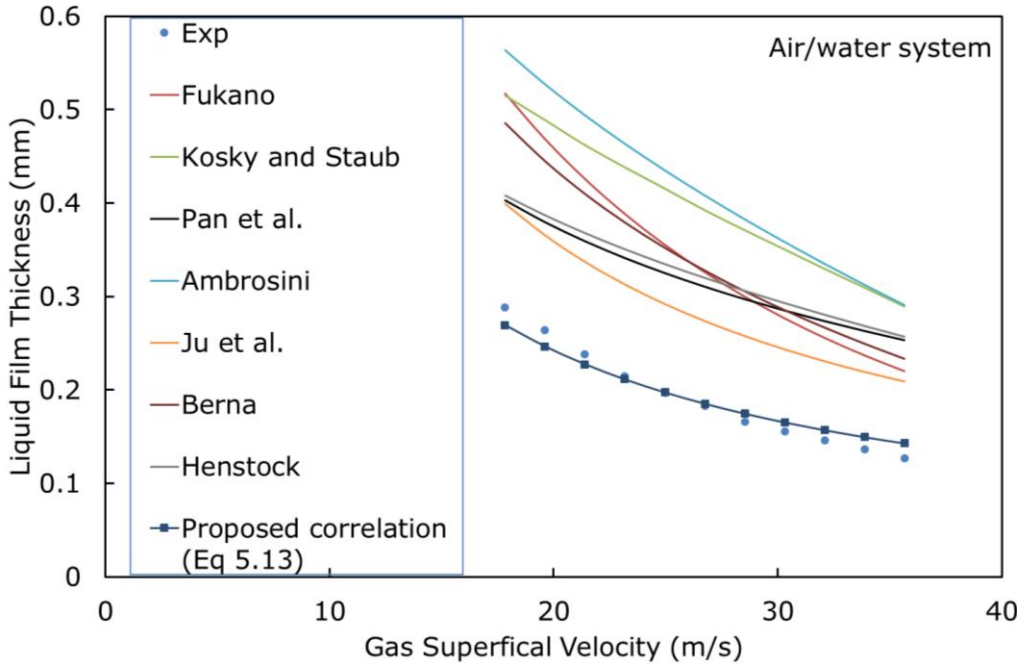


Figure 5.33: Comparison of measured liquid film thickness with predicted correlations for different gas superficial velocity and liquid superficial velocity of 0.089m/s for air/water system.

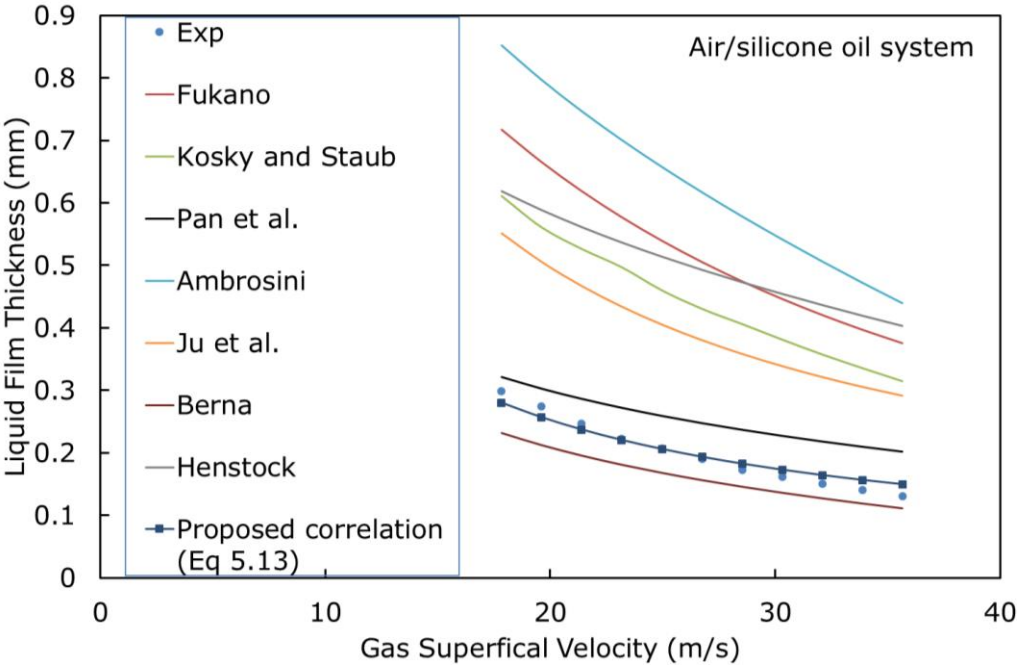


Figure 5.34: Comparison of measured liquid film thickness with predicted correlations for different gas superficial velocity and liquid superficial velocity of 0.094m/s for air/silicone oil system.

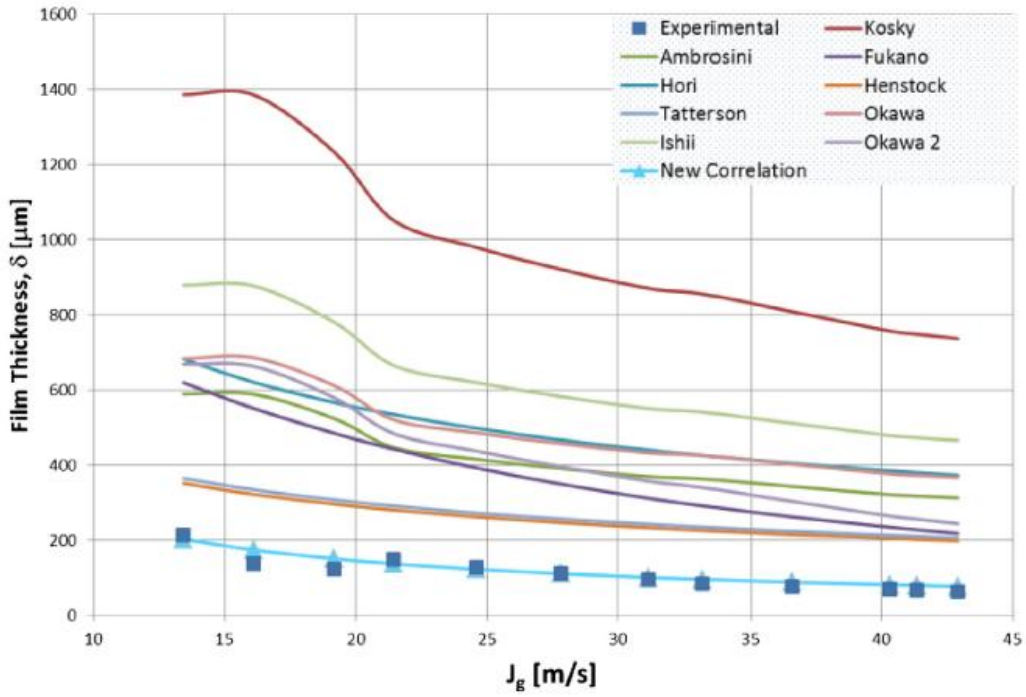


Figure 5.35: The example of the results obtained for the correlations evaluated by Berna et al. (2014) for air/water system.

As discussed above, the film thickness is affected by superficial velocity, density and viscosity of both liquid and gas phases, pipe diameter, entrainment and surface tension. Therefore, any model should include the effect of all these parameters to predict the film thickness close to the experimental data with efforts to minimise the physical constants derived from the experimental data. There will still be variation between the prediction and the measurements because of the entrance effect and the accuracy of the measurement devices. The acceptable variation limit depends on the importance of the liquid film thickness measurement to the process industry. An effort was made to get a model to fit current experiment data which is a modified version of Ju et al. (2015) as it showed a similar trend to current experimental data for an air/water system.

The modification was made to the gas Weber number [$\frac{\rho_g U_{gs}^2 D}{\sigma}\left(\frac{(\rho_l-\rho_g)}{\rho_g}\right)^{1/3}$ instead of $\frac{\rho_g U_{gs}^2 D}{\sigma}\left(\frac{(\rho_l-\rho_g)}{\rho_g}\right)^{1/4}$ ] and introduced a new dimensionless parameter (Film Reynolds number, $Re_{lf}$^-0.05) and surface tension ratio between liquid surface tension ($\sigma_l$) and water surface tension ($\sigma_w$) as shown in Equation (5.13):

$$\frac{\delta}{\delta_{max}} = \tanh\left(14.22 We_l^{0.24} We_g''^{-0.47} N_{\mu_l}^{0.21} Re_{lf}^{-0.05}\right)\left(\frac{\sigma_l}{\sigma_w}\right)^{0.28} \quad (5.13)$$

$$We_g'' = \frac{\rho_g U_{gs}^2 D}{\sigma}\left(\frac{(\rho_l-\rho_g)}{\rho_g}\right)^{1/3} \quad (5.14)$$

$$Re_{lf} = (1-E)Re_l \quad (5.15)$$

The new model can predict current experiment data within ±15% for air/water and air/silicone oil systems. Further work in the future is still required to introduce a model that can fit any experimental data with less dependency on physical constants derived from the experimental data.

## 5.5. Summary

The liquid film thickness results were analysed for air/water and air/silicone oil systems at gas superficial velocities ranging from 17.83 m/s to 35.66 m/s, and liquid superficial velocities ranging from 0.018m/s to 0.089m/s with water, and from 0.018m/s to 0.094m/s with silicone oil. From the results and discussion, the following could be summarised:

- The development of ultrasonic pulse-echo technique to measure the liquid film thickness was presented using static and dynamic conditions.

- Different processing methods of ultrasonic signals were utilised to calculate the liquid film thickness. A new processing method was suggested for film thickness less than 0.5 mm.

- The ultrasonic technique was compared against liquid film thicknesses calculated using theoretical calculation (Equation 5.10) based on a knowledge of liquid volume and the area of the test bench top. Both measurements showed good agreement with each other.

- The ultrasonic technique was also compared against two other measurement techniques (Multi-Pin Film Sensor and concentric probe) based on conductance measurements. The relative deviation between ultrasonic and the other two techniques was within +/-5%.

- The average (mean) liquid film thickness decreases with increasing gas and liquid superficial velocity for both air/water and air/silicone oil systems.

- The liquid film thickness of air/silicone oil system shows similar trend behaviour to the ones obtained for the air/water system regardless of the liquid physical properties.

- The change of viscosity and surface tension of the liquid phase has a slight effect on the mean liquid film thickness where this effect is almost negligible at high gas superficial velocity regardless of liquid superficial velocity.

- Different correlations to predict liquid film thicknesses were used. None of these correlations was able to predict the liquid film thickness for both air/water and air/silicone oil systems.

- A new correlation (Equation 5.13) is proposed which is a modified of Ju et al. (2015) correlation. The proposed correlation was able to predict current experimental data with ±15% for both air/water and air/silicone oil systems.

# CHAPTER 6

# WALL SHEAR STRESS MEASUREMENTS

The wall shear stress plays a significant role in the prediction of the pressure drop measurement and the liquid film velocity profile in annular two-phase flow (Hewitt and Hall-Taylor, 1970, Alekseenko et al., 1994, Azzopardi, 2006). The wall shear stress has a direct impact on the frictional pressure drop. The importance of the wall shear stress is reflected by the number of the measurement techniques that were developed due to the difficulty to measure it as discussed in Chapter 2. The waves in the interface between the gas and liquid film affect the interfacial shear stress, hence the wall shear stress. Understanding the relationship between the pressure drop, the wall shear stress and the liquid film will help to develop models for predicting one of these parameters. In the current study, the wall shear stress was measured using commercial glue on flush mounted hot film probe from Dantec dynamics (Dantec 55R47). The wall shear stress measurements were conducted for air/water and air/silicone oil systems between gas superficial velocities ranging from 17.83 m/s to 35.66 m/s, and liquid superficial velocities ranging from 0.018 m/s to 0.089 m/s with water, and from 0.018 m/s to 0.094 m/s with silicone oil.

In this chapter, the experimental results of the two-phase wall shear stress using a hot film probe for air/water and air/silicone oil systems are presented. Section 6.1, discusses the effect of gas and liquid superficial velocity on two-phase wall shear stress. Viscosity and surface tension influence on the wall shear stress is presented in Section 6.2. The prediction of the wall shear stress using the

frictional pressure drop and the triangular relationship was compared to the measured wall shear stress in Section 6.3. Finally, the relationship between the wall shear stress, liquid film thickness, and pressure drop is discussed in section 6.4.

## 6.1. Effect of gas and liquid superficial velocity on wall shear stress

The gas and liquid superficial velocity influence the wall shear stress as illustrated in Figure 6.1 for an air/water system between gas superficial velocities ranging from 17.83 m/s to 35.66 m/s and water superficial velocities ranging from 0.018m/s to 0.089m/s. The results in Figure 6.1 show that the average (mean) wall shear stress increases when the gas and liquid superficial velocity increases. These experimental trends and behaviour in a vertical upward annular flow were reported by previous researchers including Owen (1986), Govan et al. (1989) and Wolf (1995).

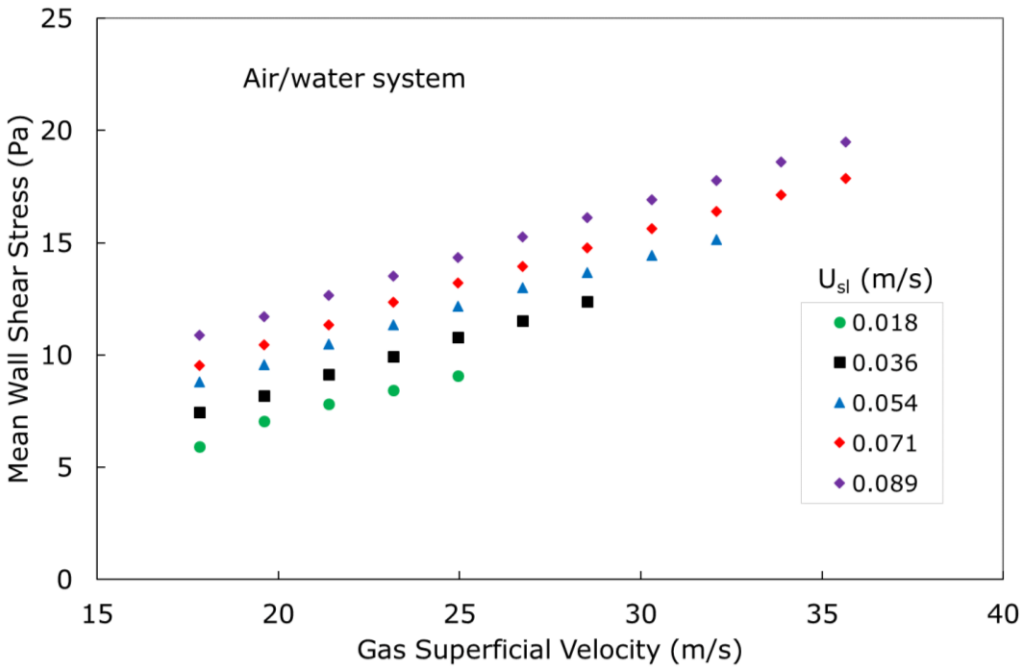


Figure 6.1: Effect of gas and liquid superficial velocity on the mean wall shear stress for an air/water system.

The liquid film in the annular flow is associated with disturbance waves that contribute to the wall shear stress as they are the main cause of entrainment that enhances the liquid film velocity when deposited back into the liquid film. When the liquid superficial velocity increases, the frictional force on the wall increases leading to an increase in the wall shear stress. The increase in the gas superficial velocity will increase the liquid superficial velocity hence the wall shear stress due to the increase in the momentum transfer by the entrainment-deposition interchange (Govan et al., 1989, Fore and Dukler, 1995). When the droplet is entrained into the gas core, it is accelerated by the gas core velocity. Then when the droplet is deposited on the liquid film, all its momentum is transferred to the liquid film and hence increases the liquid film velocity.

For the air/silicone oil system, the influence of gas and liquid superficial velocity is shown in Figure 6.2 between a gas superficial velocity ranging from 17.83 m/s to 35.66 m/s and a liquid superficial velocity ranging from 0.019m/s to 0.094m/s with silicone oil. From Figure 6.2, the wall shear of air/silicone oil system increases with increasing gas and liquid superficial velocities. Figure 6.1 and Figure 6.2 showed that air/water and air/silicone oil systems have a similar trend in behaviour when the gas and liquid superficial velocity increases even with different fluid properties. The influence of the liquid properties (i.e viscosity and surface tension) on the wall shear stress will be discussed in Section 6.3.

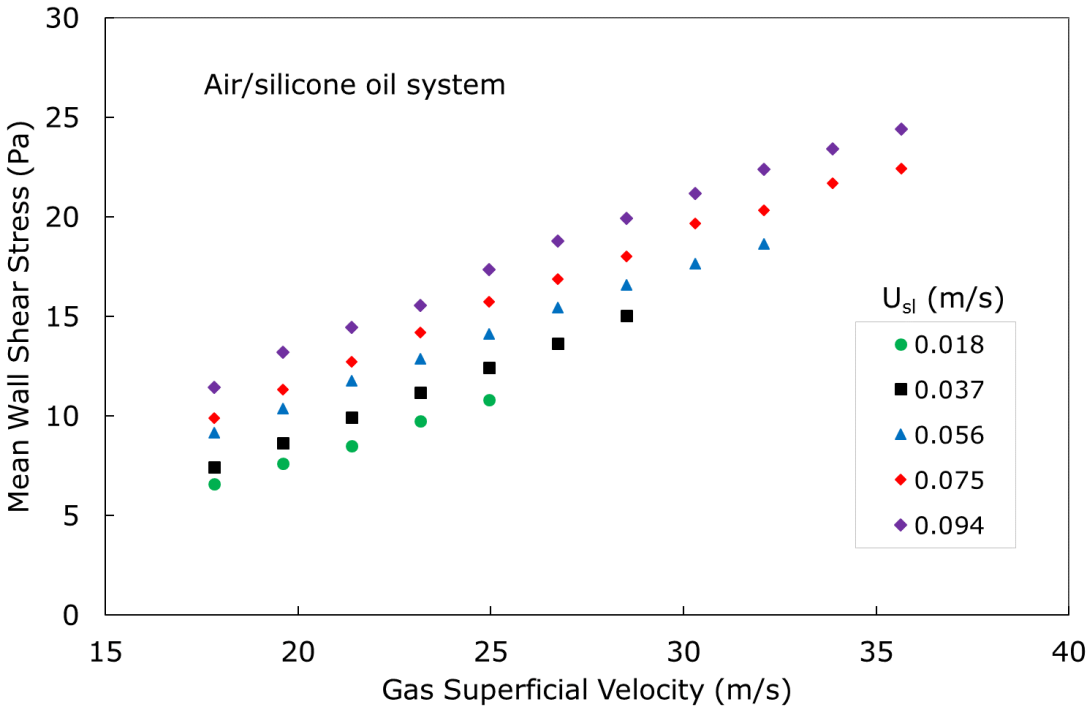


Figure 6.2: Effect of gas and liquid superficial velocity on the mean wall shear stress of air/silicone oil system.

## 6.2. Effect of viscosity and surface tension on wall shear stress

In the current study, the mean wall shear stress of the air/silicone oil system is higher than the wall shear stress of the air/water system as shown in Figure 6.3. Figure 6.3 illustrates the results for gas superficial velocities ranging from 17.83 m/s to 35.66 m/s and water superficial velocities (0.018, 0.054 and 0.089 m/s) and silicone oil superficial velocities (0.018, 0.056 and 0.094 m/s).The difference in the wall shear stress between air/water and air/silicone oil systems is small at low gas superficial velocity (17.83 m/s) and keeps increasing with increasing gas superficial velocity regardless to liquid superficial velocities. As shown in Section 6.1, the wall shear stress of air/water and air/silicone oil systems increases with increasing gas and liquid superficial velocities. The difference between them starts from 5% at low gas superficial velocity (17.83 m/s) to a maximum of 25% at high gas superficial velocity (36.66 m/s). However, the increase in the difference between them (Figure 6.3), could be related to the difference in the viscosity and the surface tension.

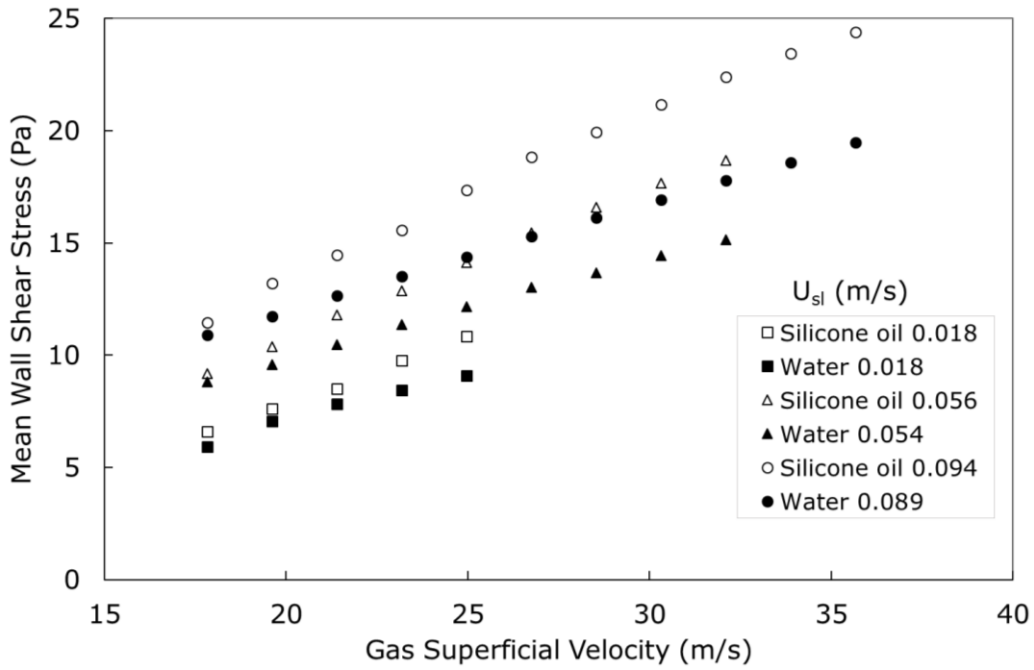


Figure 6.3: Effect of viscosity and surface tension on the mean wall shear stress of air/water and air/silicone oil systems at different gas and liquid superficial velocities.

As discussed in Section 2.4, the wall shear stress can be estimated by using the relationship between the wall shear stress ($\tau_w$), liquid viscosity ($\mu_l$) and film velocity gradient ($\frac{\partial u}{\partial y}$) that is given by equation (6.2):

$$\tau_w = \mu_l \frac{\partial u}{\partial y} \tag{6.1}$$

This relationship is only true for all Newtonian fluid where the dynamic viscosity is constant at all velocity gradient which means the influence of the viscosity on wall shear stress is constant. In annular flow, the measurement of the velocity profile of the thin liquid film is difficult to be measured accurately using conventional instrumentation such as hot wire, Laser Doppler Velocimetry (LDV) and Particle Image Velocimetry (PIV) close to the wall (Salari and Tabar, 2011). The film velocity profile is influenced by the liquid film velocity

and liquid film thickness due to the presence of the waves at the interface. As discussed in Chapter 4, the liquid film velocity is influenced by the momentum transfer due to the entrainment-deposition interchange which is influenced by viscosity and surface tension. The calculated entrainment rate in air/silicone oil system is higher than the air/water system and hence the entrainment-deposition interchange. Therefore, the momentum transfer on the silicone oil film is expected to be higher than the water film.

Due to the higher in the viscosity and film velocity of air/silicone oil system compared to the air/water system, a high wall shear stress of air/silicone oil system is anticipated compared to air/water system. The increase in the difference of the wall shear stress between the air/water system and the air/silicone oil could be related to the gradual increase in the momentum transfer due to the increase in the entrainment-deposition interchange.

## 6.3. Prediction of the wall shear stress

There is no particular correlation to predict the wall shear stress in annular two-phase flow similar to those correlations made for predicting interfacial friction factor as summarised by Aliyu et al. (2017), therefore interfacial shear stress. There is no satisfactory correlation for predicting the interfacial shear stress where all of the existing correlations assume the interface as wall roughness and the interface is smooth (Pan et al., 2015b). Pan et al. (2015b) showed that the interfacial shear stress is affected by the disturbance wave height and the entrainment-deposition interchange. For the thin liquid film, the wall shear stress

is assumed to be equal to the interfacial shear stress (Hewitt, 1982, Govan et al., 1989). As shown in Chapter 4, this assumption is not always valid.

In contrast, the wall shear stress is usually calculated from the knowledge of the total pressure drop. It is calculated from the frictional pressure drop based on the separated flow model or using triangular relationship. The wall shear stress ($\tau_w$) calculation from the frictional pressure drop ($\left(\frac{dp}{dz}\right)_f$) is expressed by Equation (6.2):

$$\tau_w = \frac{D}{4}\left(\frac{dp}{dz}\right)_f \tag{6.2}$$

where D is the internal pipe diameter.

The triangular relationship relates three variables together which are pressure drop (or wall shear stress), film thickness, and film flowrate. Anyone of those parameters can be calculated when the other two of these variables are known. The triangular relationship consists of four steps as described by Owen (1986), Govan (1990) and Zangana (2011). The first step is performing a momentum balance on the gas core element for a circular tube (Figure 6.4) to calculate the interfacial shear stress. The second step is applying a momentum balance on the liquid film element to obtain shear stress distribution. In the first and second steps, the acceleration is assumed negligible, and the interface is smooth. The third step is calculating the velocity distribution using Equation (6.1). Then, the final step is calculating the film flowrate using the calculated shear stress and velocity distribution in step two and three. The triangular relationship also assumes that the wall shear stress is equal to the interfacial shear stress. In the current study, steps one and two were only applied to obtain the shear stress.

More details about it can be found in Hewitt and Hall-Taylor (1970), Owen (1986), Govan (1990) and Zangana (2011).

The momentum balance equation on the gas core element is given by Equation (6.3):

$$\tau_i = -\frac{r_i}{2}\left(\rho_c g + \frac{dp}{dz}\right) \tag{6.3}$$

The momentum balance equation on the liquid film element is given by Equation (6.4):

$$\tau(r) = \tau_i \frac{r_i}{r} + \frac{1}{2}\left(\rho_l g + \frac{dp}{dz}\right)\left(\frac{r_i^2 - r^2}{r}\right) \tag{6.4}$$

where $r_i$ is the interfacial radius $(r_0 - \delta)$, $r_0$ is the pipe radius, $\delta$ is film thickness, r is given by $((r_i + r_0)/2) \approx r_0$, $\rho_c$ is the gas core density, $\rho_l$ is the liquid density, g is gravitational acceleration, $\tau_i$ is the interfacial shear stress, $\tau(r)$ is the shear stress at radius (r) and $\frac{dp}{dz}$ is the total measured pressure drop.

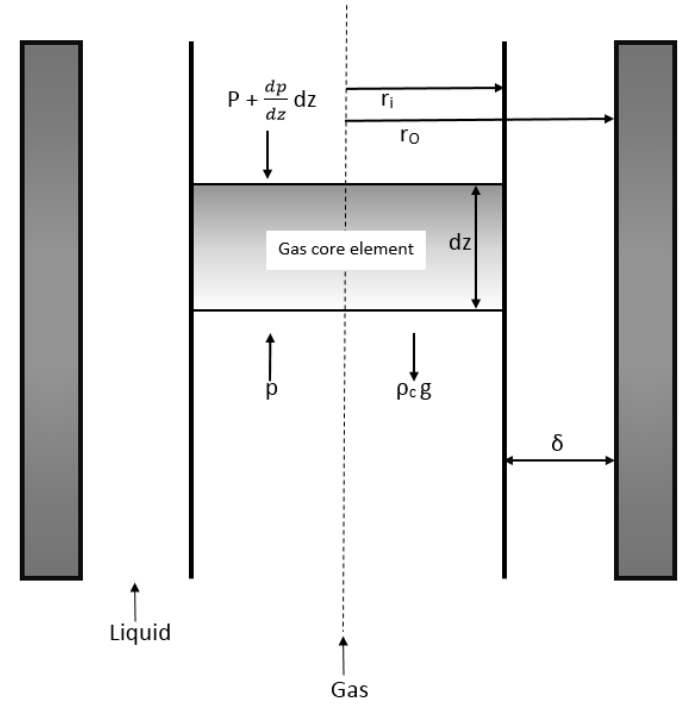


(a) Gas core Force Balance

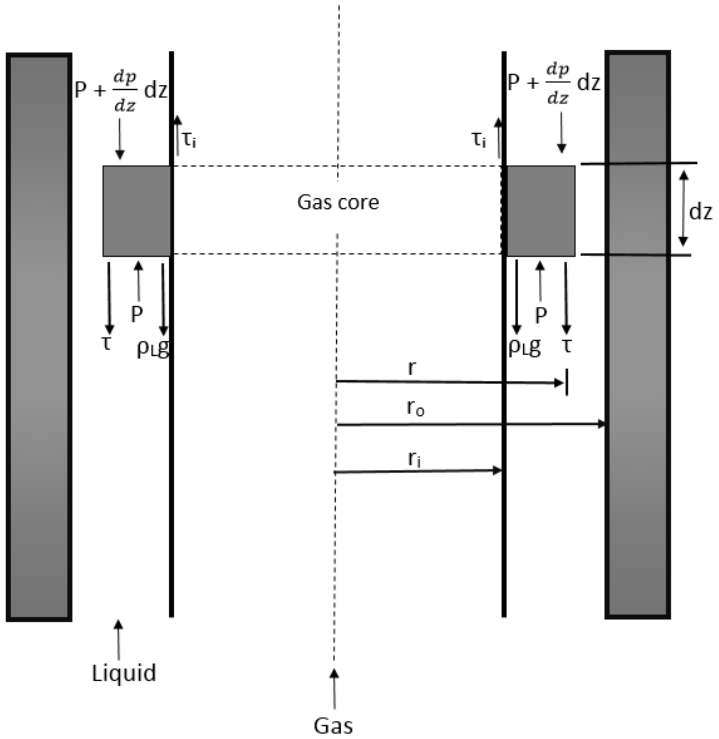


(b) Liquid Film Force Balance

Figure 6.4: Force balance on control element for gas and liquid film (Owen, 1986).

As shown and discussed in Chapter4, the pressure drop was better predicted by using characteristic shear stress and the interfacial shear stress calculated using the correlation proposed by Pan et al. (2015b). Hence, the shear stress calculated using the frictional pressure drop (Equation 6.2) is the characteristic shear stress ($\tau_c$) rather than the wall shear stress ($\tau_w$). Therefore, the wall shear stress was back calculated using the characteristic shear stress equation (4.5).

$$\tau_c = \frac{2}{3}\tau_w + \frac{1}{3}\tau_i \tag{4.5}$$

Both methods of calculating the wall shear stress have to be compared using the same set of data. Therefore, the interfacial shear stress was calculated using the Pan et al. (2015b) correlation and the one derived from momentum balance on the gas core (Equation 6.3).

The wall shear stress calculated from the frictional pressure drop and triangular relationship using the interfacial shear stress based on the Pan et al. (2015b) correlation are shown in Figure 6.5 and 6.6 for air/water and air/silicone oil systems respectively.

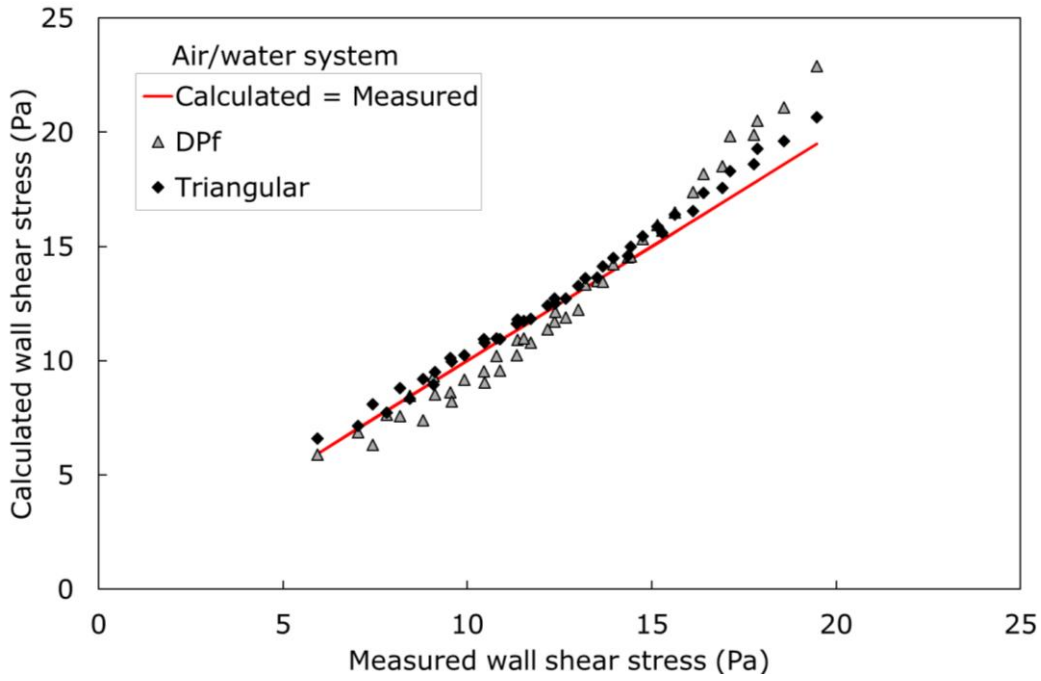


Figure 6.5: The wall shear stress calculated from the frictional pressure drop and triangular relationship using the interfacial shear stress based on the Pan et al. (2015b) correlation for an air/water system.

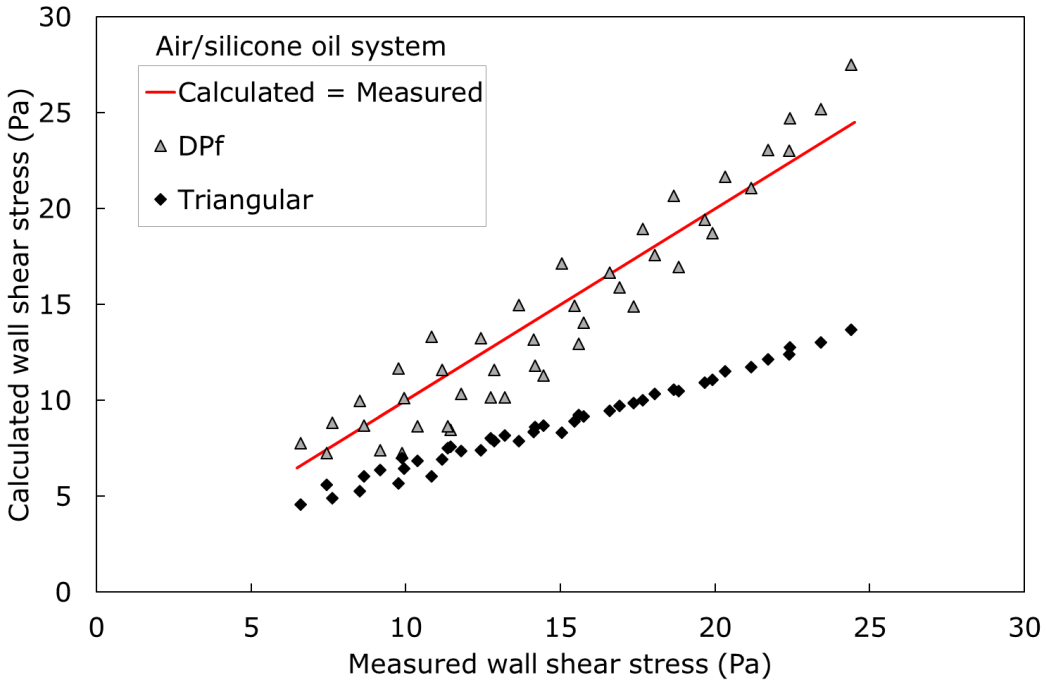


Figure 6.6: The wall shear stress calculated from the frictional pressure drop and triangular relationship using the interfacial shear stress based on the Pan et al. (2015b) correlation for an air/silicone oil system.

From Figure 6.5 and 6.6, it is clear that the frictional pressure drop was able to predict the measured wall shear stress for both air/water system and air/silicone oil system. The frictional pressure drop predicted the measured wall shear stress with a relative error of ±15% for the air/water system and ±25% for the air/silicone oil system. However, the triangular relationship predicted the measured wall shear stress of air/water system better than the frictional pressure drop. The triangular relationship predicted the measured wall shear stress with a relative error of ±10% for the air/water system and under predicted the measured shear stress by a maximum relative error of -42% for the air/silicone oil system. The variation was calculated using relative error:

$$\text{Relative error } (\%) = \left[\frac{(\tau_{\text{Pred}} - \tau_{\text{Exp}})}{\tau_{\text{Exp}}}\right] \times 100\% \qquad (6.5)$$

The wall shear stresses calculated from the frictional pressure drop and triangular relationship using the interfacial shear stress calculated from the momentum balance on the gas core are shown in Figure 6.7 and 6.8 for air/water and air/silicone oil systems respectively.

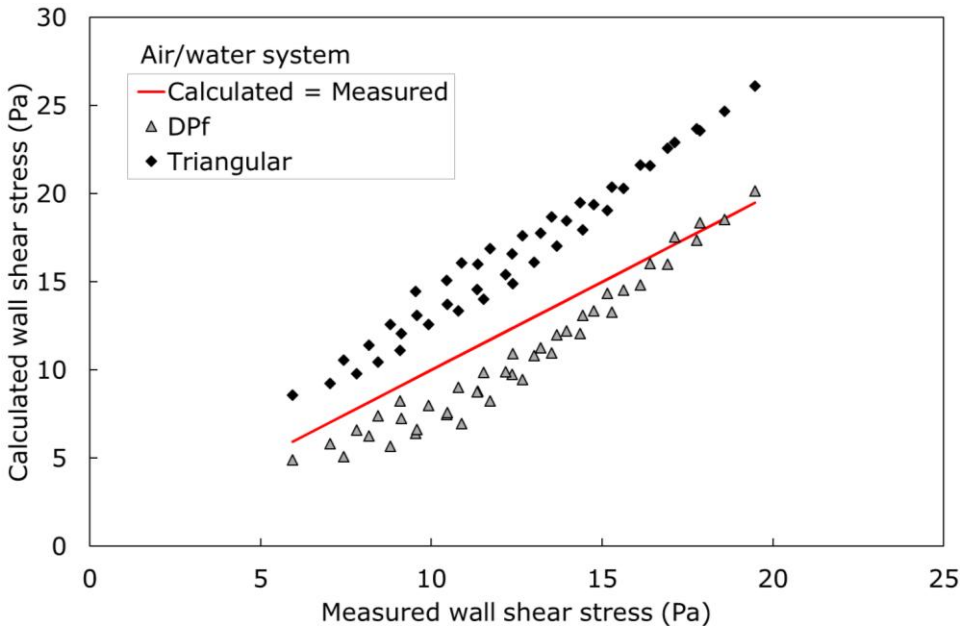


Figure 6.7: The wall shear stress calculated from the frictional pressure drop (DPf) and triangular relationship (Triangular) using the interfacial shear stress calculated from the momentum balance on the gas core for an air/water system.

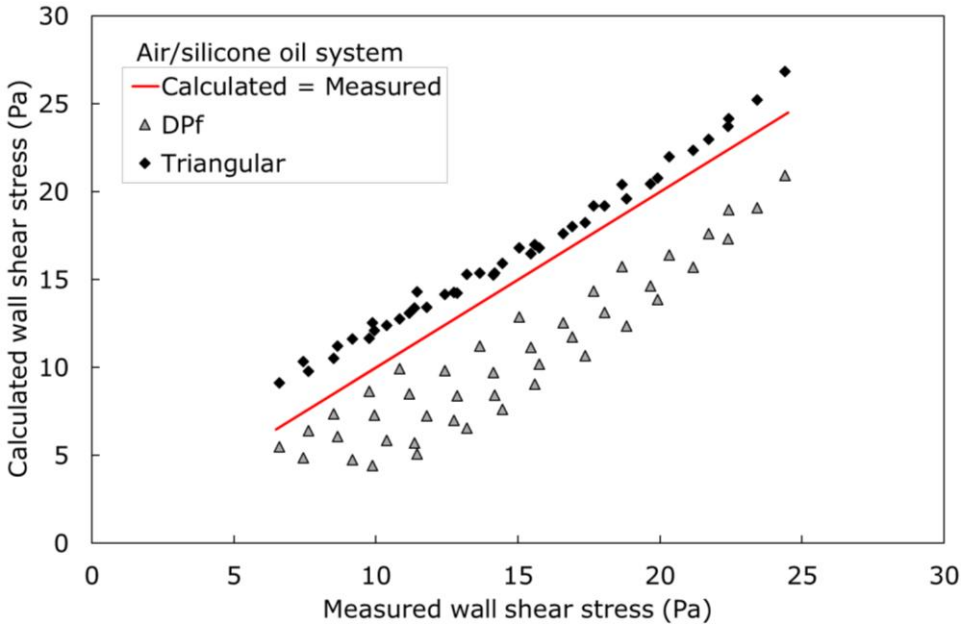


Figure 6.8: The wall shear stress calculated from the frictional pressure drop (DPf) and triangular relationship (Triangular) using the interfacial shear stress calculated from the momentum balance on the gas core for an air/silicone oil system.

It is clear from Figure 6.7 that the predicted wall shear stress for air/water system by the frictional pressure drop was better than the triangular relationship. The frictional pressure drop predicted the measured wall shear stress with a relative error of +/-35% compared to ±48% by the triangular relationship for the air/water system. In contrast, the triangular relationship predicted the measured wall shear stress of air/silicone oil system better than the frictional pressure drop as shown in Figure 6.8. The triangular relationship predicted the measured wall shear stress with a relative error of ±36% compared to ±55% by the frictional pressure drop for the air/silicone oil system. The difference between the two models to predict the wall shear stress could be related to different factors, for instance, the triangular relationship assumes the liquid film is smooth and the wall shear stress is equal to the interfacial shear stress. In addition, the accuracy of the triangular relationship depends on the accuracy of entrainment calculation and pressure drop and film thickness measurements. On the other hand, the frictional pressure drop accuracy depends on the accuracy of the void fraction and the pressure drop measurements. The accuracy of the measured wall shear stress is also contributed where Govan et al. (1989) showed that the difference between single phase calibration and two-phase calibration is ±10%.

In general, the prediction of the wall shear stress by the frictional pressure drop and triangular relationship using the interfacial shear stress calculated based on Pan et al. (2015b) was better compared to those using the interfacial shear stress calculated from momentum balance on the gas core. The triangular relationship shows a better prediction for the wall shear stress of the air/water system when the Pan et al. (2015b) correlation was used for the interfacial shear stress calculation. However, it shows a better prediction for the wall shear stress of the

air/silicone oil system when using the interfacial shear stress calculated from momentum balance on the gas core. Owen (1986) used the triangular relationship to calculate the wall shear stress using the experimental pressure drop and film flowrate results of Martin (1983). He found that the calculated wall shear stress is higher than Martin's experimental wall shear stress by 50%.

## 6.4. Relationship between pressure drop, film thickness and wall shear stress

The measurements of pressure drop, film thickness, and wall shear stress were recorded simultaneously which enabled comparative analysis between them for both air/water and air/silicone oil systems. From the average (mean) results of these three measurements, both pressure drop and wall shear stress increase with increasing gas superficial velocity where the film thickness decreases. The film thickness is associated with the disturbance waves which affect the interfacial shear stress and wall shear stress and hence the pressure drop. The relationship of disturbance wave height with the interfacial shear stress and pressure drop is inversely proportional where the decrease in the disturbance wave height leads to an increase the interfacial shear stress and pressure drop (Pan et al., 2015b). As shown in Chapter 5, the disturbance wave's height reduced with increasing the gas superficial velocity.

Film thickness and pressure drop relationship could be related to the liquid entrainment. The entrainment rate is contributing to the pressure drop by 20% according to Fore and Dukler (1995) and 14.5% as per Pan et al. (2015b). On the other hand, the reduction of the film thickness is related to the increase of entrainment rate (Sawant et al., 2008, Al-Sarkhi et al., 2012). Also, the gravitational pressure drop contributes to the total pressure drop where the film thickness influences the gravitational pressure drop by affecting the gas void fraction as per the momentum force balance. The gas void fraction is calculated based on the measured liquid film thickness. Figure 6.9 and 6.10 show the influence of film thickness on the pressure drop for an air/water system and an air/silicone oil system respectively. In both systems, the pressure drop decreases with increasing film thickness. Both film thickness and pressure drop were obtained between gas superficial velocities ranging from 17.83 m/s to 35.66 m/s and liquid superficial velocities ranging from 0.018 m/s to 0.089 m/s with water and from 0.018 m/s to 0.094 m/s with silicone oil.

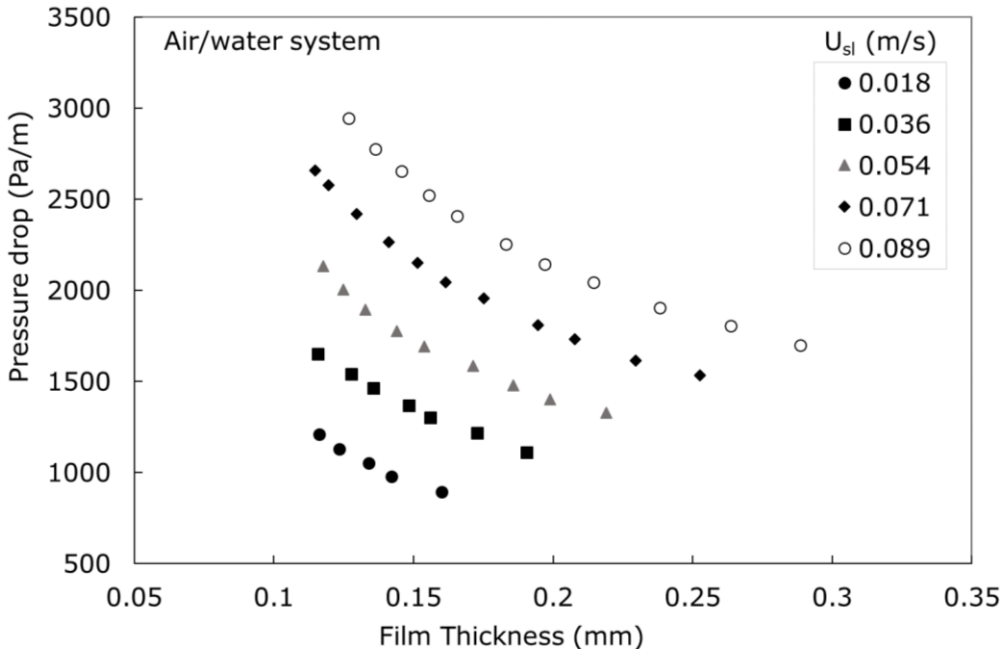


Figure 6.9: Influence of film thickness on pressure drop for air/water system at gas superficial velocities ($U_{sg}$) ranging from 17.83 m/s to 35.66 m/s and liquid superficial velocities ($U_{sl}$) ranging from 0.018 m/s to 0.089 m/s.

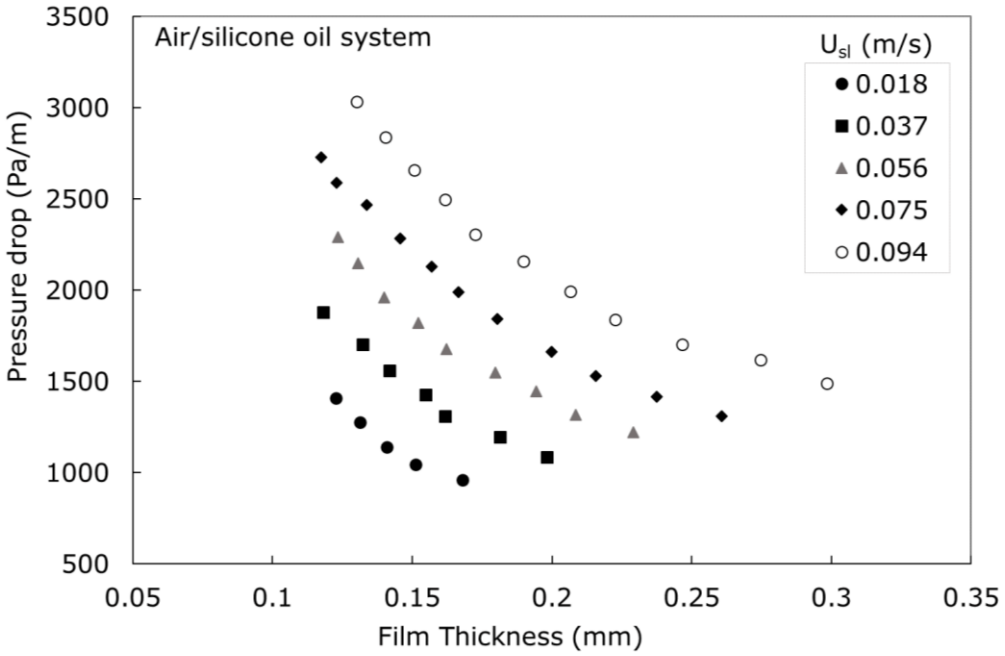


Figure 6.10: Influence of film thickness on pressure drop for air/silicone oil system at gas superficial velocities ($U_{sg}$) ranging from 17.83 m/s to 35.66 m/s and liquid superficial velocities ($U_{sl}$) ranging from 0.018 m/s to 0.094 m/s.

The wall shear stress has a direct impact on the pressure drop through the frictional pressure drop (Equation 6.2) based on the momentum force balance. The relationship between them is directly proportional where the increase in the wall shear stress will lead to an increase in the frictional pressure drop. The influence of wall shear stress on pressure drop is illustrated in Figure 6.11 and 6.12 for air/water and air/silicone oil systems respectively. In both systems, the pressure drop increases with increasing wall shear stress.

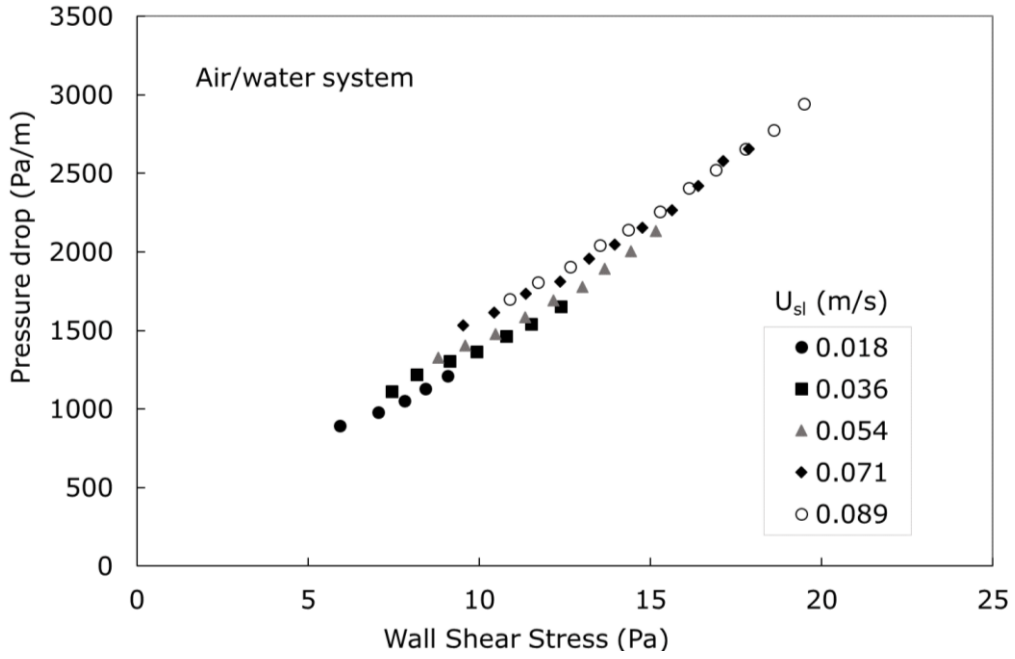


Figure 6.11: Influence of wall shear stress on pressure drop for air/water system at different gas ($U_{sg}$) and liquid ($U_{sl}$) superficial velocities.

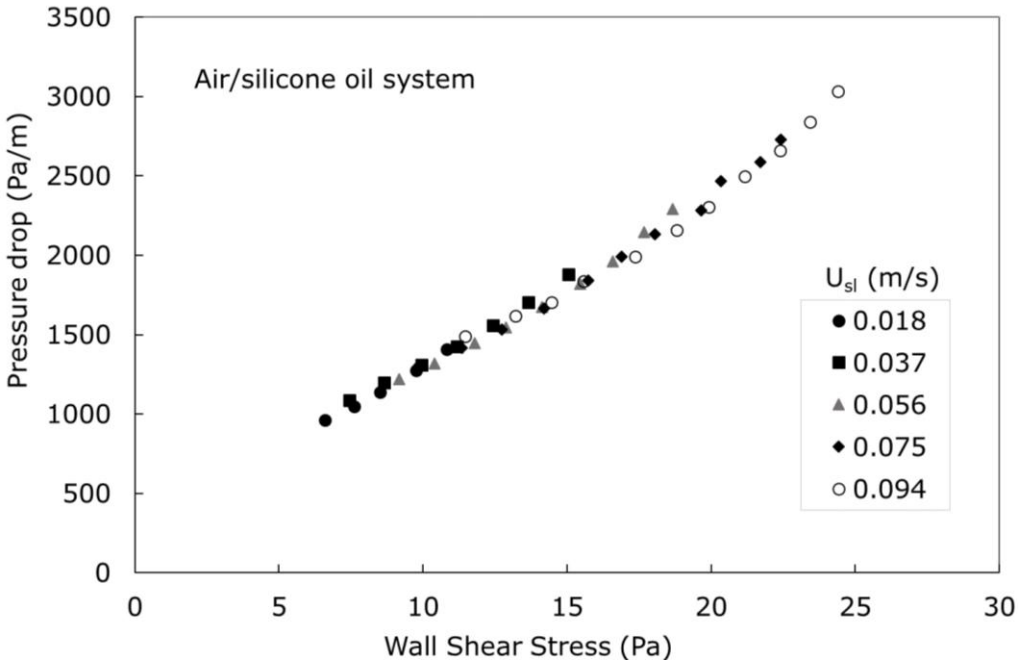


Figure 6.12: Influence of wall shear stress on pressure drop for air/silicone oil system at different gas ($U_{sg}$) and liquid ($U_{sl}$) superficial velocities.

Martin (1983) showed that the presence of large disturbance wave peak in the film thickness is reflected a large peak in the wall shear stress. Martin used the hot-film probe for measuring instantaneous shear stress and pin conductance probes for film thickness measurement. However, Martin measured the film thickness and wall shear stress at the same vertical position with small circumferential separation between them. Owen (1986) and Govan et al. (1989) used the time series data of the wall shear stress to determine disturbance wave frequencies. In the current study, the film thickness probe (Ultrasonic sensor) and the wall shear stress probe (Hot film probe) are separated by 140 mm in vertical (axial) direction. An example of the time series data of film thickness and wall shear stress for air/water system and air/silicone oil systems are shown in Figure 6.13 and 6.14 respectively.

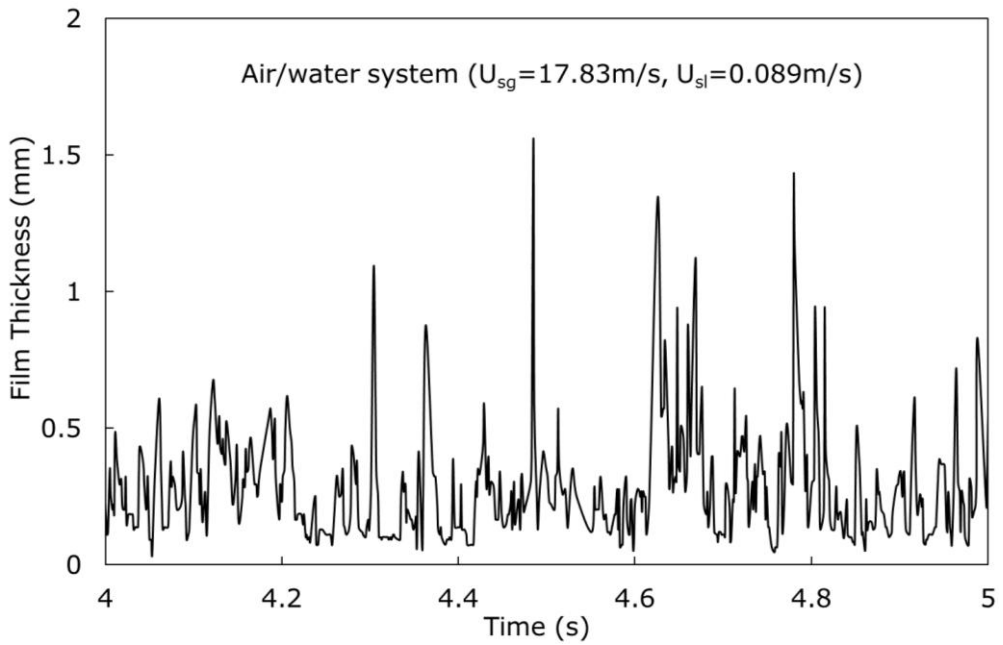


(a) Film Thickness

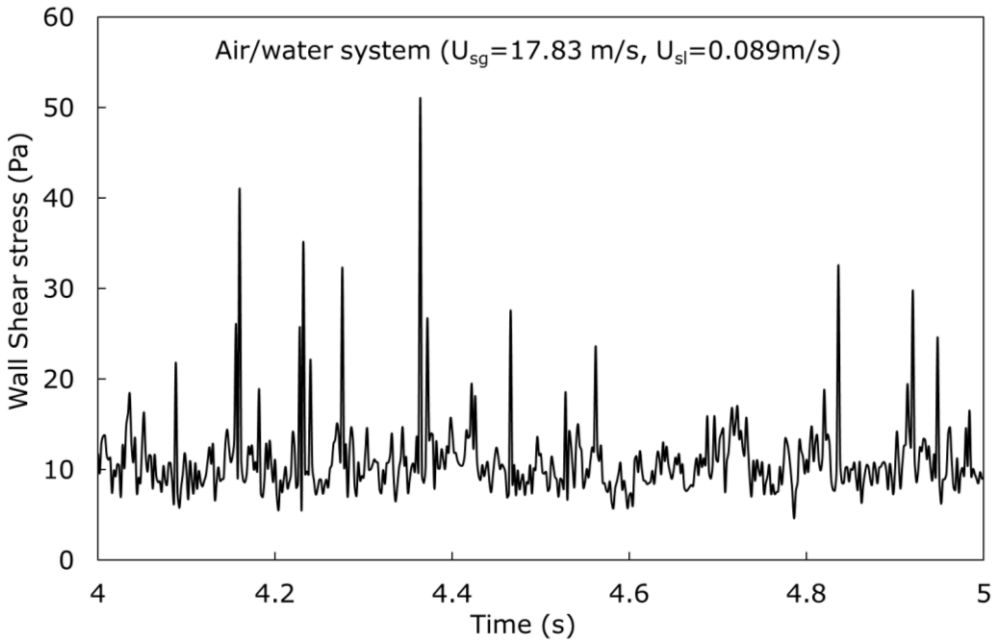


(b) Wall shear stress

Figure 6.13: Time series data of film thickness (a) and wall shear stress (b) for air/water system at gas superficial velocity ($U_{sg}$) of 17.83 m/s and liquid superficial velocity ($U_{sl}$) of 0.089 m/s.

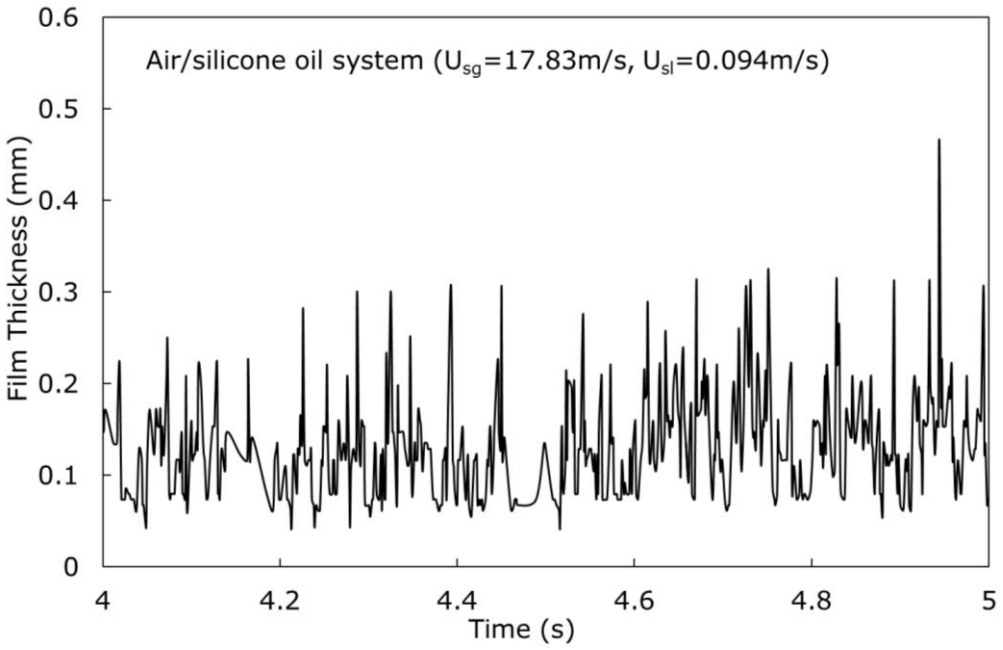


(a) Film Thickness

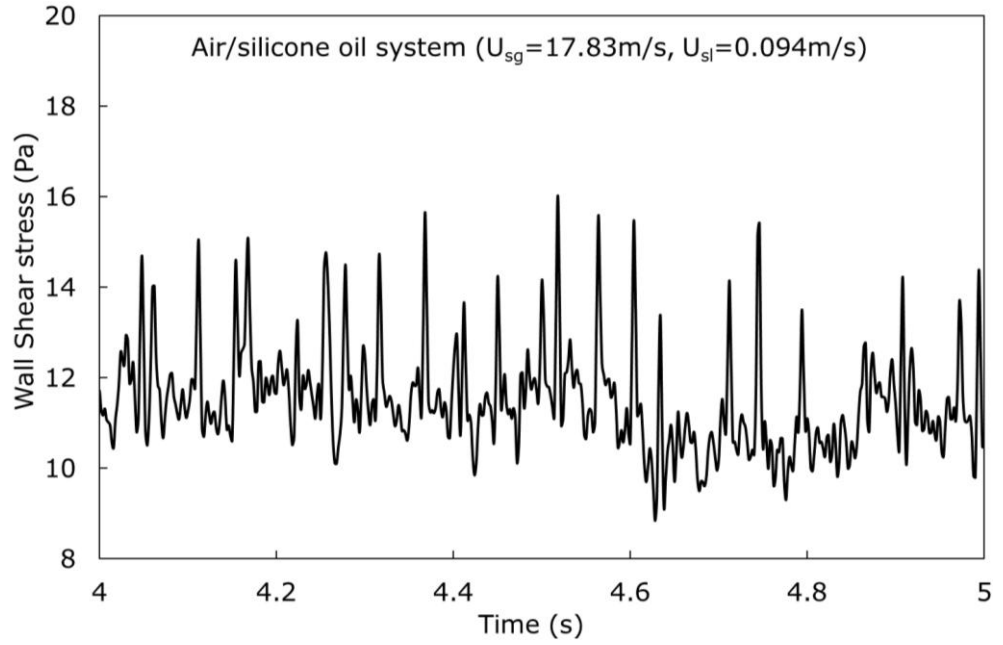


(b) Wall shear stress

Figure 6.14: Time series data of film thickness (a) and wall shear stress (b) for air/silicone oil system at gas superficial velocity ($U_{sg}$) of 17.83 m/s and liquid superficial velocity ($U_{sl}$) of 0.094 m/s.

Disturbance wave frequency can be measured by counting the number of peaks in the time series or using Power Spectral Density function available in MATLAB software as described in Chapter 5. The counting method could be done manually which is very subjective and depends on personal judgment. It can also be done by setting a threshold level and counting the number of peaks above the threshold using a built-in function in MATLAB software. However, there is no set of rules to define the threshold level which again depends on personal judgment. For example, Zhao et al. (2013) used a threshold level of 1.6 times the mean film thickness and Alekseenko et al. (2014) used 1.5 times the base film thickness. In contrast, Power Spectral Density was a preferable method by most of the researchers in the literature such as Martin (1983), Owen (1986) and Wolf (1995). In the current study, Power Spectral Density was preferred and used to determine the frequency of the film thickness and wall shear stress data. Figure 6.15 shows the frequency of film thickness and wall shear stress for an air/water system between gas superficial velocities ranging from 17.83 m/s to 35.66 m/s and liquid superficial velocities of 0.054 m/s and 0.089 m/s. The frequency of film thickness and wall shear stress increases with increasing gas and liquid superficial velocities. These results agree with the findings by Martin (1983) and Wolf (1995). However, the frequency is not identical as stated by Martin (1983). This could be attributed to the separation distance between the two sensors compared to Martin (1983) setup as discussed above. In addition, the accuracy of both measurement techniques contributes to the discrepancy between the two measurements.

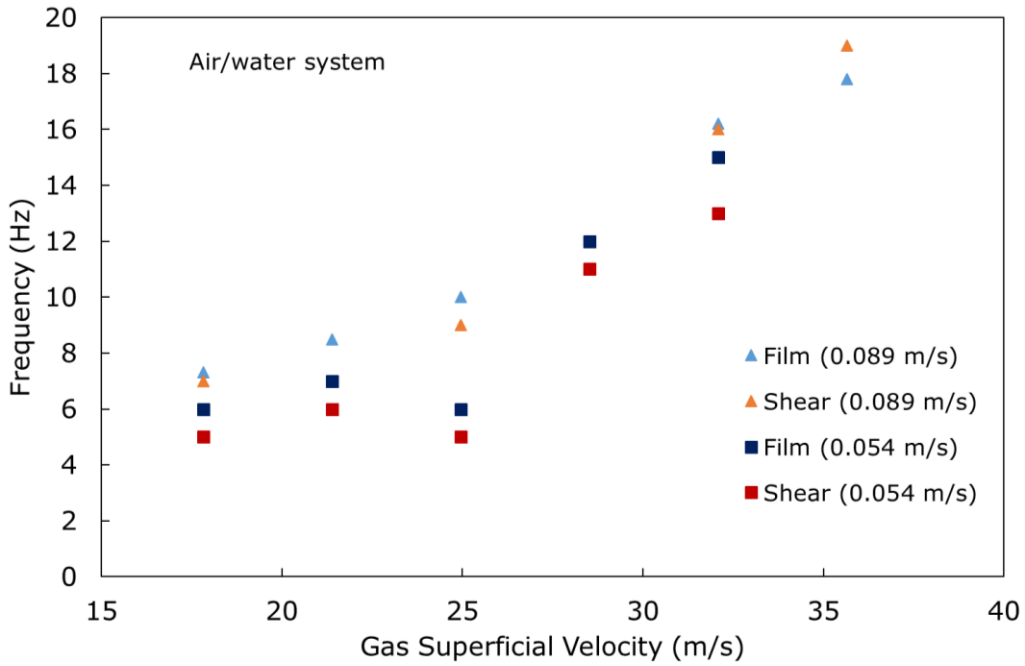


Figure 6.15: Frequency of film thickness and wall shear stress for an air/water system between different gas superficial velocities ($U_{sg}$) and liquid superficial velocities ($U_{sl}$) of 0.054 m/s and 0.089 m/s.

The frequency of film thickness and wall shear stress for air/silicone oil system between gas superficial velocities ranging from 17.83 m/s to 35.66 m/s and liquid superficial velocities of 0.056 m/s and 0.094 m/s are illustrated in Figure 6.16. The frequency of both film thickness and wall shear stress are low and not affected by increasing gas and liquid superficial velocity. These low frequencies are attributed to the effect of viscosity and surface tension.

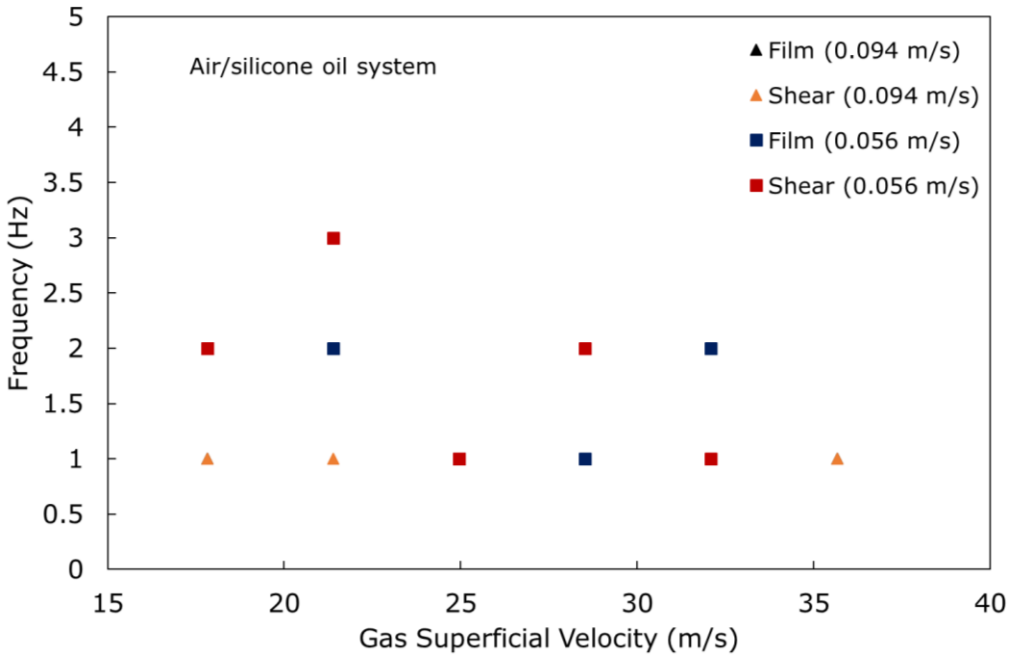


Figure 6.16: Frequency of film thickness and wall shear stress for an air/silicone oil system between different gas superficial velocities ($U_{sg}$) and liquid superficial velocities ($U_{sl}$) of 0.056 m/s and 0.094 m/s.

## 6.5. Summary

The wall shear stress data were analysed for air/water system and air/silicone oil system at gas superficial velocities ranging from 17.83 m/s to 35.66 m/s, and liquid superficial velocities ranging from 0.018 m/s to 0.089 m/s with water, and from 0.018 m/s to 0.094 m/s with silicone oil. From the results and discussion, the following could be summarised:

- The wall shear stress of the air/silicone oil system shows a similar trend behaviour to the one obtained for the air/water system regardless of the physical properties of the liquid. The average (mean) wall shear stress increases with increasing the gas and liquid superficial velocities for both air/water and air/silicone oil systems.

- The wall shear stress is affected by the viscosity and the surface tension of the liquid where there is a difference between the wall shear stress of the air/water system and the wall shear stress of the air/silicone oil system. The difference keeps increasing with increasing the gas superficial velocity regardless of liquid superficial velocity.

- The prediction of the wall shear stress was checked using the frictional pressure drop and the triangular relationship. It was well predicted using the frictional pressure drop by considering the characteristic shear stress for both air/water and air/silicone oil system.

- The interfacial shear stress was calculated by using the Pan et al. (2015b) correlation and the momentum balance on the gas core. The use of interfacial shear stress using the Pan et al. (2015b) correlation to calculate the wall shear stress shows a better prediction for both air/water and air/silicone oil system.

- The relationship between the wall shear stress, the pressure drop and the film thickness was evaluated. Both wall shear stress and pressure drop increase with increasing the gas superficial velocities where the liquid film decreases. The pressure drop decreases with increasing the liquid film thickness and increases with increasing the wall shear stress.

- The disturbance waves affect the wall shear stress where the large disturbance wave peak is associated with a large wall shear stress peak. It was confirmed by comparing the frequency of film thickness and wall shear stress using Power Spectral Density analysis.

# CHAPTER 7

# CONCLUSION AND FUTURE WORK

## 7.1. Conclusion

The two-phase upward annular flow regime, which is the most frequently observed flow regime in industrial applications, was studied. Understanding about its characteristics has led to the development of correlations to predict its parameters such as pressure drop, liquid film thickness and wall shear stress. However, most of the previous studies were conducted using air as the gas phase and water as the liquid phase. In the current study, the aim was to understand the annular flow regime behaviour and the relationship between its parameters using air as the gas phase and silicone oil as the liquid phase. Following this, the suitability of existing correlations developed for an air/water systems were assessed against the new experimental data obtained from an air/silicone oil system.

The total pressure drop, film thickness and wall shear stress were first studied using the air/water system and the experimental results were compared with the existing correlations for each one. Then, the experiments were conducted using the air/silicone oil system where the results were compared with the results using the air/water system. Also, the experimental results using the air/silicone oil system were compared with the existing correlations developed using the air/water system. The experiments were conducted on a vertical test facility with

a 34.5mm inner diameter (ID) and a test section made of acrylic resin (Perspex™). The experiment conditions were identified by defining the point where the annular flow exists and meets Wallis parameter ($U_g^*$) and Kutateladze number ($Ku_g$) criteria as shown in Chapter 4. The experiments were conducted for air/water and air/silicone oil systems between gas superficial velocity ranging from 17.83 m/s to 35.66 m/s, and liquid superficial velocity ranging from 0.018 m/s to 0.089 m/s with water, and from 0.018 m/s to 0.094 m/s with silicone oil.

The measurement of liquid film thickness was the most challenging where the widely and preferable measurement techniques are based on conductance measurement as per evaluation in Chapter 2. However, silicone oil is a non-conducting medium. Therefore, development of a measurement technique that is not depending on the liquid properties was necessary. An ultrasonic pulse echo technique was utilised to measure the liquid film thickness which was evaluated using static and dynamic conditions as presented in Chapter 5. The total pressure drop was measured using a remote seal differential pressure transducer and the wall shear stress was measured using a glue-on hot film sensor.

The experimental work carried out in this research has yielded the following important findings and conclusions:

1. The behaviour of total pressure drop, liquid film thickness and wall shear stress using an air/silicone oil follow similar trend behaviour of an air/water system with increasing gas and liquid superficial velocities even though there is a difference in fluid properties between both systems.

2. In both air/water and air/silicone oil systems, the total pressure drop and wall shear stress increase with increasing gas and liquid superficial velocities where the liquid film thickness decreases. These results in annular flow agree with the published work using an air/water system.

3. In both air/water and air/silicone oil systems, the total pressure drop increases with increasing wall shear stress and decrease with increasing the liquid film thickness.

4. The difference in fluid properties (viscosity and surface tension) between air/water and air/silicone oil systems influenced the total pressure, film thickness and wall shear stress. However, the influence on the total pressure drop and wall shear stress is significant compared to the liquid film thickness. The total pressure drop of air/silicone oil system is lower than the total pressure of air/water system at low gas superficial velocity. Then, it keeps increase with increasing gas superficial velocity until it becomes greater than the total pressure drop of air/water system. The liquid film thickness has been affected slightly where this effect is almost negligible at high gas superficial velocity regardless of liquid superficial

velocity. In other hand, the difference in fluid properties has much impact on the wall shear stress where there is a difference between the wall shear stress of the air/water system and the wall shear stress of the air/silicone oil system. The difference keeps increasing with increasing the gas superficial velocity regardless of liquid superficial velocity.

5. Most of the available correlations could predict the total pressure drop, liquid film thickness and wall shear stress with relative deviation of ±50% or even higher in some cases. This large deviation margin was attributed to many factors such as pipe diameter, gas and liquid superficial velocities, liquid viscosity and surface tension. In addition, the gas/liquid injection method and the inherent inaccuracy of the data used for making the correlations are also contributed according to Hewitt (1982) and Owen (1986). Liquid film thickness correlations contain constants that were based on the experimental data used to develop them. These constants might be the cause of the variation.

6. The ultrasonic measurement technique was developed and tested for measuring liquid film thickness using static and dynamic conditions as discussed in Chapter 5. It was demonstrated to be able to measure the film thickness on dynamic condition with relative deviation of ± 5% when compared against well-known conductance measurement techniques (Multi-Pin Film Sensor and concentric probe).

7. A new processing method called Baseline removal method was developed for ultrasonic measurement. The method is simple and easy to implement assuming the system is not vibrating and the temperature is constant during measurement recording time.

## 7.2. Future Work

From the current study, it was noted that there is a room for further experimental studies. The following recommendations are suggested for future work:

1. The characteristics of annular flow and the relationship between total pressure drop, liquid film thickness and wall shear stress can be further tested using liquid with different surface tensions and viscosities such as silicone oil with higher viscosities. However, it is better to use a liquid which doesn't consist of water to alter its surface tension and viscosity in order to avoid the influence of water properties on the measurement.

2. The entrainment fraction was calculated using a correlation derived based on experimental data using an air/water system. Therefore, the entrainment fraction needs to be measured to assess the uncertainty of the entrainment correlations with different surface tension and viscosity using the same entrainment measurement technique like sampling probe method or liquid film removal method. Hence, developing a correlation suitable with liquid different than water.

3. The injection method has an impact on the measurement according to Hewitt (1982) and Owen (1986). Therefore, further experiments are required using different injection methods such as porous wall injector and axial jet injector. The experiments have to be conducted under the same experimental condition and different fluids properties to assess the effect of the injection method.

4. Investigate the possibility of developing a correlation for predicting liquid film thickness that can fit any experimental data with less dependency on physical constants derived from the experimental data and can be used with different liquid properties.

# REFERENCES

ABBAS HASAN, B. AZZOPARDI, B. HEWAKANDAMBY, YOUSUF ALAUFI, N.J. WATSON & MOHAMMED, S. K. 2016. Experimental characterization of interfacial wave structure of a falling liquid film in a vertical large pipe diameter. Proceedings of 9th International Conference on Multiphase Flow (ICMF), 2016 Firenze-Italy.

AL-SARKHI, A., SARICA, C. & QURESHI, B. 2012. Modeling of droplet entrainment in co-current annular two-phase flow: A new approach. *International Journal of Multiphase Flow,* 39**,** 21-28.

ALAMU, M. B. 2010. *Investigation of periodic structures in gas-liquid flow*. Ph.D. Thesis, University of Nottingham.

ALEKSEENKO, S. V., CHERDANTSEV, A. V., HEINZ, O. M., KHARLAMOV, S. M. & MARKOVICH, D. M. 2014. Analysis of spatial and temporal evolution of disturbance waves and ripples in annular gas–liquid flow. *International Journal of Multiphase Flow,* 67**,** 122-134.

ALEKSEENKO, S. V., NAKORI͡AKOV, V., POKUSAEV, B. G. E. & FUKANO, T. 1994. *Wave flow of liquid films*, Begell House New York.

ALIYU, A. M., BABA, Y. D., LAO, L., YEUNG, H. & KIM, K. C. 2017. Interfacial friction in upward annular gas–liquid two-phase flow in pipes. *Experimental Thermal and Fluid Science,* 84**,** 90-109.

AYAZ, U. K., IOPPOLO, T. & OETUEGEN, M. V. 2013. Direct measurement of wall shear stress in a reattaching flow with a photonic sensor. *Measurement Science & Technology,* 24.

AZZOPARDI, B. 1983. *Mechanisms of entrainment in annular two phase flow*, UKAEA Atomic Energy Research Establishment.

AZZOPARDI, B. 1986. Disturbance wave frequencies, velocities and spacing in vertical annular two-phase flow. *Nuclear Engineering and Design,* 92**,** 121-133.

AZZOPARDI, B. J. 1997. Drops in annular two-phase flow. *International Journal of Multiphase Flow,* 23, Supplement**,** 1-53.

AZZOPARDI, B. J. 2006. *Gas-liquid flows,* Begell house New York.

BABA MUSA, A. & YUENG, H. 2016. Non-invasive classification of gas–liquid two-phase horizontal flow regimes using an ultrasonic Doppler sensor and a neural network. *Measurement Science and Technology,* 27**,** 084002.

BAKER, O. 1954. Simultaneous Flow of Oil and Gas. *The oil and gas,* 53**,** 185-195.

BARBOSA, J., HEWITT, G., KÖNIG, G. & RICHARDSON, S. 2002. Liquid entrainment, droplet concentration and pressure gradient at the onset of annular flow in a vertical pipe. *International Journal of Multiphase Flow,* 28**,** 943-961.

BEGGS, D. H. & BRILL, J. P. 1973. A Study of Two-Phase Flow in Inclined Pipes.

BELT, R. J. 2007. *On the liquid film in inclined annular flow.* Ph.D. Thesis, Delft University of Technology.

BELT, R. J., VAN'T WESTENDE, J. M. C., PRASSER, H. M. & PORTELA, L. M. 2010. Time and spatially resolved measurements of interfacial waves in vertical annular flow. *International Journal of Multiphase Flow,* 36**,** 570-587.

BERCA, E.-L. 2007. *Instrumentation development for wall shear-stress applications in 3D complex flows.* EPFL.

BERNA, C., ESCRIVÁ, A., MUÑOZ-COBO, J. & HERRANZ, L. 2014. Review of droplet entrainment in annular flow: Interfacial waves and onset of entrainment. *Progress in Nuclear Energy,* 74**,** 14-43.

BILANIUK, N. & WONG, G. S. 1993. Speed of sound in pure water as a function of temperature. *The Journal of the Acoustical Society of America,* 93**,** 1609-1612.

BOYER, C., DUQUENNE, A.-M. & WILD, G. 2002. Measuring techniques in gas–liquid and gas–liquid–solid reactors. *Chemical Engineering Science,* 57**,** 3185-3215.

BRUUN, H. 1996. Hot-film anemometry in liquid flows. *Measurement Science and Technology,* 7**,** 1301.

BRUUN, H. H. 1995. Hot-wire anemometry-principles and signal analysis.

CHALLIS, R. E., WILKINSON, G. P. & FREEMANTLE, R. J. 1998. Errors and uncertainties in the ultrasonic pulse-echo reflectometry method for

measuring acoustic impedance. *Measurement Science and Technology,* 9**,** 692.

CHEEKE 2002. Fundamentals and applications of ultrasonic wave. *Fundamentals and Applications of Ultrasonic Waves.* CRC Press.

CHEN, Z. Q., HERMANSON, J. C., SHEAR, M. A. & PEDERSEN, P. C. 2005. Ultrasonic monitoring of interfacial motion of condensing and non-condensing liquid films. *Flow Measurement and Instrumentation,* 16**,** 353-364.

CHENG, H., HILLS, J. & AZZORPARDI, B. 1998. A study of the bubble-to-slug transition in vertical gas-liquid flow in columns of different diameter. *International journal of multiphase flow,* 24**,** 431-452.

CHISHOLM, D. 1967. A theoretical basis for the Lockhart-Martinelli correlation for two-phase flow. *International Journal of Heat and Mass Transfer,* 10**,** 1767-1778.

CHISHOLM, D. 1972. Equation for Velocity Ratio in Two-Phase Flow. *Nat. Eng. Lab. Rep.(U. K.)***,** 13.

CICCHITTI, A., LOMBARDI, C., SILVESTRI, M., SOLDAINI, G. & ZAVATTARELLI, R. 1960. Two-phase cooling experiments: pressure drop, heat transfer and burnout measurements. Centro Informazioni Studi Esperienze, Milan.

CLARK, W. W. 2002. LIQUID FILM THICKNESS MEASUREMENT. 14**,** 74.

COGNET, G., LEBOUCHE, M. & SOUHAR, M. 1984. Wall shear measurements by electrochemical probe for gas-liquid two-phase flow in vertical duct. *AIChE journal,* 30**,** 338-341.

COLLIER, J. G. & HEWITT, G. F. 1964. *Film thickness measurements,* Chemical Engineering Division, Atomic Energy Research Establishment.

CONTE, G. 2000. *An experimental study for the characterisation of gas/liquid flow splitting at T-junctions.* PhD, University of Nottingham.

CONTE, G. & AZZOPARDI, B. J. 2003. Film thickness variation about a T-junction. *International Journal of Multiphase Flow,* 29**,** 305-328.

COSTIGAN, G. & WHALLEY, P. 1997. Slug flow regime identification from dynamic void fraction measurements in vertical air-water flows. *International Journal of Multiphase Flow,* 23**,** 263-282.

DESCAMPS, M., OLIEMANS, R., OOMS, G. & MUDDE, R. 2008. Air–water flow in a vertical pipe: experimental study of air bubbles in the vicinity of the wall. *Experiments in Fluids,* 45**,** 357-370.

DURST, F., MÜLLER, R. & JOVANOVIC, J. 2004. Determination of the measuring position in laser-Doppler anemometry. *Experiments in fluids,* 6**,** 105-110.

ETEBARI, A. 2008. Recent innovations in wall shear stress sensor technologies. *Recent Patents on Mechanical Engineering,* 1**,** 22-28.

FACHUN, L., HONGFENG, Z., HAO, Y. & YUAN, S. 2016. Gas–liquid two-phase flow pattern identification by ultrasonic echoes reflected from the

inner wall of a pipe. *Measurement Science and Technology,* 27**,** 035304.

FERNHOLZ, H. H., JANKE, G., SCHOBER, M., WAGNER, P. M. & WARNACK, D. 1996. New developments and applications of skin-friction measuring techniques. *Measurement Science and Technology,* 7**,** 1396.

FORE, L. B. & DUKLER, A. E. 1995. Droplet deposition and momentum transfer in annular flow. *AIChE Journal,* 41**,** 2040-2046.

FRIEDEL, L. Improved friction pressure drop correlations for horizontal and vertical two-phase pipe flow. European two-phase group meeting, Ispra, Italy, 1979.

FUKANO, T. & FURUKAWA, T. 1998. Prediction of the effects of liquid viscosity on interfacial shear stress and frictional pressure drop in vertical upward gas–liquid annular flow. *International journal of multiphase flow,* 24**,** 587-603.

GOVAN, A. H. 1990. *Modeling of Vertical Annular and Dispersed Two-Phase Flow.* Ph.D. Thesis, , Imperial College London, UK.

GOVAN, A. H., HEWITT, G. F., OWEN, D. G. & BURNETT, G. 1989. Wall shear stress measurements in vertical air-water annular two-phase flow. *International Journal of Multiphase Flow,* 15**,** 307-325.

HAGIWARA, Y. E. E., H.TSUTSUI, K.SUZUKI 1988. Simultaneous measurement of liquid film thickness, wall shear stress and gas flow turbulence of horizontal wavy two phase flow. *International Multiphase flow,* 15**,** 421-431.

HAMAD, F. A. & HE, S. 2010. Evaluation of hot-film, dual optical and Pitot tube probes for liquid–liquid two-phase flow measurements. *Flow Measurement and Instrumentation,* 21**,** 302-311.

HANRATTY, T. J. 2013. *Physics of Gas-Liquid Flows*, Cambridge University Press.

HANRATTY, T. J. & CAMPBELL, J. A. 1996. Measurement of wall shear stress. *Fluid mechanics measurements(2 nd revised and enlarged edition)(A 97-29735 07-35), Washington, DC, Taylor & Francis, 1996***,** 575-648.

HARITONIDIS, J. 1989. The Measurement of Wall Shear Stress. *In:* GAD-EL-HAK, M. (ed.) *Advances in Fluid Mechanics Measurements.* Springer Berlin Heidelberg.

HENSTOCK, W. H. & HANRATTY, T. J. 1976. The interfacial drag and the height of the wall layer in annular flows. *AIChE Journal,* 22**,** 990-1000.

HEWITT, G., LACEY, P. & NICHOLLS, B. 1965. *Transitions in film flow in a vertical tube,* AERE, Chemical Division Harwell.

HEWITT, G. F. 1978. Measurement of two phase flow parameters. *NASA STI/Recon Technical Report A,* 79**,** 47262.

HEWITT, G. F. 1982. Handbook of multiphase systems, McGraw-Hill, Hetsroni ed.

HEWITT, G. F. & HALL-TAYLOR, N. 1970. *Annular two-phase flow,* Pergamon.

HEWITT, G. F., KING, S. & LONEGRORE, P. 1961. *Holdup and pressure drop measurement in the two-phase annular flow of air-water mixtures*, UKAEA Atomic Energy Research Establishment, Harwell Research Group.

HEWITT, G. F. & ROBERTS, D. 1969. Studies of two-phase flow patterns by simultaneous X-ray and flash photography. DTIC Document.

HUTCHINS, N. & CHOI, K.-S. 2002. Accurate measurements of local skin friction coefficient using hot-wire anemometry. *Progress in Aerospace Sciences,* 38**,** 421-446.

ISHIGAI, S., NAKANISI, S., KOIZUMI, T. & OYABU, Z. 1972. Hydrodynamics and Heat Transfer of Vertical Falling Liquid Films: Part 1, Classification of Flow Regimes. *Bulletin of JSME,* 15**,** 594-602.

ISHII, M. & MISHIMA, K. 1989. Droplet entrainment correlation in annular two-phase flow. *International Journal of Heat and Mass Transfer,* 32**,** 1835-1846.

JACKSON, M. L. 1955. Liquid films in viscous flow. *AIChE Journal,* 1**,** 231-240.

JAWOREK, A. & KRUPA, A. 2004. Gas/liquid ratio measurements by rf resonance capacitance sensor. *Sensors and Actuators A: Physical,* 113**,** 133-139.

JU, P., BROOKS, C. S., ISHII, M., LIU, Y. & HIBIKI, T. 2015. Film thickness of vertical upward co-current adiabatic flow in pipes. *International Journal of Heat and Mass Transfer,* 89**,** 985-995.

KAJI, R. & AZZOPARDI, B. J. 2010. The effect of pipe diameter on the structure of gas/liquid flow in vertical pipes. *International Journal of Multiphase Flow,* 36**,** 303-313.

KANG, H. C. & KIM, M. H. 1992. THE DEVELOPMENT OF A FLUSH-WIRE PROBE AND CALIBRATION METHOD FOR MEASURING LIQUID-FILM THICKNESS. *International Journal of Multiphase Flow,* 18**,** 423-437.

KARAPANTSIOS, T. D., PARAS, S. V. & KARABELAS, A. J. 1989. Statistical characteristics of free falling films at high reynolds numbers. *International Journal of Multiphase Flow,* 15**,** 1-21.

KLAUSNER, J. F., ZENG, L. Z. & BERNHARD, D. M. 1992. Development of a film thickness probe using capacitance for asymmetrical two-phase flow with heat addition. *Review of Scientific Instruments,* 63**,** 3147-3152.

LEVY, S. 1999. Two-Phase Flow in Complex Systems. Wiley-Interscience.

LOCKHART, R. & MARTINELLI, R. 1949. Proposed correlation of data for isothermal two-phase, two-component flow in pipes. *Chem. Eng. Prog,* 45**,** 39-48.

LOUREIRO, J. B. R., SOUSA, F., ZOTIN, J. L. Z. & FREIRE, A. P. S. 2010. The distribution of wall shear stress downstream of a change in roughness. *International Journal of Heat and Fluid Flow,* 31**,** 785-793.

LU, Q., SURYANARAYANA, N. V. & CHRISTODOULU, C. 1993. Film Thickness Measurement with an Ultrasonic Transducer. *Experimental Thermal and Fluid Science,* 7**,** 354-361.

LYU, T. H. & MUDAWAR, I. 1991. Statistical investigation of the relationship between interracial waviness and sensible heat transfer to a falling liquid film. *International Journal of Heat and Fluid Flow,* 34**,** 1451-1464.

MAGRINI, K. L., SARICA, C., AL-SARKHI, A. & ZHANG, H.-Q. 2012. Liquid Entrainment in Annular Gas/Liquid Flow in Inclined Pipes.

MARTIN, C. J. 1983. *Annular two phase flow.* Ph.D. Thesis, University of Oxford.

MASALA, T., HARVEL, G. & CHANG, J.-S. 2007. Separated two-phase flow regime parameter measurement by a high speed ultrasonic pulse-echo system. *Review of Scientific Instruments,* 78**,** 114901.

MURAI, Y., TASAKA, Y., NAMBU, Y., TAKEDA, Y. & GONZALEZ A, S. R. 2010. Ultrasonic detection of moving interfaces in gas–liquid two-phase flow. *Flow Measurement and Instrumentation,* 21**,** 356-366.

NAKORYAKOV, V., KASHINSKY, O. & KOZMENKO, B. 1986. Experimental study of gas-liquid slug flow in a small-diameter vertical pipe. *International journal of multiphase flow,* 12**,** 337-355.

NAKORYAKOV, V. E., KASHINSKY, O. N. & KOZMENKO, B. K. 1984. Electrochemical Method for Measuring Turbulent Characteristics of Gas-Liquid Flows. *In:* DELHAYE, J. M. & COGNET, G. (eds.) *Measuring Techniques in Gas-Liquid Two-Phase Flows.* Springer Berlin Heidelberg.

NAUGHTON, J. W. & SHEPLAK, M. 2002. Modern developments in shear-stress measurement. *Progress in Aerospace Sciences,* 38**,** 515-570.

NG, T. W., NARAIN, A. & KIVISALU, M. T. 2009. Fluorescence and Fiber-Optics Based Real-Time Thickness Sensor for Dynamic Liquid Films. *Journal of Heat Transfer,* 132**,** 031603-031603.

OHBA, K., ORIGUCHI, T. & SHIMANAKA, Y. Multi-fiber optic liquid film sensor. Proceedings of the 4th Sensor Symposium, 1984. 33-37.

OHBA, K., TAKADA, H., KAWAKAMI, N. & NAGAE, K. 1992. Twin fiber optic liquid film sensor for simultaneous measurement of local film thickness and velocity in two-phase annular flow. DTIC Document.

OHNUKI, A. & AKIMOTO, H. 2000. Experimental study on transition of flow pattern and phase distribution in upward air–water two-phase flow along a large vertical pipe. *International journal of multiphase flow,* 26**,** 367-386.

OLIEMANS, R. V. A., POTS, B. F. M. & TROMPÉ, N. 1986. Modelling of annular dispersed two-phase flow in vertical pipes. *International Journal of Multiphase Flow,* 12**,** 711-732.

OMEBERE-IYARI, N. K. & AZZOPARDI, B. J. 2007. A Study of Flow Patterns for Gas/Liquid Flow in Small Diameter Tubes. *Chemical Engineering Research and Design,* 85**,** 180-192.

OWEN, D. & HEWITT, G. Data and Analysis of Pressure Gradient and Liquid Entrainment in Vertical Annular Gas-Liquid Flow. European Two-Phase Flow Group Meeting, Marchwood, GB, 1985.

OWEN, D. G. 1986. *An experimental and theoretical analysis of equilibrium annular flows.* Ph.D. Thesis, University of Birmingham.

PAN, L.-M., HE, H., JU, P., HIBIKI, T. & ISHII, M. 2015a. Experimental study and modeling of disturbance wave height of vertical annular flow. *International Journal of Heat and Mass Transfer,* 89**,** 165-175.

PAN, L.-M., HE, H., JU, P., HIBIKI, T. & ISHII, M. 2015b. The influences of gas–liquid interfacial properties on interfacial shear stress for vertical annular flow. *International Journal of Heat and Mass Transfer,* 89**,** 1172-1183.

PAN, L. & HANRATTY, T. J. 2002. Correlation of entrainment for annular flow in vertical pipes. *International Journal of Multiphase Flow,* 28**,** 363-384.

PARK, J. R. & CHUN, M.-H. 1984. Liquid Film Thickness Measurement by An Ultrasonic Pulse Echo Method. *Korean Nuclear Society,* 17.

PERRON, A., KISS, L. I. & VERREAULT, R. 2006. A multifibre optic sensor to measure the liquid film thickness between a moving bubble and an inclined solid surface. *Measurement Science & Technology,* 17**,** 1594-1600.

POVEY, M. J. 1997. *Ultrasonic techniques for fluids characterization*, Academic Press.

PRESTON, J. 1954. The determination of turbulent skin friction by means of Pitot tubes. *Journal of the Royal Aeronautical Society,* 58**,** 109-121.

RATHAKRISHNAN, E. 2007. *Instrumentation, Measurements, and Experiments in Fluids*, CRC Press.

SALARI, M. & TABAR, M. M. 2011. Accurate wall positioning of the hot-wire sensor using a high aspect-ratio rectangular nozzle. *Flow Measurement and Instrumentation,* 22**,** 138-143.

SAWANT, P., ISHII, M. & MORI, M. 2008. Droplet entrainment correlation in vertical upward co-current annular two-phase flow. *Nuclear Engineering and Design,* 238**,** 1342-1352.

SCHMIDT, J., GIESBRECHT, H. & VAN DER GELD, C. 2008. Phase and velocity distributions in vertically upward high-viscosity two-phase flow. *International Journal of Multiphase Flow,* 34**,** 363-374.

SCOTT, D. S. 1963. Properties of cocurrent gas-liquid flow. *Advances in chemical engineering,* 4**,** 199-277.

SEKOGUCHI, K. & MORI, K. 1997. New development of experimental study on interfacial structure in gas–liquid two-phase flow. *Experimental Heat Transfer, Fluid Mechanics and Thermodynamics,* 2**,** 1177-1188.

SERIZAWA, A., NAGANE, K., KAMEI, T., TAKAHASHI, O. & KAWARA, Z. 1994. NON-INTRUSIVE MEASUREMENT OF DYNAMIC BEHAVIOR OF A LIQUID FILM FLOW. *Proceedings of the German-Japanese Symposium on Multi-Phase Flow***,** 51-51.

SHAHA, J. 1999. *Phase interactions in transient stratified flow.* Ph.D. Thesis, Imperial College London (University of London).

SHEDD, T. A. & NEWELL, T. A. 1997. An Automated Optical Liquid Film Thickness Measurement Method. Air Conditioning and Refrigeration Center. College of Engineering. University of Illinois at Urbana-Champaign.

SHEPLAK, M., CATTAFESTA, L., NISHIDA, T. & MCGINLEY, C. B. 2004. *MEMS shear stress sensors: promise and progress,* Defense Technical Information Center.

TAITEL, Y., BORNEA, D. & DUKLER, A. E. 1980. Modelling flow pattern transitions for steady upward gas-liquid flow in vertical tubes. *AIChE Journal,* 26**,** 345-354.

THAN, C., TEE, K., LOW, K. & TSO, C. 1993. Optical measurement of slope, thickness and velocity in liquid film flow. *Smart Materials and Structures,* 2**,** 13.

TIBIRIÇÁ, C. B., DO NASCIMENTO, F. J. & RIBATSKI, G. 2010. Film thickness measurement techniques applied to micro-scale two-phase flow systems. *Experimental Thermal and Fluid Science,* 34**,** 463-473.

VAN DER MEULEN, G. P. 2012. *Churn-annular gas-liquid flows in large diameter vertical pipes.* PhD, University of Nottingham.

WADA, S., KIKURA, H. & ARITOMI, M. 2006. Pattern recognition and signal processing of ultrasonic echo signal on two-phase flow. *Flow Measurement and Instrumentation,* 17**,** 207-224.

WALLIS, G. B. 1962. The transition from flooding to upwards cocurrent annular flow in a vertical pipe. United Kingdom Atomic Energy Authority.

WALLIS, G. B. 1969. *One-dimensional two-phase flow*, McGraw-Hill.

WANG, Z., GABRIEL, K. S. & MANZ, D. L. 2004. The influences of wave height on the interfacial friction in annular gas–liquid flow under

normal and microgravity conditions. *International journal of multiphase flow,* 30**,** 1193-1211.

WATSON, N. J. 2015. Ultrasound Tomography. *In:* M WANG (ed.) *Industrial tomography: systems and applications.* Woodhead Publishing.

WHALLEY, P. & MCQUILLAN, K. 1985. *The development and use of a directional wall shear stress probe,* UKAEA Atomic Energy Research Establishment.

WINTER, K. G. 1977. An Outline of the Techniques Available For the Measurement of Skin Friction In Turbulent Boundary Layers. 18**,** 1-57.

WOLF, A. 1995. *liquid film structure in annular two-phase flow.* Ph.D. Thesis, , University of London, Imperial College.

WOOD, A. B. 1941. *A text book of sound,* G. Bell and Sons, London.

YU, S. C. M. & TSO, C. P. 1995. Simulation of fiber optic sensors in determination of thin liquid film thicknesses. *Advances in Engineering Software,* 22**,** 55-62.

YU, S. C. M., TSO, C. P. & LIEW, R. 1996. Analysis of thin film thickness determination in two-phase flow using a multifiber optical sensor. *Applied Mathematical Modelling,* 20**,** 540-548.

ZABARAS, G., DUKLER, A. E. & MOALEM-MARON, D. 1986. Vertical upward cocurrent gas-liquid annular flow. *AIChE Journal,* 32**,** 829-843.

ZANGANA, M. H. S. 2011. *Film behaviour of vertical gas-liquid flow in a large diameter pipe.* Ph.D. Thesis, University of Nottingham.

ZHAO, Y. 2014. *Wave behaviour in vertical multiphase flow.* Ph.D. Thesis, Imperial College London.

ZHAO, Y., MARKIDES, C. N., MATAR, O. K. & HEWITT, G. F. 2013. Disturbance wave development in two-phase gas–liquid upwards vertical annular flow. *International Journal of Multiphase Flow,* 55**,** 111-129.

ZHENG, D. & CHE, D. 2007. An investigation on near wall transport characteristics in an adiabatic upward gas–liquid two-phase slug flow. *Heat and mass transfer,* 43**,** 1019-1036.

# APPENDIX

## 7.3. Appendix A:

## Operating Instruction of MiniCTA Anemometer 54T42

# 1. MiniCTA Anemometer 54T42

## 1.1 Introduction

The MiniCTA version 54T42 is a versatile anemometer that can be used with many of Dantec's wire and film/fiber-film probes. The MiniCTA is mounted in a small box equipped with BNC connectors and operated from a 12 VDC power adapter or alternatively by a battery. It is especially designed for measurements in air of velocity and turbulence in subsonic flows with moderate frequency content. With a proper set-up measurements of low velocities and fluctuations in water can also be performed.

The flexible and compact unit is well suited for educational purposes and for field measurements. Its small size makes it well suited for building into test models close to the probe. The CTA electronics is optimised for use with wire probes in air (bandwidth >= 10 kHz at 50 m/sec). The anemometer has an operational resistance range (probe + cable) of 4-36 Ohms and can be configured to operate with probes with cold resistances above 20 Ohms (depending on probe overheat selection!).

Note:

The overheat resistance is preset at the factory to match Dantec 55P11-16 and 55P61-64 wire probes connected with 4 m probe cables to the MiniCTA. (The default setting accepts cable lengths of 1 - 10 m). The MiniCTA is ready for use without any adjustments for these combinations. For use with other probes or cable lengths longer than 10 m (max. 20 m) an adjustment of the overheat and cable compensation will be necessary.

Overheat adjustment, signal conditioning and selecting cable compensation are performed via DIP-switches and jumpers inside the box. The overheat adjustment is assisted by the MiniCTA software package or by an Excel spreadsheet, which can be downloaded from Dantec Dynamics web site.

A proper grounding of the MiniCTA is necessary for correct measurements, especially important for water applications! See paragraph 1.3.1.

## 1.3 Installation

The anemometer has two BNC connectors (one for the probe cable and one for the output voltage) and one input connector for the power adapter. *It is important to connect the probe and probe cable to the box and - if necessary - to adjust the overheat, before the power adapter is connected and power is switched on, in order to avoid burn-out of the probe.*

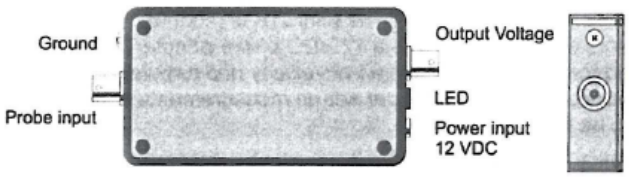


***Fig. 1.*** *The MiniCTA box with connections for probe input, output voltage, power input and ground-connection. A LED indicates that the power is connected.*

Connect the coax cable (4 m Dantec no. 9006A1863 supplied with the anemometer) with its probe support to the Probe input BNC connector on the CTA-box and insert the probe into the probe support. Connect the BNC connector marked 'Output' to a voltmeter or data acquisition system, see Fig. 1. Finally connect the power supply to the power input. If a custom power supply is used it must be a double-isolated 12 VDC type with positive center pin (minimum 0.5 A output). It is recommended to connect the MiniCTA output signal differentially to the A/D board input, as the power supply is floating. If more MiniCTA's are attached to the same power supply, their outputs must be connected differentially.

Do not turn the line power on until you have checked that the overheat is correctly adjusted inside the MiniCTA box (see below) and the probe is connected/mounted!

### 1.3.1 Grounding of the MiniCTA

There is no ground connection through the double-isolated DC Power Adaptor for the MiniCTA and the MiniCTA acts as a floating signal source. It is therefore most important to use differential input, when the anemometer voltage is acquired via an A/D board - and also to connect the anemometer signal ground to the Analog input ground (or PC ground) via a resistor in order to avoid noise problems. For this purpose the cabinet of the MiniCTA box is provided with a ground terminal screw. Alternatively, the shield of the output cable can be used as shown in Fig. 2. When more MiniCTA's are connected to the same A/D board, it is mandatory that all outputs must be grounded via their own resistor.

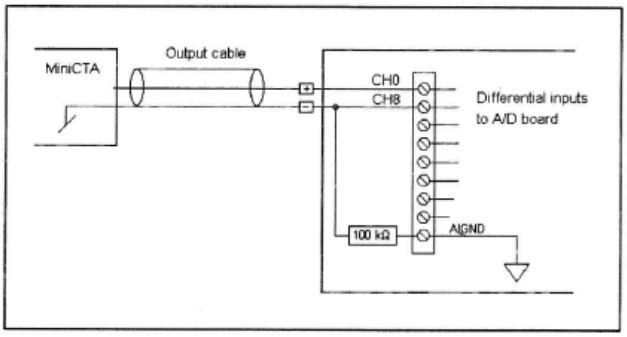


***Fig. 2.*** *Connecting and grounding of the MiniCTA output signal via a 100 kΩ resistor.*

For A/D boards (with no dedicated signal ground connection) connected to the PC via a USB cable it is advised to use the PC ground/chassis as signal ground. However, it must then be checked that the USB cable shield is properly connected to the PC chassis.

### 1.3.2 Grounding of the MiniCTA in water applications

For all CTA-applications in water (only fresh water should be used!) a grounding electrode should be placed in the water close to the CTA-probe. The electrode should be connected via a thick wire to the MiniCTA ground connection. The complete measurement system/chain should be connected to the same ground connection. The objective is to eliminate any potential differences to avoid electrical strike-through of the probe insulation.

Except for the special precautions needed when measuring in water/liquids CTA probes and probe cables should normally be electrically insulated from any conductive parts.

### 1.3.3 Electromagnetic Interference

Due to the nature of the CTA measurement system with a servo-loop with relatively high bandwidth it is not possible to build a CTA system that can pass standard EMC tests. CTA systems should always be used in so-called 'controlled EMC environments'. However, with a proper grounding of the MiniCTA system to a ground reference 'far away' from the ground reference for e.g. the wind tunnel motor control system it should still be possible to minimize electromagnetic interference. This also means that the MiniCTA system should be kept well away from all motor cables etc. because it might be a matter of simple magnetic coupling if the motor cables are not shielded carefully with proper grounding of the shield.

## 1.4 General set up

### 1.4.1 Factory settings

The overheat resistance is preset at the factory to match 55P11-16 and 55P61-64 wire probes connected with 4 m probe cables to the MiniCTA. (The defult setting accepts cable lengths of 1 - 10 m). The system is ready for use without any adjustments for these combinations. For use with other probes or cable lengths longer than 10 m (max. 20 m) an adjustment of the overheat will be necessary. To change the settings DIP switches inside the MiniCTA box must be set in a correct manner as described below.

***Warning! An incorrect setting may result in damaged probes!***

| Probe type $R_{20} \geq 3.2\ \Omega$ | Cable length | Recommended decade setting ($20 R_T$) | DIP switch SW1 | DIP switch SW2 | DIP switch SW3 |
|---|---|---|---|---|---|
| | | | | | |
| Wire probes | 9006A1863 | | 1 • | • • | • |
| 55P11-16 | 4 m | 140 Ω | 0 • • • | • • | • • • |
| 55P61-64 | | | 4 3 2 1 | 4 3 2 1 | 4 3 2 1 |

***Fig. 3.*** *Factory overheat setup. Dots indicate switch in down position. For SW1 switches Dip_3, and Dip_4 are used to set the cable compensation according to cable length (4 or 20 m).*

### 1.4.2 Selecting cable length

The MiniCTA is preset at the factory to match wire probes connected with 4 -10 m probe cables (RG-58 coax cable - 50 Ohms impedance). If longer cables than 10 m (max. 20 m) are used the cable length setting inside the MiniCTA should be changed to the 20 m setting. SW1 switch 4 & 3 are used to set the cable length (see Fig. 3). The standard 4 m setting corresponds to a switch setting with Dip_4 = 1 and Dip_3 = 0. The 20 m setting corresponds to Dip_4 = 0 and Dip_3 =1.

### 1.4.4 Overheat calculation using Excel spreadsheet

The overheat can be calculated using the MS Excel spreadsheet "54T42 MiniCTA - overheat calculation", which can be found on the installation CD or downloaded from Dantec Dynamics web site www.dantecdynamics.com - Look for the MiniCTA System page.

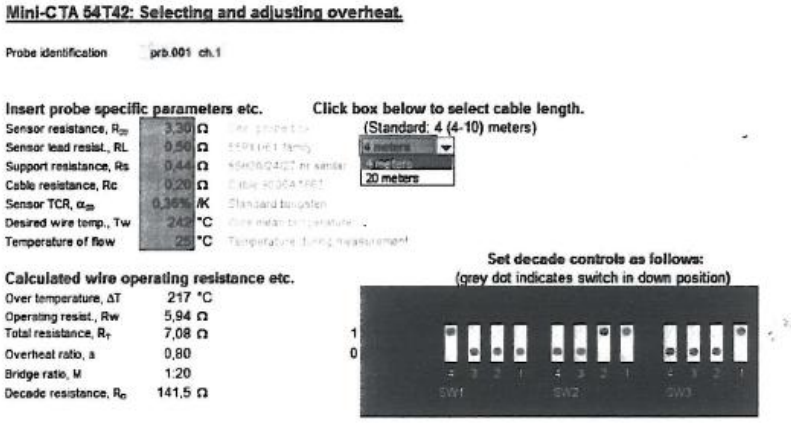


***Fig. 4.*** *Overview of "MiniCTA overheat spreadsheet".*

1) Before starting check that spreadsheet is the correct for use with the 54T42 version of the MiniCTA.

2) First enter the probe and channel number for a correct documentation of your system settings.

3) Select the cable length **4 meters** (for 1-10 m cables) or **20 meters** for cables longer than 10 m (max. allowed cable length is 20 m).

4) Then enter the data from the probe box and the data for the probe support and the probe cable together with the desired wire operating temperature $T_W$ (= 242°C) and the ambient temperature during measurement, $T_{amb}$ (= 25°C).

Insert probe specific parameters etc.

| | | | |
|---|---|---|---|
| Sensor resistance, $R_{20}$ | 3,30 | Ω | On probe box |
| Sensor lead resist., RL | 0,50 | Ω | 55P11/61 family |
| Support resistance, Rs | 0,40 | Ω | 55H20/24/27 or similar |
| Cable resistance, Rc | 0,20 | Ω | Cable 9006A1863 |
| Sensor TCR, $\alpha_{20}$ | 0,36% | /°K | Standard tungsten |
| Desired wire temp., Tw | 242 | °C | Wiremean temperature |
| Temperature of flow, $T_{amb}$ | 25 | °C | Temperature during measurement |

## Appendix B:

## Experiment Results

### 1. Pressure drop, liquid film thickness and wall shear stress of an air/water system

| Liquid superficial velocity, m/s | Gas superficial velocity, m/s | DP, Pa/m | Liquid film thickness, mm | Wall shear stress, Pa |
|---|---|---|---|---|
| 0.018 | 17.829 | 894.393 | 0.160 | 5.931 |
| 0.018 | 19.612 | 981.178 | 0.142 | 7.046 |
| 0.018 | 21.394 | 1052.298 | 0.134 | 7.820 |
| 0.018 | 23.177 | 1131.680 | 0.123 | 8.438 |
| 0.018 | 24.960 | 1212.437 | 0.116 | 9.078 |
| 0.036 | 17.829 | 1111.390 | 0.191 | 7.441 |
| 0.036 | 19.612 | 1218.500 | 0.173 | 8.182 |
| 0.036 | 21.394 | 1304.528 | 0.156 | 9.131 |
| 0.036 | 23.177 | 1367.412 | 0.148 | 9.925 |
| 0.036 | 24.960 | 1465.672 | 0.136 | 10.797 |
| 0.036 | 26.743 | 1543.139 | 0.128 | 11.525 |
| 0.036 | 28.526 | 1652.139 | 0.116 | 12.385 |
| 0.054 | 17.829 | 1328.792 | 0.219 | 8.799 |
| 0.054 | 19.612 | 1402.329 | 0.199 | 9.581 |
| 0.054 | 21.394 | 1478.223 | 0.186 | 10.476 |
| 0.054 | 23.177 | 1586.092 | 0.171 | 11.350 |
| 0.054 | 24.960 | 1692.919 | 0.154 | 12.169 |
| 0.054 | 26.743 | 1777.549 | 0.144 | 13.012 |
| 0.054 | 28.526 | 1893.394 | 0.133 | 13.666 |
| 0.054 | 30.309 | 2003.101 | 0.125 | 14.439 |
| 0.054 | 32.092 | 2133.411 | 0.118 | 15.151 |
| 0.071 | 17.829 | 1532.849 | 0.252 | 9.533 |
| 0.071 | 19.612 | 1614.919 | 0.230 | 10.443 |
| 0.071 | 21.394 | 1733.983 | 0.208 | 11.355 |
| 0.071 | 23.177 | 1810.408 | 0.195 | 12.357 |
| 0.071 | 24.960 | 1956.362 | 0.175 | 13.209 |
| 0.071 | 26.743 | 2045.247 | 0.161 | 13.959 |
| 0.071 | 28.526 | 2152.993 | 0.151 | 14.762 |
| 0.071 | 30.309 | 2267.009 | 0.141 | 15.626 |
| 0.071 | 32.092 | 2421.906 | 0.130 | 16.401 |
| 0.071 | 33.875 | 2578.556 | 0.119 | 17.127 |
| 0.071 | 35.657 | 2657.534 | 0.115 | 17.873 |
| 0.089 | 17.829 | 1700.852 | 0.289 | 10.885 |

| | | | | |
|---|---|---|---|---|
| 0.089 | 19.612 | 1806.638 | 0.264 | 11.720 |
| 0.089 | 21.394 | 1904.904 | 0.238 | 12.663 |
| 0.089 | 23.177 | 2044.163 | 0.214 | 13.519 |
| 0.089 | 24.960 | 2142.932 | 0.197 | 14.359 |
| 0.089 | 26.743 | 2255.702 | 0.183 | 15.280 |
| 0.089 | 28.526 | 2409.383 | 0.166 | 16.114 |
| 0.089 | 30.309 | 2521.938 | 0.155 | 16.919 |
| 0.089 | 32.092 | 2656.715 | 0.146 | 17.769 |
| 0.089 | 33.875 | 2776.160 | 0.136 | 18.595 |
| 0.089 | 35.657 | 2944.783 | 0.127 | 19.478 |

## 2. Pressure drop, liquid film thickness and wall shear stress of an air/silicone oil system

| Liquid superficial velocity, m/s | Gas superficial velocity, m/s | DP, Pa/m | Liquid film thickness, mm | Wall shear stress, Pa |
|---|---|---|---|---|
| 0.018 | 17.829 | 962.607 | 0.168 | 6.595 |
| 0.018 | 19.612 | 1047.170 | 0.151 | 7.622 |
| 0.018 | 21.394 | 1139.766 | 0.141 | 8.515 |
| 0.018 | 23.177 | 1275.533 | 0.131 | 9.755 |
| 0.018 | 24.960 | 1408.092 | 0.123 | 10.833 |
| 0.037 | 17.829 | 1087.184 | 0.198 | 7.451 |
| 0.037 | 19.612 | 1197.919 | 0.182 | 8.642 |
| 0.037 | 21.394 | 1309.756 | 0.162 | 9.957 |
| 0.037 | 23.177 | 1426.285 | 0.155 | 11.174 |
| 0.037 | 24.960 | 1559.974 | 0.142 | 12.437 |
| 0.037 | 26.743 | 1703.318 | 0.132 | 13.654 |
| 0.037 | 28.526 | 1878.011 | 0.118 | 15.049 |
| 0.056 | 17.829 | 1220.365 | 0.229 | 9.164 |
| 0.056 | 19.612 | 1316.449 | 0.209 | 10.388 |
| 0.056 | 21.394 | 1446.465 | 0.194 | 11.791 |
| 0.056 | 23.177 | 1547.384 | 0.180 | 12.870 |
| 0.056 | 24.960 | 1675.978 | 0.162 | 14.134 |
| 0.056 | 26.743 | 1819.828 | 0.152 | 15.445 |
| 0.056 | 28.526 | 1961.305 | 0.140 | 16.589 |
| 0.056 | 30.309 | 2147.135 | 0.131 | 17.663 |
| 0.056 | 32.092 | 2292.378 | 0.123 | 18.668 |
| 0.075 | 17.829 | 1309.227 | 0.261 | 9.886 |
| 0.075 | 19.612 | 1416.499 | 0.237 | 11.347 |
| 0.075 | 21.394 | 1531.127 | 0.216 | 12.740 |
| 0.075 | 23.177 | 1664.013 | 0.200 | 14.189 |

| | | | | |
|---|---|---|---|---|
| 0.075 | 24.960 | 1842.634 | 0.180 | 15.741 |
| 0.075 | 26.743 | 1991.622 | 0.167 | 16.902 |
| 0.075 | 28.526 | 2130.946 | 0.157 | 18.041 |
| 0.075 | 30.309 | 2283.352 | 0.146 | 19.664 |
| 0.075 | 32.092 | 2466.751 | 0.134 | 20.332 |
| 0.075 | 33.875 | 2588.077 | 0.123 | 21.713 |
| 0.075 | 35.657 | 2728.690 | 0.117 | 22.421 |
| 0.094 | 17.829 | 1491.378 | 0.298 | 11.459 |
| 0.094 | 19.612 | 1618.623 | 0.275 | 13.196 |
| 0.094 | 21.394 | 1705.191 | 0.247 | 14.464 |
| 0.094 | 23.177 | 1837.686 | 0.223 | 15.580 |
| 0.094 | 24.960 | 1992.495 | 0.207 | 17.356 |
| 0.094 | 26.743 | 2158.020 | 0.190 | 18.814 |
| 0.094 | 28.526 | 2305.455 | 0.173 | 19.923 |
| 0.094 | 30.309 | 2495.540 | 0.162 | 21.169 |
| 0.094 | 32.092 | 2659.801 | 0.151 | 22.385 |
| 0.094 | 33.875 | 2840.632 | 0.141 | 23.426 |
| 0.094 | 35.657 | 3033.200 | 0.130 | 24.406 |